Approximate Continuation of Harmonic Functions in Geodesy

A Weighted Least-Squares Approach Based on Splines with Extension to the Multiscale Adaptive Case

zur Erlangung des Doktorgrades
der
Fakultät für Elektrotechnik, Informatik und Mathematik
der
Universität Paderborn

vorgelegt von
Gabriela Jager geb. Constantinescu
aus Iaşi

Paderborn, 2010

Angefertigt mit Genehmigung
der Fakultät für Elektrotechnik, Informatik und Mathematik
der Universität Paderborn

Betreuung: Prof. Dr. Angela Kunoth, Universität Paderborn

Diese Arbeit ist mit Unterstützung des
EU-IHP Projektes *Breaking Complexity*, des
SFB/TR 32 *Patterns in Soil-Vegetation-Atmosphere-Systems*, mit einem
Promotionsstipendium aus Gleichstellungsmitteln der Universität Bonn und mit einem
Promotionsabschlußstipendium der Universität Paderborn
entstanden.

to my father
and his fascination with science

Danksagung

Ich möchte mich zunächst bei meiner Betreuerin Frau Prof. Dr. Angela Kunoth für das Vertrauen und die vielfältige Unterstützung während den Jahren meines Promotionsstudiums und der Erstellung meiner Doktorarbeit bedanken. Ihre Anleitung als überzeugte Mathematikerin, komplementär zu mir als Informatikerin, hat mein Verständnis von Problemlösen grundlegend geändert und gereift.

Ebenso möchte ich Herrn Prof. Dr. Wolf-Dieter Schuh meinen Dank aussprechen. Durch seine Zusammenarbeit mit Frau Kunoth konnte diese geodätische Problemstellung überhaupt in einer mathematischen Dissertation bearbeitet werden. Er hat mich in die Welt der theoretischen Geodäsie eingeführt und mir dabei ein tieferes Verständis des Systems Erde gegeben. Diese Erfahrungen haben nicht nur meine Augen für die versteckte Geodäsie im Alltag geöffnet, sondern auch meinen Enthusiasmus für Interdisziplinarität gefördert.

Nicht nur für das gründliche Korrekturlesen, sondern auch für die vielen fachlichen und nicht fachlichen, anregenden und konstruktiven Gespräche und für das Dasein, wenn das Wetter schlecht war, möchte ich mich bei Roland Pabel bedanken. Mein Dank geht außerdem an meine Kollegen innerhalb der Arbeitsgruppe Komplexe Systeme und an die ehemaligen Kollegen am Institut für Numerische Simulation für die gute Arbeitsatmosphäre und die Kaffeerunden am Nachmittag.

Bei meinen Eltern bedanke ich mich für ihre Unterstützung und die Art, wie sie meine Einstellung zum Lernen, Arbeiten und nach vorne Blicken geprägt haben.

Meinem Mann danke ich für das Korrekturlesen und die kreative Mischung aus Motivation und Kritik.

Zuletzt möchte ich den Beitrag meines Sohnes Nils würdigen, der immer für eine schöne Abwechslung gesorgt hat.

Zusammenfassung

Diese Dissertation beschäftigt sich mit der mathematischen Modellierung des Erdschwerefelds und der numerischen Lösung der resultierenden partiellen Differentialgleichung. Die Rekonstruktion aus Messdaten stellt ein schlecht gestelltes Datenanpassungsproblem mit hunderttausenden von Parametern dar. Wir betrachten die Randwertaufgabe der Potentialtheorie, welche sich mit der analytischen Fortsetzung des äußeren Potentialfeldes der Erde beschäftigt und zu deren Anwendungen z.B. GPS- und Navigationssysteme zählen.

Diese Dissertation ist in Zusammenarbeit mit Prof. Dr. Wolf-Dieter Schuh vom Institut für Geodäsie und Geoinformation der Universität Bonn entstanden, der die Defizite der klassischen Darstellung des Potentialfeldes mittels harmonischer Kugelfunktionen erläutert und den großen rechnerischen Aufwand bei deren Anwendung bemängelt hat. Da harmonische Kugelfunktionen einen globalen Träger haben und die Menge der Daten umfangreich ist, entstehen große, voll besetzte Systemmatrizen. Diese machen Berechnungen sehr aufwendig. Zudem muss die Darstellung immer wieder neu bestimmt werden, wenn neue Daten verfügbar werden. Diese Darstellung erlaubt keine Berechnung auf beschränkten Gebieten, auch wenn die Daten inhomogen verteilt sind. Eine wichtige Inspiration für unsere Arbeit war [99], worin erste Finite-Elemente-Ansätze für dieses Problem untersucht wurden. Seitdem sind Multiskalen-basierte Methoden für PDEs entwickelt worden, die die Möglichkeit für adaptive und effiziente Darstellungen mit sich bringen. Die Anwendung adaptiver Verfahren für dieses geodätische Randwertproblem ist in der Literatur jedoch noch nicht zu finden, obwohl dies wegen der Inhomogenität der Daten unerlässlich ist.

Wir beschäftigen uns daher insbesondere mit der Multiskalenapproximation von gravimetrischen Daten zur globalen Erdschwerefeldbestimmung und mit Datenanpassungs- und Modellierungsproblemen auf der Erdoberfläche bzw. im Außenraum unter Beachtung der Harmonizität des Erdpotentials. Zunächst werden einige Grundlagen aus der Geodäsie, der Theorie der PDEs und deren Diskretisierung, Minimierungsprobleme und iterative Lösungsverfahren für Gleichungssysteme dargestellt. Dann werden Basisfunktionen entwickelt, die ein Optimum bezüglich der widersprüchlichen Forderungen nach Harmonizität und Lokalität bzw. Exaktheit und Anpassung an unregelmäßige Daten gewährleisten. Hier haben wir uns für eine hierarchische Konstruktion mittels Tensorprodukten von B-Splines und B-Spline-Wavelets entschieden.

Die Darstellung eines Potentialfeldes muss die Laplace-Gleichung mit Dirichlet-Randbedingungen erfüllen. In der geodätischen Aufgabenstellung geht die Eindeutigkeit der Lösung verloren, da die Randbedingungen nur diskret und über Teilen des Randgebietes gegeben sind. Um trotzdem eine Lösung zu finden, verwenden wir einen Data-Fitting-Ansatz über den Randgebieten und erzwingen die Harmonizität durch eine Regularisierung auf dem Gebiet der Fortsetzung. Für die adaptive, iterative Version dieser Methode werden unter Berücksichtigung der Erfahrungen mit Multiskalen-Techniken für Datenanpassungsprobleme aus [17,18] die Wavelet-basierten adaptiven Methoden für PDEs [22,30] erweitert. Wir untersuchen die Bestimmung des Gewichtparameters für die Regularisierung und die Verwendung unterschiedlich angepasster Basen. Im Zusammenhang mit der Adaptivität beschäftigt sich die Arbeit mit zusätzlichen Faktoren, wie z.B. dem Thresholding und den Abbruchkriterien. Diese unterscheiden sich von denen, die in Ansätzen für reine Datenanpassungsprobleme oder partielle Differentialgleichungen eingesetzt werden.

Abstract

The reconstruction of the earth's potential field from geometric and gravimetric data is an ill-posed data fitting problem with tens of thousands of parameters. One employs its essential property stating that the potential field is harmonic, i.e., it fulfills the Laplace equation. In practice, the representation and determination of the gravity field includes the continuation of gravity measurements together with the treatment of noise and outliers. The upward continuation problem statement leads to the solution of the exterior Dirichlet boundary value problem for the Laplace equation with respect to given continuous values at the borders of the domain. Difficulties when solving the boundary problem in geodesy occur due to incomplete boundary conditions which affect the uniqueness of the solution. In addition, high accuracy requirements have to be fulfilled. The exterior boundary value problem is then essentially ill posed and we depend on employing representations in terms of harmonic basis functions or some regularization technique.

This work resulted from the collaboration with Prof. Dr. Wolf-Dieter Schuh from the Institute for Geodesy and Geoinformation of the University of Bonn, who explained about the bottleneck in the classical representation of potential fields. This representation of fields in terms of spherical harmonics allows a harmonic extension of the data without an explicit treatment of the ill–posedness. Since spherical harmonics are globally supported basis functions and due to millions of available data points, their employment entails large, fully populated system matrices. Considering the very large amount of data, this approach is computationally very expensive. Furthermore, it is confined to spherical domains.

The main inspiration of this thesis is [99], where finite element methods to this fundamental problem of geodesy were considered. We have witnessed since end of 70s the development of more and more ingredients generalizing finite elements, in particular for the fast numerical solution of partial differential equations by means of multiscale approaches. Their substantial advantage resides in the potential for adaptivity.

Here, we investigate formulations based on regularized least-squares functionals and localized representations based on multiscale finite elements and wavelets. Instead of solving the exterior Dirichlet problem, we consider the Laplace equation on a bounded domain. We construct continuations of potential fields using only local information by a data fitting ansatz with respect to the boundary conditions corroborated with a simultaneous regularization enforcing the harmonicity over the interior of the domain. We employ generalized multiscale finite element and wavelet approaches to higher orders. We consider for computations tensor products of cubic B-splines and B-spline wavelets. For the adaptive version of our method we employ a representation in terms of a hierarchical B-splines construction. The approach works with an iterative, coarse-to-fine strategy. The attention goes to differently designed refinements in order to better comply with the regularization and with issues related to the ill–posed nature of the problem. It includes the determination of the weight parameter for the regularization. Due to the adaptivity, we also investigate additional parameters of the algorithm, like thresholding parameters and stopping criteria, which differ from the ones considered within a plain data fitting or plain partial differential equation ansatz.

Contents

Chapter 1

Introduction

har·mon·ic
– adjective

1. pertaining to harmony, as distinguished from melody and rhythm.
2. marked by harmony; in harmony; concordant; consonant.
3. *Physics.* a single oscillation whose frequency is an integral multiple of the fundamental frequency.
4. *Mathematics.*
   a. (of a set of values) related in a manner analogous to the frequencies of tones that are consonant.
   b. capable of being represented by sine and cosine functions.
   c. (of a function) satisfying the Laplace equation.

– noun

5. *Music.* overtone.

Dictionary.com Unabridged [75]

1.1 Motivation

Remember the proverbial apple. Newton, sitting under a tree more than 300 years ago, meditated about the basic principles and concepts of gravitation. Gravity is a complex force of nature with a deep impact for all of us. It holds us literally with the feet on the ground. It is often assumed that gravity on the surface of the earth has a constant value, but in fact it changes subtly. Mostly, we say that the force of gravity on the surface of the earth is a constant $g \simeq 9.81 ms^{-2}$, yet it is the subject of variation from place to place and time. The idealized value of $9.81 ms^{-2}$ refers to the earth as a homogeneous sphere. In reality, there are lots of factors causing variations to this not–so–constant value. Some of them are: the rotation of the earth, mountains, ocean tides and the less visible deviations in density of the earth's interior. These effects of gravity variations, or anomalies, have a

deep impact in hydrology, oceanography, glaciology and geophysics and provide important information for understanding the *System Earth*. Such deviations in gravity help to describe e.g. ocean flows, whose investigation is essential for hydrology and climate studies. Besides that, the analysis of gravity anomalies or deviations help us to understand better the variations in the upper layers of the earth and the geodynamics associated with the lithosphere. Further, the study of gravity is fundamental for all applications involving satellites, global height-reference systems and positioning.

The accurate modeling of all these anomalies requires large series of measurements of the gravitational potential field [12]. Current and planned satellite missions (CHAMP [68], GRACE [108], GOCE [40]) are designed to determine the structure of the earth's gravity field with very high precision. For example, the objective of the gravity mission GOCE is to determine gravity-field anomalies with an accuracy of 1 mGal, to determine the geoid, a reference equipotential surface of the gravity field, with an accuracy of 1-2 cm and to achieve the above at a spatial resolution better than 100 km.

The reconstruction of the earth's potential field from geometric and gravimetric data is an ill-posed data fitting problem with tens of thousands of parameters. One employs its essential property stating that the potential field is harmonic, i.e., it fulfills the Laplace equation. In practice, the representation and determination of the gravity field includes the continuation of gravity measurements together with the treatment of noise and outliers, see e.g. [10, 127, 131]. This is an important application and allows the transformation of gravimetric data from and to different height levels, i.e., the downward or upward continuation of a (two-dimensional) field to a level surface everywhere below or above the observation locations. As a simple example, the use of ground gravity data in well surveyed areas, continued upward to satellite altitude, is a calibration and validation method for satellite gravity gradient observations. These include not only topographic measurements. The navigation system alone, that we all take for granted in our everyday life, is based on the Global Positioning System (GPS), and relies on well calibrated satellites.

We deal in this work with the upward continuation of the potential field. By the continuation of a function one generally understands some enlargement of its definition range and the determination of the appropriate values the function would take over the domain augmentation. This action mostly takes place by interpolation or extrapolation. In order to construct the continuation, one requires the available function values together with some kind of information on the data, which is more or less determinative for the solution. The continuation of harmonic functions designates therefore the extension by means of a function which is harmonic itself.

By definition, harmonic functions are n-dimensional, real valued, twice continuously differentiable functions which satisfy the Laplace equation, i.e., the sum of their second derivate is null:

$$u : I\!R^n \to I\!R, \quad \Delta u(x) := \sum_{i=1}^{n} \frac{\partial^2 u}{\partial x_i^2} = 0, \; x = (x_1, \ldots, x_n). \tag{1.1}$$

So the upward continuation problem statement leads to the solution of the exterior Dirichlet boundary value problem for the Laplace equation with respect to the given continuous values at the borders of the domain. This can be formulated as follows: let

$\Omega_{\text{ext}} \subset I\!R^3$ be the space *outside* of a bounded simply connected domain. Let f be a continuous function defined over the boundary $\partial\Omega_{\text{ext}}$. We want to determine the function $u : \mathcal{C}^2(\Omega_{\text{ext}}) \cap \mathcal{C}^0(\partial\Omega_{\text{ext}}) \rightarrow I\!R$ which is harmonic over Ω_{ext} and which takes the given boundary value f at $\partial\Omega_{\text{ext}}$:

$$\left\{ \begin{array}{rcl} \Delta u = & 0 & \text{on } \Omega_{\text{ext}}, \\ u = & f & \text{on } \partial\Omega_{\text{ext}}. \end{array} \right. \tag{1.2}$$

This problem has many solutions when no restrictions are imposed at distant points of space. We can assure the uniqueness of the solution if we require the solution to be bounded, or even stronger, if we require it to go to zero. This means, that no other masses are contained in the domain so the field does indeed attenuate. The solution of the exterior Dirichlet problem (1.2) has a solution for every continuous function prescribed on its boundary, see [48, 82, 126] for the analytical, integral representation of the solution. Accordingly, for $\partial\Omega_{\text{ext}}$ a sphere in $I\!R^3$ with radius R and for any $f \in L_2(\partial\Omega_{\text{ext}})$ there exists one and only one harmonic continuation u of f over the infinite space Ω_{ext} with u regular at infinity:

$$u(x) = \frac{1}{4\pi R} \int_{\partial\Omega_{\text{ext}}} \frac{|x|^2 - R^2}{|x-y|^3} f(y) dw_R \tag{1.3}$$

with w_R the surface element on the sphere of radius R. Handling such a theoretical formulation in geodetic application is simply idealistic, since it cannot be evaluated. Also, the information of the earth's gravity field as derived from the available observing and measuring techniques is incomplete. In this geodetic setup, the data is available only discrete, badly scattered and at various heights over the surface of the earth. Difficulties when solving the boundary problem occur due to incomplete boundary conditions, which affect the uniqueness of the solution, and high accuracy requirements.

The concept of a well-posed problem goes back to [61], who took the point of view that every mathematical problem which corresponds to some physical or technological problem must be well-posed. Accordingly, for a well–posed problem a solution should exist which is uniquely determined and the problem should be stable. By stable one understands, that an arbitrary small change in the data does not lead to large changes in the solution. The Laplace equation per se is not problematic. But in our case, the unicity of the solution is not granted due to incomplete boundary conditions. The exterior boundary value problem is then essentially ill posed and we depend on employing representations in terms of harmonic basis functions or some regularization technique.

Usually the continuation of harmonic functions and potential data is based on *interpolating* the data in terms of Ansatz functions like the spherical harmonics, see e.g. [47, 48]. Spherical harmonics are harmonic basis functions defined on the sphere. Developed within extensive and elaborated long standing mathematical theory, they are constructed by considering the separable solution of the Laplace equation. This standard choice representation of potential fields makes a mathematical tool widespread among various disciplines. Spherical harmonics are perfectly suited to generate three dimensional functions from two dimensional data. They allow a harmonic extension of the data without an explicit treatment of the ill–posedness, as any linear combination of spherical harmonics is also a harmonic function. They further allow arbitrary high accuracy up to the accuracy provided by the data. Of course, in dependency on the type and resolution of the available data,

there is no guarantee that the obtained solution is indeed also a good one [114]. There are still some substantial drawbacks. Since spherical harmonics are globally supported basis functions and due to millions of available data points, their employment entails large, fully populated system matrices. This type of application would block computer clusters for ages making their employment hardly affordable as one data set would cost two weeks on a cluster. Within an iterative process, each entry of the system matrix had to be recomputed. Yet the system matrix would not fit in the available storage, which significantly slows down computations. Further, also due to the global support, the complete coefficient set of the representation based on spherical harmonics must be recomputed, even when only some local information is added to the model. More computational power will not ease the burden substantially and accuracy demands are always rising. A new approach is necessary and local models in terms of locally supported basis functions hold the key.

Such modern approaches have been provided e.g. by [39]. There, a global gravity field represented by a spherical harmonic expansion up to a moderate degree has to be derived at first. It is then refined by regionally adapted high resolution refinements being parameterized by splines as space localizing base functions. Their basis functions are isotropic and homogeneous harmonic spline functions [48] on a grid generated by a uniform subdivision. Their work is therefore restrained to the sphere, depending on a spherical harmonic expansion and is not adaptive in a constructive way. We point to [48] for another broad and insightful work on multiscale approaches in potential theory. This includes e.g. the harmonic wavelet methods, see also [81, 100] for more on wavelets in geodesy. What we are still missing are robust adaptive techniques for handling such large scattered data sets in an ill–posed context.

The idea for this interdisciplinary thesis arose from discussions between Prof. Dr. Angela Kunoth, my advisor engaged in the numerical analysis of partial differential equations and approximation theory, and Prof. Dr. Wolf-Dieter Schuh from the Institute of Geodesy and Geoinformation, University of Bonn, working on theoretical geodetic issues like gravity field modeling and satellite data analysis. Following a scientific event, Prof. Schuh told Prof. Kunoth about the unavoidable numerical burden in geodetic applications, like the continuation of gravity potential data. Since the gravity field is harmonic outside the earth's surface, its continuation implies the construction of an appropriate harmonic extension. He explained about the bottleneck in the classical representation of potential fields in terms of spherical harmonics. Prof. Dr. Wolf-Dieter Schuh also mentioned the work of his PhD advisor, P. Meissl in *The use of finite elements in physical geodesy* [99], who investigated the feasibility of applying the finite element method to this fundamental problem of geodesy. Distinctively, [99] also used a finite number of elements extending to infinity decaying in radial direction to partition the infinite space. The upward continuation is obtained by

$$\int_{\Omega_{\text{ext}}} (\Delta u)^2 d\Omega_{\text{ext}} \to \min, \quad u = f \text{ at } \partial\Omega_{\text{ext}}, \tag{1.4}$$

where Ω_{ext} is the outer space of the sphere, $\partial\Omega_{\text{ext}}$ is its surface and f are the observed values at the surface. To our knowledge, his work has not yet been further pursued, but the author argued for the use of locally based representations of the gravitational field and of the infinite space.

The resulting collaboration was in search for a proper representation of the potential field, which should be determined from a heap of unhomogenous, incomplete and eventually erroneous data. This representation should deal with the intrinsic ill–posed nature of the problem and with difficult data fitting aspects. Further, it should meet the requirements in terms of complex data availability issues, high accuracy demands and computational costs. By intrinsically solving the Laplace equation, the representation should secondly take into account the harmonicity of the task function, the potential field. This work is therefore concerned with this important issue arising in geophysics and geodesy: the approximate continuation of harmonic functions.

On the mathematical side, we have witnessed since then the development of more and more ingredients generalizing the Finite Elements end of 70s, in particular for the fast numerical solution of partial differential equations by means of multiscale approaches. We mention preconditioning involving the hierarchical finite element basis [151], multigrid methods [31] and wavelets [29, 33]. These constructions have been mainly developed in terms of linear basis functions, e.g., splines. Their substantial advantage resides in the potential for adaptivity, that is employing an increasing number of degrees of freedom only where necessary.

The key of our approach lies in fully understanding the potential and the underlying boundary value problem, together with the reasonably handling of the physical interpretation within the mathematical formulation. The basic idea is to extent the approach by Meissl [99] to modern tools from data fitting and numerical solution for partial differential equations. Here, we investigate alternative problem formulations based on regularized least-squares functionals and localized representations based on multiscale finite elements and wavelets. We extend and adapt some of the coarse–to–fine data fitting with regularization techniques of [16, 17] based on (tensor products of) linear spline wavelets to the geodetical problem. We attempt to construct continuations of potential fields on bounded domains using only local information, specifically incomplete boundary conditions. The outcome is a weighted least squares approach to the approximate continuation of harmonic functions based on tensor products of B-splines. The continuation is constructed by a three dimensional data fitting ansatz with regard to the boundary conditions corroborated with a simultaneous regularization enforcing the harmonicity over the interior of the domain. We choose to employ generalized multiscale finite element and wavelet approaches to higher orders in order to discretize the regularization term. For computations we consider tensor products of cubic B-splines and B-spline wavelets.

We take a not necessarily cuboid domain Ω. It is considered tangent to a mass or source of the field. The domain spans the space up to the desired upward continuation target and contains the available data points. They are situated mainly but not necessarily at the bottom, that is, near the mass, and eventually on the top side, and make up the given boundary conditions, see Figure 1.1. Alternatively, the mass can intersect the domain. The potential is not harmonic within a mass. The continuation computed there is simply meaningless. By this we do not have to treat intricated geometries in order to describe the surface. Although we handle the upward continuation, we consider the potential at satellite height to be given, since this smooth data is well known. Furthermore, we consider the representation of a multivariate function in terms of locally supported basis functions

$\Psi := \{\psi_\lambda : \lambda \in \Lambda\}$ with Λ a set of indices for the basis Ψ, e.g. uniform tensor products of cubic B-splines. An approximate continuation of a harmonic function would then be constructed by determining the expansion coefficients $\mathbf{d} = (d_\lambda)_{\lambda\in\Lambda}$ of the representation

$$u(x) := \sum_{\lambda\in\Lambda} d_\lambda \psi_\lambda(x) \,, \quad x \in \Omega, \tag{1.5}$$

such that the error on the boundary and the Laplacian of the continuation over the entire domain are simultaneously minimized

$$J_\eta(u_\eta) := \sum_{i=1}^{M} (u_\eta(x_i) - z_i)^2 + \eta \int_\Omega |\Delta u_\eta(x)|^2 \, dx. \tag{1.6}$$

By that we combine a data fitting ansatz with a weighted regularization term and solve the resulting normal equation system directly or iteratively to obtain the coefficients. Instead of solving the exterior Dirichlet problem, we consider the Laplace equation on a bounded domain. The problem still remains ill–posed. The theory states again that unicity of the solution requires boundary data available on entire $\partial\Omega$. But it is in fact given on just one or two sides of the cuboid instead of six and therefore incomplete. The determined representation can afterwards be evaluated everywhere and the boundary data has been continued upwards. The regularization term actually determines the basis functions whose support does not contain data points, so the choice of a proper weight parameter is essential for the results. At this point we discuss some estimators for the weight parameter adjusted to both available data and considered basis.

Figure 1.1. *Set up diagram: cuboid tangent to a sphere outside of it.*

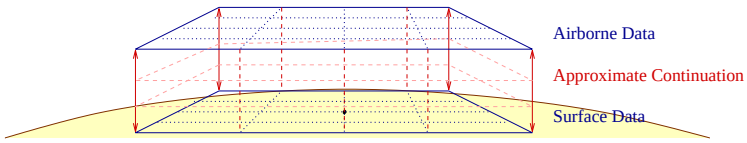

Later, we construct an adaptive version of our method. For that, we consider the concepts of the wavelet-based adaptive methods for partial differential equations as in [22, 29, 30]. The degrees of freedom should accumulate where more information needs to be represented. For this, we employ a representation in terms of a hierarchical B-splines construction or wavelet decompositions of finite element spaces. The approach works with an iterative, coarse-to-fine strategy based on anisotropic, isotropic or sparse bases [14]. In our work the attention goes to differently designed refinements to better comply with the regularization and with issues related to the ill–posed nature of the problem. It includes the determination of the weight parameter η. Due to the adaptivity, we also investigate the additional parameters of the algorithm, like thresholding parameters and stopping criteria, which differ from the ones considered within a plain data fitting or plain partial differential equation ansatz.

This work does intentionally not include a detailed discussion on the costs of the method. The established approaches to the modeling of the potential field and to the upward continuation of harmonic function are based on spherical harmonics. This is a computationally costly and global model where all coefficients are computed at once. Our method on the other hand is designed to handle local data and makes adaptive or parallel computations on bounded domains accessible. Further, it consists of an adaptive, iterative coarse–to–fine algorithm which can be terminated when the desired accuracy has been reached. These approaches can therefore by nature not be properly and plausibly compared by relationing running times or memory requirements. But we do investigate the spectral condition numbers of the resulted matrices and the number of iterations required to solve the systems, which is indeed relevant and decisive, independent from implementation or machine. The programs have been implemented in MATLAB version 7.9.0.529 (R2009B, The MathWorks [98]).

1.2 Structure of the Work

The work proceeds within the introduction in Chapter 2 *Harmonic Functions* with a look at some of their properties and surrounding theoretical issues. We see in particular their occurrence in natural sciences. Moreover, we present the representative of this function class per se, namely the spherical harmonic functions, and specify their numerical handling in the approximation theory.

The following Chapter 3 *The Earth's Gravitational Field* describes the geodetical background of our problem statement. We first give an insight of the main theoretical statements and the fundamental relationships on potential fields. The most important properties of the earth's gravitational field are presented and classical representation methods via spherical harmonic are introduced. We also study why for example the gravitational field is harmonic or about the non–uniqueness issues arising in geodetic boundary problems. These incidentally lead to the fact that the local continuation of the gravity field is an ill-posed one.

We are then ready to present in Chapter 4 *New Approach: Least-Squares with Regularization* our new approach in terms of regularized data fitting by means of weighted least squares. We discuss the general setup, the employed tools and their theoretical background. This will be accompanied by a presentation and discussion of the concrete choices in terms of approximation spaces, namely the tensor product B-spline spaces, we made in order to conduct experiments and some alternative formulations for comparison purposes.

The short chapter on the *Two Dimensional Illustration of the Method* is meant to give the reader an intuitive view over the procedure. We shortly analyze its behavior and dependencies on input factors, e.g., the structure of the domain and available datasets or the less intuitive aspect, the weight parameter for regularization term. This will point to the aspects to be investigated for the less straightforward, three dimensional case.

The following chapter 6 *Numerical Results* then displays a series of experiments investigating the feasibility of our approach for the continuation problem of harmonic functions. The tests deal with bounded domains and uniformly refined sets of basis functions. We answer here the question of how one can choose the essential weight parameter when deal-

ing with such a numerically instable process. Tests are undertaken with several differently constructed test datasets. Further, we discuss the effect of iterative system solvers over the results of the method.

As a significant maturation of the proposed setup, the work included in Chapter 7 *Adaptivity: Experiments with the Hierarchical Cubic B-Splines Basis* a discussion of an adaptive version of the method. We hereby try to meet the high exactness requirements without wasting degrees of freedom and to refine only where necessary. Several aspects resulting from data-fitting issues in a refinable setup, like hierarchical bases and stopping criteria will be treated. Their interaction with the regularization term enforcing the harmonicity will be investigated.

In the last chapter, *Conclusions*, the results will be finally summarized and discussed.

Chapter 2

Harmonic Functions

Potential theory is the mathematics of equilibrium.

Brownian Motion and Potential Theory [69]

2.1 Preliminaries

The term *harmony* originates from the Greek and is commonly used to describe the quality of sound. The harmonic functions, which are essential within this work, inherited their name through a parallel to physics. There, the movement of a point on a vibrating string is called a harmonic motion. Essential is that this motion can be described by means of the sine and cosine functions, which are sometimes called harmonics. In classical Fourier analysis, functions on the unit circle are expanded in terms of sines and cosines. For the n-dimensional sphere, such expansions take place in terms of harmonic polynomials, which are then also called spherical harmonics. Later, the word harmonic was used not only to describe homogeneous polynomials, but denoted any function that is a solution of the Laplace equation.

The first encounter of the harmonic functions seems to go back to the 18th century. The Laplace equation occurs in papers of L. Euler [41] and J. d'Alembert [32] from 1761, in connection with problems of hydromechanics and the first studies of functions of a complex variable. But the break-through came with the appearance of the papers of P.S. Laplace [89,90] where he discloses his investigations on the theory of the gravitational potential and celestial mechanics. Yet, Jacobi in the 2nd and 26th, together with Dirichlet in the 17th band of Crelle's journal refers to Legendre as that person, who introduced the spherical harmonics. They are the angular portion of the solution to Laplace's equation in spherical coordinates. Legendre thereby triggered Laplace's investigations on these functions [66]. Further, Legendre's major work on elliptic integrals provided basic analytical tools for mathematical physics. Harmonic functions play now an essential role in potential theory.

2.2 Some Basic Notation

These introductory concepts on harmonic functions, Laplace equation and potential theory can be found e.g. [4, 5, 42, 82, 120]. See Appendix B for all notation used. Generally,

Definition 2.2.1 (Domain). *$\Omega \subset \mathbb{R}^n$ is called a domain if it is an open set and connected. We say a domain Ω is connected if, for all two points $x, y \in \Omega$ we have a continuous curve $C \subset \Omega$ connecting x and y. Further, $\partial\Omega$ is the boundary of Ω and $\bar{\Omega} = \Omega \cup \partial\Omega$.*

Definition 2.2.2 (Harmonic function). *A harmonic function is a real-valued, twice continuously differentiable function $u : \Omega \to \mathbb{R}$ with $u \in \mathcal{C}^2(\Omega) \cap \mathcal{C}^0(\partial\Omega)$, $\Omega \subset \mathbb{R}^n$ an open subset, which satisfies Laplace's equation in n dimensions, i.e.,*

$$\frac{\partial^2 u}{\partial x_1^2} + \frac{\partial^2 u}{\partial x_2^2} + \cdots + \frac{\partial^2 u}{\partial x_n^2} = 0 \tag{2.1}$$

everywhere on Ω.

This can be abbreviated as

$$\nabla^2 u = 0 \quad \text{or} \quad \Delta u = 0. \tag{2.2}$$

This equation arises in several physical applications, such as potential fields in gravitation and electro-statics or velocity potential fields in fluid dynamics. The most important properties of harmonic functions can be deduced from Laplace's equation.

Proposition 2.2.3 (Regularity theorem for harmonic functions). *Harmonic functions are infinitely differentiable. Further, harmonic functions are real analytic.*

If u is a harmonic function on Ω, then all partial derivatives of u are also harmonic functions on Ω. The Laplace operator Δ and the partial derivative operator will commute on this class of functions.

Proposition 2.2.4 (Maximum principle). *If the domain Ω is connected, then a harmonic function u attains its maximum and minimum on the boundary of Ω. If local maxima or minima are attained in the interior of Ω, u is constant.*

The following property illustrates the relationship between harmonic functions and spheres, which is vital for the study of harmonic function theory.

Proposition 2.2.5 (Mean value property). *If $B(x, r)$ is a ball with center x and radius r which is completely contained in the domain Ω, then the value $u(x)$ of the harmonic function u at the center of the ball is given by the average value of u on the surface of the ball; this average value is also equal to the average value of u in the interior of the ball. This means,*

$$u(x) = \frac{1}{\omega_n r^{n-1}} \int_{\partial B(x,r)} u \, dS = \frac{n}{\omega_n r^n} \int_{B(x,r)} u \, dV \tag{2.3}$$

where ω_n is the surface area of the unit n–dimensional sphere.

The uniform limit of a convergent sequence of harmonic functions is still harmonic. This is true because any continuous function satisfying the mean value property is harmonic.

Theorem 2.2.6 (Liouville's theorem). *If u is a bounded harmonic function defined on all of $\mathbb{R}^n$, then u is constant.*

The following three boundary value problems for the Laplace equation are encountered in potential theory.

Definition 2.2.7 (Dirichlet problem for the Laplace equation). *Find a solution $u = u(x, y, z),\ u \in \mathcal{C}^2(\Omega) \cap \mathcal{C}^0(\partial\Omega)$ on a domain $\Omega \subset \mathbb{R}^3$ with respect to the given data at the boundary $\partial\Omega$:*

$$\begin{cases} \Delta u(x,y,z) = & 0 & \text{in } \Omega, \\ u = & f & \text{on } \partial\Omega. \end{cases} \tag{2.4}$$

The Dirichlet problem for the Laplace equation is also known as the *first boundary problem of potential theory.*

Definition 2.2.8 (Neumann problem for the Laplace equation). *Find a solution $u = u(x, y, z),\ u \in \mathcal{C}^2(\Omega) \cap \mathcal{C}^0(\partial\Omega)$ on a domain $\Omega \subset \mathbb{R}^3$ with respect to the given at the boundary $\partial\Omega$:*

$$\begin{cases} \Delta u(x,y,z) = & 0 & \text{in } \Omega, \\ \frac{\partial u}{\partial \mathbf{n}} = & g & \text{on } \partial\Omega \end{cases} \tag{2.5}$$

where $\mathbf{n}$ denotes the (typically exterior) normal to the boundary $\partial\Omega$ and $\frac{\partial u}{\partial \mathbf{n}}$ the normal derivative.

Definition 2.2.9 (Mixed problem for the Laplace equation). *Find a solution $u = u(x, y, z),\ u \in \mathcal{C}^2(\Omega) \cap \mathcal{C}^0(\partial\Omega)$ on a domain $\Omega \subset \mathbb{R}^3$ with respect to the given at the boundary $\partial\Omega = \Gamma_1 \cup \Gamma_2$:*

$$\begin{cases} \Delta u(x,y,z) = & 0 & \text{in } \Omega, \\ u = & f & \text{on } \Gamma_1 \\ \frac{\partial u}{\partial \mathbf{n}} = & g & \text{on } \Gamma_2. \end{cases} \tag{2.6}$$

We deal in our work with the Dirichlet problem for the Laplace equation. In general, a boundary value problem should be well–posed. This means: a solution exists, is unique and depends continuously on the input data, in our case on boundary data and the boundary topology. Using the Maximum principle, one can prove the existence and the uniqueness of the solution for the Dirichlet boundary problem for the Laplace equation: If $f \in \mathcal{C}^0(\partial\Omega)$, then the problem has at most one solution. The remaining question is if such a solution exist. One can indeed prove that if both the boundary $\partial\Omega$ and the function f taken at the boundary are smooth enough, then one can construct a harmonic function with respect

to the boundary conditions. The way to this result is intricated and starts with the case when the boundary is a ball. Literature discussing this issue includes [5, 82].

Unfortunately, we will later see that, the problem statement in the geodetical setup of this work deals with an ill–posed Dirichlet problem. This is a result of incomplete boundary conditions, i.e., the function f is not specified over the entire $\partial\Omega$. Hereby, the uniqueness of the solution gets lost. At this point, the construction of some solution is easy. The difficulty resides in constructing a physically meaningful one. We will do this by means of regularization.

2.3 Harmonic Functions in Natural Sciences

Harmonic functions are important in many areas of applied mathematics since they are the solution of the Laplace equation and thereby they describe the behavior of electric, gravitational, and fluid potentials. Harmonic functions are also known as potential functions in physics and engineering. Many functions satisfy this equation, e.g. the electrostatic potential, the velocity potential of irrotational flow in an incompressible fluid, the gravitational potential or the displacement of an elastic membrane.

Example 2.3.1. *Some common harmonic functions are*

- *functions which describe conditions of equilibrium such as the temperature or electrical charge distribution over a region in which the value at each point remains constant: the function* $u(x_1, x_2) = \ln(x_1^2 + x_2^2)$ *defined on the punctured space* $\mathbb{R}^2 \setminus \{0\}$ *describes the electric potential due to a line charge, and the gravity potential due to a long cylindrical mass;*

- $u(x) = |x|^{2-n}$ *with* $|x|$ *the euclidean norm of* $x = (x_1, ..., x_n)$*, defined also on the punctured space* $\mathbb{R}^n \setminus \{0\}$ *for space dimension* $n \geq 3$*, is an essential harmonic function; it represents the class of harmonic function which are also rotational invariant; for* $n = 3$ *we obtain a core function in potential theory,* $u = 1/\sqrt{x_1^2 + x_2^2 + x_3^2} = 1/r$ *with* r *the radius from the origin;*

- $u(x_1, x_2) = \exp(x_1)\sin(x_2)$ *on* $\mathbb{R}^2$*;*

- *the constant, linear and affine functions on all of* $\mathbb{R}^n$*; for example, the electric potential between the plates of a capacitor, and the gravity potential of a slab;*

- $u(x_1, x_2, x_3) = 8x_1^5 - 40x_1^3x_2^2 + 15x_1x_2^4 - 40x_1^3x_3^2 + 30x_1x_2^2x_3^2 + 15x_1x_3^4$ *on* $\mathbb{R}^3$ *is an homogeneous harmonic polynomial;*

- *since the Laplacian commutes with every partial derivate, further harmonic functions can be obtained by partial derivation.*

The potential theory overlaps with the study of harmonic functions as solution of the Laplace equation mostly when harmonic functions are described by their singularities. Singularities can have the form of a point, an eventually infinite line and represent here

Function	Singularity
$\frac{1}{r}$	Unit point charge at origin
$\frac{x_1}{r^3}$	x_1-directed dipole at origin
$-\ln(r^2 - x_3^2)$	Line of unit charge density on entire x_3-axis
$-\ln(r + x_3)$	Line of unit charge density on negative x_3-axis
$\frac{x_1}{r^2 - x_3^2}$	Line of x-directed dipoles on entire x_3 axis
$\frac{x_1}{r(r+x_2)}$	Line of x_1-directed dipoles on negative x_3 axis

Table 2.1. *Several harmonic functions that can be described by their singularities.*

the boundary conditions. For descriptive purposes we use this time the terminology of electrostatics. The singularities of the harmonic functions depicted in table 2.1 are associated with charge densities. Hence, these harmonic functions are proportional to the electrostatic potential due to the corresponding charge distribution. See Table 2.1 for some examples of charge distributions. There, $r := \sqrt{x_1^2 + x_2^2 + x_3^2}$ in Cartesian coordinates.

Take as a further example the gravitational potential energy of any point mass m in the gravitational field of a point mass M, given for GM the gravity-mass constant by

$$U = -\frac{GMm}{r}. \tag{2.7}$$

As this term is the multiplication of $f(x) = \frac{1}{r}$ by a constant, it is easy to see that the gravitational field is harmonic outside of the point mass. This also holds for an external point of a body having a spherically symmetric mass density with total mass M, where r is again the radius from the center of mass. In fact, the gravitational potential satisfies Laplace's equation in the region outside every mass. Evidently, a similar behavior exhibits the electric potential outside electric charges.

Regarding application in fluid dynamics, we can point to an exercise from [146] to find a simple model for the temperature in the eye, where the eye is a sphere, the eyelids are circular and the steady state temperature is described by Laplace's equation. Here the z-axis is taken straight through the middle of the eye, and we can assume that the temperature does only depend on r, θ and not on ϕ. One looks for the steady state temperature as it is described by Laplace's equation. The computation of the solution leads to another key equation of potential theory, namely the Legendre equation.

We should not forget the application of harmonic functions in elasticity or for minimal surfaces. The position and configuration of a stretched elastic membrane in a given space is determined by the height at each surface point of the membrane [69]. The function of the height of each point fulfills the Laplace equation. The study of functions describing such resulting surfaces belongs also to potential theory. Rather unexpectedly, this has applications in financial economics. In [116] the authors treat volatility surfaces as analogous to this elastic membrane at equilibrium stretched in three-dimensional space. The paper identifies an equilibrium relationship that exists between implied (option) volatility,

strike prices and expiration dates. In equilibrium the implied volatility of an option must be the average of the implied volatilities of nearby options under analysis. This calls for the mean value property of harmonic function.

Some less obvious but modern applications of the harmonic functions go to robotics and motion planning. They can be used via artificial potential fields to generate smooth, collision-free paths without the threat of spurious local minima. To argue this intuitively, remember that a harmonic function attains its minimum and maximum values only on the boundary and any critical points of the function in the interior must be saddle points. A robot could get stuck at a minimum, but when it reaches a saddle point there must be a way out practically by changing the direction of motion. One strategy could be for example to set obstacles to a constant high potential and regions at a low potential. The gradient of the resulted potential is aligned with the surface normals of the obstacles. If this function is used for path generation, it will tend to repel the robot away from obstacles. The gradient can be used to determine eventually the correct velocity. See [24, 25, 83] for more details.

Harmonic functions find via spherical harmonics employment for a variety of purposes in computer graphics. We can mention the theoretically founded approaches in the approximation, representation, reconstruction and retrieval of three dimensional objects, as for example in [123]. Intuitively, spherical harmonics are associated with star shaped objects, but one can find in the literature various normalization procedures to handle complex objects or sets.

Further, spherical harmonics are an established tool in lighting rendering that can effectively deliver real-time dynamic global illumination with highly realistic shading and shadowing at a very high performance. Generally, spherical harmonic lighting techniques involve replacing parts of standard lighting equations [77] with spherical functions that have been projected into frequency space using the spherical harmonics as a basis. It was introduced by [137] as a technique for ultra realistic lighting of models. One evaluates an approximation of the rendering equation at each vertex of the geometry of the scene by projecting its different components onto the spherical harmonic basis during a pre-process step. Later, the rendering equation can be reconstructed from the computed coefficients.

Another approach is the use of disk harmonic functions for adaptive optic simulation as an alternative to Zernike basis functions see [101]. The disk harmonic functions form a complete, orthonormal basis defined on the unit circle and are the set of eigenfunctions of the Laplacian. Atmospheric turbulences and deformable mirror corrections are represented in terms of these functions.

2.4 Spherical Harmonics

Though only indirectly related with the upward continuation approach of this thesis, a deep understanding of the spherical harmonics will help us give a better insight on the properties of the potential field. We had already mentioned that potential fields can be formulated in terms of spherical harmonics and expansion coefficients. For example, the attenuation of the anomalies with the hight can be or the amount of information carried by each spherical harmonic degree can be best described in this formulation. We also

employ linear combinations of spherical harmonics to generate test datasets.

However, spherical harmonics are important in many theoretical and practical applications. Some of the first complete works on spherical harmonics include [71, 139, 147]. Relevant for us is their employment in the representation and approximation of the gravitational field, geoid, and magnetic field of planetary bodies. They are also used in the computation of atomic electron configurations, e.g., the solutions to the time-independent Schrödinger equation for hydrogen-like atoms are based on spherical harmonics [57]. A modern application is their use in characterization of the cosmic microwave background radiation, a form of electromagnetic radiation filling the universe. Here, computing the power spectrum takes place by decomposing the map of the sky into spherical harmonics [134, 138]. We had already mentioned that spherical harmonics also serve different purposes in computer graphics, e.g. for recognition of three dimensional shapes or for the realization of lightening effects.

Spherical harmonics are usually defined either as a solution of the three dimensional Laplace equation or through the Fourier transformation on the sphere. We will first concentrate on the first approach; the link to Fourier analysis will be discussed in the following subsection. Recall from Definition 2.2.2, Laplace's equation is a linear second-order differential equation and the solution are twice-differentiable real-valued functions, $u = u(x, y, z)$ of real variables, from now on denoted as x, y, and z in Cartesian coordinates, such that

$$\frac{\partial^2 u}{\partial x^2} + \frac{\partial^2 u}{\partial y^2} + \frac{\partial^2 u}{\partial z^2} = 0 \quad \text{or} \quad \Delta u(x, y, z) = 0 \tag{2.8}$$

with Δ the Laplace operator. Further, the Dirichlet problem for Laplace's equation is to find a solution u on a domain Ω such that the solution u on the boundary of the domain $\partial\Omega$ is equal to a given function:

$$\begin{cases} \Delta u(x, y, z) = & 0 & \text{in } \Omega, \\ u = & g & \text{on } \partial\Omega. \end{cases} \tag{2.9}$$

For a deeper understanding, we can also write the Laplace equation in spherical coordinates. In order to keep coherent notation with geodetical and geophysical literature, we work here with the physical instead of the mathematical version of the spherical coordinates. This means, θ is the co-latitude or polar angle, ranging from $0 \leq \theta \leq \pi$ and ϕ, the azimuth or longitude, ranging from $0 \leq \phi < 2\pi$. The spherical coordinates (r, θ, ϕ) are then related to the Cartesian coordinates (x, y, z) by

$$\begin{cases} r = \sqrt{x^2 + y^2 + z^2} & r \in [0, \infty), \\ \theta = \arccos(z/r) & \theta \in [0, \pi], \\ \phi = \arctan(y/x) & \phi \in [0, 2\pi), \end{cases} \quad , \quad \begin{cases} x = r\sin(\theta)\cos(\phi) & x \in I\!R, \\ y = r\sin(\theta)\sin(\phi) & y \in I\!R, \\ z = r\cos(\theta) & z \in I\!R. \end{cases} \tag{2.10}$$

We can now write the Laplace operator in spherical coordinates:

$$\Delta = \frac{1}{r^2}\frac{\partial}{\partial r}\left(r^2\frac{\partial}{\partial r}\right) + \frac{1}{r^2\sin(\theta)}\frac{\partial}{\partial\theta}\left(\sin(\theta)\frac{\partial}{\partial\theta}\right) + \frac{1}{r^2\sin^2(\theta)}\frac{\partial^2}{\partial\phi^2}. \tag{2.11}$$

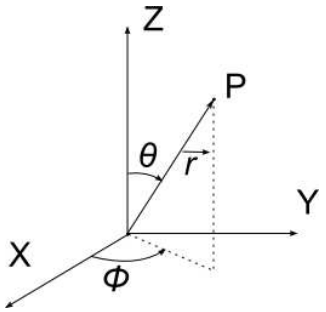

Figure 2.1. *Spherical coordinates of a point* $P(r, \phi, \theta)$.

From this point we deal with the explicit derivation and construction of spherical harmonics. Now we assume that $u(r, \theta, \phi) = R(r)\Gamma(\theta, \phi)$, and separate the radial and angular variables. When the solution of the Laplace equation u can be indeed written as the product of a function of r, $R(r)$, and a function of the angles θ and ϕ, namely $\Gamma(\theta, \phi)$, the function Γ is called a spherical harmonic. We assume the existence of a variable separable solution of the form $u(r, \theta, \phi) = R(r)\Theta(\theta)\Phi(\phi)$. We insert $u(r, \theta, \phi)$ in the Laplace equation based upon the spherical coordinates version of the operator (2.11) and obtain

$$\Delta R(r)\Theta(\theta)\Phi(\phi) = \frac{\Theta\Phi}{r^2}\frac{d}{dr}\left(r^2\frac{dR}{dr}\right) + \frac{R\Phi}{r^2\sin(\theta)}\frac{d}{d\theta}\left(\sin(\theta)\frac{d\Theta}{d\theta}\right) + \frac{R\Theta}{r^2\sin^2(\theta)}\frac{d^2\Phi}{d\phi^2} \;=\; 0. \tag{2.12}$$

The detailed calculation of the separation of variables can be found in Appendix A. We provide here directly the solution parts. The azimuthal separation, i.e. the part depending on regarding ϕ, deals with the ordinary differential Sturm-Liouville equation

$$\frac{d^2\Phi}{d\phi^2} = -m^2\Phi, \tag{2.13}$$

and yields due to the Single-valuedness Principle

$$\Phi_m(\phi) = e^{im\phi}, \quad m = \ldots, -3, -2, -1, 0, 1, 2, 3, \ldots. \tag{2.14}$$

Further, the polar angle separation, i.e. of θ, leads to the associated Legendre differential equation

$$(1 - x^2)\frac{d^2\Theta}{dx^2} - 2x\frac{d\Theta}{dx} + \Theta\left(\ell(\ell + 1) - \frac{m^2}{1 - x^2}\right) \;=\; 0, \tag{2.15}$$

whose canonical solution are the associated Legendre functions $\Theta(\theta) = P_\ell^m(x)$ with $x = \cos(\theta)$

$$P_\ell^{(m)}(\cos\theta) = (-1)^m(\sin\theta)^m \;\frac{d^m}{d(\cos\theta)^m}\left(P_\ell(\cos\theta)\right). \tag{2.16}$$

The radial separation deals with the radius dependent parts in equation (A.6) and yields a sum of the two possible powers

$$R(r) \;=\; ar^\ell + br^{-(\ell+1)}. \tag{2.17}$$

We can now finally assemble the separable solution of the form $u(r,\theta,\phi) = R(r)\Theta(\theta)\Phi(\phi)$ of the Laplace equation in spherical coordinates as product of the azimuthal, polar and radial terms described in (A.5, A.14, A.28):

$$u(r,\theta,\phi) \;=\; \sum_{l=0}^{\infty}\sum_{m=-\ell}^{\ell}\Big(a_{\ell m}r^{\ell} + b_{\ell m}r^{\ell+1}\Big)\,P_{\ell}^{m}(\cos\theta)e^{im\phi} \tag{2.18}$$

or in terms of the here to be described spherical harmonics

$$u(r,\theta,\phi) \;=\; \sum_{l=0}^{\infty}\sum_{m=-\ell}^{\ell}\Big(a_{\ell m}r^{\ell} + b_{\ell m}r^{\ell+1}\Big)\,Y_{\ell}^{m}(\theta,\phi) \tag{2.19}$$

whereas:

Definition 2.4.1 (Spherical harmonics). *The spherical harmonic of degree m and order ℓ is [71, 147]*

$$Y_{\ell}^{m}(\theta,\phi) \;=\; P_{\ell}^{m}(\cos(\theta))e^{im\phi} \;=\; P_{\ell}^{m}(\cos(\theta))(\cos(m\phi) + i\sin(m\phi)). \tag{2.20}$$

Please notice for clarity, the meaning of degree ℓ and order m for spherical harmonic $Y_{\ell}^{m}(\theta,\phi)$ or for an associated Legendre function $P_{\ell}^{m}(\theta)$ differs the common meaning of degree and order as in the case of classic polynomials; there we say, a polynomial of degree n has order $k = n+1$.

Before discussing orthogonality issues for spherical harmonics, please recall the orthogonality identities for the generalized Legendre polynomials (A.16 - A.17) and that the functions

$$\sin(nx),\; n = 1,2,\ldots \quad \text{and} \quad \cos(nx),\; n = 1,2,\ldots \tag{2.21}$$

form an orthogonal set for the interval $x \in [0, 2\pi]$, i.e.,

$$\int_0^{2\pi} \sin(nx)\sin(mx)dx = 0, \quad m \neq n \tag{2.22}$$

$$\int_0^{2\pi} \cos(nx)\cos(mx)dx = 0, \quad m \neq n \tag{2.23}$$

$$\int_0^{2\pi} \sin(nx)\cos(mx)dx = 0. \tag{2.24}$$

Several different normalizations are in common use for the spherical harmonic functions. The disciplines of geodesy and spectral analysis use the fully normalized version. We will work therefore with the following definition:

$$Y_{\ell}^{m}(\theta,\phi) = \sqrt{(2\ell+1)\frac{(\ell-m)!}{(\ell+m)!}}\,P_{\ell}^{m}(\cos\theta)\,e^{im\phi} \tag{2.25}$$

with

$$\frac{1}{4\pi}\int_{\theta=0}^{\pi}\int_{\phi=0}^{2\pi} Y_{\ell}^{m}\,Y_{\ell'}^{m'}\,d\Omega = \delta_{\ell\ell'}\,\delta_{mm'}. \tag{2.26}$$

Most real applications regard still the spherical harmonics as the real part of Y_ℓ^m. In their original definition, spherical harmonics are four-dimensional. But applications on the sphere require two-dimensional functions defined on the sphere. Therefore, depending on the sign of the m, the sin or cos parts of the complete spherical harmonics remain:

$$Y_\ell^{mc} = \sqrt{\frac{2\ell+1}{4\pi}\frac{(\ell-m)!}{(\ell+m)!}}\cos(m\phi)P_\ell^m(\cos(\theta)), \quad m \geq 0, \tag{2.27}$$

$$Y_\ell^{ms} = \sqrt{\frac{2\ell+1}{4\pi}\frac{(\ell-m)!}{(\ell+m)!}}\sin(m\phi)P_\ell^m(\cos(\theta)), \quad m \geq 0. \tag{2.28}$$

2.5 Orthogonal Expansions: Laplace Series

Laplace had already proven that spherical harmonics form a complete orthogonal system. The representation of a function as such a double series is a generalized Fourier series known as a Laplace series. This means, any real function defined on the sphere $f(\theta, \phi)$ can be expanded in terms of complex spherical harmonics by

$$f(\theta,\phi) = \sum_{\ell=0}^{\infty}\sum_{m=-\ell}^{\ell} A_\ell^m Y_\ell^m(\theta,\phi), \tag{2.29}$$

with A_ℓ^m the expansion coefficients or in terms of real spherical harmonics by

$$f(\theta,\phi) = \sum_{\ell=0}^{\infty}\sum_{m=0}^{\ell} [C_\ell^m Y_\ell^{mc}(\theta,\phi) + S_\ell^m Y_l^{ms}(\theta,\phi)] \tag{2.30}$$

with C_ℓ^m and S_ℓ^m the expansion coefficients for the sine and cosine parts respectively. The incident question is, how to determine the A_ℓ^m and S_ℓ^m, C_ℓ^m coefficients for a given function f to be written as in equation (2.29) or (2.30). This is done in a similar way as in the case of the classical Fourier series, namely by means of integration and employing the orthogonality identities for two spherical harmonics Y_ℓ^m and $Y_{\ell'}^{m'}$. We carry on the computation for the real spherical harmonics. For that, we multiply both sides of equation (2.30) by $Y_{l'}^{m'}(\theta,\phi)$, integrate and get

$$C_l^m = -\frac{(2l+1)(l-m)!}{2\pi(l+m)!}\int_0^{2\pi}\int_0^{\pi} f(\theta,\phi)P_l^m(\cos\theta)\cos(m\phi)\sin(\theta)d\theta d\phi, \tag{2.31}$$

$$S_l^m = -\frac{(2l+1)(l-m)!}{2\pi(l+m)!}\int_0^{2\pi}\int_0^{\pi} f(\theta,\phi)P_l^m(\cos\theta)\sin(m\phi)\sin(\theta)d\theta d\phi. \tag{2.32}$$

Independent from the chosen normalization, the following propositions hold for an orthogonal system of spherical harmonic functions, here for simplicity generically denoted with $\{Y_\ell^m\}_{\ell=0,1,\ldots;m=-\ell,\ldots,\ell}$. We follow the deduction line in [49] and for skip the proofs, which are based mainly on the Bernstein and Abel-Poisson summability methods. For

$F \in L^2(\Omega)$ or $F \in C(\Omega)$, the orthogonal expansion in terms of spherical harmonics yields the series

$$\sum_{\ell=0}^{\infty} \sum_{m=-\ell}^{\ell} A_\ell^m Y_\ell^m \tag{2.33}$$

with the coefficients

$$A_\ell^m = (F, Y_\ell^m)_{L^2(\Omega)} = \int_\Omega F(\theta, \phi) Y_\ell^m(\theta, \phi) d\theta d\phi. \tag{2.34}$$

Proposition 2.5.1. *The system $\{Y_\ell^m\}_{\ell=0,1,\ldots;\, m=-\ell,\ldots,\ell}$ is closed in $C(\Omega)$, that is for any given $\varepsilon > 0$ and each $F \in C(\Omega)$, there exists a linear combination*

$$\sum_{\ell=0}^{\infty} \sum_{m=-\ell}^{\ell} A_\ell^m Y_\ell^m \tag{2.35}$$

such that

$$\left\| F - \sum_{\ell=0}^{\infty} \sum_{m=-\ell}^{\ell} A_\ell^m Y_\ell^m \right\|_{C(\Omega)} \leq \varepsilon. \tag{2.36}$$

Proposition 2.5.2. *The system $\{Y_\ell^m\}_{\ell=0,1,\ldots;\, m=-\ell,\ldots,-1,0,1,\ldots,\ell}$ is closed in $C(\Omega)$ with respect to $\|\cdot\|_{L^2(\Omega)}$ that is, for any given $\varepsilon > 0$ and each $F \in C(\Omega)$, there exists a linear combination*

$$\sum_{\ell=0}^{\infty} \sum_{m=-\ell}^{\ell} A_\ell^m Y_\ell^m \tag{2.37}$$

such that

$$\left\| F - \sum_{\ell=0}^{\infty} \sum_{m=-\ell}^{\ell} A_\ell^m Y_\ell^m \right\|_{L^2(\Omega)} \leq \varepsilon. \tag{2.38}$$

Proposition 2.5.3. *The system $\{Y_\ell^m\}_{\ell=0,1,\ldots;\, m=-\ell,\ldots,\ell}$ is closed in the space $L^2(\Omega)$ with respect to $\|\cdot\|_{L^2(\Omega)}$.*

This means, any function $F \in C(\Omega)$ admits an arbitrarily close approximation by finite linear combinations of spherical harmonics. Further,

Proposition 2.5.4. *The closure of the system $\{Y_\ell^m\}_{\ell=0,1,\ldots;\, m=-\ell,\ldots,\ell}$ in $L^2(\Omega)$ is equivalent to each of the following statements:*

- *The orthogonal expansion of any element $F \in L^2(\Omega)$ converges in norm to F, i.e.,*

$$\lim_{L\to\infty} \left\| F - \sum_{\ell=0}^{L} \sum_{\ell}^{m=-\ell} (F, Y_\ell^m)_{L^2(\Omega)}\, Y_\ell^m \right\|_{L^2(\Omega)} = 0. \tag{2.39}$$

- *Parseval's identity holds. That is, for any $F \in L^2(\Omega)$ one has*

$$\|F\|^2_{L^2(\Omega)} = \sum_{\ell=0}^{\infty} \sum_{\ell}^{m=-\ell} \left| (F, Y_\ell^m)_{L^2(\Omega)} \right|^2 . \tag{2.40}$$

- *There is no strictly larger orthonormal system containing the orthonormal system $\{Y_\ell^m\}_{\ell=0,1,\ldots;\, m=-\ell,\ldots,\ell}$.*
- *The system $\{Y_\ell^m\}_{\ell=0,1,\ldots;\, m=-\ell,\ldots,\ell}$ has the completeness property: for $F \in L^2(\Omega)$, if $(F, Y_\ell^m)_{L^2(\Omega)} = 0$ for all $\ell = 0, 1, \ldots;\ m = -\ell, \ldots, \ell$ then $F = 0$.*
- *An element $F \in L^2(\Omega)$ is determined uniquely by its coefficients, that is, if the determined coefficients of two function coincide, then the functions coincide also.*

We present the uniform convergence property of the spherical harmonics for the coefficients computed as in (2.31). In [54] the authors investigate the relationship between the rapidity of convergence of these series and the smoothness of F on a spherical domain $\mathcal{S}$.

Proposition 2.5.5 (Absolute convergence of expansions in series of (surface) spherical harmonics). *Let $F(\mathbf{r}) \in \mathcal{C}^k(\mathcal{S})$ with $\mathbf{r} \in \mathcal{S}$ and $\mathcal{S}$ the unit sphere. Then in the expansion (2.30)*

$$\sum_{m=0}^{\ell} P_\ell^m(\cos\theta) \left(C_\ell^m \cos(m\phi) + S_\ell^m \sin(m\phi)\right) = \mathcal{O}\left(\frac{1}{\ell^{k-\frac{1}{2}}}\right) \tag{2.41}$$

as $\ell \to \infty$, uniformly for $\mathbf{r} \in \mathcal{S}$. The series

$$\sum_{\ell=0}^{\infty} \sum_{m=0}^{\infty} P_\ell^m(\cos\theta) \left(C_\ell^m \cos(m\phi) + S_\ell^m \sin(m\phi)\right) \tag{2.42}$$

thus converges uniformly to f for $\mathbf{r} \in \mathcal{S}$ when $k \geq 2$. Further, the series may be differentiated term-by-term up to $k-2$ times [139], [54].

Recall that a function which is continuously differentiable on the unit circle can be expressed as a uniformly convergent Fourier series. Also, a function which is continuously differentiable on the unit sphere in the three–dimensional space can be expanded in terms of a uniformly convergent series of Laplace series. This construction can be generalized for an arbitrary number of dimensions. After the introduction of spherical harmonics in arbitrary dimensions from [66], the proof of the general expansion theorem and its convergence failed until recently. For details we point to [78]. Using sufficiently high powers of the Laplace–Beltrami operator to compensate for the growth of the spherical harmonics with increasing degree, it is shown that every function $f \in \mathcal{C}^k(\mathcal{S}^{d-1})$ with $\mathcal{S}^{d-1}$ the sphere in d dimensions and $k := 2[(d+4)/3]$ [119] or $k := 2[(d+4)/4]$ [143] has a uniformly absolutely convergent Laplace series.

Though less relevant for our work, it is interesting to see how intricate this type of multidimensional approximation Laplace series are. Their employment is not user friendly and cannot keep up with modern formulations.

Figure 2.2. *The real part of spherical harmonics* $Y_\ell^{mc} = \cos(m\phi)P_\ell^m(\cos(\theta))$, $0 \geq m \geq \ell$. *The blue and red color indicates negative and positive values of* Y_ℓ^{mc}, *which are plotted at radius* $|Y_\ell^{mc}|$ *from the origin. The scale is adapted for visualization.*

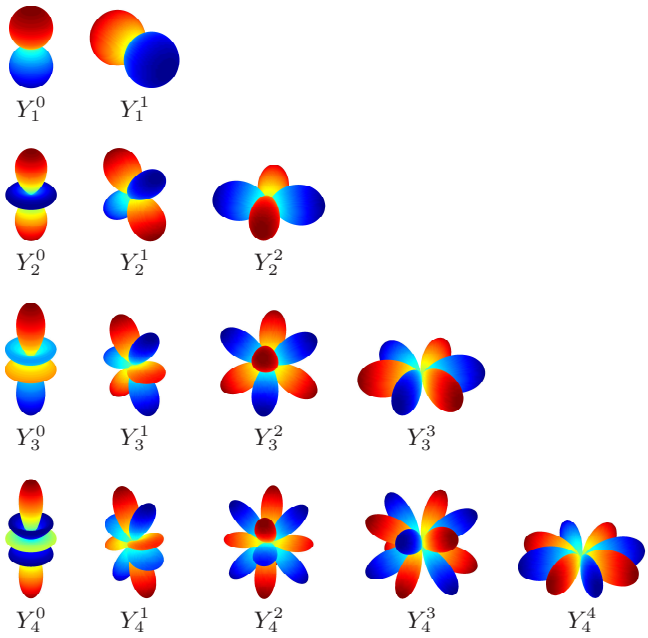

Figure 2.3. *The absolute part of spherical harmonics, dependent alone on the polar angle* θ: $|Y_\ell^m(\phi,\theta)|^2 = |P_\ell^m(\cos(\theta))e^{im\phi}|^2 = |P_\ell^m(\cos(\theta))|^2$. *The* $|Y_\ell^m|$ *values are plotted at radius* $|Y_\ell^m|$ *from the origin. The scale is adapted for visualization.*

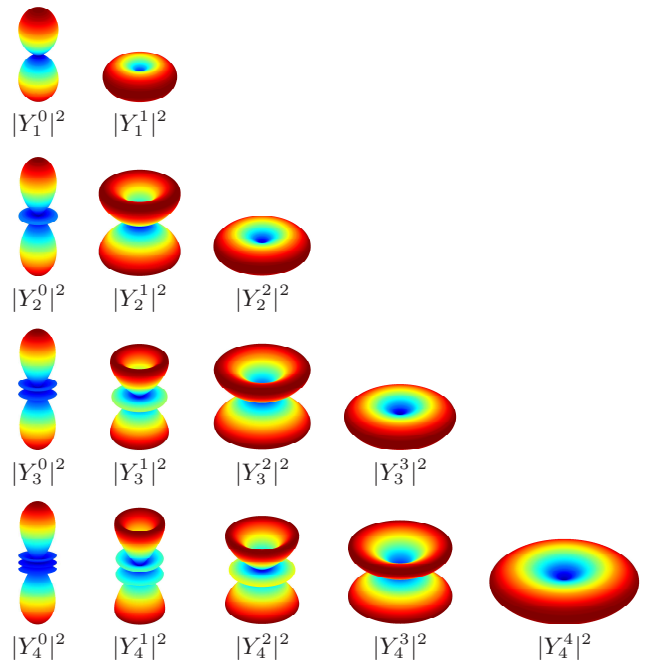

Chapter 3

The Earth's Gravitational Field

Newton's law of universal gravitation
Every particle of matter in the universe attracts every other particle with a force that is directly proportional to the product of the masses of the particles and inversely proportional to the square of the distance between them.(translated from the Latin)

Philosophiae naturalis principia mathematica [110]

Though the concept of gravity is astonishing simple, the study of the gravity of the earth is not an easy task. That is because the gravity of the earth, due to its structure, is very complex. The key of potential theory resides indeed in the study of the rather straightforward Laplace equation. But it is the size of the problem, namely the representation and the handling of a tremendous amount of data making it all quite unmanageable.

We have shortly mentioned in the introduction of this thesis the not–so–constant gravity constant and mentioned the varying nature of the earth's gravitational potential. In this chapter we discus some essential tools for its investigation, like the fundamental relationships governing gravity and its geometry. The section on classical gravity field models will help argue our own development in the continuation of harmonic functions. We also take a look at the boundary problems of geodesy and key issues of gravity data associated with it.

3.1 Preliminaries

We introduce several mathematical tools that we need when theoretically handling the earth's gravity field.

First of all, spherical coordinates are indispensable in all geosciences. For the global representation of the gravity field, the coordinates are mainly chosen so that the origin is at the center of the earth. In order to keep coherent notation with geodetical and geophysical literature, we work here with the physical instead of the mathematical version of the spherical coordinates, i.e., θ is the co-latitude or polar angle, ranging from $0 \leq \theta \leq \pi$ and ϕ, the azimuth or longitude, ranging from $0 \leq \phi < 2\pi$. Recall that the spherical

coordinates (r, θ, ϕ) are then related to the Cartesian coordinates (x, y, z) by (2.10). For local problems, a Cartesian coordinate system is still the better choice.

3.2 Fundamental Relationships

3.2.1 Gravity Acceleration and Gravity Potential

The firsts ones to theoretically handle gravity have been Galileo, who determined the magnitude of the gravitational acceleration, and Kepler, who described the orbits of planets. Yet the law of gravitational attraction was formulated by Isaac Newton (1642-1727) and published in 1687 [110].

Consider the case of a rotating system, like the earth. The gravity is defined as the force exerted on a mass m due to the gravitational attraction of the body with mass M together with the force exerted by its rotation, i.e., the centrifugal acceleration due to rotation. Further, let the point of mass M be situated at position $\mathbf{r_0}$ and the point of mass m at position $\mathbf{r}$. Then, the gravitational force between the two particles separated by a distance $r = \|\mathbf{r}_0 - \mathbf{r}\|$ is an attraction along a line connecting the two objects as

$$\mathbf{F} = -\frac{GMm}{\|\mathbf{r}_0 - \mathbf{r}\|^2}\mathbf{a}_r, \quad F = \|\mathbf{F}\| = \frac{GMm}{r^2}. \tag{3.1}$$

Here $\mathbf{a}_r = \mathbf{r}/\|\mathbf{r}\|$ is a dimensionless unit vector for the direction, pointing away from the point mass M and toward the test object. Therefore, the minus sign accounts for the fact that the force vector $\mathbf{F}$ points toward the mass M. Further, G is known as the universal gravitational constant. Its value has been determined as

$$G = 6.673 \cdot 10^{-11} m/(s^2 kg) = 6.673 \cdot 10^{-11} Nm^2/kg^2. \tag{3.2}$$

In order to obtain the gravitational attraction per unit mass g and the gravity $\mathbf{g}$ observed at distance $r = \|\mathbf{r}_0 - \mathbf{r}\|$ from M, we divide equation (3.1) by the mass m of the test object:

$$\mathbf{g} = \mathbf{F}m = -\frac{GM}{\|\mathbf{r}_0 - \mathbf{r}\|^2}\mathbf{a}_r, \quad g = \|\mathbf{g}\| = \frac{GM}{r^2}. \tag{3.3}$$

The gravitational attraction per unit mass g has the unit force per mass. It represents the acceleration of a freely falling body and points towards the attracting body; over the earth's surface it is approximately

$$g = 9.8N/kg = 9.8m/s^2 = 980Gal. \tag{3.4}$$

The units gal Gal and its derivative milligal $mGal$ are commonly used in the geodetic literature.

For real life problems, we are also interested in the total gravity resulted by several sources, namely, the vector sum of the gravity of all considered masses. Let S sources of mass M_s be situated at $\mathbf{r}_s$, $s = 1, \ldots, S$. We formalize the effect of multiple sources at a point situated at $\mathbf{r}_m$ by developing the unit vector as

$$\mathbf{g}(\mathbf{r}_m) = \sum_{s=1}^{S} \mathbf{g}_s = \sum_{s=1}^{S} -\frac{GM_s(\mathbf{r}_m - \mathbf{r}_s)}{\|\mathbf{r}_m - \mathbf{r}_s\|^3}. \tag{3.5}$$

We can further write $\mathbf{g}(\mathbf{r}_m)$ as a function of the densities ρ_s over the volume Vol_s of each of the s sources:

$$\mathbf{g}(\mathbf{r}_m) = \int_{\cup Vol_s} \sum_{s=1}^{S} -\frac{G\rho_s(\mathbf{r}_m - \mathbf{r}_s)}{\|\mathbf{r}_m - \mathbf{r}_s\|^3} d\mathrm{Vol}_s. \tag{3.6}$$

The earth's gravitation can be then similarly obtained by Newton's law of gravitation: for Vol_{Earth} the Volume, $\mathbf{r_0}$ the position and the mass element $dm = \rho dv$ of the earth (expressed by the volume density ρ and the volume element dv) and for an attracted point of unit mass situated at $\mathbf{r}$:

$$\mathbf{g}(\mathbf{r}) = G \int_{\mathrm{Vol}_{Earth}} \frac{\mathbf{r}_0 - \mathbf{r}}{\|\mathbf{r}_0 - \mathbf{r}\|^3} dm. \tag{3.7}$$

Another way of formulating the gravity field which simplifies incidental computations is by means of the potential. The three dimensional expression of the gravitational potential at a distance $r = \|\mathbf{r}_m - \mathbf{r}_{ref}\|$ from mass M is the integral along some path from the observation point at $\mathbf{r}_m$ to some reference point at $\mathbf{r}_{ref}$

$$V = -\int_{\mathbf{r}_m}^{\mathbf{r}_{ref}} \mathbf{g} \cdot d\mathbf{r} = -\int_{\mathbf{r}_m}^{\mathbf{r}_{ref}} \frac{GM}{\|\mathbf{r}_m - \mathbf{r}_{ref}\|^2} \mathbf{a}_r = GM \int_{\infty}^{r} \frac{1}{r^2} dr = -\frac{GM}{r}. \tag{3.8}$$

This means, the potential is proportional to the mass M, here the mass of the earth, and inversely proportional to the distance r. Notice, since this potential field is conservative, it does not matter which path between $\mathbf{r}_m$ and $\mathbf{r}_{ref}$ we choose. In contrast to $\mathbf{g}$, the potential V takes a scalar instead of a vector value at each point. Further, since

$$\mathbf{g} = -\mathrm{grad}V = -\nabla V, \tag{3.9}$$

$\mathbf{g}$ is perpendicular to an equipotential surface at each point. We will specify concepts like equipotential surface in the following subsection.

3.2.2 Differential and Integral Formulas for the Gravity Potential

The gravitational field of the earth is caused by its mass and indirectly by density distribution, which is inherently three-dimensional. Yet the gravitational acceleration can only be measured outside of the earth's surface. Gauss's Theorem, also known as Gauss's divergence theorem, offers a link between a surface observations and the properties of the whole body. It is the analogon to the law of conservation of mass for incompressible fluids. Let $\mathrm{Vol} \subset I\!R^3$ be a volume and $S = \partial\mathrm{Vol}$ its surface. Also, $\mathbf{n}$ is the outward pointing unit normal field of the boundary $\partial\mathrm{Vol}$. If $\mathbf{F}$ is a continuously differentiable vector field defined on a neighborhood of Vol, then the volume integral of the divergence, is equal to the net flow across the volume's boundary, i.e.

$$\int_{\mathrm{Vol}} (\nabla \cdot \mathbf{F})\, d\mathrm{Vol} = \int_{\partial\mathrm{Vol}} \mathbf{F} \cdot \mathbf{n}\, dS. \tag{3.10}$$

Consider now the flow of the gravity field and equation (3.9); we get

$$\int_{\partial\mathrm{Vol}} \mathbf{g} \cdot \mathbf{n} dS = \int_{\mathrm{Vol}} \nabla \cdot \mathbf{g} d\mathrm{Vol} = -\int_{\mathrm{Vol}} \nabla \cdot \nabla V d\mathrm{Vol} = -\int_{\mathrm{Vol}} \Delta V d\mathrm{Vol}. \tag{3.11}$$

But, on the other side, by assuming that S is a spherical surface:

$$\int_{\partial \text{Vol}} \mathbf{g} \cdot \mathbf{n} dS = -4\pi r^2 g = -4\pi GM = -4\pi G \int_{\text{Vol}} \rho d\text{Vol} \tag{3.12}$$

This tells us, how the total mass of a body M can be determined from measurements of $\nabla V = -g$ at the surface. Further, since they hold for any volume Vol, equations (3.11-3.12) provide the Poisson equation for ΔV

$$\Delta V(\mathbf{r}) = 4\pi G\rho(\mathbf{r}). \tag{3.13}$$

When we are outside the mass, this means, there is no potential negative or positive source enclosed by the surface S, thus the density is $\rho = 0$, the potential U fulfills the Laplace equation:

$$\Delta V(\mathbf{r}) = 0, \ \mathbf{r} \text{ outside Vol.} \tag{3.14}$$

Since the atmosphere does not contain relatively significant masses, up to water vapors, we can assume under certain conditions and corrections that the mass density outside the earth vanishes indeed, see [141] for details. This means that we can indeed assume, that the Laplacian of the gravity potential and of the anomalies is zero. The atmosphere has a very weak upward pull, i.e. against the attraction of the earth, but is neglected in most geodetic applications.

We proceed with some examples which will help us understand the effect of density variation of a body over its gravity field. Deviations from the average density do indeed generate variations in both scalar, vectorial and direction of the field. So we consider some reference volume generating a gravity field whose values we do not need to know. We are only interested in the deviation caused when a change in density arises. We consider for that one or more spheres with deviating density are buried underneath the w.l.o.g. flat surface and we investigate the immediate changes they inflict. These examples will help us generate test datasets for the numerical experiments with the approximate continuation.

Example 3.2.1. Gravity of a buried sphere

We defined in equation (3.3) the gravitational acceleration due to a point mass as

$$g = \|\mathbf{g}\| = \frac{Gm}{r^2}. \tag{3.15}$$

where G is the gravitational constant, m is the mass of the point mass, and r is the distance between the point mass and the observation point. Using Gauss's law, one can prove that the gravitational attraction of a sphere is identical to the gravitational attraction of a point source with the same mass. Therefore, the expression derived for the gravitational acceleration over a point mass also represents the gravitational acceleration over a buried sphere. A point mass produces both horizontal and vertical gravity attraction, but we are only interested in the vertical part. Let us consider a sphere buried at depth z and position $x = 0$, see Figure 3.2.1. Its anomalous gravity is then the vertical component of $\mathbf{g}$, which can be calculated as a function of the angle θ between the horizontal and position vector $\mathbf{r}$ of the observation point:

$$\delta g = \|\mathbf{g}\| \cos\theta = \frac{Gmz}{r^2}. \tag{3.16}$$

Now, depending on the radius $r = \sqrt{x^2 + z^2}$ *we have*

$$\delta g = \frac{Gmz}{(x^2 + z^2)^{3/2}}. \tag{3.17}$$

A last aspect to consider is the relation of the mass m *to the size and relative density of the buried sphere; for that let the case of uniform density* ρ *over the volume of the sphere* $V = \frac{4\pi r_s^3}{3}$ *for* r_s *radius of the sphere. The anomalous gravity as a function of the position of the observation point* (x, z) *translates then to*

$$\delta g_i = \frac{4\pi G z \rho r_s^3}{(x^2 + z^2)^{3/2}}. \tag{3.18}$$

Figure 3.1. *Components of the gravity vector for an arbitrary mass.*

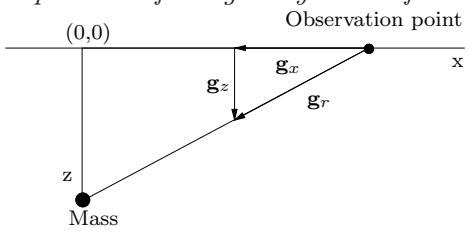

Notice how the shape of the gravity anomalies changes with the distance from the mass causing the anomaly: the values decrease fast, the isosurfaces remain circular, but get broader and in the infinity limit parallel to the surface. The understanding of the gravity of one buried point mass or sphere is not really challenging. However, it holds the key to gravity anomalies over more complicated density distributions.

Figure 3.2. *Gravity anomalies up to* $10km$ *height generated by a buried sphere. Considered geology: a massive sphere with radius* $r_S = 3km$ *and positive density deviation* $\rho_S = 0.2g/cm^3$ *buried underneath the origin at depth* $z = 6km$*. 2–dimensional section through the middle of the sphere (left) and isosurfaces of the field (right).*

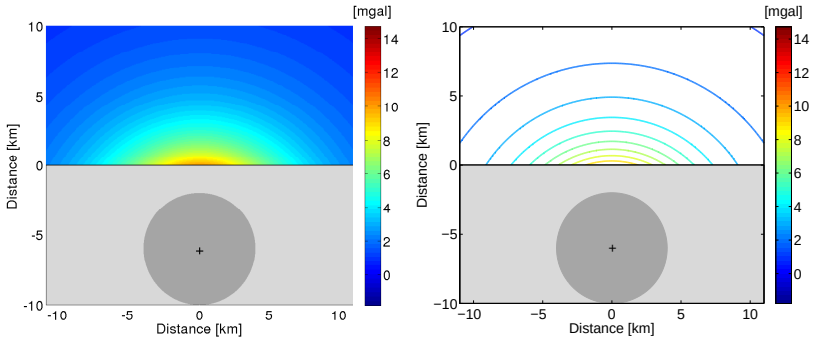

Example 3.2.2. Gravity of a set of buried spheres *We consider as an extension of 3.2.1 the example inspired by [136] which models a salt lake. This is done by assuming*

a series of buried spheres with alternating deviating densities. As we have seen, the total gravity resulted by several sources is the sum of the gravity caused by each source alone. The gravity anomaly resulted by a series of i buried spheres $(S_i, r_s(S_i), x(S_i), z(S_i))$ with radius $r_s(S_i)$ positioned at $(x(S_i), z(S_i))$ is

$$\delta g = \sum_{S_i} \frac{4\pi G z \rho(S_i) r_s(S_i)^3}{(x - x(S_i))^2 + (z - z(S_i))^2)^{3/2}}. \tag{3.19}$$

We have constructed the following geology: the same massive sphere as in example 3.2.1 but with radius $r(S_1) = 4km$ and positive density deviation $\rho(S_1) = 0.2g/cm^3$ is buried at depth $z(S_1) = 6km$. It is followed by a series of smaller spheres with alternating positive and negative density deviations:

$$\rho(S_i) = 0.3(-1)^i g/cm^3,\ i = 2, \ldots, 11, \tag{3.20}$$

radius $r(S_i) = 1km,\ i = 2, \ldots, 11$ buried on a line at depth $z(S_i) = 1km,\ i = 2, \ldots, 11$ parallel to the surface, centered in the origin. See in Figure 3.3 how the positive and negative anomalies interact and also how the anomalies caused by the smaller masses vanish faster. In fact, far away from the surface, the isosurfaces resemble the isosurfaces resulting in the case of the single buried sphere. This shows that the small mass variations near to the surface strongly influence the gravitational field geometry at low heights, but the stronger deviations generated by the greater mass dominate the field further away from the surface.

Figure 3.3. *Gravity anomalies up to $10km$ height generated by a mixture of positive and negative anomaly sources, here modeled by buried spheres. Considered geology: a massive sphere with radius $r_S = 4km$ and positive density deviation $\rho_S = 0.2g/cm^3$ buried underneath the origin at depth $z = 6km$ followed by a series of smaller spheres with alternating positive or negative density deviations $\rho(S_i) = 0.3(-1)^i g/cm^3,\ i = 2, \ldots, 11$, radius $r(S_i) = 1km,\ i = 2, \ldots, 11$ buried on a line at depth $z(S_i) = 1km,\ i = 2, \ldots, 11$. 2–dimensional section through the middle of the sphere (left) and isosurfaces of the field (right).*

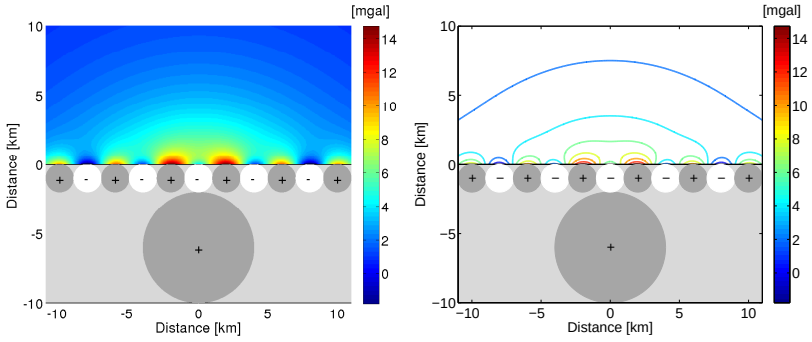

3.3 Geometry of the Gravity Field

The study of gravity potential field of the earth is associated with three surfaces:

- the topographical surface of the earth,
- the ellipsoid, a theoretical reference surface and
- the geoid, an equipotential surface of the potential field.

These surfaces define the following distances:

- the ellipsoid height relative to the ellipsoid,
- the elevation relative to the geoid and
- the geoid height (undulation) relative to the ellipsoid, see Figure 3.3.

We will describe how these surfaces and distances relate to each other [102, 136, 141].

Figure 3.4. *Schematic modeling of the potential field of the earth: the orthometric height H: surface's elevation above the geoid, h: ellipsoid height to the surface, U: undulation (geoid height) above the ellipsoid.*

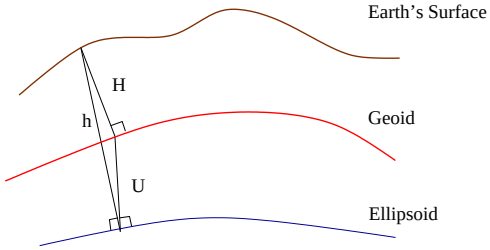

One of the established and most intuitive way to describe gravity fields is by means of equipotential surfaces. These are surfaces containing all the points outside of the mass where the gravity field takes a certain constant value. A common approximation of the form of the earth is ellipsoidal, which many applications use as reference for approximation purposes. If the earth was ellipsoidal and if it had constant density, then an equipotential surface of it would also have an ellipsoidal form. This is why an ellipsoid, also known as the normal earth and associated to the normal potential field, has been selected as a reference surface for the gravitational field of the earth.

The next key term is the geoid. Literally, geoid means earth-shaped. For our purposes, the geoid is a real equipotential surface, also known as isosurface or level surface of the earth. It is sometimes associated with an equipotential surface approximating the global mean sea-level over the ocean. It can be regarded as the surface of the hypothetical ocean at rest. It resembles in fact roughly the sea-level surface if dynamic effects like waves, tides and currents are excluded. For every point on earth, the local direction of gravity vector $\mathbf{g}$ is perpendicular to the geoid. The shape of the geoid is important for applications such as calculating satellite orbits, computations of distances like absolute height above mean

sea level or GPS. It is often described as the true physical figure of the earth, in contrast to the idealized geometrical figure of a reference ellipsoid. We will later give the exact common formulation of the normal potential field.

Figure 3.5. *Geoid, ellipsoid and topographical surface of the earth.*

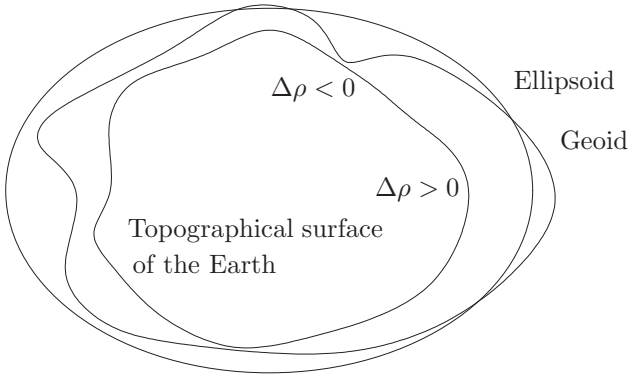

The deviation of the geoid from the ellipsoid is known as geoid undulation. It is caused, for example, by the variation of density within the mass or by the variation of the topographical surface, see Figure 3.3. Gravity around the earth varies and equipotential surfaces are not parallel to each other anymore. A density anomaly near the surface will then cause a local gravity anomaly. The difference between the real field of the earth and the theoretical normal potential field is called the anomalous field or disturbing field. The geoid undulations as deviation of the isosurfaces, the gravity anomalies as deviations of the potential field, and the gravity gradient changes reflect, but are different measures of, the density variations of the earth.

We can write in term of heights: for h the ellipsoid height relative to the ellipsoid, H the elevation relative to the geoid, and U the geoid height (undulation) relative to the ellipsoid we have:

$$h = H + U. \tag{3.21}$$

In terms of fields: for V the gravitational potential, N the normal potential and T disturbing potential it holds:

$$V = N + T. \tag{3.22}$$

Needless to say, yet the normal potential and the disturbing potential also fulfill Laplace's equation outside of the mass, that means:

$$\Delta N = 0, \quad \Delta T = 0. \tag{3.23}$$

We present as example the schematic modeling of the normal and disturbing potential field of a spherical body with varying density. Since absolute values carry no relevant information for this example, scales have been omitted. Though the computations are three–dimensional, we show for the sake of simplicity two–dimensional sections through the center of the body and isosurfaces of these cuts. The normal field is defined to be that of the sphere with uniform density. Notice its circular, parallel to each other isosurfaces.

In order to construct veridic anomalies, we have in fact evaluated and properly scaled some terms of the geoid potential model EGM96 [92]. This time, the isosurfaces are not circular anymore. They present deviations to the isosurfaces of the normal field. Notice also, that the deviations of the equipotential surfaces near to the surface, i.e., near to the anomalous masses, are stronger than the deviations of the isosurfaces at larger distances.

Figure 3.6. *Schematic modeling of the normal and disturbing potential field of a spherical body with varying density: 2–dimensional sections through the center of the body and isosurfaces of these cuts.*

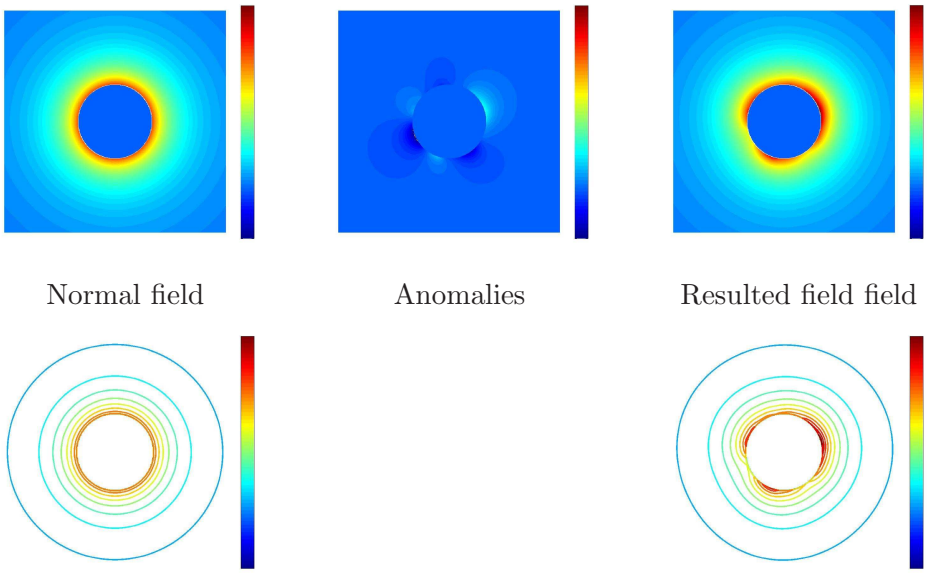

3.4 Classical Gravity Field Model: The Spherical Harmonics Representation

Global gravity field or geoid models of the earth are mostly based on spherical harmonic expansions. As we have seen in Section 2.4, spherical harmonics are harmonic basis functions resulted by constructing a solution of the Laplace equation in spherical coordinates by means of the separation of variables, see Section 2.4 for the detailed discussion. They are relevant for theoretical and practical applications and are used e.g. for the computation of the atomic electron configurations, the representation of the magnetic fields of planetary bodies, and the characterization of the cosmic microwave background radiation.

The gravitational potential V in the spherical harmonic representation in the exterior space of the earth is given for $x = (r, \theta, \phi)$ the spherical coordinates of a computation point x with r the geocentric radius, θ the spherical co-latitude and ϕ the longitude of x

by

$$V^{\infty}(r,\theta,\phi) = \frac{GM_1}{r}\sum_{n=0}^{\infty}\sum_{m=0}^{n}\left(\frac{a_1}{r}\right)^n \left(C_n^m\cos(m\phi) + S_n^m\sin(m\phi)\right) P_n^m(\cos\theta) \tag{3.24}$$

with the gravity-mass constant GM_1 value, the equatorial scale factor a_1, corresponding the best fitting earth ellipsoid, and P_n^m the (fully normalized) Legendre functions. Yet, the geodetic information is limited. The geopotential models embody therefore a truncated set of harmonic coefficients and are available with four components: the set of (fully normalized) coefficients C_n^m and S_n^m from degree $n = 0,\ldots,N$ and order $m = 0,\ldots,n$, which are elaborately determined from numerous satellite and terrestrial observations, the gravity-mass constant GM_1, the equatorial scale factor a_1 and the permanent tide system.

3.4.1 Determination of the Model

Recall from chapter 2.4 the construction of spherical harmonics and from subsection 2.5 the Laplace series. We stay with the geodetic formulation and use from now on the (fully normalized) Legendre functions, i.e.

$$Y_n^m = \begin{cases} Y_n^{mc} &= \cos(m\phi)P_n^m(\cos(\theta)), \quad m \geq 0, \\ Y_n^{ms} &= \sin(m\phi)P_n^m(\cos(\theta)), \quad m < 0 \end{cases} \tag{3.25}$$

and the normalization

$$\frac{1}{4\pi}\int_{\mathcal{S}} Y_n^m(\theta,\phi)Y_{n'}^{m'}(\theta,\phi)ds = \delta_{nn'}\delta_{mm'}. \tag{3.26}$$

We look for a solution V of the exterior boundary value problem for the Laplace equation with Dirichlet boundary conditions. We write V as a linear combination of spherical harmonics with the expansion coefficients C_n^m of the spherical harmonic of degree n and order m

$$V^{\infty}(r,\theta,\phi) = \frac{GM_1}{r}\sum_{n=0}^{\infty}\sum_{m=0}^{n}\left(\frac{a_1}{r}\right)^n \left(C_n^m\cos(m\phi) + S_n^m\sin(m\phi)\right) P_n^m(\cos\theta). \tag{3.27}$$

According to the orthogonality condition of the spherical harmonics on the sphere, the coefficients C_n^m and S_n^m can be computed from the available data on the sphere of radius R. The computation of these coefficients is analogous to the computation of coefficients in a classical Fourier series. This means, we multiply both sides in equation (3.27) by $Y_{n'}^{m'}(\theta,\phi)$, integrate over the sphere of radius R, and by means of equations (3.26) obtain

$$C_n^m = \frac{1}{4\pi}\int_s V(r,\theta,\phi)Y_n^{mc}(\theta,\phi)ds, \tag{3.28}$$

$$S_n^m = \frac{1}{4\pi}\int_s V(r,\theta,\phi)Y_n^{ms}(\theta,\phi)ds. \tag{3.29}$$

Of course, not all, but only an infinite number of coefficients can be determined, let alone the fact that $V(\mathcal{S})$ is not everywhere continuously available. E. g., the well established EGM96, the NASA GSFC and NIMA Joint Geopotential Model [92] contains a total of 130317 model coefficients up to spherical harmonic degree and order 360 yielding a spatial resolution of 30 arc minutes. Table 3.1 shows the first coefficients of this model. In order to satisfy higher accuracy requirements, work has been undertaken to update EGM96 using new satellite data. It was expected that the new version contains coefficients for a model with spherical harmonic degree larger than 2000. The official Earth Gravitational Model EGM2008 has been already publicly released by the National Geospatial-Intelligence Agency (NGA) EGM Development Team [115]. This gravitational model is complete up to spherical harmonic degree and order 2159, contains additional coefficients extending to degree 2190 and order 2159 and models gravity field variations with a wavelength of 5 arc minutes.

Figures 3.14-3.16 present the map of the undulations of the geoid based on the EGM96 [92] gravity model up to the spherical harmonic expansion degree 10, 30 and 300 respectively. Notice the incremental refinement of the representation e.g. in the area between Russia and China. On the other side, figures 3.17-3.19 present a map of the *representation error* for geoid undulations of the EGM96 [92] gravity model up to the spherical harmonic expansion degree 10, 30 and 300 respectively, compared to the EGM96 [92] gravity model up to the spherical harmonic expansion degree 360. Notice the structure of the deviations. See also the the areas where the deviation has sharp variations, like the west coast of South America or in the seas south of Japan. Here, the missing high degree coefficients are significant.

3.4.2 Coefficients Significance

The dimension of the space spanned by spherical harmonics of degree n is $2n+1$; for each spherical harmonic of degree n the geoid model contains $n+1$ coefficients C_n^m for the cos–functions, from order $m=0$ to order $m=n$, and n coefficients S_n^m for the sin–functions, from degree $m=1$ to degree $m=n$. The sin–coefficients $S_{n,0}$ for $m=0$ are set to 0, as $\sin(m\phi)=0$ for all ϕ. The approximated potential reads

$$V^N(r,\theta,\phi) = \frac{GM_1}{r}\sum_{n=0}^{N}\sum_{m=0}^{n}\left(\frac{a_1}{r}\right)^n \left(C_n^m\cos(m\phi)+S_n^m\sin(m\phi)\right)P_n^m(\cos\theta). \tag{3.30}$$

The term for $n=0$ is represented by GM_1/r as $S_{0,0}$ does not exist and $C_{0,0}=1$. The first degree coefficients are inadmissible, that is $C_{1,m}=0$ and $S_{1,m}=0$ if the origin is at the center, as they are associated with an arbitrary shift of the center of the mass. Also, $C_{2,0}$ is defined in a specific permanent tide system. The spherical harmonic summation (3.30) can therefore be given in the form

$$V^N(r,\theta,\phi) = \frac{GM_1}{r}\left[1+\sum_{n=2}^{N}\sum_{m=0}^{n}\left(\frac{a_1}{r}\right)^n \left(C_n^m\cos(m\phi)+S_n^m\sin(m\phi)\right)P_n^m(\cos\theta)\right]. \tag{3.31}$$

Recall from Section 3.3, the difference between the measured gravity potential and the theoretical estimated potential of an idealized, best fitting the earth, ellipsoidal body

Table 3.1. *The first of the set of (fully normalized) coefficients C_n^m and S_n^m for the EGM96, the NASA GSFC and NIMA Joint Geopotential Model [92]; the corresponding gravity-mass constant GM_1, the equatorial scale factor a_1.*

degree n	order m	C_n^m	S_n^m
2	0	-0.484165371736e-03	0.000000000000e+00
	1	-0.186987635955e-09	0.119528012031e-08
	2	0.243914352398e-05	-0.140016683654e-05
3	0	0.957254173792e-06	0.000000000000e+00
	1	0.202998882184e-05	0.248513158716e-06
	2	0.904627768605e-06	-0.619025944205e-06
	3	0.721072657057e-06	0.141435626958e-05
4	0	0.539873863789e-06	0.000000000000e+00
	1	-0.536321616971e-06	-0.473440265853e-06
	2	0.350694105785e-06	0.662671572540e-06
	3	0.990771803829e-06	-0.200928369177e-06
	4	-0.188560802735e-06	0.308853169333e-06
5	0	0.685323475630e-07	0.000000000000e+00
	1	-0.621012128528e-07	-0.944226127525e-07
	2	0.652438297612e-06	-0.323349612668e-06
	3	-0.451955406071e-06	-0.214847190624e-06
	4	-0.295301647654e-06	0.496658876769e-07
	5	0.174971983203e-06	-0.669384278219e-06
6	0	-0.149957994714e-06	0.000000000000e+00
	1	-0.760879384947e-07	0.262890545501e-07
	2	0.481732442832e-07	-0.373728201347e-06
	3	0.571730990516e-07	0.902694517163e-08
	4	-0.862142660109e-07	-0.471408154267e-06
	5	-0.267133325490e-06	-0.536488432483e-06
	6	0.967616121092e-08	-0.237192006935e-06

$$GM_1 = 3986004.415e+8\frac{m^3}{s^2}$$
$$a_1 = 6378136.3m$$

is known as gravity anomaly. Then the geoid undulation produced by the anomalous potential, that is the deviation of an equipotential surface to the reference ellipsoid, given by the Bruns' formula [67, 80], to the maximal degree N from the geopotential model is

$$U^N(r,\theta,\phi) = \frac{GM_1}{r\gamma}\sum_{n=2}^{N}\sum_{m=0}^{n}\left(\frac{a_1}{r}\right)^n\left(\delta C_n^m\cos(m\phi) + S_n^m\sin(m\phi)\right)P_n^m(\cos\theta). \qquad (3.32)$$

Here γ is the normal gravity on the surface of the reference ellipsoid and δC_n^m are the fully normalized coefficients that have been reduced by the even zonal harmonics of the reference ellipsoid.

To the maximal degree of a spherical harmonics model, i.e. $N = 360$ for EGM96,

Figure 3.7. *(Half) wavelength* $w = \frac{2\pi a_1}{2n+1}$ *per degree* n *of the spherical harmonic decomposition of the earth's potential field.*

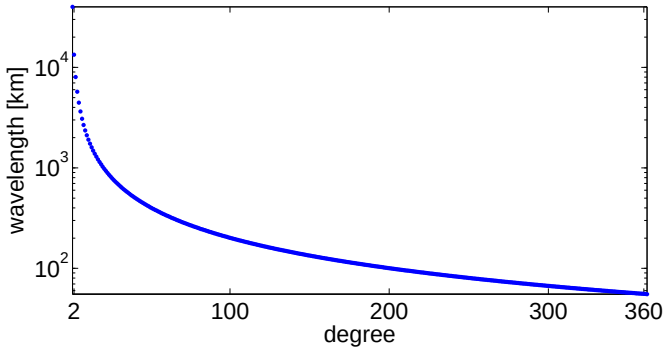

Figure 3.8. *Signal amplitude* $\sigma_n^2 = R\sum_{m=0}^{n}\left(C_n^{m2} + S_n^{m2}\right)$ *per degree* n *of the spherical harmonic coefficients of the geoid model EGM96.*

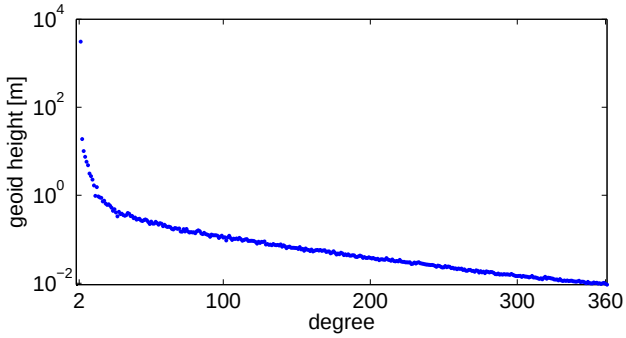

corresponds to a minimal wavelength w calculated for $a_1 = 6378.135km$ as

$$w = \frac{2\pi a_1}{2N+1} \;=\; 55.5825\ km. \tag{3.33}$$

Figure 3.7 shows the wavelength per degree of the spherical harmonic decomposition up to the maximal degree of EGM96.

In order to compare geoid models, one computes the signal amplitude of the geoid model, namely the degree variances, that are the variances σ_n per spherical harmonic degree n as

$$\sigma_n^2 = R\sum_{m=0}^{n}\left(C_n^{m2} + S_n^{m2}\right), \quad n = 2,\ldots,N. \tag{3.34}$$

The coefficients of a spherical harmonic expansion, C_n^m, S_n^m for Y_n^{mc} and Y_n^{ms} respectively may depend on the choice of the coordinates but the signal amplitude per degree of the coefficients set is constant for all choices of the coordinate system. This information is very important [118], especially corroborated with the fact that the geoid model employs the (fully normalized) Legendre functions. This means that the so called basis functions of the spherical harmonic representation make a complete orthogonal system on the surface

of the sphere Ω_s and have been normalized such that

$$\int\int_{\Omega_s} Y_n^{mc}(\theta,\phi)^2 d\Omega_s(\theta,\phi) = \int\int_{\Omega_s} \cos^2(m\phi) P_n^m(\cos(\theta))^2 d\Omega_s(\theta,\phi) = 1, \quad (3.35)$$

$$\int\int_{\Omega_s} Y_n^{ms}(\theta,\phi)^2 d\Omega_s(\theta,\phi) = \int\int_{\Omega_s} \sin^2(m\phi) P_n^m(\cos(\theta))^2 d\Omega_s(\theta,\phi) = 1. \quad (3.36)$$

In this context, the statement in the dependence of variances per degree is, that the smaller the degree $n = 1, \ldots$, the greater the influence of the coefficient set for spherical harmonics of degree n in the summation (3.30).

We further rewrite equation (3.30):

$$V(r,\theta,\phi) = \frac{GM_1}{a_1} \sum_{n=0}^{N=360} \sum_{m=0}^{n} \left(\frac{a_1}{r}\right)^{n+1} \left(C_n^m \cos(m\phi) + S_n^m \sin(m\phi)\right) P_n^m(\cos\theta). \quad (3.37)$$

For an arbitrary point

$$x = (a_1, \theta, \phi) \quad (3.38)$$

situated on the surface of the earth, the potential is

$$V(a_1,\theta,\phi) = \frac{GM_1}{a_1} \sum_{n=0}^{N} \sum_{m=0}^{n} \left(\frac{a_1}{a_1}\right)^{n+1} \left(C_n^m \cos(m\phi) + S_n^m \sin(m\phi)\right) P_n^m(\cos\theta). \quad (3.39)$$

But for a point

$$x = (a_1 + h, \theta, \phi) \quad (3.40)$$

where h could be for example the height of a satellite, the potential reads

$$V(a_1+h,\theta,\phi) = \frac{GM_1}{a_1} \sum_{n=0}^{N} \sum_{m=0}^{n} \left(\frac{a_1}{a_1+h}\right)^{n+1} \left(C_n^m \cos(m\phi) + S_n^m \sin(m\phi)\right) P_n^m(\cos\theta). \quad (3.41)$$

The factor

$$F_h^n = \left(\frac{a_1}{a_1+h}\right)^{n+1} = \left(\frac{a_1}{r}\right)^{n+1} \quad (3.42)$$

for a point with radius $r = a_1 + h$ with respect to the radius r is called attenuation factor and describes the field attenuation with the altitude. It is further dependent on the spherical harmonic degree n, $n = 0, \ldots, N$ for which it has been computed. This means, fractions of V^N which are described using only spherical harmonics of degree n attenuate at different rates. The higher the degree n, the faster the attenuation, see Figure 3.9.

Figure 3.9. *Attenuation factor* $F_h^n = \left(\frac{a_1}{a_1+h}\right)^n$ *varying with* h*, the distance from Earth, for different spherical harmonic degrees.*

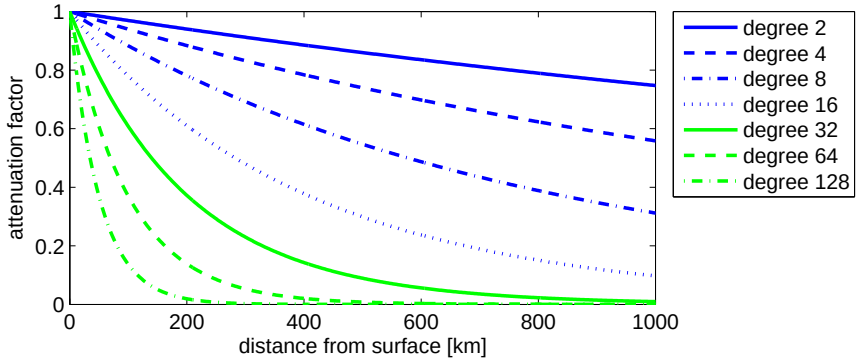

Due to the very fast, exponential drop of the model coefficients with the degree (see the signal amplitude per degree of the geoid model EGM96 in Figure 3.8), and also due to the factor $\left(\frac{a_1}{r}\right)^{n+1}$, which is smaller than 1 and decreases with increasing h, the smaller degree terms in the expansion V^N or U^N strongly influence the computation of the undulation values.

3.4.3 Convergence Issues

The convergence of a spherical harmonic expansion of the earths external gravitational potential has long been a point of discussion and has really raised the spirits. One can easily show that convergence can be assured for points of radius $r \geq r_1$ with r_1 the radius of the smallest sphere around the origin that completely encloses the mass of the earth. The radius r_1 is simply the maximum value that the radius of the earth can take and defines the so called Brillouin sphere [103]. The incident question is, whether $r \geq r_1$ is indeed necessary, i.e., if the spherical expansion converges everywhere outside the earth's surface. One can find in [105] a long list of established authors that have provided a wrong proof of convergence or divergence.

Figure 3.10. *The smallest sphere around the origin that completely encloses the masses of the earth.*

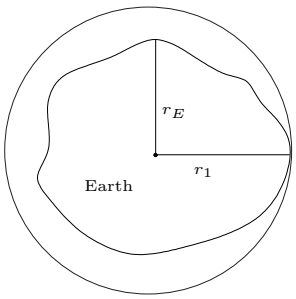

We found the following excerpt from [106], page 2, written by Prof. Dr. Helmut Moritz

to best possible describe the status of the discussion at the moment

> *Torben Krarup solved the problem of convergence or divergence of a spherical-harmonic development of the earths external gravitational potential at the earths surface. This was an old discussion among important people, which Krarup definitively solved by showing that it is a non-problem. Even if this series were originally convergent, it could be made divergent by an arbitrary small change of the potential (the well-known sand grain) [...] Which was much more important and difficult to prove, was that the opposite is also true. By an arbitrarily small change, the potential at the earth surface can be made convergent, even if the original potential expression was divergent. In mathematical terms, the set of convergent potentials were dense in the set of all potentials, in much the same sense as the set of rational numbers are dense within the set of real numbers. Measurements are always finite, with a definite number of reliable digits, and can thus always considered rational numbers. In the same way, measured spherical-harmonic series can always be considered convergent. By realizing this, Torben Krarup made a giant contribution to geodetic thinking. In my opinion, this was his greatest contribution, because he proved the convergence problem to be a non-problem. Still, few people have understood this, and convergence discussions still flare up from time to time.* [106]

Although the question of convergence has been found as meaningless, convergence can be still proved under some special assumptions, see [103] or [104]. Yet, the external potential cannot be generally be expanded by a spherical harmonic series which converges at the surface. Still, it is possible to approximate it uniformly by a finite linear combination of spherical harmonics on and outside of its surface. These linear combinations are dense within the set of convergent potentials: the appropriate linear combinations are then constructed by truncation of the corresponding spherical harmonic series [103], page 68.

3.4.4 Deficiencies of the Spherical Harmonic Representation

The spherical harmonic representation is well established, leaves space for little surprises but meets several critical limitations.

The first deficiency is related to the very high resolution demands which means that very large sets of coefficients must be computed. E.g., the official Earth Gravitational Model EGM2008 released by the National Geospatial-Intelligence Agency (NGA) EGM Development Team [115] complete to spherical harmonic degree and order 2159, contains more than 2 million coefficients extending to degree 2190 and order 2159 and models gravity field variations with a wavelength of 5 arc minutes. Further, the spherical harmonics are globally supported basis functions. The consequences are various. For example, updating a representation due to locally enhanced measurement data requires the new computation of the entire representation coefficients set. This requires handling very large and fully populated matrices.

Secondly, although the spherical harmonic representation is intrinsically global and not appropriate for regional representation, computations need to come up with irregularly distributed data. Measurements are not available over the entire surface of the earth, have

been taken at various heights and are eventually noisy. There are for example satellite-only models, although satellites have problems flying over poles due to missing light. The alternative is a combination of solutions involving both terrestrial and surface data, which is also not everywhere available. Alone in Africa there are large surfaces not covered at all. Complicated calibration and correction computations are necessary to compensate for the missing homogeneity in order to allow the determination of the model. But these techniques cannot compensate for the missing information.

These aspects rise the question of alternative representation methods. The wish list includes that the chosen basis functions are locally supported so that local computations and updates for the representation of the potential field can be undertaken. Heterogeneous data resolution calls for adaptivity and support of the variate data types and sources. Furthermore, the representation must regard the fact that the potential is harmonic everywhere outside the masses.

3.5 Boundary Problems in Geodesy

The geodetic boundary value problem is the determination of the earth's external gravity field and of the geoid from gravity related measurements. As measurements are generally provided on a surface, but the unknown gravity field is required in the complete three dimensional external space of the earth, we have to deal with the the solution of a boundary value problem. Since the exterior gravitational potential V, the disturbing potential T or the undulation U, which is directly calculated from T, are harmonic outside all masses, the boundary problems evolve around the Laplace equation. Just as in Section 2.2, depending on the type of the available boundary data, three different types can be formulated. The main difference resides in the fact that we now have an unbounded domain Ω outside of a spherical domain or of any domain representing the earth, where the solution has to be determined, see Figure 3.5. This unbounded domain represents the entire space outside the mass. Its surface becomes then the boundary $\partial\Omega$.

Figure 3.11. *Domain of boundary problems in Geodesy.*

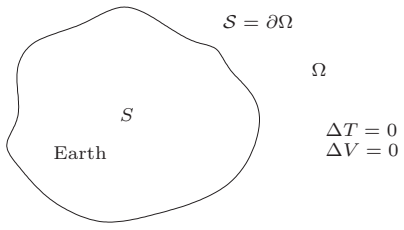

Further, in infinity, the disturbing potential, just as the potential itself, is regular, i.e. it takes the value null at an infinite distance from the mass:

$$T(\vec{x}) \to 0, |\vec{x}| \to \infty, \tag{3.43}$$

$$V(\vec{x}) \to 0, |\vec{x}| \to \infty. \tag{3.44}$$

This yields the regularity condition occurring in each geodetic boundary value problem.

3.5.1 Classical Upward Continuation of the Potential Field

We will concentrate on the so-called *first problem of geodesy* or also known as a refinement of the *first problem of potential theory*. It is in fact the Dirichlet boundary value problem for the Laplace equation. We are looking for a harmonic function. This can be e.g. the exterior gravitational potential, the disturbing potential or the computed undulation, here generically denoted by V in terms of the values taken at the boundary $V(S)$. Here, $V(S)$ stays for the surface of the earth, or, simplified, the surface of a sphere of radius R. We also assume that the boundary values are available as continuous functions.

Definition 3.5.1 (Dirichlet problem for the Laplace equation outside of the sphere). *Find solution $V \in \mathcal{C}^2(\Omega) \cap \mathcal{C}^0(\partial\Omega)$ on a domain Ω outside of a sphere containing the masses with respect to the given data the boundary $\partial\Omega$, the surface $\mathcal{S}$ of the sphere:*

$$\begin{cases} \Delta V(x,y,z) = & 0 & \text{in } \Omega, \\ V = & V(\mathcal{S}) & \text{on } \partial\Omega. \end{cases} \tag{3.45}$$

Since harmonic functions can be represented by linear combinations of spherical harmonics, which evolve intrinsically around spherical domains, recall from Section 2.4 the construction of spherical harmonics model. We stay with the geodetic formulation. We look for a solution V as a linear combination of spherical harmonics with the coefficient C_n^m for the spherical harmonic of degree n and order m. The coefficients C_n^m can be computed from the data on the sphere of radius R as in 3.28 and the representation yields

$$V(r,\theta,\phi) = \sum_{n=0}^{\infty} \left(\frac{R}{r}\right)^{n+1} \sum_{m=-n}^{n} C_n^m Y_n^m(\theta,\phi), \tag{3.46}$$

$$C_n^m = \frac{1}{4\pi} \int_s V(r,\theta,\phi) Y_n^m(\theta,\phi) ds. \tag{3.47}$$

We have therefore constructed a solution of the spherical Dirichlet boundary problem. Through equations (3.27) and (3.28) we have determined the representation of the harmonic function V anywhere in the exterior of the sphere S by computing the representation coefficients from the boundary values over the surface of the sphere $V(\mathcal{S})$. Though equation (3.27) can also be evaluated for points (r,θ,ϕ) inside the sphere, thus $r \geq R$, the values do not show the potential field inside the sphere, since the potential satisfies the Laplace equation only outside of the masses.

We have thereby constructed the upward continuation of the gravity data available on the sphere. But this calculation is not really feasible for application purposes. First, the data is required to be continuous over the entire sphere of radius R in order to at least theoretically even begin to compute the integral. Gravity measurements however are in fact discrete values. Further, in order to obtain accurate results, one has to deal with with huge amounts of data and the computation integral gets very intricated. Computations take therefore a very long time even on modern machines and the complexion is not justifiable. Last but not least, the model fails if only locally distributed data is available.

Another way is by means of least-squares collocation. We will not specify the method since it out scopes this work and there is plenty of literature available, see e.g. [99,103]. The

method is flexible and also mathematically very elegant. It is yet numerically problematic since it requires the a priori knowledge of the covariance function, which is critical to the solution, and also the inversion of large, full covariance matrices.

3.5.2 Interpretation and Non-uniqueness of Gravity Data

Before beginning the discussion, take a look again at the example of a buried sphere. We considered the fact that the gravitational attraction of a sphere equals that of a point source. Computing the gravitational attraction of a buried body is simple, but interpreting the local measurements of the generated anomaly is not, since, as we have seen in our example, more than one mass distribution can generate the same gravity anomaly. The non-uniqueness of the solution is the Achilles' heel of the inverse problems in geophysics. It holds also for the propagation of the geoid deviations: the continuation of different anomaly measurement configurations can lead to the same deviations at greater distances.

Example 3.5.2. *This example should give a first hint to the non-uniqueness problems in geodesy. To these problems belongs the fact that two different geologies can create the same anomaly and potential isosurface outside of the mass. We simply consider a buried sphere as in example 3.2.1. The mass of the sphere is the same, but now the sphere is smaller and, subsequently, of a higher density difference. The different mass distributions do indeed lead to the same gravity anomaly.*

This means, one can continue the gravity field outside the surface without knowing how the mass is distributed underneath the surface. We can differentiate between the upward and the downward continuation, depending on where the gravity data is provided, on the surface or in satellite hight. Yet the unicity of the solution of the Laplace equation is given by the boundary conditions, which must therefore be available even on the entire surface enclosing the mass, i.e. the earth. When can still attempt to construct continuation on isolated segments of the outer space of the earth, that is, to construct a local field continuation. The local upward continuation of the gravity field, together with theoretical and applicative aspects, is the subject of this work and will be specified in the following chapters.

Figure 3.12. *Nonuniqueness of the gravity anomalies with respect to the generating source: Gravity anomalies up to* $10km$ *height generated by a buried sphere. First considered geology: a massive sphere with radius* $r_S = 2km$ *and density deviation* $\rho_S = 1.6g/cm^3$ *buried at depth* $z = 6km$*. 2–dimensional section through the middle of the sphere (left) and isosurfaces of the field (right).*

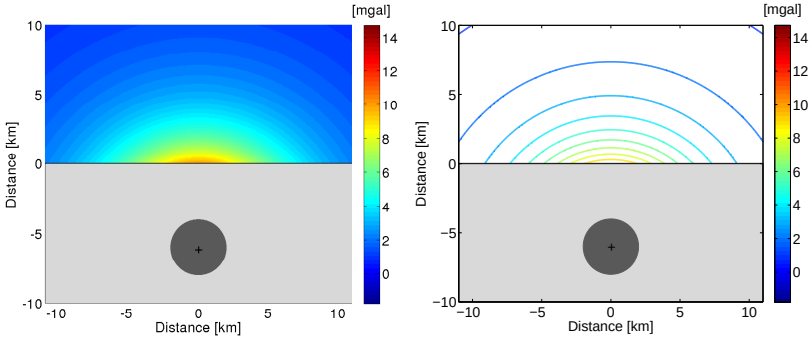

Figure 3.13. *Gravity anomalies up to* $10km$ *height generated by a buried sphere. Second considered geology: a massive sphere with radius* $r_S = 3km$ *and positive density deviation* $\rho_S = 0.2g/cm^3$ *buried underneath the origin at depth* $z = 6km$*. 2–dimensional section through the middle of the sphere (left) and isosurfaces of the field (right).*

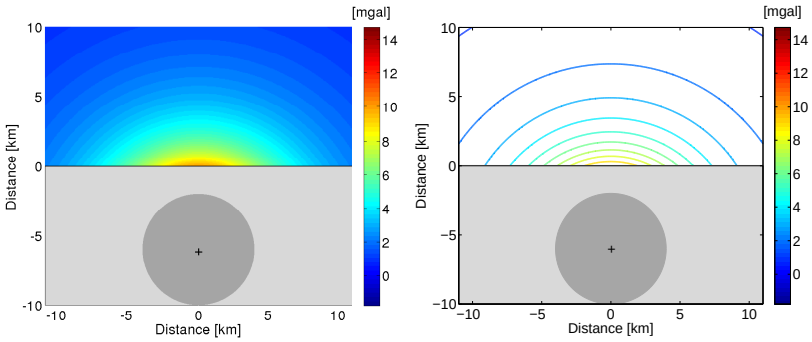

Figure 3.14. *Map of the undulations of the geoid, in centimeters, based on the EGM96 [92] gravity model up to the spherical harmonic expansion degree 10.*

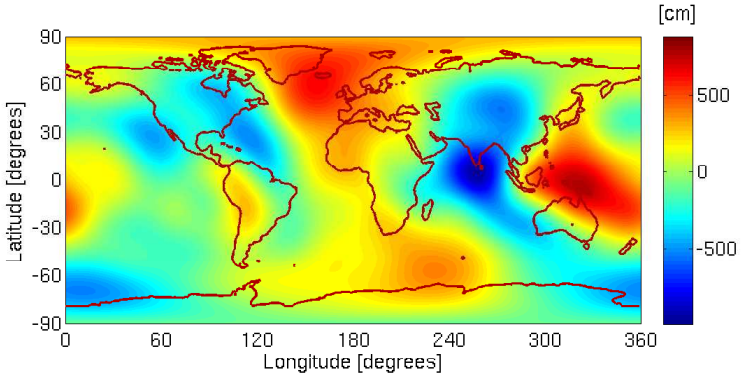

Figure 3.15. *Map of the undulations of the geoid, in centimeters, based on the EGM96 [92] gravity model up to the spherical harmonic expansion degree 30.*

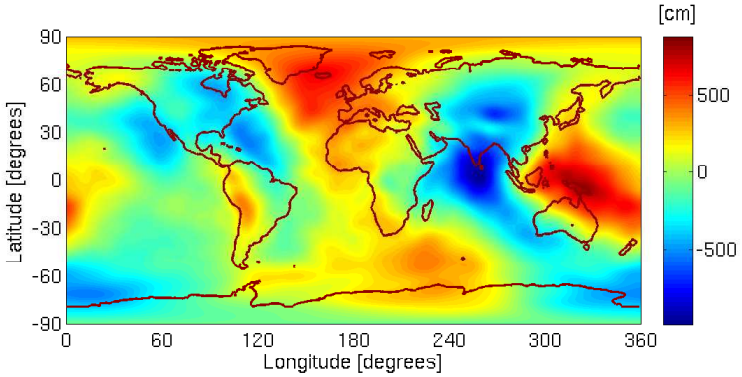

Figure 3.16. *Map of the undulations of the geoid, in centimeters, based on the EGM96 [92] gravity model up to the spherical harmonic expansion degree 300.*

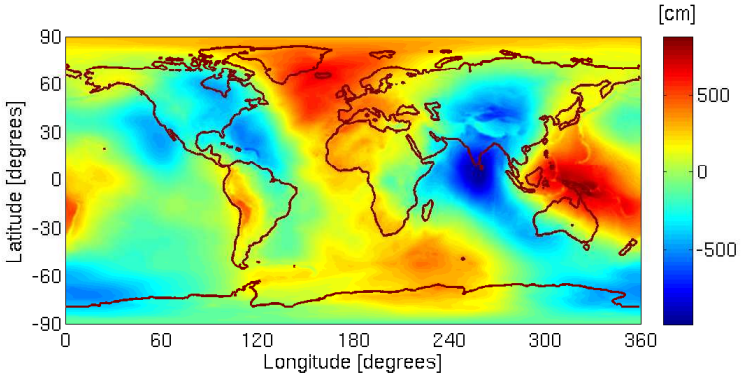

Figure 3.17. *Map of the* representation error *for geoid undulations of the EGM96 [92] gravity model up to the spherical harmonic expansion degree 10, compared the EGM96 [92] gravity model up to the spherical harmonic expansion degree 360, in centimeters.*

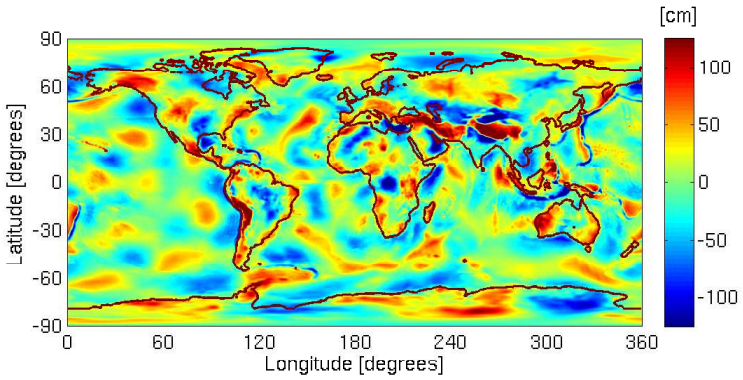

Figure 3.18. *Map of the* representation error *for geoid undulations of the EGM96 [92] gravity model up to the spherical harmonic expansion degree 30, compared the EGM96 [92] gravity model up to the spherical harmonic expansion degree 360, in centimeters.*

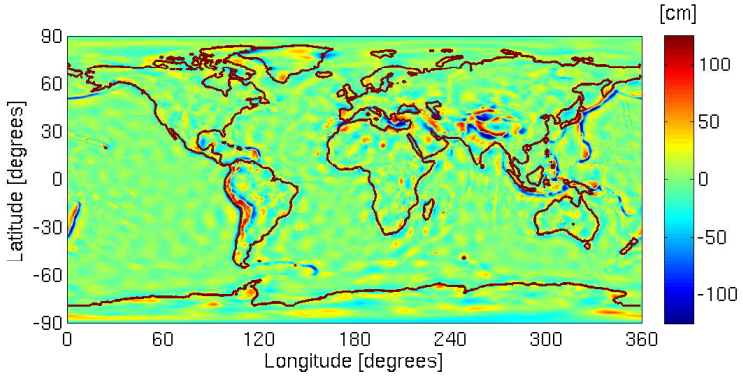

Figure 3.19. *Map of the* representation error *for geoid undulations of the EGM96 [92] gravity model up to the spherical harmonic expansion degree 100, compared the EGM96 [92] gravity model up to the spherical harmonic expansion degree 360, in centimeters.*

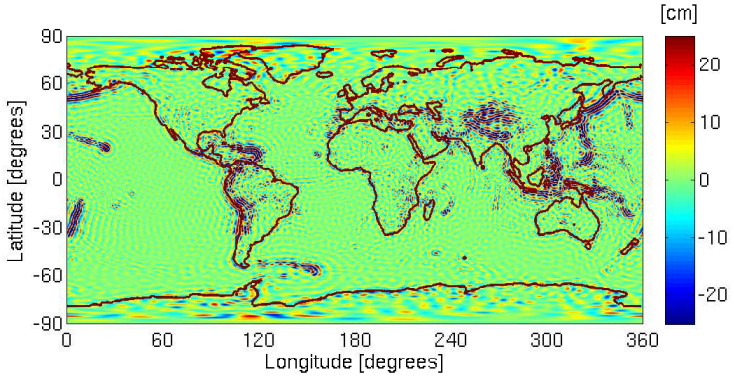

Chapter 4

New Approach: Least Squares with Regularization

In a true zero-defects approach, there are no unimportant items.

Philip Crosby, Reflections on Quality

In the previous chapter we have seen the main difficulties concerning the spherical harmonic representation and the upward continuation of the potential field. We look for another representation and an appropriate formulation of the upward continuation problem. In order to accommodate modern applications, our wish list includes the possibility of local and additionally, adaptive computations on bounded domains. We are also interested in a numerically – friendly method. Therefore we tend to work with formulations in terms of locally supported basis functions. Considering the data is heterogeneous available, the method should be able to cope with irregular distributions and noise.

Our work has been essentially inspired by P. Meissl, The use of finite elements in physical geodesy [99]. He compared several current methods of computational physical geodesy and investigated the feasibility of applying the finite element method to the fundamental problem of geodesy. For that, he considered the discretization of the potential outside of a sphere by means of Finite Elements. Distinctively, [99] used also a finite number of specially designed elements of infinite size to elaborately partition the infinite space by employing elements extending to infinity in radial direction, see Figure 4.1. In order to use functions which conform to the potential attenuation with the height, functions have been considered that they tend to zero also as the square of the distance from sphere:

$$f(r) \sim r^{-2} \quad \text{as} \quad r \to \infty. \tag{4.1}$$

The upward continuation is then obtained by

$$\int_{\Omega} (\Delta V)^2 d\Omega \to \min, \quad V = g \text{ at } \partial\Omega, \tag{4.2}$$

where Ω is the outer space of the sphere, $\partial\Omega$ its surface and g observed values at the surface. The experiments considered irregularly distributed observation points covering the entire surface of the sphere. In the absence of data homogeneity and regularity,

the Finite Element method turned out to be indeed asymptotically superior to spherical harmonics with respect to computational efficiency. Although there is the possibility of a local refinement, the problem remains, that observation points covering the entire surface of the sphere are still a must, i.e., one cannot compute on a bounded domain alone. Additionally, a large number of parameters are necessary to describe the potential on the reference surface due to poor conditioning.

Figure 4.1. *Domain partitions as in [99] Meissl, The Use of Finite Elements in Physical Geodesy, reproduced from pages 47 and 88 respectively.*

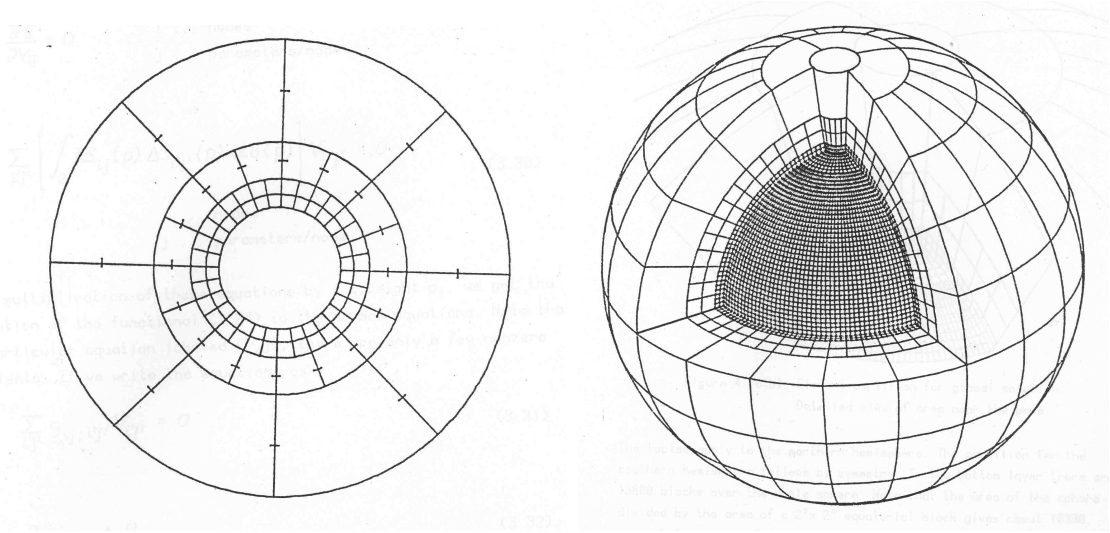

4.1 General Setup, Justification

On the way to another development we consider at first another choice of representation for the outer space of the earth. Here, a finite cuboid tangent lays at the surface of a sphere, outside of it, practically spanning the potential field of the earth between surface and satellite height, see Figure 1.1. We aim at local computations, i.e., the data is not available over the entire sphere but rather clustered. Without restriction of generality, we consider the smallest cuboid containing the data points and spanning the space up to the desired upward continuation target. Since geodetic applications mostly deal with surface and/or airborne data, our method takes just observation points situated on the upper and/or lower side of the cuboid and builds a local continuation. For a cuboid high enough we could also assume that the values on top of it are zero, considering in fact that the field has attenuated for points far away in outer space.

We consider the representation of a multivariate function in terms of locally supported basis functions on some fixed target domain $\Omega \subset \mathbb{R}^3$. An *approximate continuation* of a harmonic function would then be constructed from given data on a sub-domain $\Gamma \subset \Omega$ (typically consisting of boundary regions) and returning the expansion coefficients of the representation living on entire Ω. The given data may be discrete (point values) or

continuous (a function on Γ) and is assumed to stem from a harmonic function.

We start with a classical full grid data-fitting ansatz, as in [17]. Specifically, let Ω be some cuboid domain and let

$$\Omega_{\#} := \{x_i \in \Omega : i = 1, \ldots, N\} \tag{4.3}$$

consist of (not necessarily) uniformly gridded observation points covering all of Ω. For a subset of $M \ll N$ observation points of $\Omega_{\#}$ defining $\Gamma_{\#}$, let $z_i \in \mathbb{R}$ be given function values. The set

$$P_\Gamma := \{(x_i, z_i) : x_i \in \Gamma_{\#}, i = 1, \ldots, M\} \tag{4.4}$$

will then be the set of *input observation points*. We seek the representation of these data points in terms of a function expanded by linear combination of a locally supported basis $\Psi := \{\psi_\lambda : \lambda \in \Lambda\}$ with Λ a set of indices for the basis Ψ defined on Ω. So we determine the expansion coefficients $\mathbf{d} = (d_\lambda)_{\lambda\in\Lambda}$ for

$$u(x) := \sum_{\lambda\in\Lambda} d_\lambda \psi_\lambda(x) \,, \quad x \in \Omega, \tag{4.5}$$

which minimizes the functional

$$J(u) := \sum_{i=1}^{M} (u(x_i) - z_i)^2 \,. \tag{4.6}$$

In this setup of a least squares ansatz, the equations are assembled from observations alone. Further, in our case the observation points are available only on some subset Γ of the domain Ω. They are mostly clustered at the boundaries. At least when we are considering a full grid basis, but also in an adaptively constructed basis, some basis functions will have not contain any data points at all. Their coefficients cannot be determined. As a consequence, observations alone are not sufficient to determine the representation of the continuation. But the harmonicity of the potential field is not automatically implied in the generical data fitting representation, as it happens in the case of the spherical harmonics representation. We have also chosen not to consider harmonic basis functions since this property is not compatible with bounded support. Therefore, we search for a way to regard additional and essential information on the regularity of the solution. In order to obtain a continuation which is as close as possible to being harmonic, we suggest a combined strategy: simultaneously minimize the data fitting error over the sub-domain Γ and the Laplacian of the complete reconstruction over the full target domain Ω.

The enforcement of the harmonicity condition for the solution will be achieved by regarding an additional regularization term including the second derivative of u. This term consists of the integral of the Laplacian of the constructed continuation and will be minimized simultaneously with the reconstruction error of the available information points, here also called boundary data. This complementing integral will give the additional contribution to the normal equations under the control of a weight parameter, here named η. Of course, as also mentioned in [99], complete harmonicity is not granted by and eventually incompatible with this field representation and we can only target on an

approximate fulfillment of Laplace's equation. We will later see that this indulgence in complying with the harmonicity condition can be in fact beneficial.

The (upward) harmonic continuation of the boundary data is constructed by determining the coefficients $\mathbf{d} = (d_\lambda)_{\lambda\in\Lambda}$ for

$$u_\eta(x) := \sum_{\lambda\in\Lambda} d_\lambda \psi_\lambda(x), \quad x \in \Omega \tag{4.7}$$

which minimizes the functional

$$J_\eta(u_\eta) := \sum_{i=1}^{M} (u_\eta(x_i) - z_i)^2 + \eta \int_\Omega |\Delta u_\eta(x)|^2 \, dx \tag{4.8}$$

for a given weight parameter $\eta \geq 0$ and Δ the Laplace operator. This is what we call the *weighted least-squares approach with regularization.*

The main ingredient of this representation is the chosen basis $\Psi = \{\psi_\lambda : \lambda \in \Lambda\}$ with Λ the set of indices for the basis Ψ defined on Ω. As we have already mentioned, we consider only locally supported basis functions. The advantages are various. In contrast to the classical spherical harmonics approach, the matrices of resulting system of equations are sparse. This leads to more efficient computations. Also in contrast to globally supported representations, only some of the representation coefficients must be recomputed when updating the available data, namely those in the neighborhood of the corrected or added data points. Since the basis functions have compact support, we can undertake local computations, e.g., build the upper continuation over Europe alone without having to solve the problem over the entire outer space around the earth. Considering refinable representations calls for adaptive techniques. This will help construct the continuation with best possible accuracy only there, where this is really needed, e.g. along a trajectory, or only where finer data resolution is available.

The additional regularization term in (4.8), which makes the resulting continuation harmonic and determines the representation, emerges to be both the strength and Achilles' heel of the approach. The regularization itself, i.e., the minimization of the laplacian of the representation, makes the method naturally resistant against white noise. But deciding how to choose the weight parameter $\eta \geq 0$ in order to correctly determine the system may not be trivial. In a set up with homogeneous, globally distributed, error free data with sufficient resolution, the choice of η should be more or less irrelevant, since the laplacian should turn out null anyway. But we deal with an intrinsic ill posed problem. Experiments will show, choosing η too small leads to unsolvable systems and choosing it too large yields over–smoothed solutions. The detailed discussion will accompany the numerical experiments in Chapter 6.

4.2 Construction of the Solution

We choose at this point some arbitrary locally supported basis for Ψ constructed on the domain Ω in order to assure the evaluation of the two terms in (4.8). Let $L := \#\Lambda$ be the number of elements in the set of indices Λ on Ψ. Given the set of M information data

points in

$$P_\Gamma = \{(x_i, z_i) : x_i \in \Gamma_\#, i = 1, \ldots, M\}, \tag{4.9}$$

we look for $u_\eta : \Omega \to I\!R$ to approximately satisfy

$$u_\eta(x_i) = z_i, \ i = 1, \ldots, M, \tag{4.10}$$

$$\Delta u_\eta = 0 \quad \text{over } \Omega \tag{4.11}$$

where

$$u_\eta = \sum_{\lambda \in \Lambda} d_\lambda \psi_\lambda \tag{4.12}$$

is a function that is a linear combination of L given basis functions living over Ω

$$\Psi = \{\psi_\lambda : \lambda \in \Lambda\}. \tag{4.13}$$

As mentioned, our approach simultaneously minimizes the data fitting error over the information data points and the laplacian of the computed solution of the continuation problem. The terms in (4.8) generate under the basis Λ the two system matrices. The system matrix is than the weighted sum of these two.

4.2.1 Data Fitting

We can solve this data-fitting problem of finding the coefficients $d_\lambda, \lambda \in \Lambda$ to minimize

$$J(u) = \sum_{i=1}^{M} (u(x_i) - z_i)^2 \tag{4.14}$$

by classically solving the linear least squares problem translated in the matrix form

$$\|\mathbf{A}\mathbf{d} - \mathbf{z}\|_2^2 \to \min, \tag{4.15}$$

with

$$\mathbf{A} := (\mathbf{A}_{i\ell})_{\substack{i = 1 \ldots M \\ \ell = 1 \ldots L}}, \ \mathbf{A}_{i\ell} := \psi_\ell(x_i), \quad \mathbf{d} = (d_\lambda)_{\lambda \in \Lambda}, \quad \mathbf{z} = (z_i)_{(x_i, z_i) \in P_\Gamma}. \tag{4.16}$$

The unknowns of the system are $\mathbf{d} = (d_\lambda)_{\lambda \in \Lambda}$, the expansion coefficients. Notice that we have more information data points than basis functions. This is due to the nature of the upward continuation setup, where numerous but badly distributed points are available to determine the solution of an ill-posed problem. This means,

$$\mathbf{A} \in I\!R^{M \times L}, \quad M \gg L. \tag{4.17}$$

Since the system is over determined, we consider another matrix formulation of the problem. It is possible, that there is no solution to the system. However, if one solution u_η exists, than we have $\sum_{i=1}^{M} (u_\eta(x_i) - z_i)^2 = 0$. Intuitively we expect, that the data-fitting residual $\mathbf{A}\mathbf{d} - \mathbf{z}$ must be perpendicular on $\{Ax : x \in I\!R^L\}$ if $\mathbf{A}\mathbf{d} - \mathbf{z} \to \min$. The

minimum is attained where the gradient of $\sum_{i=1}^{M}\left(u_\eta(x_i)-z_i\right)^2$ is zero. So, taking the $\frac{\partial}{\partial d_\lambda}$ derivatives of $\sum_{i=1}^{M}\left(u_\eta(x_i)-z_i\right)^2$ for $\lambda\in\Lambda$ gives the first share of the normal equations of the data-fitting part of the problem. On minimizing $\sum_{i=1}^{N}(z_i-u_\eta(x_i))^2$, we require $\forall\lambda\in\Lambda$:

$$\begin{aligned}\frac{\partial}{\partial d_\lambda}\left(\sum_{i=1}^{M}(z_i-u_\eta(x_i))^2\right) &= \sum_{i=1}^{M}\frac{\partial}{\partial d_\lambda}\left(z_i-u_\eta(x_i)^2\right)\\ &= \sum_{i=1}^{M}2\left(z_i-u_\eta(x_i)\right)\frac{\partial}{\partial d_\lambda}u_\eta(x_i)\ =\ 0.\end{aligned}\tag{4.18}$$

As $u_\eta(x_i)=\sum_{\lambda'\in\Lambda}d_{\lambda'}\psi_{\lambda'}(x_i)$, than $\frac{\partial}{\partial d_\lambda}u_\eta(x_i)=\psi_\lambda(x_i)$. We need therefore:

$$\sum_{i=1}^{M}2\left(z_i-u_\eta(x_i)\right)\psi_\lambda(x_i)=\sum_{i=1}^{M}2\left(z_i-\sum_{\lambda'\in\Lambda}d_{\lambda'}\psi_{\lambda'}(x_i)\right)\psi_\lambda(x_i)=0,\tag{4.19}$$

or finally,

$$\sum_{i=1}^{M}z_i\psi_\lambda(x_i)=\sum_{\lambda'\in\Lambda}d_{\lambda'}\left(\sum_{i=1}^{M}\psi_{\lambda'}(x_i)\psi_\lambda(x_i)\right).\tag{4.20}$$

Rewriting this in a matrix form we set:

$$\mathbf{M}\mathbf{d}=\mathbf{b}\tag{4.21}$$

with the entries of the observation matrix $\mathbf{A}$ and of the crossed-product matrix $\mathbf{M}=\mathbf{A}^{\mathrm{T}}\mathbf{A}$ defined by

$$\mathbf{M}:=(\mathbf{M}_{\ell\ell'})_{\ell,\ell'=1\ldots L},\ \mathbf{M}_{\ell\ell'}:=\sum_{i=1}^{M}\psi_\ell(x_i)\psi_{\ell'}(x_i).\tag{4.22}$$

The vector $\mathbf{d}=(d_\lambda)_{\lambda\in\Lambda}$ solves the minimization of $\sum_{i=1}^{M}\left(u(x_i)-z_i\right)^2,(x_i,z_i)\in P_\Gamma$ when $\mathbf{d}$ solves

$$\mathbf{A}^T\mathbf{A}\mathbf{d}=\mathbf{A}^T\mathbf{z}.\tag{4.23}$$

Furthermore, $\mathbf{b}=\mathbf{A}^{\mathrm{T}}\mathbf{z}$ is the right hand side for $\mathbf{z}$ the vertical values from the input observation points set $P_\Gamma=\{(x_i,z_i):\ x_i\in\Gamma_\#,\ i=1,\ldots,M\}$. The available information is processed to the right hand side as

$$\mathbf{b}=\mathbf{A}^{\mathrm{T}}\mathbf{z},\ \mathbf{b}:=(\mathbf{b}_\ell)_{\ell=1,\ldots,L},\ \mathbf{b}_\ell=\sum_{i=1}^{M}z_i\psi_\ell(x_i).\tag{4.24}$$

The normal equation system has at least one solution which is unique if the quadratic matrix $\mathbf{M}=\mathbf{A}^T\mathbf{A}$ with size$(\mathbf{M})=(L,L)$ has full rank. Yet, since the data is badly scattered and depending on the cardinality and support size of the considered basis, the

matrix will most probably not be invertible. [17] investigated some invertibility criteria for the matrix M depending on the data to be fitted. He reduced this issue to a local check if the support of each basis function contains a sufficient number of properly distributed data points. But since in our case the data is available scattered at the boundary and the basis functions should not have a large support, we are bound to fail this intuitive criteria.

If we would want to solve simply $\mathbf{Ad} = \mathbf{z}$ with direct solvers like the QR methods, we would have difficulties exploiting the sparse nature of $\mathbf{A}$. The alternatives are iterative methods like conjugate gradients for least squares. Solving the normal equation system $\mathbf{A}^T\mathbf{Ad} = \mathbf{A}^T\mathbf{z}$ is not always preferred to solving $\mathbf{Ad} = \mathbf{z}$. This is because information may get lost within the additions in $\mathbf{M}_{\ell\ell'} = \sum_{i=1}^{M} \psi_\ell(x_i)\psi_{\ell'}(x_i)$ and $\mathbf{b}_\ell = \sum_{i=1}^{M} z_i\psi_\ell(x_i)$. But when the different levels are orthogonal with respect to L_2, the matrices turn out to be block diagonal. Not only that they are sparse and symmetric, but they have further good numerical properties. A conditioning of the basis has then a positive effect on the condition number of the results system matrix. The sequence of matrices $\mathbf{M} = \mathbf{A}^T\mathbf{A}$ for varying basis levels has uniformly bounded condition numbers if the considered basis is uniformly stable [17]. See Chapter 7 to find more on stability issues.

4.2.2 Enforcing Harmonicity

It remains to adapt the harmonicity constraint to the matrix formulation. For this we write $\int_\Omega |\Delta u(x)|^2 \, dx$, the H^2 semi-norm of $u_\eta(x) = \sum_{\lambda\in\Lambda} d_\lambda\psi_\lambda(x)$ as a quadratic form over the expansion coefficients $\mathbf{d} = (d_\lambda)_{\lambda\in\Lambda}$

$$\begin{aligned} |u_\eta|_{H^2}^2 dx &= \int_\Omega \Big|\Delta \sum_{\lambda\in\Lambda} d_\lambda\psi_\lambda(x)\Big|^2 dx = \int_\Omega \Big|\sum_{\lambda\in\Lambda} d_\lambda\Delta\psi_\lambda(x)\Big|^2 dx \\ &= \int_\Omega \Big(\sum_{\lambda\in\Lambda} d_\lambda\Delta\psi_\lambda(x)\Big)\Big(\sum_{\lambda'\in\Lambda} d_{\lambda'}\Delta\psi_{\lambda'}(x)\Big)dx \\ &= \sum_{\lambda,\lambda'\in\Lambda} d_\lambda d_{\lambda'} \int_\Omega \Delta\psi_\lambda\Delta\psi_{\lambda'}dx \\ &=: \mathbf{d}^{\mathrm{T}}\mathbf{G}\mathbf{d} \end{aligned} \tag{4.25}$$

with

$$\mathbf{G} := (\mathbf{G}_{\ell\ell'})_{\ell,\ell'=1\ldots L},\ \mathbf{G}_{\ell\ell'} := \int \Delta\psi_\ell(x)\Delta\psi_{\ell'}(x)dx. \tag{4.26}$$

4.2.3 Resulting System of Equations

As we have seen, the minimization of the functional (4.8) can be computed by solving the following normal equations:

$$(\mathbf{M} + \eta\mathbf{G})\,\mathbf{d} = \mathbf{b}, \quad \mathbf{M} = \mathbf{A}^{\mathbf{T}}\mathbf{A}, \quad \mathbf{b} = \mathbf{A}^{\mathbf{T}}\mathbf{z}. \tag{4.27}$$

Since the system matrix $\mathbf{M} + \eta\mathbf{G}$ is symmetric and positive definite, we can employ both a direct or an iterative solver. In order to assess the quality of the obtained approximation, we compare u_η on Ω with an original data set on the full domain

$P_\Omega = \{(x_i, z_i) : x_i \in \Omega_\#,\ z_i \in \mathbb{R},\ i = 1, \ldots, N\}$ obtained by a spherical harmonics approach with standard linear interpolation of the discrete values for visualization purposes. In addition, we compute an approximate continuation by solving the Laplace equation with boundary conditions derived from the original data set by means of Finite Elements and Finite Differences and also compare it to the approximate continuation u_η

4.3 Concrete Choices

4.3.1 B-Splines

This section presents the theory of B-splines of arbitrary degree which are essential for our work. B-splines have been constructed originally as convolutions of certain probability distributions, see [121]. Nowadays, one can find two approaches for defining them. First, by means of divided differences, as in de Boor's Practical Guide to Splines [35]; or by means of recurrence relations, as in texts like [72, 87]. Though B-spline properties are univocally determined, we will take a look at both procedural methods in order to gain a better understanding. We begin with a very intuitive view of B-splines, namely the average process, as in [72]. We will continue by describing aspects of the construction of the uniform B-spline basis by means of the scaled and translated B-splines. Later, we will present the boundary adaptation and its essential ingredient, the knot multiplicity.

Let Π_{n-1} denote the space of all polynomials in one variable of order at most n, i.e. degree at most $n-1$.

Definition 4.3.1 (B-splines). *The uniform B-spline b^n of degree n on the uniform mesh is defined by the recursion*

$$b^n(x) = \int_{x-1}^{x} b^{n-1}(\tilde{x})d\tilde{x} \tag{4.28}$$

starting with b^0 as the characteristic function on the interval $[0, 1)$.

Proposition 4.3.2. *The following hold for the B-splines defined above:*

(a) b^n is locally supported and positive on the interval $(0, n-1)$,

(b) b^n is piecewise polynomial that is, for any integer n

$$b^n|_{[j,j+1]} \in \Pi_{n-1}, j \in \mathbb{Z}, \tag{4.29}$$

(c) b^n is $n-1$ times continuously differentiable with discontinuities of the n-th derivative at the break points $0, \ldots, n+1$,

(d) b^n is strictly monotone on $[0, (n+1)/2]$, $[(n+1)/2, n+1]$ and is symmetric, i.e

$$b^n(x) = b^n(n+1-x), \tag{4.30}$$

(e) B-splines meet the recurrence relation

$$b^n(x) = \frac{x}{n} b^{n-1}(x) + \frac{n+1-x}{n} b^{n-1}(x-1), \tag{4.31}$$

(f) further,

$$\int_{-\infty}^{\infty} b^n(x)dx = 1. \tag{4.32}$$

We will now see how to use B-splines for interpolation purposes. For that, let $\Delta = \{\tau_i\}_{i=0,\ldots,l+1}$ be a knot sequence of $l+2$ points with

$$a = \tau_0 < \tau_1 < \ldots < \tau_{l+1} = b. \tag{4.33}$$

Definition 4.3.3 (Univariate spline space). *For a knot sequence Δ and degree k, let the space*

$$S_{k,\Delta} = \left\{ S \in \mathcal{C}^{k-2}([a,b]) : S|_{[\tau_i,\tau_{i+1})} \in \Pi_k, \forall i = 0,\ldots,l \right\} \tag{4.34}$$

be the spline space of order k and knot sequence Δ.

In order to discuss the dimension of this space, we make use of the following construction in terms of truncated power functions.

Definition 4.3.4 (Truncated power function). *Given a function f, the truncated power function is defined as*

$$f_+^n := \begin{cases} f^n & \text{if } f \geq 0 \\ 0 & \text{if } f < 0 \end{cases}. \tag{4.35}$$

Let $f \in S_{k,\Delta}$, then

$$f|_{[\tau_i,\tau_{i+1}]} = p_{i+1} \in \Pi_{k-1}. \tag{4.36}$$

The corroboration with the continuity conditions

$$(p_{i-1} - p_i)^{(j)}(\tau_i) = 0, j = 0,\ldots,k-2 \tag{4.37}$$

leads to

$$p_{i+1}(x) = p_i(x) + c_i(x-\tau_i)^{k-1} \tag{4.38}$$

with constant c_i. We write f for $x \in [\tau_i, \tau_{i+1}]$ as

$$f(x) = p_1(x) + \sum_{j=1}^{i} c_j(x-\tau_j)^{k-1} \tag{4.39}$$

and in terms of truncated powers for $x \in [a,b]$

$$f(x) = p_1(x) + \sum_{j=1}^{l} c_j(x-\tau_j)_+^{k-1}. \tag{4.40}$$

The set

$$\left\{ 1, \ldots, x^k, (x-\tau_1)_+^k, \ldots, (x-\tau_l)_+^k \right\} \tag{4.41}$$

with linearly independent functions belonging to $S_{k,\Delta}$ is also a basis for $S_{k,\Delta}$. Yet these basis functions are globally supported, which is disadvantageous from the computational point of view. Therefore, we look for locally supported basis functions. In fact, we will see that B-splines build a minimal supported basis for $S_{k,\Delta}$.

Definition 4.3.5 (B-Splines). *For a knot sequence $\Delta = \{\tau_i\}_{i=0,\dots,l+1}$ with*

$$a = \tau_0 < \tau_1 < \ldots < \tau_{l+1} = b \tag{4.42}$$

we define the B-splines $N_{i,k}(x)$ of order k with respect to $\tau_i, \dots, \tau_{i+k}$ for $k = 1, \dots, l$ and $i = 0, \dots, l-k+1$ recursively by

$$N_{i,1}(x) = \chi[\tau_i, \tau_{i+1}](x) = \begin{cases} 1 & \text{if} \quad x \in [\tau_i, \tau_{i+1}] \\ 0 & \text{otherwise,} \end{cases} \tag{4.43}$$

$$N_{i,k}(x) = \frac{x - \tau_i}{\tau_{i+k-1} - \tau_i} N_{i,k-1}(x) + \frac{\tau_{i+k} - x}{\tau_{i+k} - \tau_{i+1}} N_{i+1,k-1}(x). \tag{4.44}$$

Proposition 4.3.6. *The following properties hold for the B-splines defined in 4.3.5*

(a) (local support) $\operatorname{supp} N_{i,k} \subseteq [\tau_i, \tau_{i+k}]$,

(b) (not-negativity) $N_{i,k}(x) > 0$ for all $x \in [a, b]$,

(c) (point wise polynomial) $N_{i,k}(x)|_{[\tau_i, \tau_{i+k})} \in \Pi_k$,

(d) (partition of unity) $\sum_i N_{i,k}(x) = 1$ for all x,

(e) (recursion formula for derivation of B-splines)

$$N'_{i,k}(x) = (k-1) \left(\frac{N_{i,k-1}(x)}{\tau_{i+k-1} - \tau_i} - \frac{N_{i+1,k-1}(x)}{\tau_{i+k} - \tau_{i+1}} \right), \tag{4.45}$$

(f) (recursion formula for derivation of B-splines series) for $\alpha_i \in \mathbb{R}$ coefficient for $N_{i,k}$ it holds [35]

$$\left(\sum_i \alpha_i N_{i,k}(x) \right)' = \sum_i (k-1) \frac{\alpha_i - \alpha_{i-1}}{\tau_{i+k-1} - \tau_i} N_{i,k-1}(x), \tag{4.46}$$

(g) (recursion formula for integration of B-splines series) for $\alpha_i \in \mathbb{R}$ coefficient for $N_{i,k}$ it holds [35]

$$\int_{\tau_1}^{x} \sum_i \alpha_i N_{i,k}(x) = \sum_{i=1}^{s-1} \left(\sum_{j=1}^{i} \frac{\alpha_j (\tau_{j+k} - \tau_j)}{k} \right) N_{i,k+1}(x) \tag{4.47}$$

with s so, that $x \in [\tau_1, \tau_s]$.

B-spline series are a very important tool for the local representation of a spline function. The following proposition due to Marsden [97] shows us how to generate other polynomials in Π_k. For that, we define the extended knot sequence by means of knot multiplicity at the boundaries

$$T := \{\theta_i\}_{i=1,\ldots,n+k} \tag{4.48}$$

with $\theta_i < \theta_{i+k}$ for $i = 1, \ldots, n$, and

$$\theta_1 = \ldots = \theta_k = a < \theta_{k+1} \leq \ldots \leq \theta_n < b = \theta_{n+1} = \ldots = \theta_{n+k}. \tag{4.49}$$

Further, let $\mathcal{N}_k(T)$ be the set of all linear combinations of the B-splines over the knot sequence T:

$$\mathcal{N}_k(T) = \mathcal{N}_{k,T} := \operatorname{span}\{N_{i,k} : i = 1, \ldots, n\}, \tag{4.50}$$

which means that each element $S \in \mathcal{N}_k(T)$ can be written in terms of B-spline series as

$$S(x) = \sum_{i=1}^{n} c_i N_{i,k}(x), \quad x \in [a, b]. \tag{4.51}$$

Proposition 4.3.7 (Marsden's Identity). *For all $x \in [a, b]$ and $\sigma \in \mathbb{R}$ it holds*

$$(x - \sigma)^{k-1} = \sum_{i=1}^{n} \prod_{j=1}^{k-1} (\theta_{i+j} - \sigma) N_{i,k}(x) \tag{4.52}$$

$$= \sum_{i=1}^{n} \varphi_{i,k}(\sigma) N_{i,k}(x), \tag{4.53}$$

whereas

$$\phi_{i,k}(\sigma) := \Pi_{j=1}^{k1}(\theta_{i+j} - \sigma). \tag{4.54}$$

Here are some direct, yet essential consequences.

Corollary 4.3.8. $\Pi_{k-1} \subseteq \mathcal{N}_k(T)$.

Corollary 4.3.9. $\sum_i N_{i,k}(x) = 1$ *for all* $x \in [a, b]$.

Proposition 4.3.10 (Linear independence over the interval). *If* $\sum_{i=1}^{n} c_i N_{i,k}(x) = 0$ *for* $x \in (c, d) \subseteq [a, b]$ *and* $(c, d) \cap (\theta_i, \theta_{i+k}) \neq \emptyset$, *then* $c_i = 0$.

Proposition 4.3.11. *For the knot sequence Δ and the extended knot sequence T as defined in 4.48 with identical outer knots, i.e. for $\tau_i \in \Delta$ and $\theta_{i+k} \in T$ it holds $\tau_i = \theta_{i+k}, i = 0, \ldots l + 1$, we have*

$$S_{k,\Delta} = \mathcal{N}_{k,T}, \tag{4.55}$$

i.e. the B-splines of order k build a basis for the spline function space $S_{k,\Delta}$.

In order to discuss the stability of the B-spline basis, we present another essential concept.

Definition 4.3.12 (Dual basis). *A vector space V has a corresponding dual vector space V^* of the same size as V consisting of all linear functionals on V. So for us, the set of linear functionals $\{\lambda_j\}_{j=1,\dots,n}$ defined on $S_{k,\Delta}$ is called a dual basis if*

$$\lambda_j N_{i,k} \;=\; \delta_{ji} = \begin{cases} 1 & \text{if } i = j \\ 0 & \text{else} \end{cases}. \tag{4.56}$$

The dual basis is very useful since for the B-spline series we have, that, if $s = \sum_{i=1}^{n} c_i N_{i,k}$ then

$$\lambda_i s = c_i, \quad i = 1 \dots, n. \tag{4.57}$$

This further allows us to correlate the size of the spline and the size of its coefficients.

Proposition 4.3.13 (Stability of the B-splines basis). *For the B-spline series $\sum_{i=1}^{n} c_i N_{i,k}$ and $\mathbf{c} = \{c_i\}_{i=1,\dots,n}$ it holds*

$$C_k \|\mathbf{c}\|_\infty \leq \left\| \sum_{i=1}^{n} c_i N_{i,k} \right\|_{\infty,[a,b]} \leq \|\mathbf{c}\|_\infty. \tag{4.58}$$

The upper bound is a consequence of the division of unity property (4.3.9). The lower bound follows from (4.57). Once we have constructed a dual basis, we choose C_k as

$$C_k = \frac{1}{\max_{1\leq i\leq n} \|\lambda_i\|}, \quad \|\lambda_i\| = \sup_{s\in S_{k,\Delta}, s\neq 0} \frac{|\lambda_i s|}{\|s\|_\infty}. \tag{4.59}$$

Proposition (4.3.13) states that the B-splines build an unconditionally stable basis for $S_{k,\Delta}$ because the B-spline series $\sum_{i=1}^{n} c_i N_{i,k}$ can be, independently from the knot sequence Δ, lower and upper estimated by the coefficients $\{c_i\}_{i=1,\dots,n}$. Therefore, one can say that a B-spline basis is well conditioned. Adaptive computations in terms of multiscale basis require that the equation (4.58) in terms of the L_2–norm holds. For that we present in Chapter 7 the L_p–normalized B-spline basis and include a detailed discussion on the underlying stability issues.

Since in our work we employ nested B-spline spaces defined on nested grids, which are practically nested knot sequences, we now consider the uniform knot sequence

$$T^h := \{\theta_i\}_{i=1,\dots,n+k} \tag{4.60}$$

over $[a, b]$ with $\theta_i < \theta_{i+k}$ for $i = 1, \dots, n$, and for mesh size h:

$$a < \theta_1 < \theta_2 = \theta_1 + h < \dots < \theta_n = \theta_{n-1} + h < b = \theta_{n+1} = a + h(n-1). \tag{4.61}$$

Obviously,

$$T^h \subset T^{h/2}. \tag{4.62}$$

Then let the B-splines $N_{i,k}^h$ be the B-splines $N_{i,k}$ with respect to the uniform knot sequence T^h

$$N_{i,k}^h = N_{i,k}(T^h). \tag{4.63}$$

The following statement is important for the construction of the hierarchical B-splines basis.

Proposition 4.3.14 (Grid refinement). *[72] The subdivision formula for B-spline holds as: the B-spline $N_{i,k}^h$ defined over T^h can be expressed as a linear combination of the B-splines $N_{i,k}^{h/2}$ defined over $T^{h/2}$:*

$$N_{i,k}^h = 2^{-k+1} \sum_{l=0}^{k} \binom{k}{l} N_{2i+l,k}^{h/2}. \tag{4.64}$$

Proof 4.3.15. *The proof succeeds by induction for k; we present here the main arguments, see [72] for details. We begin with the piecewise linear, i.e., 2nd order B-splines; it is clear that*

$$N_{i,2}^h = \frac{1}{2} \sum_{l=0}^{2} \binom{2}{l} N_{2i+l,2}^{h/2} = \frac{N_{2i,2}^{h/2}}{2} + N_{2i+1,2}^{h/2} + \frac{N_{2i,2}^{h/2}}{2} \tag{4.65}$$

holds. For the inductory step we first consider the recursion formula for the derivation of B-splines as in (4.45) for uniform knot sequence with mesh size h; here we have $\theta_{i+1} = \theta_i + h$ for $i = 1, \ldots, n$ and the derivation can be carried out as

$$\begin{aligned} {N_{i,k}^h}'(x) &= (k-1) \left(\frac{N_{i,k-1}^h(x)}{\theta_{i+k-1} - \theta_i} - \frac{N_{i+1,k-1}^h(x)}{\theta_{i+k} - \theta_{i+1}} \right) \\ &= h^{-1} \left(N_{i,k-1}^h(x) - N_{i+1,k-1}^h(x) \right). \end{aligned} \tag{4.66}$$

We now derivate (4.64); the left side derivatives are as in (4.66) and the right side becomes:

$$2^{-k+1} \sum_{l=0}^{k} \binom{k}{l} {N_{2i+l,k}^{h/2}}' = 2^{-k+1} \sum_{l=0}^{k} \binom{k}{l} \left(\frac{h}{2} \right)^{-1} \left(N_{2i+l,k-1}^{h/2} - N_{2i+l+1,k-1}^{h/2} \right). \tag{4.67}$$

Considering that both sides vanish at the knots of the sequence, we have to prove the equivalent statement

$$N_{i,k-1}^h(x) - N_{i+1,k-1}^h(x) = 2^{-k+2} \sum_{l=0}^{k} \binom{k}{l} \left(N_{2i+l,k-1}^{h/2} - N_{2i+l+1,k-1}^{h/2} \right). \tag{4.68}$$

From the induction hypotheses, it holds:

$$N_{i,k-1}^h = 2^{-k+2} \sum_{l=0}^{k-1} \binom{k-1}{l} N_{2i+l,k-1}^{h/2}, \tag{4.69}$$

$$N_{i+1,k-1}^h = 2^{-k+2} \sum_{l=0}^{k-1} \binom{k-1}{l} N_{2i+2+l,k-1}^{h/2}. \tag{4.70}$$

The rest of the proof follows regarding that

$$N^h_{i+1,k-1}(x) = N^h_{i,k-1}(x-h), \tag{4.71}$$

$$N^{h/2}_{2i+l,k-1}(x-h) = N^{h/2}_{2i+l+2,k-1}(x) \tag{4.72}$$

and with an exercise in combinatorial computation when comparing the coefficients for each of the B-splines.

4.3.2 Tensor Product Spaces

As our work deals with representation of multivariate data, we have turned to one of the most uncomplicated, yet multivariate spline formulations, namely tensor product B-splines. This particular choice allows for computations to be carried out dimension–wise in terms of one-dimensional B-spline bases, which is very convenient. Consider for that e.g. the aspects of differential nature involved in our continuation of harmonic functions. The computation of the Laplacian of a solution involves indeed a separation of the dimensions and we can profit from the tensor product construction.

In order to further discuss the essential aspects of tensor product B-splines, we begin with a brief characterization of the tensor products in terms of vector and Hilbert spaces as in [93]. Later, we will transfer these properties to multivariate construction via tensor-product B-splines.

The tensor product is a formal bi-linear multiplication of two modules or vector spaces. The tensor product of two vector spaces V and W over a field, denoted by $V \otimes W$, also called the tensor direct product, is a way of creating a new vector space and has a formal definition by the method of generators and relations.

Definition 4.3.16. *The vector space $V \otimes W$ is spanned by elements of the form $v \otimes w$ with $v \in V$ and $w \in W$.*

The following basic proprieties of tensors operands hold by construction.

Proposition 4.3.17.

(a) $(v_1 + v_2) \otimes w = v_1 \otimes w + v_2 \otimes w,\ v_1, v_2 \in V,\ w \in W,$

(b) $v \otimes (w_1 + w_2) = v \otimes w_1 + v \otimes w_2,\ v \in V,\ w_1, w_2 \in W,$

(c) $\alpha(v \otimes w) = (\alpha v) \otimes w = v \otimes (\alpha w),\ v \in V,\ w \in W,\ \alpha$ *scalar,*

(d) $0 \otimes w = v \otimes 0 = 0.$

Further, in terms of properties of the resulting space we have the following.

Proposition 4.3.18.

(a) for V and W, the resulting tensor product space $V \otimes W$ is also a vector space,

(b) for $\{v_i\}_{i=1,\ldots,n}$ and $\{w_j\}_{j=1,\ldots,m}$ bases of V and W, respectively, the tensor product set $\{v_i \otimes w_j\}_{i=1,\ldots,n,j=1,\ldots,m}$ forms a basis for $V \otimes W$,

(c) $\dim(V \otimes W) = \dim(V)\dim(W)$.

Each $u \in U = V \otimes W$ has therefore the unique representation

$$u = v_i \otimes w_j, \quad v_i \in V,\ w_j \in W. \tag{4.73}$$

Consider in more detail the tensor product of Hilbert spaces. For this we remember that a Hilbert space is a vector space with a norm $\|\cdot\|$ induced by a scalar product $\langle\cdot,\cdot\rangle$. So, for the tensor product of two Hilbert spaces, we are interested in an inner product for the resulting tensor product space in terms of the inner products associated to the original spaces. This will allow us to formulate some statements about the dual space of the tensor product space.

Let H_1 and H_2 be two Hilbert spaces with inner products $\langle\cdot,\cdot\rangle_1$ and $\langle\cdot,\cdot\rangle_2$, respectively. Let the vector spaces $H = H_1 \otimes H_2$ be the tensor product of H_1 and H_2. For H, we define the inner product

$$\langle u_1 \otimes u_2, v_1 \otimes v_2\rangle := \langle u_1, v_1\rangle_1 \langle u_2, v_2\rangle_2 \tag{4.74}$$

for all $u_1, v_1 \in H_1$ and $u_2, v_2 \in H_2$.

Consider the completion under the inner product. For the resulting Hilbert space H, the tensor product of the Hilbert spaces H_1 and H_2, we have the following incidental property.

Proposition 4.3.19. *For $\{v_i^1\}_{i=1,\ldots,\dim(H_1)}$ and $\{v_i^2\}_{i=1,\ldots,\dim(H_2)}$ orthonormal bases of H_1 and H_2, respectively,*

$$\{v_i^1 \otimes v_j^2\}_{i=1,\ldots,\dim(H_1),\ j=1,\ldots,\dim(H_2)} \tag{4.75}$$

is an orthonormal basis of $H_1 \otimes H_2$.

Referring to $(H_1 \otimes H_2)^\star$ as the dual space of the tensor product space $H_1 \otimes H_2$, containing all linear functionals $H_1 \otimes H_2$, it can be naturally identified with the space of all bi-linear functionals on $H_1 \times H_2$. In other words, every bi-linear functional is a functional on the tensor product space, and vice versa. Further, if H_1 and H_2 are finite dimensional, as it happens for the considered spaces in our set-up, there is a natural isomorphism between $H_1^\star \otimes H_2^\star$ and $(H_1 \otimes H_2)^\star$. Last but not least, the tensors of the linear functionals are bi-linear functionals. See [93] for more details about the approximation theory of tensor product spaces.

4.3.3 Tensor Product Splines

In the case of the univariate spline space we have a knot sequence $\Delta = \{\tau_i\}_{i=0,\ldots,l+1}$ with

$$a = \tau_0 < \tau_1 < \ldots < \tau_{l+1} = b \tag{4.76}$$

and degree k, the space $S_{k,\Delta}$ as the spline space of order k and knot sequence Δ. For the extended knot sequence $T = \{\theta_i\}_{i=1,\ldots,n+k}$ as defined by means of knot multiplicity at the boundaries with $\theta_i < \theta_{i+k}$ for $i = 1, \ldots, n$, and

$$\theta_1 = \ldots = \theta_k = a < \theta_{k+1} \leq \ldots \leq \theta_n < b = \theta_{n+1} = \ldots = \theta_{n+k}, \tag{4.77}$$

we have $\mathcal{N}_{k,T} = \text{span}\{N_{i,k}\}_{i=1,\ldots,n}$. Then for Δ and T with identical inner knots, for $\tau_i \in \Delta$ and $\theta_{i+k} \in T$ with $\tau_i = \theta_{i+k},\ i = 0, \ldots l+1$, it follows

$$S_{k,\Delta} = \mathcal{N}_{k,T}, \quad \dim(S_{k,\Delta}) = \dim(\mathcal{N}_{k,T}) = n = k + l. \tag{4.78}$$

This means, the B-splines of order k are a basis for the spline function space $S_{k,\Delta}$.

We follow here the line of [132] to discuss the tensor product construction.

Definition 4.3.20 (Tensor-product polynomial). *We define for the d-dimensional knot sequence $\Delta^j = \{\tau_i^j\}_{i=0,\ldots,l^j+1,\ j=1,\ldots,d}$ with*

$$a^j = \tau_0^j < \tau_1^j < \ldots < \tau_{l^j+1}^j = b^j \tag{4.79}$$

and degrees $\mathbf{k} = (k^1, \ldots, k^d)$ the d-variate spline $N_{\mathbf{i},\mathbf{k}}$ as d-dimensional products of d 1-dimensional terms of the form

$$N_{\mathbf{i},\mathbf{k}} = \prod_{j=1}^{d} N_{i^j,k^j}, \quad \mathbf{i} = (i^1, \ldots i^d), i^j = 1, \ldots n^j, \quad \mathbf{k} = (k^1, \ldots k^j) \tag{4.80}$$

and the the space of tensor-product polynomial splines by

$$\mathcal{S} = \otimes_{j=1}^{d} S_{k^j,\Delta^j} = \text{span}\{N_{\mathbf{i},\mathbf{k}}\}_{i^d=1,\ldots,n^d}^{j=1,\ldots,d} \tag{4.81}$$

$$= \text{span}\{N_{i^1,k^j}^1 \cdots N_{i^j,k^j}^j \cdots N_{i^d,k^j}^d\}_{i^d=1,\ldots,n^d}^{j=1,\ldots,d}. \tag{4.82}$$

We have immediately:

Proposition 4.3.21. *$\mathcal{S}$ is a linear space with*

$$\dim \mathcal{S} = \prod_{j=1}^{d} (n^j) = \prod_{j=1}^{d} (l^j + k^j). \tag{4.83}$$

Each function in $\mathcal{S}$ is defined on the d-dimensional rectangle

$$H = \otimes_{j=1}^{d} [a^j, b^j] = \{\mathbf{x} = (x^1, \ldots, x^d) : a^j \leq x^j \leq b^j, j = 1, \ldots, d\}. \tag{4.84}$$

Obviously, we can tensor product B-spline spaces of different orders or defined on different knot sequences. Depending on these aspects, their properties are more or less sparse to describe. We begin though with the most general ones.

Proposition 4.3.22.

(a) (local support) $\operatorname{supp} \mathrm{N}_{\mathbf{i},\mathbf{k}} \subseteq \otimes_{\mathrm{j}=1}^{\mathrm{d}} [\tau_{\mathrm{ij}}, \tau_{\mathrm{ij}+\mathrm{kj}}]$,

(b) (not-negativity) $N_{\mathbf{i},\mathbf{k}}(x) > 0$ *for all* $x \in [a^j, b^j]$,

(c) (point wise polynomial) $N_{\mathbf{i},\mathbf{k}}(x)|_{[\tau_{ij},\tau_{ij}+k^j)} \in \Pi_{k^j}$,

(d) (partition of unity) $\sum N_{\mathbf{i},\mathbf{k}}(x) = 1$ *for all* $x \in [a^j, b^j]$,

(e) (smoothness) the spline $N_{\mathbf{i},\mathbf{k}}$ *is* n^j *times continuously differentiable with respect to each variable* x^j.

The last property gives us for a tensor-product spline series $s(x)$:

$$s(x) \;=\; \sum_{\mathbf{i}} c_{\mathbf{i}} N_{\mathbf{i},\mathbf{k}}(x) \;=\; \sum_{\substack{j=1,\dots,d \\ i^d=1,\dots,n^d}} c_{\mathbf{i}} N^1_{i^1,k^j}(x^1) \cdots N^j_{i^j,k^j}(x^j) \cdots N^d_{i^d,k^d}(x^d). \tag{4.85}$$

Due to the tensor-product structure separating the variables, all the derivatives of a series can be written directly in terms of the derivatives of the tensor functions, namely

$$D^{\alpha^1}_{x^1} \cdots D^{\alpha^d}_{x^d}\; s(x) = \sum_{i^1=1}^{n^1} \cdots \sum_{i^d=1}^{n^d} c_{\mathbf{i}} D^{\alpha^1}_{x^1} N^1_{i^1,k^j}(x^1) \cdots D^{\alpha^d}_{x^d} N^d_{i^d,k^d}(x^d). \tag{4.86}$$

These derivatives exist, they are continuous and their smoothness is controlled by the knot multiplicity. In our case, knot multiplicity issues are relevant only for the splines living at the boundaries. Further, the coefficients of the derivatives and of the antiderivatives can also be recursively computed using the tools for the one dimensional case, e.g. (4.45).

Recall the subdivision formula for the univariate B-spline $N^h_{i,k}$ defined over the uniform knot sequence T^h in terms of the B-splines $N^{h/2}_{i,k}$defined over $T^{h/2}$and the thereby defined coefficients denoted here $a_l, l = 0, \dots, k$:

$$N^h_{i,k} = 2^{-k+1} \sum_{l=0}^{k} \binom{k}{l} N^{h/2}_{2i+l,k} =: \sum_{l=0}^{k} a_l N^{h/2}_{2i+l,k}. \tag{4.87}$$

We can formulate a similar refinement equation for the tensor product splines. For $\mathbf{i} = (i^1, \dots i^d), i^j = 1, \dots, n^j$ and $\mathbf{k} = (k^1, \dots, k^j)$

$$N_{\mathbf{i},\mathbf{k}} = \prod_{j=1}^{d} N^{h^j}_{i^j,k^j} = \prod_{j=1}^{d} \sum_{l=0}^{k} a_{lj} N^{h^j/2}_{2i^j+l,k^j}. \tag{4.88}$$

One can eventually further develop the formulation until the knot sequences T^{h^j} have the same level for each direction of the tensor product. We specify here only the case where

$N_{\mathbf{i},\mathbf{k}}$ is isotropic, this means it tensors one dimensional basis functions with identical grid size h and degree k on each direction:

$$N_{\mathbf{i},\mathbf{k}} = \prod_{j=1}^{d} N_{i^j,k}^{h} = \prod_{j=1}^{d} \sum_{l=0}^{k} a_{lj} N_{2i^j+l,k^j}^{h/2} \tag{4.89}$$

$$= \sum_{\substack{j=1,\ldots,d \\ l_j=0,\ldots,k}} \prod_{j=1}^{d} a_{lj} \prod_{j=1}^{d} N_{2i^j+l^j,k}^{h/2}. \tag{4.90}$$

We are now ready to construct a dual basis for the tensor product space.

Proposition 4.3.23. *For each $j = 1, \ldots, d$ let the set of linear functional $\{\lambda_i^j\}_{i=1,\ldots,n^j}$ defined on S_{k^j,Δ^j} be a dual basis of S_{k^j,Δ^j}. Then the set*

$$\{\lambda_{\mathbf{i},\mathbf{k}}\}_{i^d=1,\ldots,n^d}^{j=1,\ldots,d} = \{\lambda_{i^1,k^j}^1 \cdots \lambda_{i^j,k^j}^j \cdots \lambda_{i^d,k^j}^d\}_{i^d=1,\ldots,n^d}^{j=1,\ldots,d} \tag{4.91}$$

forms a dual basis for the dual of tensor product space $\otimes_{j=1}^{d} S_{k^j,\Delta^j}$.

For more details about the approximation by means of tensor product splines see [132], Chapter 12.

4.4 Computing the Solution

We choose here (tensor product of) cubic spline basis of level l for Ψ constructed on the (multivariate) domain Ω with $L = \#\Lambda$, the number of elements in the index set Λ over Ψ. For the given information data points in $P_\Gamma = \{(x_i, z_i) : x_i \in \Gamma_\#, i = 1, \ldots, M\}$, we want to determine $u_\eta : \Omega \to I\!R$, $u_\eta = \sum_{\lambda\in\Lambda} d_\lambda \psi_\lambda$ such that the functional (4.8) is minimized. The coefficient set $\mathbf{d} = \{d_\lambda\}_{\lambda\in\Lambda}$ is then computed by solving the following equation system:

$$(\mathbf{M} + \eta\mathbf{G})\,\mathbf{d} = \mathbf{b}, \quad \mathbf{M} = \mathbf{A}^\mathbf{T}\mathbf{A}, \quad \mathbf{b} = \mathbf{A}^\mathbf{T}\mathbf{z}, \quad \mathbf{z} = (z_i)_{(x_i,z_i)\in P_\Gamma} \tag{4.92}$$

with

$$\mathbf{A} = (\mathbf{A}_{i\ell})_{\substack{i=1,\ldots,M \\ \ell=1,\ldots,L}}, \ \mathbf{A}_{i\ell} = \psi_\ell(x_i), \tag{4.93}$$

$$\mathbf{M} = (\mathbf{M}_{\ell\ell'})_{\ell,\ell'=1,\ldots,L}, \ \mathbf{M}_{\ell\ell'} = \sum_{i=1}^{M} \psi_\ell(x_i)\psi_{\ell'}(x_i) \tag{4.94}$$

and

$$\mathbf{G} = (\mathbf{G}_{\ell\ell'})_{\ell,\ell'=1,\ldots,L}, \ \mathbf{G}_{\ell\ell'} = \int \Delta\psi_\ell(x)\Delta\psi_{\ell'}(x)dx. \tag{4.95}$$

Since information data points are available only over a subset of the domain, there exist basis functions whose support does not contain any of these points. Therefore, the matrix

$\mathbf{M}$ itself will be most probable not invertible. However, depending on the value for η weighing $\mathbf{G}$, the system 4.92 can still be solved.

Another aspect to be considered is the tensor structure of the considered basis. We have decided to employ this type of multivariate basis functions due to the differential type of the problem, more exactly due to the additional term $\int_\Omega |\Delta u_\eta(x)|^2$ in the functional (4.8) which has to be minimized.

Recall, that the basis functions $\Psi = \{\psi_\lambda : \lambda \in \Lambda\}$ with Λ set of indices for the basis are a d-variate spline $N_{\mathbf{i},\mathbf{k}}$ build as d-dimensional products of d 1-dimensional functions and of the type

$$N_{\mathbf{i},\mathbf{k}} = \prod_{j=1}^{d} N_{i^j,k^j}, \quad \mathbf{i} = (i^1,\dots,i^d), i^j = 1,\dots n^j, \quad \mathbf{k} = (k^1,\dots,k^j) \tag{4.96}$$

defined for the d-dimensional knot sequence $\Delta^j = \{\tau_i^j\}_{i=0,\dots,l^j+1,\ j=1,\dots,d}$ over the domain Ω. Recall that the derivative of a B-spline is also a B-spline.

We see how the elements $\mathbf{G}_{\ell\ell'}, \mathbf{G}_{\ell\ell'} = \int \Delta\psi_\ell(x)\Delta\psi_{\ell'}(x)dx$ can be fragmented dimension-wise for $x = (x_1,\dots,x_d) \in \Omega$. First we rewrite

$$\begin{aligned}
\Delta\psi_\ell(x) =& \Delta \prod_{i=1}^{d} \psi_\ell^i(x_i) \\
=& \sum_{j=1}^{d} \frac{d^2}{dx_j^2} \prod_{i=1}^{d} \psi_\ell^i(x_i) \\
=& \sum_{j=1}^{d} \psi_\ell^j(x_j)'' \prod_{i=1,i\neq j}^{d} \psi_\ell^i(x_i).
\end{aligned} \tag{4.97}$$

We have now for the elements of $\mathbf{G}$:

$$\begin{aligned}
\mathbf{G}_{\ell\ell'} =& \int \Delta\psi_\ell(x)\Delta\psi_{\ell'}(x)dx \\
=& \int \left[\sum_{j=1}^{d} \psi_\ell^j(x_j)'' \prod_{i=1,i\neq j}^{d} \psi_\ell^i(x_i)\right] \left[\sum_{j'=1}^{d} \psi_{\ell'}^{j'}(x_j)'' \prod_{i=1,i\neq j'}^{d} \psi_{\ell'}^i(x_i)\right] dx \\
=& \int \left[\sum_{j=1}^{d}\sum_{j'=1}^{d} \psi_\ell^j(x_j)''\psi_{\ell'}^{j'}(x_j)'' \prod_{i=1,i\neq j}^{d} \psi_\ell^i(x_i) \prod_{i=1,i\neq j'}^{d} \psi_{\ell'}^i(x_i)\right] dx \\
=& \sum_{j=1}^{d}\sum_{j'=1}^{d} \int \left[\psi_\ell^j(x_j)''\psi_{\ell'}^{j'}(x_j)'' \prod_{i=1,i\neq j}^{d} \psi_\ell^i(x_i) \prod_{i=1,i\neq j'}^{d} \psi_{\ell'}^i(x_i)\right] dx.
\end{aligned} \tag{4.98}$$

Now we can group and separate the inner integral of the product by the dimensions of the terms. In each of the d dimensions only two-paired terms appear. Each entry is then the sum of a number of products with d terms, which are one dimensional products of the

form $\psi^i_\ell(x_i)\psi^i_{\ell'}(x_i)$, $\psi^i_\ell(x_i)''\psi^i_{\ell'}(x_i)$ or $\psi^i_\ell(x_i)\psi^i_{\ell'}(x_i)''$. This means, the matrix $\mathbf{G}$ in the d-dimensional case is in fact a sum of the Kronecker product of d matrices for the respective one-dimensional bases:

$$\mathbf{G} = \sum_{j=1}^{d}\sum_{j'=1}^{d} \otimes_{i=1}^{d} \mathbf{G}^{jj'i} \tag{4.99}$$

with

$$\mathbf{G}^{jj'i}_{ll'} = \begin{cases} \int \psi^i_l(x_i)\psi^i_{l'}(x_i)dx_i, & j \neq i, j' \neq i, \\ \int \psi^i_l(x_i)''\psi^i_{l'}(x_i)dx_i, & j = i, j' \neq i, \\ \int \psi^i_l(x_i)\psi^i_{l'}(x_i)''dx_i, & j \neq i, j' = i, \\ \int \psi^i_l(x_i)''\psi^i_{l'}(x_i)''dx_i, & j = i, j' = l. \end{cases} \tag{4.100}$$

and ψ^i_l the one-dimensional basis function in each of the $i = 1, \ldots, d$ dimensions.

Recall, that the Kronecker product, denoted by $\otimes$, is an operation on two matrices of arbitrary size resulting in a block matrix. If $\mathbf{A}$ is an m-by-n matrix and $\mathbf{B}$ is a p-by-q matrix, then the Kronecker product $\mathbf{A} \otimes \mathbf{B}$ is the mp-by-nq block matrix with $\mathbf{A} \otimes \mathbf{B}$ at the position mn, pq equal to $\mathbf{A}_{mn}\mathbf{B}_{pq}$. See Figure 3.5 for a comparison of typical sparsity pattern of the matrix $\mathbf{G}$ for a one– and two–dimensional uniform (tensor product of) B-spline bases.

Figure 4.2. *Typical sparsity pattern of the matrix* $\mathbf{G}$ *for a one dimensional B-spline basis (left) and for a two-dimensional tensor product of B-spline basis (right); blue points show the* nz *non-zero elements.*

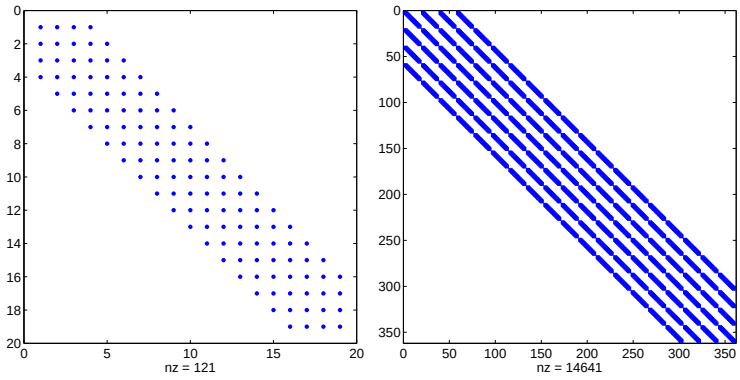

Consider further the sparsity pattern of matrix $\mathbf{M}$. Here, we have considered a two-dimensional B-spline basis level four in lexicographic order. See Figure 4.3 (left) for the case where points cover uniformly the entire domain such that the support of all basis function contain points. Here, the system of equations can be solved for $\eta = 0$ also. However, this changes when a significant amount of information points is left out and the supports of some basis functions does not contain any data points at all. We consider a classical set-up for our continuation problem, where e.g. the middle of the domain contains no data points. See Figure 4.3 (middle) and (right) for the sparsity pattern of the matrix $\mathbf{M}$ when information points are available only at the four boundaries (middle) or at two

of the four boundaries of a rectangular domain (right). Without the contribution of the term $\eta\mathbf{G}$, enforcing the harmonicity of the continuation, no solution can be computed.

Figure 4.3. *Sparsity pattern of the matrix* $\mathbf{M}$ *for a two-dimensional tensor product of B-splines basis and information points: uniformly distributed over the entire domain (left), only at the four boundaries of a rectangular domain (middle) and only two of the four boundaries of a rectangular domain (right); blue points show the* nz *non-zero elements.*

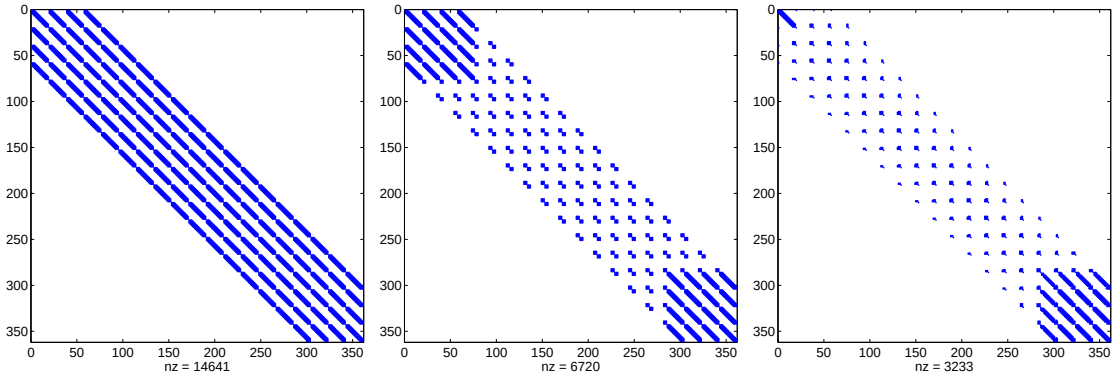

Further, Figure 4.4 shows the sparse pattern of the matrix $\mathbf{M}$ when the basis is not uniform anymore. We have considered conversely a complete multiscale tensor product of B-splines basis. In this case, certain B-splines on several successive levels are added to the basis. A detailed discussion on multiscale approaches for tensor product B-splines will follow in Chapter 7. We just mention here that the sparsity pattern presents a typical finger structure. The higher the levels, the support of less basis functions contains data points and more basis functions contain none at all. Therefore, the sparser areas of the matrix are associated with higher leveled basis functions.

Figure 4.4. *Sparsity pattern of the matrix* $\mathbf{M} = (\mathbf{M}_{\ell\ell'})_{\ell,\ell'=1,\dots,L}$, $\mathbf{M}_{\ell\ell'} = \sum_{i=1}^{M} \psi_\ell(x_i)\psi_{\ell'}(x_i)$ *for a complete multi-scale tensor product of B-splines basis; blue points show the* nz *non-null elements.*

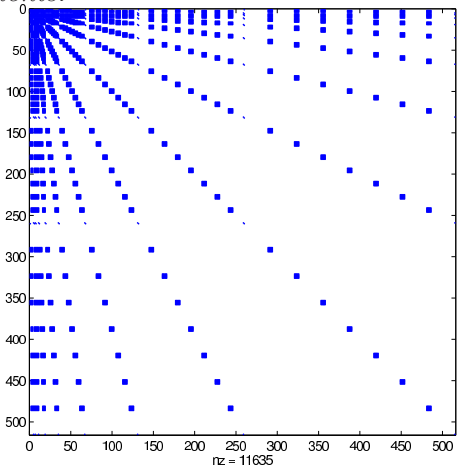

Even if the coefficient matrix $\mathbf{A}$ is not symmetric and nonsingular, the normal equation matrix $\mathbf{M} = \mathbf{A}^\mathbf{T}\mathbf{A}$ will be symmetric and positive definite, just as the matrix $\mathbf{G}$. Hence, iterative methods as the conjugate gradient method can be applied. However, the convergence may be relatively slow even with data available on the full grid. Conditioning is improved by adding information about harmonicity to the pure data-fitting ansatz. But the ill–conditioning issues remain as a consequence of the intrinsic ill posing of the continuation problem. Iterative methods are a better choice since solving directly such a large system of equations with tens to hundred thousands of degrees of freedom is not always practicable due to memory problems and performance issues.

With regard to the regularization effect of our least squares method, one might consider the premature interruption of the iterative solver. Intuitively we have that gradient methods by construction determine first the coarser shares of the solution and later the higher frequencies. This regularization effect of cutting off the iterative process has already been studied for data fitting problems with splines in [145] or for more generalized ill posed problems in [63].

Recall that our target functions are harmonic and therefore smooth; isolated spikes for example are not to be expected. So we don't need to considerably worry about an essential loss of accuracy when choosing reasonable stopping criteria for the iteration. Our experiments include results obtained with direct solvers, there, when systems are small enough, and results obtained with the conjugate gradients method, where large systems arise, e.g. for solutions comprising high–level three dimensional tensor product of B-splines basis.

4.5 Alternative Formulations for Comparison Purposes

Additionally to our least squares approach, we consider two alternative, classical partial differential equation formulations adequate for bounded domains. We compute an approximate continuation by solving the Laplace boundary value problem by means of finite elements, see e.g. [11], and finite differences, see e.g. [60].

We have chosen these methods for comparison purposes as they both belong, just as spherical harmonics, to long standing mathematical theory on approximation. But finite elements and finite differences can be employed to solve the Laplace equation on bounded domains. Further, we know that they solve the Laplace equation correctly up to the accuracy of the available boundary conditions, which can be also in discrete form. Yet both finite elements and finite differences require complete boundary conditions, this means available over the entire $\partial\Omega$, and cannot be employed directly for our upward continuation problem. So they show us merely which solution one should expect using the complete boundary conditions at the given discretization and classical partial differential approaches. This should later stand as comparison to the solution obtained using our weighted least squares approach and incomplete boundary conditions at the same discretization.

4.5.1 Finite Elements

A different reconstruction using a finite-element(FE)-solver is the following. We consider the Laplace equation with Dirichlet boundary conditions

$$\Delta u = 0 \quad \text{in } \Omega, \qquad u = f \quad \text{on } \Gamma \tag{4.101}$$

where $\Gamma := \partial\Omega$ is the whole boundary of the cuboid consisting of its six faces. The boundary data f which are required to be continuous for the FE method are obtained as follows. We take the extreme boundary layer grids of $\Gamma_\#$ on all six sides of the cuboid and interpolate them using bi-linear functions. Problem (4.101) is then solved using the finite element package ALBERTA of the software program [125]. The domain Ω is split into tetrahedrons; the coarsest grid consists of six tetrahedrons which are further refined by bisection until approximately the same resolution, as in the grid of the available data, is achieved. On this fine decomposition of the domain, we use linear finite elements (first order Lagrangian functions) as basis functions to approximate u. The resulting system of linear equations is solved iteratively by the method of conjugate gradients. We call this the *finite element approach*.

4.5.2 Finite Differences

We consider the potential equation with Dirichlet boundary conditions (4.101) where $\Gamma := \partial\Omega$ is the whole boundary of the cuboid consisting of its six faces. The boundary data f in this case required to be gridded. The basic idea is to approximate differential quotients by a second-order centered difference. Problem (4.101) is then solved using a three dimensional seven-point stencil. The resulting system of linear equations can also be solved exactly or iteratively by the method of conjugate gradients. We call this the *finite differences approach*.

Chapter 5

Two Dimensional Illustration of the Method

Picture – noun
A representation in two dimensions of something wearisome in three.

Ambrose Bierce, The Devil's Dictionary [9]

The least squares approach for the approximate continuation problem has been designed to help with the construction of the upward continuation of the potential field of the earth. Hence, it deals with three dimensional data sets. Since volumes are not easily displayed on paper-type media, we depend mostly on sections. So we considered the illustration of several two-dimensional harmonic continuation experiments with synthetic harmonic functions, in order to get a more intuitive understanding of its behavior, in particular of the trade-off between data fit and harmonicity constraints.

As presented in the previous section, instead of solving the exterior boundary value problem for the Laplace equation, the approximate continuation is constructed by a method that takes information point values situated on different sub-domains Γ of a target domain Ω and returns coefficients for (tensor product of) splines living on Ω. It simultaneously minimizes the data fit error over the sub-domain and the Laplacian of the complete reconstruction.

5.1 From the Boundary Data to the System of Equations

Let for the domain $\Omega = [0,1]^2$

$$\Omega_{\#} = \{(x_i, z_i)\}_{i=1,\ldots,N}, x_i \in [0,1]^2,\ z_i \in I\!R \tag{5.1}$$

be a cloud of not coinciding uniformly gridded data points on Ω. They are defined by the corresponding horizontal values: $\mathbf{x} = \{(x_i)\}_{i=1,\ldots,N}$ for multi index $x = (x_1, x_2)$ and vertical values $\mathbf{z} = \{(z_i)\}, z_i = f(x_i), \forall i = 1, \ldots, N$, which result from the evaluation of a harmonic test function f at the observation points x_i. In our case, we have a total of

$$(2^7 + 1)^2 = 16641 \tag{5.2}$$

points. The test function has been constructed starting from the harmonic function

$$f : [0,1]^2 \to I\!R, \quad f(x_1, x_2) = \exp^{-x_1} \sin(x_2). \tag{5.3}$$

In order to work with a more challenging test case, we consider variations where the parameters are multiplied by a coefficient. Further, for an easier understanding of the numerical results, the function has been modified such that

$$f : [0,1]^2 \to [-1,1]. \tag{5.4}$$

Altogether, the test function for the two–dimensional experiment reads as:

$$f_1(x_1, x_2) = \exp^{-10x_1} \cdot \sin(10x_2) + \exp^{-10+10x_1} \cdot \sin(10 - 10x_2). \tag{5.5}$$

See Figure 5.1 for a view of the test function f_1 evaluated over the full grid $\Omega_{\#}$.

Figure 5.1. *Considered test function f_1.*

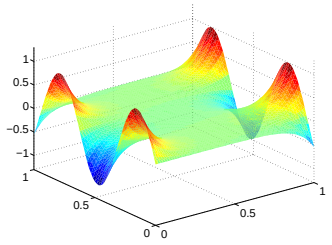

A key point for our harmonic continuation approach is the set P_Γ of available data points. Depending on its structure, we might be able or we might not be able to construct a good approximate continuation. Recall, the theory states, that, in order to be able to correctly solve Dirichlet's problem for the Laplace equation information at the entire boundary of the domain is required. This translates to a configuration of the information points set as in Figure 5.2 (a). In this case we could solve the problem via a classical finite elements or finite differences approach. However, in our problem statement inspired by the geodetic application, boundary conditions are incomplete, i.e., there are boundary segments that contain no data points. Figure 5.2 (b-f) shows some possible boundary data configurations. In this case, the solution is not unique anymore, but still determined through the second term in the functional (4.8) enforcing the harmonicity and the considered weight parameter η.

Initial experiments have shown which kind of configuration of the boundary data points provide a good reconstruction of the test function. See Figures 5.2 (a,b) for some other examples of reasonable boundary data configurations. Figures 5.2 (c,d) are only with reservations to consider. Figures 5.2 (e,f) depict an example of boundary data configurations for which, independent from the choice of the weight parameter, i.e., in spite of the regularization, no proper continuation can be constructed. Here, the resulting system of equations could not be solved since the system matrix was not invertible. Independent from the term controlling the Laplacian of the continuation, when too little information

Figure 5.2. *Example of boundary data configurations P_Γ. (a,b): Configurations for which good approximate continuation results can be expected. Information points are either over the entire boundary available or protruding into the domain. (e,f): Configurations for which no approximate continuation can be constructed. Information data points are insufficient.*

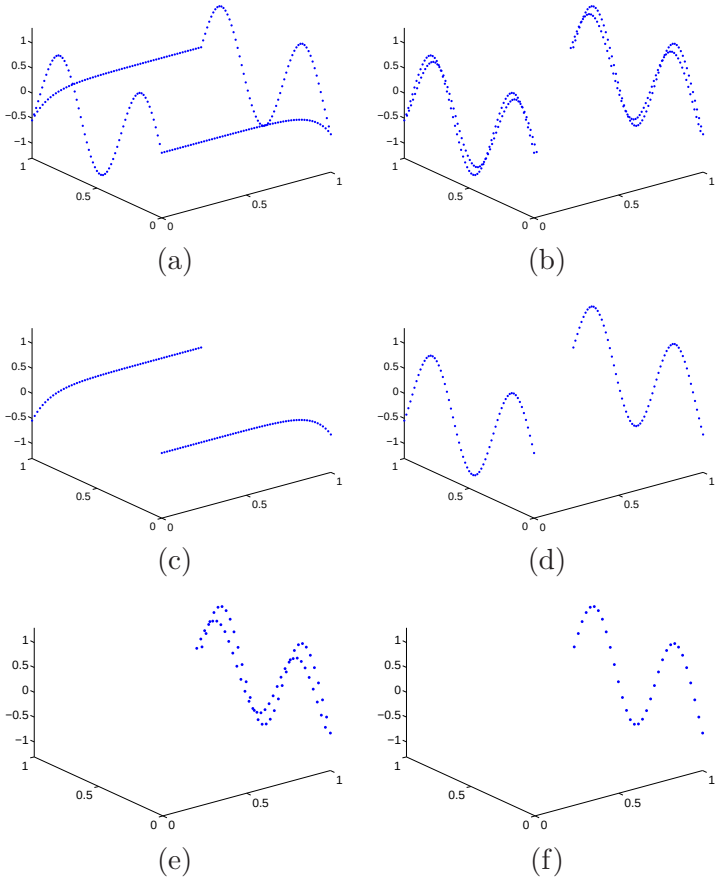

points are available compared to the cardinality of the considered basis, the system cannot be solved. On the other side, in case of the reasonable configurations, the support of a sufficient number of basis functions, but not of all, contains one or more information points, and thus having an essential contribution in determining the equation system. Is is interesting to see that the configurations in Figure 5.2 (a,b) provide good results, but the configuration in Figure 5.2 (d) is worse. The intuitive explanation could be at first, that the missing boundary information along some direction might be practically replaced by the directional, gradient type information given by the two lines of points available along the other direction. In fact, Figure 5.2 (e) shows a pure upward continuation set up where data is available, even though two–layered, on only one side of the domain.

Further, we consider for Λ a two dimensional tensor product B-spline basis with level $l = 4$, i.e., we have in both the x_1 and x_2 direction a one dimensional B-spline basis of

level 4. This means we have a number of

$$(2^l + 3)^2 = 19^2 = 361 \tag{5.6}$$

lexicographically ordered basis functions. Next, we describe how the system of equations is practically assembled. We are looking for $u_\eta(x) = \sum d_\lambda \psi_\lambda(x)$ with $\mathbf{d} = \{(d_\lambda)\}_{\lambda\in\Lambda}$ the coefficients for the functions ψ_λ belonging to an isotropical, two–dimensional tensor product B-spline basis Λ indexed by λ such that

$$\sum_{i=1}^{N}(u_\eta(x_i) - z_i)^2 + \eta \int |\Delta u_\eta(x)|^2 dx \to \min. \tag{5.7}$$

This results in solving the following system of normal equations:

$$(\mathbf{M} + \eta\mathbf{G})\,\mathbf{d} = \mathbf{b} \tag{5.8}$$

with

$$\mathbf{M}_{\ell\ell'} = \sum_{i=1}^{M} \psi_\ell(x_i)\psi_{\ell'}(x_i), \quad \mathbf{G}_{\ell\ell'} = \int \Delta\psi_\ell(x)\Delta\psi_{\ell'}(x)dx, \quad \mathbf{b}_\ell = \sum_{i=1}^{M} z_i\psi_\ell(x_i). \tag{5.9}$$

We write the two dimensional tensor product basis functions

$$\psi_\ell(x) = \psi_{\ell_1}(x_1)\psi_{\ell_2}(x_2),\ x = (x_1, x_2) \tag{5.10}$$

with $\ell = 1, \ldots, \#\Lambda$ and ψ_{ℓ_1}, ψ_{ℓ_2} the corresponding one dimensional B-spline basis functions. The system matrices can then be written explicitly following the line in Section 4.4 as

$$\mathbf{M}_{\ell\ell'} = \sum_{i=1}^{M} \psi_\ell(x_i)\psi_{\ell'}(x_i) = \sum_{i=1}^{M} \psi_{\ell_1}(x_{i_1})\psi_{\ell_2}(x_{i_2})\psi_{\ell_1'}(x_{i_1})\psi_{\ell_2'}(x_{i_2}) \tag{5.11}$$

and

$$\begin{aligned}
\mathbf{G}_{\ell\ell'} &= \int \Delta\psi_\ell(x)\Delta\psi_{\ell'}(x)dx = \int (\partial_{x_1x_1}\psi_\ell(x) + \partial_{x_2x_2}\psi_\ell(x))(\partial_{x_1x_1}\psi_{\ell'}(x) + \partial_{x_2x_2}\psi_{\ell'}(x)) \\
&= \int \left(\psi_{\ell_1}(x_1)''\psi_{\ell_2}(x_2) + \psi_{\ell_1}(x_1)\psi_{\ell_2}(x_2)''\right)\left(\psi_{\ell_1'}(x_1)''\psi_{\ell_2'}(x_2) + \psi_{\ell_1'}(x_1)\psi_{\ell_2'}(x_2)''\right)dx \\
&= \int (\psi_{\ell_1}(x_1)''\psi_{\ell_2}(x_2)\psi_{\ell_1'}(x_1)''\psi_{\ell_2'}(x_2) + \psi_{\ell_1}(x_1)''\psi_{\ell_2}(x_2)\psi_{\ell_1'}(x_1)\psi_{\ell_2'}(x_2)'' \\
&\quad + \psi_{\ell_1}(x_1)\psi_{\ell_2}(x_2)''\psi_{\ell_1'}(x_1)''\psi_{\ell_2'}(x_2) + \psi_{\ell_1}(x_1)\psi_{\ell_2}(x_2)''\psi_{\ell_1'}(x_1)\psi_{\ell_2'}(x_2)'')dx \\
&= \int \psi_{\ell_1}(x_1)''\psi_{\ell_1'}(x_1)''dx_1 \int \psi_{\ell_2}(x_2)\psi_{\ell_2'}(x_2)dx_2 \\
&\quad + \int \psi_{\ell_1}(x_1)''\psi_{\ell_1'}(x_1)dx_1 \int \psi_{\ell_2}(x_2)\psi_{\ell_2'}(x_2)''dx_2 \\
&\quad + \int \psi_{\ell_1}(x_1)\psi_{\ell_1'}(x_1)''dx_1 \int \psi_{\ell_2}(x_2)''\psi_{\ell_2'}(x_2)dx_2 \\
&\quad + \int \psi_{\ell_1}(x_1)\psi_{\ell_1'}(x_1)dx_1 \int \psi_{\ell_2}(x_2)''\psi_{\ell_2'}(x_2)''dx_2.
\end{aligned} \tag{5.12}$$

We mention shortly that the matrices $\mathbf{M}$, $\mathbf{G}$ as well as their weighted sum $\mathbf{M} + \eta\mathbf{G}$ can be regarded as sparse. This is because we deal in this ansatz with locally supported basis functions. The support of each basis function does not carry all the evaluation points, if any. Take a look at Figure 5.3 for a plot of these matrices as resulted by constructing an approximate continuation and at their sparsity patterns. We considered the level 4 tensor product B-spline basis, lexicographically sorted, and two boundary data configurations. Information data points are available as two layered, on either one (as in Figure 5.2(a)) or on two parallel sides (as in Figure 5.2(b)) of the four boundary segments of the rectangular domain. The matrices of size 361×361, i.e., a maximum of 130321 elements where 361 is the number of basis functions in the considered two dimensional basis.

Figure 5.3. *Example of matrices resulted within the approximate continuation method for B-spline tensor product of level 4. For each matrix, nnz denotes the number of actual non zero positions. Left: Matrix* $\mathbf{G}$*. Middle: Matrix* $\mathbf{M}$ *when information data points are available as in Figure 5.2(e). Right: Matrix* $\mathbf{M}$ *when information data points are available as in Figure 5.2(b).*

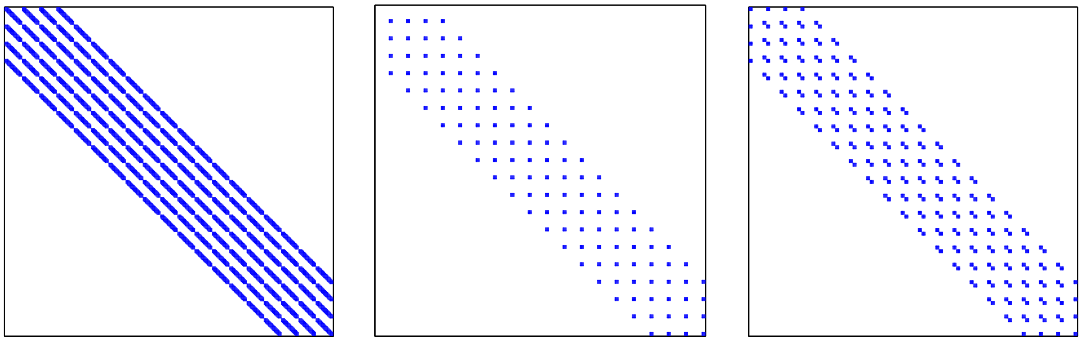

$nnz = 14641$ $nnz = 1936$ $nnz = 3872$

5.2 Variation of the Weight Parameter vs. Boundary Data Configurations

We detail the successful continuations presented in Figures 5.4, 5.5 and 5.6. We choose an interval for the weight parameter empirically as

$$\eta \in [10^{-20}, 10^{10}] \tag{5.13}$$

and logarithmically sample the interval when choosing values. It is clear that the weight parameter depends at least on the scaling of the considered basis. The lower bound of the interval has proved to provide only little effective regularization and the upper value leads already to over smoothed solutions.

Considering the small size of the resulting system of equation of $\#\Lambda = 361$ degrees of freedom, we solve the system directly. For each constructed boundary data set P_Γ as a subset of the full grid $\Omega_\#$, the results show the boundary error as $E_{bnd,\infty}$

$$E_{bnd,\infty} := \max\{\mathrm{abs}(f(x) - u_\eta(x)),\ x \in P_\Gamma\}, \tag{5.14}$$

the total error as $E_{\Omega,\infty}$

$$E_{\Omega,\infty} := \max\{\text{abs}(f(x) - u_\eta(x)),\ x \in \Omega_\#\} \tag{5.15}$$

and the harmonicity of the entire reconstruction $E_{\Omega,\Delta}$ computed as

$$E_{\Omega,\Delta} := \mathbf{dGd} \tag{5.16}$$

with $\mathbf{d}$ the determined coefficient vector of the tensor product spline representation. For each of the three test cases presented in Figures 5.4, 5.5, 5.6, notice how the boundary error gets larger with increasing values for the weight parameter controlling the harmonicity term. This is obvious, since only the boundary information points are significant for the reconstruction when less harmonicity constraint is present. Boundary data alone determines the system and is hence represented. Yet, with too little regularization, the continuation is unsatisfactory and at a first glance, simply not smooth enough. This is why our minimization objective, namely the total error, shows a slightly different behavior as compared to the boundary error. For too small weight parameters, the boundary values are well fitted but the total error is high. On the other side, both the boundary and the total error are out of scope for too large weight parameters. Here, the regularization is too strong and boundary conditions get disregarded. The laplacian of the reconstruction nearly vanishes with larger η, which is at this point no surprise, since it is a direct subject of the minimization.

As expected, not any weight parameter is a good one. We still have a relatively large and, most importantly, compact interval of proper choices for η. It is essential, that for two similar values of η the resulting continuation is also similar. This is reflected by the continuous aspect of the three evaluators: the boundary error, the total error and the harmonicity. A more detailed discussion about how to choose a proper value follows for the relevant three dimensional application in the following chapter handling the numerical results.

For visualization purposes, Figure 5.7 shows a series of continuation results. We deal with the same setup of the level $l = 4$ tensor product B-spline basis spanned over $[0, 1]^2$ and over a full uniform grid $\Omega_\#$ of $(2^7+1)^2$ points. We construct the approximate continuation with our least squares approach for the boundary datasets depicted in each image as black points at the positions $(x, f(x)), x \in P_\Gamma$. We set the weight parameter as

$$\eta \in \{10^{-17}, 10^{-15}, 10^{-10}, 10^{-1}, 10^{4}\}. \tag{5.17}$$

These values have no specific meaning but have given best insight on the influence of the weight parameter over the resulting continuation.

It is further interesting to see in corroboration with Figures 5.4, 5.5 and 5.6, that the continuation results are better for a larger interval of weight parameters when the information points are available along the side of the domain presenting the essential oscillations of the function. Recall, the test function resulted as a dimension–wise product of sin and exp functions whereas the sin terms yield stronger oscillations.

Figure 5.4. *Continuation results (right) for the boundary data configuration (left).*

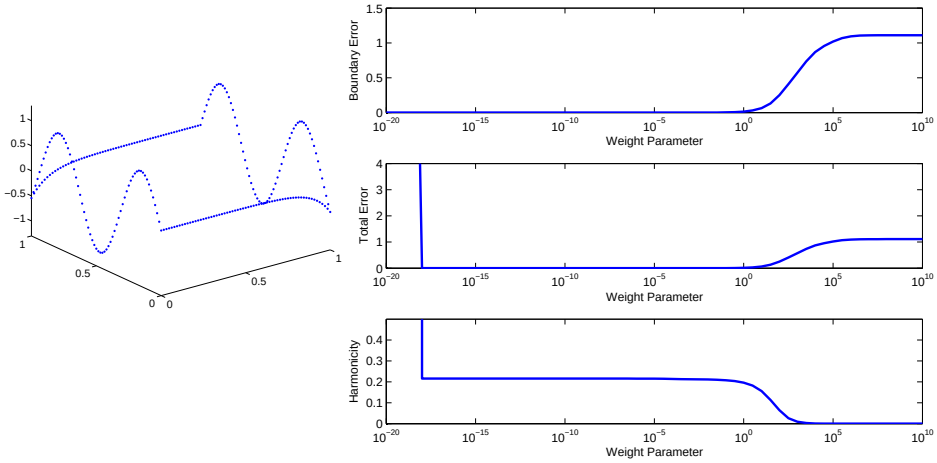

Figure 5.5. *Continuation results (right) for the boundary data configuration (left).*

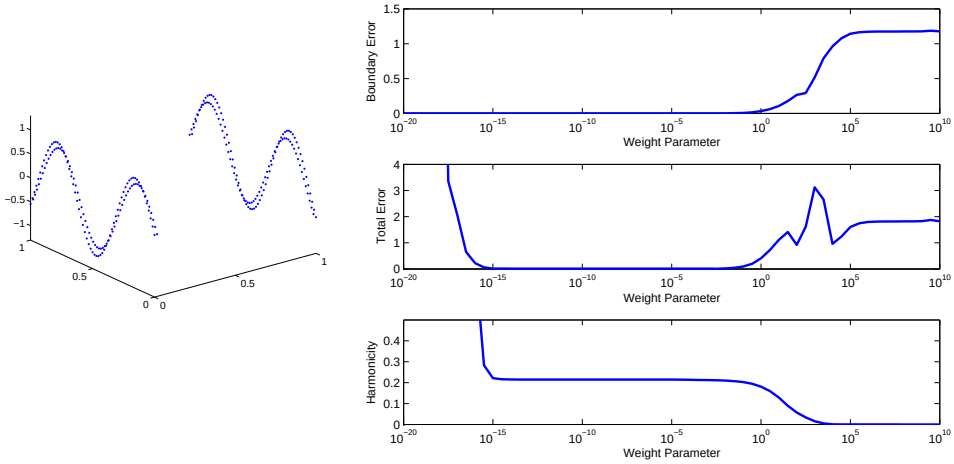

Figure 5.6. *Continuation results (right) for the boundary data configuration (left).*

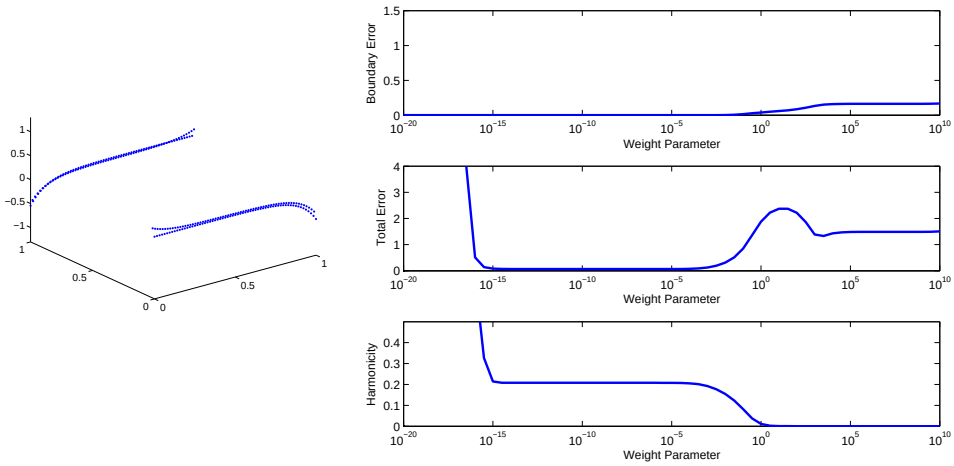

Figure 5.7. *Approximate continuation results for different boundary data configurations and weight parameter. For each case, the black dots show available information and the respective weight parameter η is printed above the plot.*

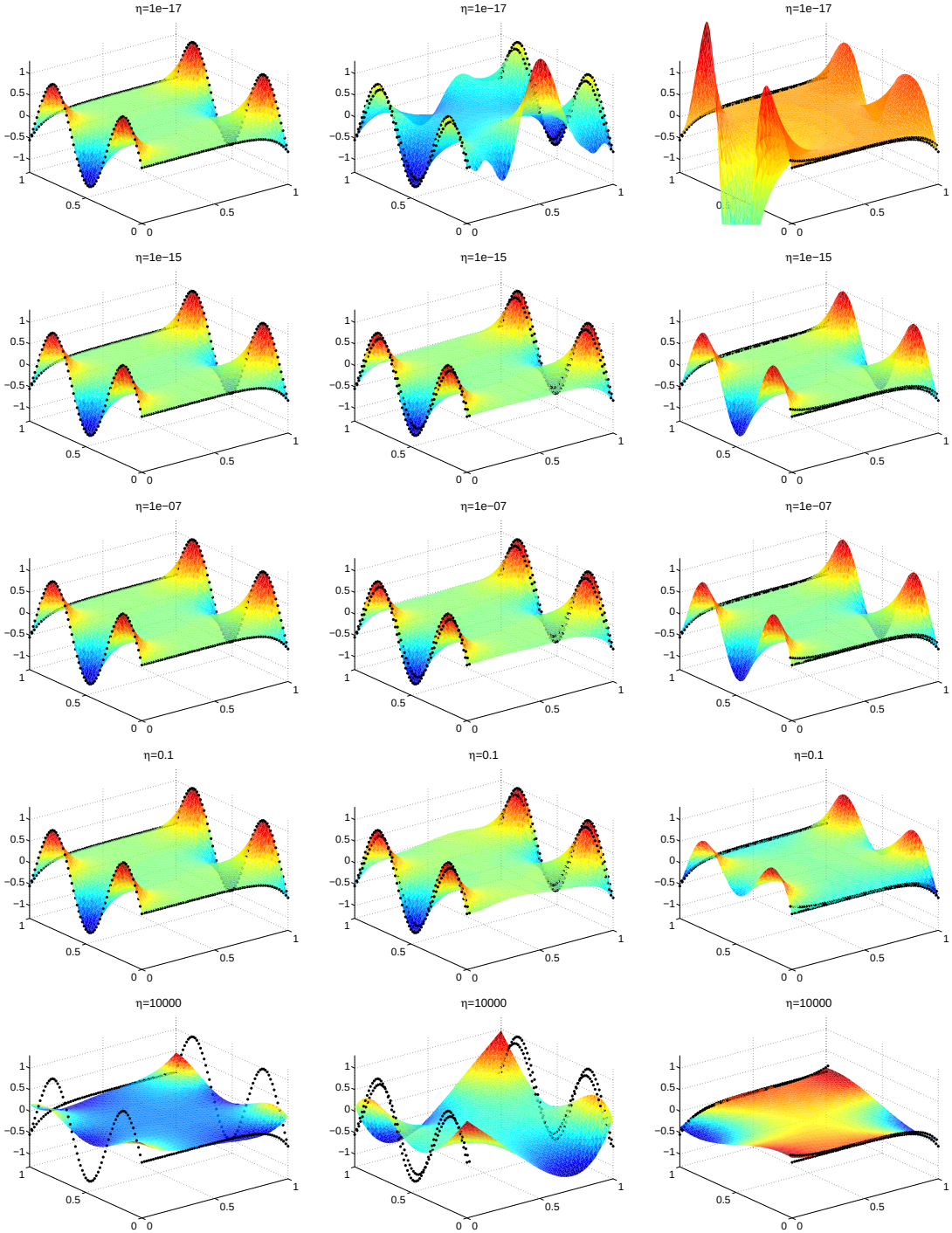

5.3 Variation of the Basis Cardinality vs. Strongly Incomplete Boundary Data

Other experiments show the expected regularization effect behavior of the least squares approach. For this, we consider another test function. We have the same cloud of not coinciding uniformly gridded data points $\Omega_{\#} = \{(x_i, z_i)\}_{i=1,\ldots,N}, x_i \in [0,1]^2, z_i \in I\!R$ on the domain $\Omega = [0,1]^2$. They are defined by vertical values $\mathbf{z} = \{(z_i)\}, z_i = f(x_i), \forall i = 1,\ldots,N$ where test function reads as:

$$f_2(x_1, x_2) = \exp^{-10+10x_1} \cdot \sin(10 - 10x_2). \tag{5.18}$$

See Figure 5.8 for a view of the test function f evaluated over the full grid $\Omega_{\#}$. As you notice, the function strongly variates on one instead of two sides of the quadratic domain. By this, we have constructed a two dimensional parallel to the three dimensional, geodetic set up. Remember, there we would have one mass generating the potential field. So the information spreads from the surface in radial direction to infinity and can be, for simplicity, regarded as unidirectional. Here, we have the domain situated outside of some mass generating the greatest field anomalies on the part of the domain nearest to the mass source. This anomalies attenuate with the distance from the source. So on the opposite side of the domain, the information has gotten lost and the function is smooth.

Figure 5.8. *Considered test function f_2.*

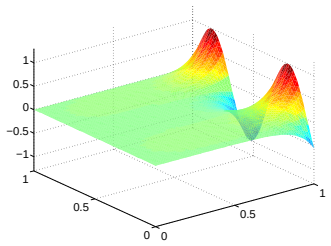

We can further see that the quality of the constructed continuation increases with the level of the considered B-spline basis and naturally with the number of the basis functions whose support contains data points. However, it is not a good idea to simply increase the level of the basis without the appropriate raise in available data points, since then the coefficients of more basis functions have to be determined.

The quality of the constructed continuation increases naturally also with the number of the basis functions whose support contains data points. Intuitively, the more the information points are spread in the domain, the better posed is the problem and the more complete is the matrix $\mathbf{M}$. This leads to a better reconstruction. So when the boundary conditions are available indeed on two parallel sides, which span between them the entire continuation space, good continuation results are expected. Take a look at Figure 5.9 for some experiments. We have fixed the weight parameter to

$$\eta = 10^{-7}. \tag{5.19}$$

This value is empirically selected, provides good results but is again not the optimal value for each case. Remember that we have normalized the test function so they reach to

Figure 5.9. *Approximate continuation (up) and continuation error (down) for different tensor product spline basis level $l = 5, 6$ and 7, weight parameter $\eta = 10^{-7}$. For each case, the black dots show available information points: two lines of points on one side and one line of points of the other side of the domain.*

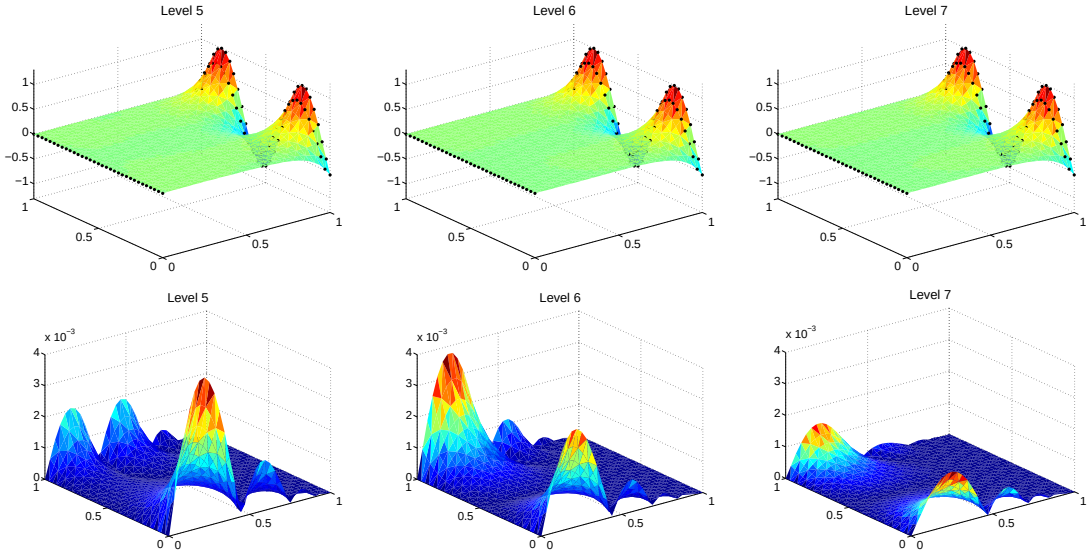

take values between -1 and 1. Notice also the scale of the continuation error. We have a maximum of 4e-3 for level 5.

We also take a look at the case, where information points are available only on one of the four sides. This translates for the geodetic approach to the classical upward continuation problem, where the gravimetric measurement are available only on the surface or near to it. Figure 5.10 shows the approximate continuation results. We fix the weight parameter to some good but not necessarily optimal $\eta = 10^{-7}$. The basis function levels vary from 5 to 7. The lowest considered level has provided very poor results. It is still very pleasant to see how well the available information has been upward continued. The regularization term can indeed imitate the effect of attenuation with the distance from the source. No considerable artifacts are generated as long as the available information has been properly represented.

Notice also the scale of the continuation error. We have $\max(|u_\eta(x) - f_1(x)|) = 4e-3$ for level 5 when the information normalized to one was also available on the opposite side of the domain, see Figure 5.9. But here, where data is given only on the side near to the information source, the continuation error is greater. It ranges up to $\max(|u_\eta(x) - f_2(x)|) = 0.2$ at the points most distant to the available information. This is indeed the price in accuracy of the solution in this ill posed formulation.

Figure 5.10. *Approximate continuation (up) and continuation error (down) for different tensor product spline basis level $l = 5, 6$ and 7, weight parameter $\eta = 10^{-7}$. For each case, the black dots show available information points with only two lines of points on one side of the domain.*

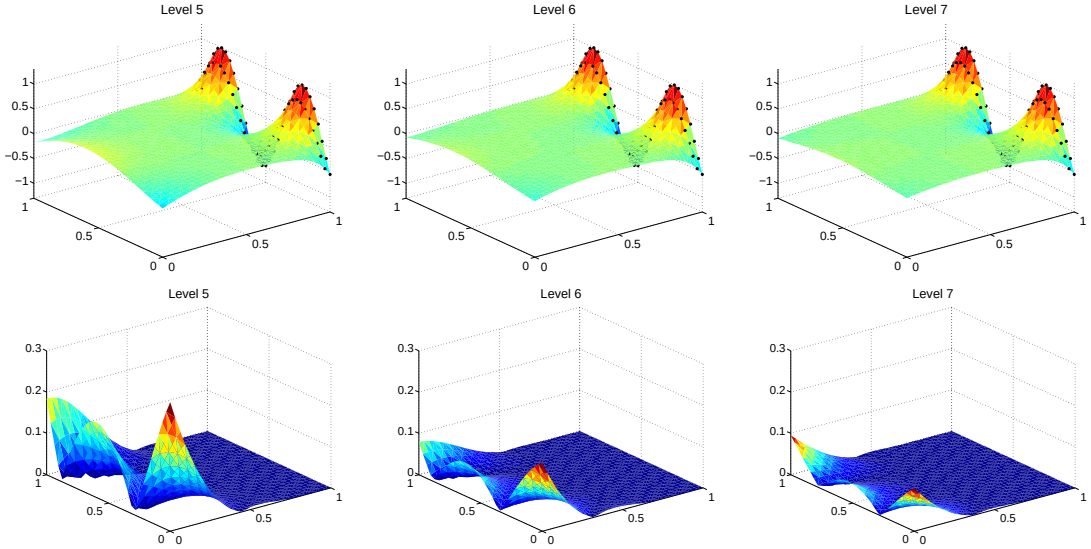

Chapter 6

Numerical Results

> However beautiful the strategy, you should occasionally look at the results.
>
> Sir Winston Churchill

This chapter on the numerical results of our least squares approach comprises several three dimensional experimental sets for the approximate continuation of harmonic functions. This will help us to investigate the behavior of the least squares approach for the continuation problem with respect to different problem set up parameters.

We consider at this point only isotropic, fully gridded tensor products of B-splines bases Ψ. The discussion also includes issues like test function types. The method will first be tested for synthetic harmonic functions chosen as linear combination of spherical harmonics. We further employ geopotential undulation datasets obtained by the evaluation of the geopotential model EGM96. We specify issues evolving around the structure and consistency of the available information point sets which are relevant for the result of the continuation.

The dependence of the continuation results on the weight parameter also requires a deeper investigation. The experiments will consider the solution of the system of equations for weight parameters η spanning a relatively large interval Υ as, e.g.

$$\eta \in \Upsilon, \quad \Upsilon := \{10^{-20}, 10^{-19.99}, 10^{-19.98}, \ldots, 10^{9.98}, 10^{9.99}, 10^{10}\} \tag{6.1}$$

for the differently designed information point set P_Γ. Choosing the weight parameter η in the equation system is an important ingredient of the weighted least-squares approach. We look towards the design of an application oriented continuation method. Therefore we should a priori be able to chose the weight parameter so that a good continuation is obtained. We will see, that this parameter depends on the size and topology of the information point sets and on the considered tensor product basis. Our attention will go to this interrelationship.

Last but not least, the use of iterative system solvers and the effect of the premature interruption of the procedure will also be into more detail.

6.1 Algorithm

At this point, the algorithm of the approximate continuation of harmonic functions with our regularized least squares approach can be summarized as in Algorithm 6.1.1. For given information data points in P_Γ, we assemble the matrices of the equation system as presented in Chapter 4. We compute the representation coefficients $\mathbf{d}$ for a weight parameter η. The determined reconstruction can then be evaluated over the entire Ω and the boundary data has been harmonically continued.

Algorithm 6.1.1.

1. *Preprocessing: scale the given domain and the information point set* $P_\Gamma = \{(x_i, z_i), i = 1, \ldots, M\}$ *to* $\Omega = [0,1]^3$.
2. *Choose resolution* $2^{-\ell}$ *for the cubic splines* $\Psi = \{\psi_\lambda : \lambda \in \Lambda\}$ *defined on* Ω *and build the matrices* $\mathbf{A}$, $\mathbf{M}$, $\mathbf{G}$ *and the vector* $\mathbf{b}$ *as*

$$\mathbf{A} = (\mathbf{A}_{i\ell})_{\substack{i=1,\ldots,M \\ \ell=1,\ldots,L}},\ \mathbf{A}_{i\ell} = \psi_\ell(x_i), \quad \mathbf{M} = \mathbf{A}^\mathbf{T}\mathbf{A}, \quad \mathbf{b} = \mathbf{A}^T\mathbf{z},$$

$$\mathbf{G} = (\mathbf{G}_{\ell\ell'})_{\ell,\ell'=1,\ldots,L},\ \mathbf{G}_{\ell\ell'} = \int \Delta\psi_\ell(x)\Delta\psi_{\ell'}(x)dx.$$

3. *Choose the value for the weight parameter* η.
4. *Solve* $(\mathbf{M} + \eta\mathbf{G})\,\mathbf{d} = \mathbf{b}$ *to determine the spline coefficients* $\mathbf{d} = (d_\lambda)_{\lambda\in\Lambda}$ *of the approximate continuation* $u_\eta(x) = \sum_{\lambda\in\Lambda} d_\lambda\psi_\lambda(x),\ x \in \Omega$.

6.2 Numerical Setup

6.2.1 Input

We work with cuboid domains Ω where the information points P_Γ are available on two of its six parallel boundary sides, as inspired by geodetic applications, see Figure 1.1. We consider the full grid as

$$\Omega_\#{}^{n\times e\times h} := \{x_i \in \Omega :\ i = 1, \ldots, N\}. \tag{6.2}$$

This is a set consisting of $n \cdot e \cdot h$ uniformly gridded observation points covering the domain Ω. Here, n is the number of points in the north-south direction, e in the east-west direction and h for the height. It leads to the following mesh size per axis:

$$d_n = \frac{1}{n},\ d_e = \frac{1}{e} \text{ and } d_h = \frac{1}{h}. \tag{6.3}$$

Then the data set on the full domain is

$$P_\Omega{}^{n\times e\times h} := \{(x_i, z_i) :\ x_i \in \Omega_\#,\ z_i \in \mathbb{R}, i = 1, \ldots, N\}. \tag{6.4}$$

For a subset of $M \ll N$ observation points of $\Omega_\#$ defining $\Gamma_\#$, let $z_i \in \mathbb{R}$ be the given function values. The set

$$P_\Gamma := \{(x_i, z_i) : x_i \in \Gamma_\#, i = 1, \ldots, M\} \tag{6.5}$$

is then the set of *input observation points*. In general, P_Γ contains points situated at the boundaries of $\Omega_\#$. For the weighted least squares approach P_Γ contains one or two layers of points at the upper and/or lower boundary side. ${P_\Gamma}^{b,t}$ denotes an information point set with b layers of information points at the bottom boundary side and t layers of information points at the top boundary side of our cuboid domain ${\Omega_\#}^{n\times e\times h}$.

For the finite differences and the finite elements approach as described in Section 4.5, the points situated at all boundary sides of the gridded cuboid ${\Omega_\#}^{n\times e\times h}$ have to be known, accordingly to the theoretical setup. We denote this set of points with ${P_\Gamma}^{fd}$. Practically,

$${P_\Gamma}^{fd},\ {P_\Gamma}^{b,t} \subset {\Omega_\#}^{n\times e\times h} \tag{6.6}$$

and yield the same resolution, i.e. the same grid sizes d_n, d_e and d_h as in equation (6.3), see Figure 6.1. Further, we have for example

$${P_\Gamma}^{1,1} \subset {P_\Gamma}^{fd}, \quad {P_\Gamma}^{2,1} \not\subset {P_\Gamma}^{fd}, \tag{6.7}$$

as ${P_\Gamma}^{2,1}$ contains an additional layer of points near to the bottom boundary.

We further solve the resulting system of equations directly or iteratively for the considered basis and some weight parameter η assembled as in Section 4.2.3. For comparison purposes, reconstructions using finite elements or finite differences as described in Section 4.5 will be made available.

6.2.2 Tensor Product of B-Splines Basis

Most of the applications with data-fitting or partial differential equations in literature, e.g. [17, 151], work with linear basis functions. But since we know the stringent condition on our solution, namely the harmonicity, a smoother representation is more appropriate. We consider therefore cubic splines of minimal degree in order to ensure the evaluation of the regularization term involving the second derivative of the solution in the functional (4.8). Meissl already analyzed in his work [99] whether spline bases of higher degree, in particular quintic splines, provide better continuation results. He found that this is not the case. Therefore, we stay from the first place with tensor products of cubic splines. The basis functions of the three dimensional tensor product of a cubic B-spline basis that occurs on a given level l are tensor products of the one dimensional B-splines on level l constructed on the knot succession $T^{2^{-l}}$ with mesh size 2^{-l}:

$$2^{-l}\left[0,\ 0,\ 0,\ 0,\ 1,\ 2, \ldots,\ 2^l - 2,\ 2^l - 1,\ 2^l,\ 2^l,\ 2^l,\ 2^l\right]. \tag{6.8}$$

Each one of the $2^l + 3$ one–dimensional basis functions is compactly supported and so is each of the $\left(2^l + 2\right)^3$ three–dimensional ones. One finds below a comparison between the support of the one dimensional B-spline basis functions and the number of basis functions in the one– and three–dimensional tensor product of B-Spline basis for a given level.

Table 6.1. *Tensor product of B-splines basis: level–wise comparison of support and cardinality.*

Level l	Support $H = 4/2^l$	dof of 1D basis	dof of tensor product 3D basis
2	1	7	343
3	0.5	11	1331
4	0.25	19	6859
5	0.125	35	42875

6.2.3 Measures of Error and Validation

The harmonic continuation of local data is an ill-posed problem, as the unicity of the solution is lost due to incomplete boundary conditions. The best solution is hard to find and a compromise in the error measurements has been done. From the geodetic point of view, when constructing the continuation over a certain bounded domain, i.e. local continuation, the aim is a correct reconstruction in the middle of the domain. This is motivated by the fact that the continuation near to the boundaries would also require information from the region outside of the domain, which is not available. For clarity, the method minimizes the functional over the entire domain, yet in the end we are most interested to evaluate the error over the middle of it.

We define accordingly the points over the middle of the domain normalized to one $P_\Omega \subset [0,1]^3$ as ${P_\Omega}^{mid}$, see Figure 6.1, the set of points situated between the first and last quarter of the width and breadth of the domain, but the entire height of the cuboid domain

$$ {P_\Omega}^{mid} \subset P_\Omega, \quad {P_\Omega}^{mid} = [0.25, 0.75] \times [0.25, 0.75] \times [0, 1]. \tag{6.9} $$

The continuation error in the middle and the error over the boundary information point set P_Γ are then given as

$$ E_{2,\mathrm{bnd}} := \sqrt{\sum_{x_i \in P_\Gamma} \left(u_\eta(x_i) - z_i\right)^2}, \tag{6.10} $$

$$ E_{2,\mathrm{mid}} := \sqrt{\sum_{x_i \in {P_\Omega}^{mid}} \left(u_\eta(x_i) - z_i\right)^2}, \tag{6.11} $$

$$ E_{\infty,\mathrm{bnd}} := \max_{x_i \in P_\Gamma} \left\{ |u_\eta(x_i) - z_i| \right\}, \tag{6.12} $$

$$ E_{\infty,\mathrm{mid}} := \max_{x_i \in {P_\Omega}^{mid}} \left\{ |u_\eta(x_i) - z_i| \right\} \tag{6.13} $$

for some given continuation u_η computed with the weight parameter η. The results for the best η in terms of $E_{2,\mathrm{mid}}$ will be detailed.

Tabelarized results of our computations present the following specifications: level of the considered tensor product of the cubic B-spline basis, considered geometry for the boundary data set, considered weight parameter and the four error measurements introduced above. Additionally, we measure the harmonicity of the resulting continuation

Figure 6.1. *Examples of relevant full grid sub-sets: boundary datasets* ${P_\Gamma}^{1,1}$, ${P_\Gamma}^{2,1}$, ${P_\Gamma}^{fd}$ *and middle of the domain* ${P_\Omega}^{mid}$.

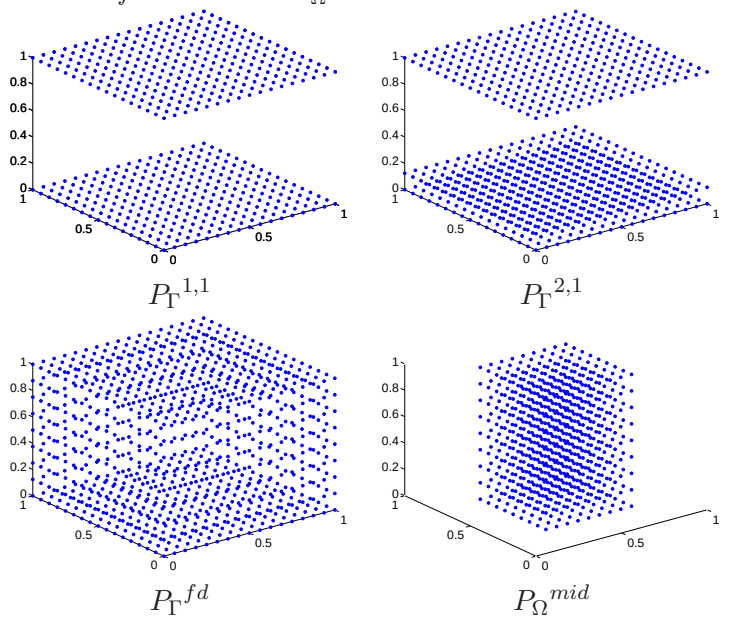

$u_\eta = \sum_{\lambda\in\Lambda} d_\lambda \psi_\lambda(x),\ x \in \Omega$, in terms of the representation coefficients $\mathbf{d} = (d_\lambda)_{\lambda\in\Lambda}$ as

$$E_{\Delta,\Omega} := \int_\Omega |\Delta u_\eta|^2 dx = \mathbf{dGd}. \tag{6.14}$$

We further consider the condition number of the system of equations to solve cond$(\mathbf{M} + \eta\mathbf{G})$, computed as the 2-norm condition number, i.e., the ratio of the largest singular value of $(\mathbf{M} + \eta\mathbf{G})$ to the smallest.

6.3 Experiments with Synthetic Harmonic Functions

6.3.1 Test Data

Our first row of experiments considers the continuation of synthetic harmonic functions. In view of the classical geopotential models based on spherical harmonics and large series of coefficients (e.g. EGM96, The NASA GSFC and NIMA Joint Geopotential Model of the Earth's gravitational potential complete to degree and order 360) we have chosen to simulate an anomalous potential field by a linear combination of low frequented spherical harmonics. Let (r, θ, λ) be the spherical coordinates of a computation point x with the geocentric radius r, the spherical co-latitude θ and the longitude λ_i of x. Considering the spherical harmonic representation of the potential field, we denote by $V^{n,m}$ the component of the spherical harmonic representation of degree n and order m:

$$V^{n,m}(r_i, \theta_i, \lambda_i) := \frac{1}{r}\left(\frac{R}{r_i}\right)^n (\cos(m\lambda_i) + \sin(m\lambda_i))\, P^{n,m}(\cos\theta_i) \tag{6.15}$$

with R the constant corresponding to the equatorial scale factor of the geopotential model and $P^{n,m}$ the (fully normalized) Legendre functions. For this particular example we set

$$R = 1, \tag{6.16}$$

choose the cubical domain Ω on top of a sphere with radius 1, set the gravity-mass constant of the model also to $GM = 1$ and evaluate the linear combination of spherical harmonics on the full grid $\Omega_{\#}$. This virtually corresponds to sampling the field outside of a source. For each x_i of the set $\Omega_{\#}$ we define z_i as the evaluation of a linear combination of spherical harmonics in x_i. Our experiments use two such constructed harmonic functions

$$f_1,\ f_2 : \mathbb{R}^3 \to \mathbb{R} \tag{6.17}$$

that resemble real potential field data by simulating the presence of a positive and a negative anomaly source and of the attenuation of the undulation with height. For the evaluation of $z_i \in \Omega_{\#}$ we choose two test functions

$$f_1(x_i) := V^{3,0}(r_i, \theta_i, \lambda_i) - V^{8,0}(r_i, \theta_i, \lambda_i), \tag{6.18}$$
$$f_2(x_i) := V^{3,1}(r_i, \theta_i, \lambda_i) - V^{6,1}(r_i, \theta_i, \lambda_i). \tag{6.19}$$

See Figure 6.2 for section views of these test functions over $\Omega_{\#}$.

Figure 6.2. *3D surface view of the two synthetic harmonic test functions $f_1 = V^{3,0} - V^{8,0}$ (left) and $f_2 = V^{3,1} - V^{6,1}$ (right) evaluated over $\Omega_{\#}$.*

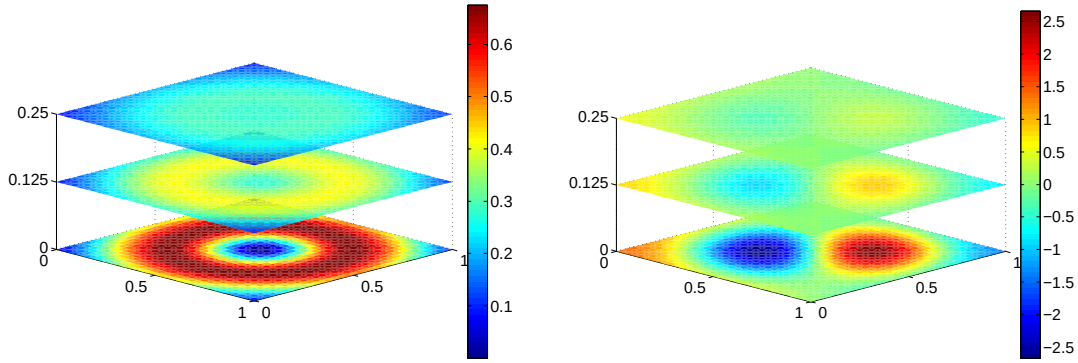

$f_1 = V^{3,0} - V^{8,0}$ $\qquad$ $f_2 = V^{3,1} - V^{6,1}$

Configuration of Data Sets and of the Boundary Data Sets

We proceed with the topological aspects. Let the Ω be the domain before normalization to one

$$\Omega = (0, 1)^2 \times (0, 0.25) \tag{6.20}$$

and let the full grid be

$$\Omega_{\#}{}^{n \times e \times h} = \{x_i \in \Omega :\ i = 1, \ldots, N\} \tag{6.21}$$

the set consisting of $n \times e \times h$ uniformly gridded observation points covering the domain Ω. In our experiments we have used synthetic harmonic data on the following full grids:

$$\Omega_{\#}{}^{16\times16\times8},\ \Omega_{\#}{}^{32\times32\times16} \text{ and } \Omega_{\#}{}^{64\times64\times32}. \tag{6.22}$$

Recall, $P_{\Gamma}{}^{b,t} \subset \Omega_{\#}$ denotes the boundary information point set with b layers of information points at the bottom boundary side and t layers of information points at the top boundary side of our cuboid domain $\Omega_{\#}{}^{n\times e\times h}$. If more then one layers at one side are included in $P_{\Gamma}{}^{b,t}$, then these are successively horizontally parallel layers from $\Omega_{\#}$ at a distance of

$$d_h = 0.25/h, \tag{6.23}$$

where 0.25 is the height of the cuboid and h the number of parallel horizontal planes in $\Omega_{\#}{}^{n\times e\times h}$. Notice that the distance between two layers decreases when the grid gets finer, that is, two layers of points for example in $\Omega_{\#}{}^{32\times32\times16}$ will span a distance twice as large as in $\Omega_{\#}{}^{64\times64\times32}$. Although the number of information points in $P_{\Gamma}{}^{2,0}$ for $\Omega_{\#}{}^{64\times64\times32}$ increases in comparison to $P_{\Gamma}{}^{2,0}$ for $\Omega_{\#}{}^{32\times32\times16}$, the information about the potential field somewhere higher above the surface is reduced.

Preliminary Continuations

Our initial full grid approximation experiments consider an isotropic tensor product basis of levels 2, 3, 4 and 5. Table 6.2 presents the experiments for a fixed set of boundary information points $P_{\Gamma}{}^{1,1}$ and varying level of the B-spline basis. For each case, the results for the best tested weight parameter η are detailed.

Further, Table 6.3 presents the experiments for a fixed set of boundary information points $P_{\Gamma}{}^{1,1}$ and $P_{\Gamma}{}^{2,0}$ and for varying levels of the B-splines basis. The attention goes to the results for an arbitrarily chosen weight parameter $\eta = 10^{-4}$. Please note the fact, that the systems of equations are solved directly, unless otherwise mentioned. In the case of the level 5 B-spline basis, due to memory issues, we could not compute the condition number of the system matrix. Instead of computing cond$(\mathbf{M} + \eta\mathbf{G})$ as the 2-norm condition number, i.e., the ratio of the largest singular value of $(\mathbf{M} + \eta\mathbf{G})$ to the smallest, we have turned to an estimator of the spectral condition number, namely CONDEST. It is a MATLAB function that computes a lower bound for the 1-norm condition number of a square matrix. CONDEST is based on the 1-norm condition estimator of Hager [62] and a block oriented generalization of Hager's estimator given by Higham and Tisseur [70]. The algorithm involves an iterative search to estimate the 1-norm of the inverse matrix without computing the inverse explicitly and calls the random function. The approximatively computed results for level 5 have been shaded gray. The results obtained for level 5 show that a finer basis does help to better fit the data. Also, a better fulfillment of the harmonicity constraint is achieved. We find that a higher level is consistent with the minimization of

$$E_{\Delta,\Omega} = \int_{\Omega} |\Delta u_{\eta}|^2 dx. \tag{6.24}$$

Table 6.2. *Results for continuation using a level 2, 3 and 4 basis,* ${P_\Gamma}^{1,1} \subset {\Omega_\#}^{32\times32\times16}$ *and* $f_1 = V^{3,0} - V^{8,0}$.

level	best η	$E_{2,\mathrm{mid}}$	$E_{\infty,\mathrm{mid}}$	$E_{2,\mathrm{bnd}}$	$E_{\infty,\mathrm{bnd}}$	$\int_\Omega \lvert\Delta u_\eta\rvert^2 dx$	cond$(\mathbf{M}+\eta\mathbf{G})$
2	5.0119e-02	1.0145e-01	1.0131e-02	6.3847e-02	1.0131e-02	3.8218e-01	4.3400e+05
3	3.4674e-10	4.2691e-02	4.8929e-03	2.6349e-02	4.8929e-03	2.0907e-01	4.4269e+13
4	3.8019e-10	1.1282e-02	7.0411e-04	1.2196e-03	1.9206e-04	1.0850e-02	6.5814e+14

Table 6.3. *Results for continuation using a fixed, arbitrarily chosen weight parameter* η *= 1e-4, level 2, 3, 4 and 5 basis,* ${P_\Gamma}^{1,1}$ *and* ${P_\Gamma}^{2,0} \subset {\Omega_\#}^{32\times32\times16}$ *and* $f_1 = V^{3,0} - V^{8,0}$. *For level 5 an estimator of the spectral condition number, CONDEST, has been employed.*

level	P_Γ	$E_{2,\mathrm{mid}}$	$E_{\infty,\mathrm{mid}}$	$E_{2,\mathrm{bnd}}$	$E_{\infty,\mathrm{bnd}}$	$\int_\Omega \lvert\Delta u_\eta\rvert^2 dx$	cond$(\mathbf{M}+\eta\mathbf{G})$
2	${P_\Gamma}^{1,1}$	1.0203e-01	1.1030e-02	6.3414e-02	1.1030e-02	3.8439e-01	6.4469e+06
3	${P_\Gamma}^{1,1}$	4.2693e-02	4.8909e-03	2.6349e-02	4.8909e-03	2.0907e-01	1.8515e+08
4	${P_\Gamma}^{1,1}$	1.1284e-02	7.0419e-04	1.2196e-03	1.9197e-04	1.0850e-02	1.0470e+10
5	${P_\Gamma}^{1,1}$	1.3097e-02	7.8635e-04	2.1110e-07	1.8632e-08	6.3327e-04	5.5803e+12

level	P_Γ	$E_{2,\mathrm{mid}}$	$E_{\infty,\mathrm{mid}}$	$E_{2,\mathrm{bnd}}$	$E_{\infty,\mathrm{bnd}}$	$\int_\Omega \lvert\Delta u_\eta\rvert^2 dx$	cond$(\mathbf{M}+\eta\mathbf{G})$
2	${P_\Gamma}^{2,0}$	2.9185e-01	1.4597e-02	8.6206e-02	1.1082e-02	4.7763e-01	2.7656e+07
3	${P_\Gamma}^{2,0}$	2.3518e-01	1.7243e-02	3.3862e-02	4.9063e-03	2.0274e-01	1.1758e+07
4	${P_\Gamma}^{2,0}$	2.4328e-02	1.4222e-03	1.5766e-03	1.9306e-04	1.0866e-02	2.0409e+08
5	${P_\Gamma}^{2,0}$	4.7541e-03	3.7943e-04	3.6473e-06	2.8598e-07	6.3748e-04	5.6484e+10

6.3.2 Variation of the Boundary Data Set

In order to assess the quality of the obtained approximation, we compare in experiments to come the continuation u_η for and differently configured input data sets P_Γ on Ω with the reference to the two test functions f_1 and f_2 on the full domain $P_\Omega = \{(x_i, z_i) : x_i \in \Omega_\#,\ z_i \in \mathbb{R}, i = 1, \ldots, N\}$.

Let us consider again the first synthetic harmonic function,

$$z_i = f_1(x_i) = V^{3,0}(r_i, \theta_i, \lambda_i) - V^{8,0}(r_i, \theta_i, \lambda_i), \quad z_i \in \Omega_\#. \tag{6.25}$$

Tables 6.4 – 6.6 display the error of the continuation for differently discretized full grids ${\Omega_\#}^{16\times16\times8}$, ${\Omega_\#}^{32\times32\times16}$ and ${\Omega_\#}^{64\times64\times32}$, and differently constructed boundary information point sets: sets with information points only at the lower side of the cuboid:

$${P_\Gamma}^{1,0}, \quad {P_\Gamma}^{2,0},$$

and sets with information points at both the lower and upper facets:

$${P_\Gamma}^{1,1},\ {P_\Gamma}^{2,1},\ {P_\Gamma}^{2,2},\ {P_\Gamma}^{3,2}.$$

For each continuation the tables present the best approximate continuation obtained from a wide range of weight parameters $\eta \in \{10^{-10}, \ldots, 10^{10}\}$.

Table 6.4. *Continuation using level* $l = 3$, $\Omega_{\#}{}^{16\times16\times8}$ *and* $f_1 = V^{3,0} - V^{8,0}$. *Continuation using finite differences and* $P_\Gamma{}^{fd}$.

P_Γ	best η	$E_{2,\text{mid}}$	$E_{\infty,\text{mid}}$	$E_{2,\text{bnd}}$	$E_{\infty,\text{bnd}}$	$\int_\Omega \lvert\Delta u_\eta\rvert^2 dx$	$\text{cond}(\mathbf{M}+\eta\mathbf{G})$
$P_\Gamma{}^{1,0}$	1.7783e-10	1.6218e+00	2.4057e-01	1.4723e-02	4.6937e-03	1.9215e-01	4.0216e+23
$P_\Gamma{}^{1,1}$	1.7783e-10	1.9020e-02	4.6937e-03	1.4742e-02	4.6937e-03	2.0886e-01	2.1572e+13
$P_\Gamma{}^{2,0}$	3.1623e-10	7.7303e-02	1.3673e-02	1.7658e-02	4.6937e-03	2.0392e-01	5.9330e+11
$P_\Gamma{}^{2,1}$	2.8184e-03	1.8842e-02	4.5774e-03	1.7755e-02	4.5774e-03	2.0927e-01	3.2813e+05
$P_\Gamma{}^{2,2}$	4.4668e-03	1.8859e-02	4.4697e-03	1.7863e-02	4.4697e-03	2.1001e-01	5.0379e+04
$P_\Gamma{}^{3,2}$	5.0119e-03	1.8863e-02	4.4671e-03	1.9115e-02	4.4671e-03	2.0972e-01	5.6062e+04
$P_\Gamma{}^{fd}$	–	2.6514e-02	3.8919e-03	–	–	–	–

Table 6.5. *Continuation using level* $l = 3$, $\Omega_{\#}{}^{32\times32\times16}$ *and* $f_1 = V^{3,0} - V^{8,0}$. *Continuation using finite differences and* $P_\Gamma{}^{fd}$.

P_Γ	best η	$E_{2,\text{mid}}$	$E_{\infty,\text{mid}}$	$E_{2,\text{bnd}}$	$E_{\infty,\text{bnd}}$	$\int_\Omega \lvert\Delta u_\eta\rvert^2 dx$	$\text{cond}(\mathbf{M}+\eta\mathbf{G})$
$P_\Gamma{}^{1,0}$	1.0471e-05	3.8038e+00	2.5948e-01	2.6318e-02	4.8927e-03	1.9237e-01	3.3636e+19
$P_\Gamma{}^{2,0}$	1.0233e-10	2.1932e-01	1.5994e-02	3.3860e-02	4.8929e-03	2.0438e-01	9.2450e+12
$P_\Gamma{}^{1,1}$	3.4674e-10	4.2691e-02	4.8929e-03	2.6349e-02	4.8929e-03	2.0907e-01	4.4269e+13
$P_\Gamma{}^{2,1}$	1.4125e-03	4.2040e-02	4.9115e-03	3.3906e-02	4.9115e-03	2.1088e-01	3.3978e+05
$P_\Gamma{}^{2,2}$	1.5849e-03	4.2090e-02	4.9093e-03	3.3938e-02	4.9093e-03	2.1234e-01	3.8117e+04
$P_\Gamma{}^{3,2}$	6.9183e-03	4.2082e-02	4.8778e-03	3.8184e-02	4.8778e-03	2.1067e-01	4.4530e+04
$P_\Gamma{}^{fd}$	–	1.8303e-02	9.9998e-04	–	–	–	–

Table 6.6. *Continuation using level* $l = 3$, $\Omega_{\#}{}^{64\times64\times32}$ *and* $f_1 = V^{3,0} - V^{8,0}$. *Continuation using finite differences and* $P_\Gamma{}^{fd}$.

P_Γ	best η	$E_{2,\text{mid}}$	$E_{\infty,\text{mid}}$	$E_{2,\text{bnd}}$	$E_{\infty,\text{bnd}}$	$\int_\Omega \lvert\Delta u_\eta\rvert^2 dx$	$\text{cond}(\mathbf{M}+\eta\mathbf{G})$
$P_\Gamma{}^{1,0}$	6.6069e-05	9.6323e+00	2.3062e-01	5.2379e-02	4.9085e-03	1.9250e-01	2.0201e+19
$P_\Gamma{}^{1,1}$	5.2481e-10	1.1193e-01	4.9089e-03	5.2440e-02	4.9089e-03	2.0923e-01	1.1687e+14
$P_\Gamma{}^{2,0}$	1.0471e-10	6.3794e-01	1.7953e-02	7.0439e-02	4.9089e-03	2.0382e-01	4.8209e+13
$P_\Gamma{}^{2,1}$	5.1286e-05	1.0977e-01	4.9107e-03	7.0485e-02	4.9107e-03	2.1429e-01	4.6494e+06
$P_\Gamma{}^{2,2}$	6.6069e-05	1.0982e-01	4.9112e-03	7.0539e-02	4.9112e-03	2.1527e-01	3.7939e+05
$P_\Gamma{}^{3,2}$	1.1749e-03	1.0984e-01	4.9231e-03	8.2300e-02	4.9231e-03	2.1373e-01	4.2481e+04
$P_\Gamma{}^{fd}$	–	1.2771e-02	2.5060e-04	–	–	–	–

Figure 6.3. *Results for* $f_1 = V^{3,0} - V^{8,0}$ *and* $\Omega_{\#}{}^{32\times32\times16}$. *Best continuation using* $P_\Gamma{}^{1,1}$ *(a),* $P_\Gamma{}^{1,0}$ *(c) and* $P_\Gamma{}^{2,0}$ *(d). Continuation using finite differences (b).*

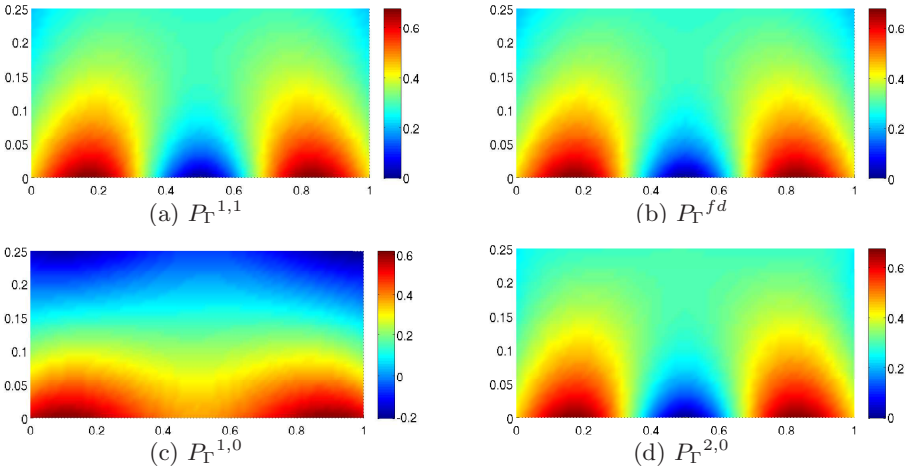

(a) $P_\Gamma{}^{1,1}$ (b) $P_\Gamma{}^{fd}$

(c) $P_\Gamma{}^{1,0}$ (d) $P_\Gamma{}^{2,0}$

Table 6.7. *Continuation using level $l = 4$, ${\Omega_\#}^{16\times16\times8}$ and $f_1 = V^{3,0} - V^{8,0}$. Continuation using finite differences and ${P_\Gamma}^{fd}$.*

${P_\Gamma}$	best η	$E_{2,\text{mid}}$	$E_{\infty,\text{mid}}$	$E_{2,\text{bnd}}$	$E_{\infty,\text{bnd}}$	$\int_\Omega \lvert\Delta u_\eta\rvert^2 dx$	$\text{cond}(\mathbf{M}+\eta\mathbf{G})$
${P_\Gamma}^{1,0}$	2.8184e-09	1.3478e+00	1.8257e-01	3.8092e-11	9.0991e-12	9.9849e-03	3.3147e+21
${P_\Gamma}^{1,1}$	1.2882e-10	5.3315e-03	7.6772e-04	2.1760e-12	4.3594e-13	1.0823e-02	5.0456e+14
${P_\Gamma}^{2,0}$	1.3804e-10	7.9610e-03	1.1742e-03	3.7814e-11	4.7161e-12	1.0823e-02	9.4770e+12
${P_\Gamma}^{2,1}$	1.1749e-10	2.7526e-05	4.3878e-06	1.1086e-11	1.4347e-12	1.0898e-02	1.0795e+12
${P_\Gamma}^{2,2}$	1.0233e-10	1.2999e-05	2.7116e-06	8.1326e-12	9.3792e-13	1.0899e-02	7.8118e+10
${P_\Gamma}^{3,2}$	1.0715e-10	5.7858e-06	1.2022e-06	2.0224e-11	3.0434e-12	1.0907e-02	3.8852e+10
${P_\Gamma}^{fd}$	–	2.6514e-02	3.8919e-03	–	–	–	–

Table 6.8. *Continuation using level $l = 4$, ${\Omega_\#}^{32\times32\times16}$ and $f_1 = V^{3,0} - V^{8,0}$. Continuation using finite differences and ${P_\Gamma}^{fd}$.*

${P_\Gamma}$	best η	$E_{2,\text{mid}}$	$E_{\infty,\text{mid}}$	$E_{2,\text{bnd}}$	$E_{\infty,\text{bnd}}$	$\int_\Omega \lvert\Delta u_\eta\rvert^2 dx$	$\text{cond}(\mathbf{M}+\eta\mathbf{G})$
${P_\Gamma}^{1,0}$	1.3183e-08	3.2736e+00	1.7555e-01	1.2175e-03	1.9206e-04	1.0005e-02	5.7865e+22
${P_\Gamma}^{1,1}$	1.2589e-10	2.0823e-02	1.2615e-03	1.5762e-03	1.9206e-04	1.0889e-02	3.5396e+13
${P_\Gamma}^{2,0}$	3.8019e-10	1.1282e-02	7.0411e-04	1.2196e-03	1.9206e-04	1.0850e-02	6.5814e+14
${P_\Gamma}^{2,1}$	2.0417e-03	1.8834e-03	1.9167e-04	1.5868e-03	1.9167e-04	1.0919e-02	2.1926e+07
${P_\Gamma}^{2,2}$	3.7154e-03	1.8836e-03	1.9066e-04	1.5954e-03	1.9066e-04	1.0914e-02	2.3632e+06
${P_\Gamma}^{3,2}$	1.0000e-10	1.8835e-03	1.9206e-04	1.7826e-03	1.9206e-04	1.1001e-02	1.2614e+11
${P_\Gamma}^{fd}$	–	1.8303e-02	9.9998e-04	–	–	–	–

Table 6.9. *Continuation using level $l = 4$, ${\Omega_\#}^{64\times64\times32}$ and $f_1 = V^{3,0} - V^{8,0}$. Continuation using finite differences and ${P_\Gamma}^{fd}$.*

${P_\Gamma}$	best η	$E_{2,\text{mid}}$	$E_{\infty,\text{mid}}$	$E_{2,\text{bnd}}$	$E_{\infty,\text{bnd}}$	$\int_\Omega \lvert\Delta u_\eta\rvert^2 dx$	$\text{cond}(\mathbf{M}+\eta\mathbf{G})$
${P_\Gamma}^{1,0}$	5.8884e-08	7.5879e+00	2.0605e-01	1.8909e-03	2.0275e-04	1.0006e-02	1.2008e+21
${P_\Gamma}^{1,1}$	1.2303e-10	2.8625e-02	7.0450e-04	1.8939e-03	2.0275e-04	1.0851e-02	1.3980e+17
${P_\Gamma}^{2,0}$	1.3183e-10	5.9780e-02	1.4291e-03	2.5510e-03	2.0275e-04	1.0894e-02	1.5705e+14
${P_\Gamma}^{2,1}$	1.2303e-03	3.9284e-03	2.0345e-04	2.5563e-03	2.0345e-04	1.0930e-02	2.2255e+07
${P_\Gamma}^{2,2}$	1.1482e-03	3.9280e-03	2.0342e-04	2.5585e-03	2.0342e-04	1.0934e-02	1.8388e+06
${P_\Gamma}^{3,2}$	2.8840e-04	3.9280e-03	2.0328e-04	2.9905e-03	2.0328e-04	1.0953e-02	1.1647e+06
${P_\Gamma}^{fd}$	–	1.2771e-02	2.5060e-04	–	–	–	–

Error measurements and the vertical sections depicted in Figure 6.3 show how the weighted least squares approach behaves. The continuation for ${P_\Gamma}^{1,0}$ is quite bad, just one layer of points gives no kind of gradient type information and the approximation does not resemble the reference dataset. On the other side, the continuation using ${P_\Gamma}^{2,0}$ is nearly as good as the one obtained with ${P_\Gamma}^{1,1}$. However, we still notice a difference in accuracy. The continuations for ${P_\Gamma}^{2,2}$ and ${P_\Gamma}^{3,2}$ yield similar errors, but the additional available information is associated with a lower condition number of the resulting system of equations for the best weight parameter.

In an intuitive scale of boundary data configurations sorted accordingly to their capacity to provide correct harmonic continuations, we could write:

$$ {P_\Gamma}^{1,0} \ll {P_\Gamma}^{2,0} < {P_\Gamma}^{1,1} < {P_\Gamma}^{2,1} < {P_\Gamma}^{2,2} \sim {P_\Gamma}^{3,2}. \tag{6.26} $$

In many cases the least squares approach produces a good continuation using information points situated only at the bottom side of the domain, as in the next example. Here, we can speak from an upward continuation in the strict sense. This is true for example for the second linear combination of spherical harmonics that we presented in our

Table 6.10. *Continuation using level $l = 3$, ${\Omega_\#}^{16\times16\times8}$ and $f_2 = V^{3,1} - V^{6,1}$. Continuation using finite differences and ${P_\Gamma}^{fd}$.*

${P_\Gamma}$	best η	$E_{2,\text{mid}}$	$E_{\infty,\text{mid}}$	$E_{2,\text{bnd}}$	$E_{\infty,\text{bnd}}$	$\int_\Omega \lvert\Delta u_\eta\rvert^2 dx$	$\text{cond}(\mathbf{M}+\eta\mathbf{G})$
${P_\Gamma}^{1,0}$	8.3176e-08	1.8981e+00	4.9260e-01	3.5102e-02	7.8406e-03	1.4753e+00	2.0898e+21
${P_\Gamma}^{1,1}$	1.0000e-10	6.0725e-02	7.8406e-03	3.5215e-02	7.8406e-03	1.7058e+00	3.8386e+13
${P_\Gamma}^{2,0}$	1.1220e-10	1.4461e-01	2.4192e-02	4.2964e-02	7.8406e-03	1.7740e+00	1.6722e+12
${P_\Gamma}^{2,1}$	1.4454e-03	4.5255e-02	7.8038e-03	4.3187e-02	7.8038e-03	1.8126e+00	2.7159e+05
${P_\Gamma}^{2,2}$	2.6915e-03	4.5256e-02	7.7201e-03	4.3468e-02	7.7201e-03	1.8180e+00	3.4138e+04
${P_\Gamma}^{3,2}$	3.8905e-03	4.5219e-02	7.6722e-03	4.7243e-02	7.6722e-03	1.8122e+00	4.4191e+04
${P_\Gamma}^{fd}$	–	1.0948e-01	1.0547e-02	–	–	–	–

Table 6.11. *Continuation using level $l = 3$, ${\Omega_\#}^{32\times32\times16}$ and $f_2 = V^{3,1} - V^{6,1}$. Continuation using finite differences and ${P_\Gamma}^{fd}$.*

${P_\Gamma}$	best η	$E_{2,\text{mid}}$	$E_{\infty,\text{mid}}$	$E_{2,\text{bnd}}$	$E_{\infty,\text{bnd}}$	$\int_\Omega \lvert\Delta u_\eta\rvert^2 dx$	$\text{cond}(\mathbf{M}+\eta\mathbf{G})$
${P_\Gamma}^{1,0}$	3.0903e-01	6.3216e+00	4.6936e-01	1.2187e-01	1.1179e-02	1.3916e+00	5.9755e+18
${P_\Gamma}^{1,1}$	1.0000e-10	1.2916e-01	8.1644e-03	6.0652e-02	8.1644e-03	1.7098e+00	1.5447e+14
${P_\Gamma}^{2,0}$	1.3804e-10	4.2205e-01	2.9538e-02	7.8851e-02	8.1644e-03	1.7860e+00	6.8541e+12
${P_\Gamma}^{2,1}$	1.0471e-10	9.6796e-02	8.1644e-03	7.8990e-02	8.1644e-03	1.8462e+00	3.9540e+11
${P_\Gamma}^{2,2}$	3.1623e-04	9.6792e-02	8.1758e-03	7.9182e-02	8.1758e-03	1.8404e+00	3.2362e+04
${P_\Gamma}^{3,2}$	2.0893e-03	9.6906e-02	8.1817e-03	8.9937e-02	8.1817e-03	1.8254e+00	2.9321e+04
${P_\Gamma}^{fd}$	–	7.5722e-02	2.6556e-03	–	–	–	–

Table 6.12. *Continuation using level $l = 3$, ${\Omega_\#}^{64\times64\times32}$ and $f_2 = V^{3,1} - V^{6,1}$. Continuation using finite differences and ${P_\Gamma}^{fd}$.*

${P_\Gamma}$	best η	$E_{2,\text{mid}}$	$E_{\infty,\text{mid}}$	$E_{2,\text{bnd}}$	$E_{\infty,\text{bnd}}$	$\int_\Omega \lvert\Delta u_\eta\rvert^2 dx$	$\text{cond}(\mathbf{M}+\eta\mathbf{G})$
${P_\Gamma}^{1,0}$	8.1283e-04	1.3071e+01	4.0414e-01	1.2025e-01	8.1774e-03	1.4796e+00	7.0816e+18
${P_\Gamma}^{1,1}$	1.0000e-10	3.2658e-01	8.1805e-03	1.2061e-01	8.1805e-03	1.7101e+00	6.2921e+14
${P_\Gamma}^{2,0}$	1.0965e-10	1.3063e+00	3.5422e-02	1.6294e-01	8.1805e-03	1.7822e+00	4.6103e+13
${P_\Gamma}^{2,1}$	1.0000e-10	2.5560e-01	8.1805e-03	1.6321e-01	8.1805e-03	1.8518e+00	2.2786e+12
${P_\Gamma}^{2,2}$	1.1749e-10	2.5552e-01	8.1805e-03	1.6351e-01	8.1805e-03	1.8551e+00	1.9947e+11
${P_\Gamma}^{3,2}$	6.0256e-04	2.5561e-01	8.1867e-03	1.9199e-01	8.1867e-03	1.8418e+00	5.3337e+04
${P_\Gamma}^{fd}$	–	5.2728e-02	6.6623e-04	–	–	–	–

experiments, namely when $z_i = V^{3,1}(r_i, \theta_i, \lambda_i) - V^{6,1}(r_i, \theta_i, \lambda_i), z_i \in \Omega_\#$. See Tables 6.10–6.12. Other experiments have shown that such upward continuation can be constructed when the dataset is relatively smooth. Of course, this works only when the source of the oscillations is underneath the bottom information points layer, conform to the upward continuation problem in geodesy. Attempting to build such a continuation for an arbitrary harmonic function, using such a reduced boundary information point set at one side, instead of six, is bounded to fail. Further, if P_Γ had points situated only at the opposite side to the source of the oscillations, we would practically deal with a pure downward continuation problem. Such a task is out of our scope. This weighted least squares approach, in the formulation presented here, is intrinsically designed to build upward continuations, and not downward, due to its smoothing effect.

Table 6.13. *Continuation using level $l = 4$, ${\Omega_\#}^{16\times16\times8}$ and $f_2 = V^{3,1} - V^{6,1}$. Continuation using finite differences and ${P_\Gamma}^{fd}$.*

P_Γ	best η	$E_{2,\text{mid}}$	$E_{\infty,\text{mid}}$	$E_{2,\text{bnd}}$	$E_{\infty,\text{bnd}}$	$\int_\Omega \lvert\Delta u_\eta\rvert^2 dx$	$\text{cond}(\mathbf{M}+\eta\mathbf{G})$
${P_\Gamma}^{1,0}$	1.0233e-01	2.8456e+00	3.9979e-01	6.4713e-03	9.1449e-04	7.8230e-02	1.3305e+18
${P_\Gamma}^{1,1}$	1.2882e-10	3.6546e-02	5.0013e-03	1.1484e-11	1.6716e-12	9.1949e-02	5.0456e+14
${P_\Gamma}^{2,0}$	1.1749e-10	2.5898e-02	4.5472e-03	9.9686e-11	1.6429e-11	9.7742e-02	1.1134e+13
${P_\Gamma}^{2,1}$	1.0715e-10	4.5858e-05	5.9947e-06	3.8159e-11	9.8068e-12	9.8614e-02	1.1837e+12
${P_\Gamma}^{2,2}$	1.1220e-10	2.6488e-05	3.7584e-06	3.7563e-11	8.9646e-12	9.8636e-02	7.1244e+10
${P_\Gamma}^{3,2}$	2.1380e-10	1.0880e-05	1.6945e-06	1.3603e-10	1.7758e-11	9.8762e-02	1.9472e+10
${P_\Gamma}^{fd}$	–	1.0948e-01	1.0547e-02	–	–	–	–

Table 6.14. *Continuation using level $l = 4$, ${\Omega_\#}^{32\times32\times16}$ and $f_2 = V^{3,1} - V^{6,1}$. Continuation using finite differences and ${P_\Gamma}^{fd}$.*

P_Γ	best η	$E_{2,\text{mid}}$	$E_{\infty,\text{mid}}$	$E_{2,\text{bnd}}$	$E_{\infty,\text{bnd}}$	$\int_\Omega \lvert\Delta u_\eta\rvert^2 dx$	$\text{cond}(\mathbf{M}+\eta\mathbf{G})$
${P_\Gamma}^{1,0}$	1.0233e-01	6.0002e+00	3.9126e-01	8.2512e-03	8.7901e-04	7.9513e-02	6.3064e+18
${P_\Gamma}^{1,1}$	2.5119e-10	7.4141e-02	4.4715e-03	3.2825e-03	3.5171e-04	9.3899e-02	1.0938e+15
${P_\Gamma}^{2,0}$	1.1220e-10	5.7784e-02	5.0482e-03	4.2851e-03	3.5171e-04	9.8566e-02	3.9591e+13
${P_\Gamma}^{2,1}$	1.5488e-03	5.3832e-03	3.5087e-04	4.3291e-03	3.5087e-04	9.8716e-02	2.0520e+07
${P_\Gamma}^{2,2}$	2.8184e-03	5.3816e-03	3.5132e-04	4.3767e-03	3.5132e-04	9.8632e-02	2.1149e+06
${P_\Gamma}^{3,2}$	1.0715e-10	5.3822e-03	3.5171e-04	4.9082e-03	3.5171e-04	9.9719e-02	1.1773e+11
${P_\Gamma}^{fd}$	–	7.5722e-02	2.6556e-03	–	–	–	–

Table 6.15. *Continuation using level $l = 4$, ${\Omega_\#}^{64\times64\times32}$ and $f_2 = V^{3,1} - V^{6,1}$. Continuation using finite differences and ${P_\Gamma}^{fd}$.*

P_Γ	best η	$E_{2,\text{mid}}$	$E_{\infty,\text{mid}}$	$E_{2,\text{bnd}}$	$E_{\infty,\text{bnd}}$	$\int_\Omega \lvert\Delta u_\eta\rvert^2 dx$	$\text{cond}(\mathbf{M}+\eta\mathbf{G})$
${P_\Gamma}^{1,0}$	5.0119e-04	1.7461e+01	5.1383e-01	4.9707e-03	3.7009e-04	8.1337e-02	2.6711e+18
${P_\Gamma}^{1,1}$	6.1660e-10	1.8815e-01	4.4659e-03	4.9896e-03	3.7017e-04	9.3947e-02	1.9047e+15
${P_\Gamma}^{2,0}$	1.0965e-10	1.5017e-01	5.3574e-03	6.7525e-03	3.7017e-04	9.8565e-02	1.9042e+14
${P_\Gamma}^{2,1}$	1.0471e-03	1.0857e-02	3.7144e-04	6.7817e-03	3.7144e-04	9.8807e-02	2.1634e+07
${P_\Gamma}^{2,2}$	1.7783e-03	1.0857e-02	3.7178e-04	6.8113e-03	3.7178e-04	9.8730e-02	2.1110e+06
${P_\Gamma}^{3,2}$	6.0256e-04	1.0868e-02	3.7135e-04	7.9850e-03	3.7135e-04	9.9088e-02	1.2297e+06
${P_\Gamma}^{fd}$	–	5.2728e-02	6.6623e-04	–	–	–	–

6.3.3 Comparison to Finite Differences

In parallel, Tables 6.7–6.15 include results of the finite differences approach. We denote with u_{fd} the continuation using the finite differences approach. The finite differences method always requires gridded information points on the entire boundary of the domain, that is all six sides of the cuboid, ${P_\Gamma}^{fd}$. For each considered full grid $\Omega_\#$, both ${P_\Gamma}^{fd}$ and e.g. ${P_\Gamma}^{2,1}$ are subsets of $\Omega_\#$, entail differently distributed data points over an identical grid and share therefore the mesh size. Hence, it makes sense to compare the finite differences continuation u_{fd} with u_η.

Though theoretically sound, the finite differences method does not always provide better results. Also, the boundary data set ${P_\Gamma}^{fd}$ as required by theory contains complete information for the solution of the Laplace equation up to the accuracy of the data. This is accompanied with a much greater complexity, as the finite differences approach has the disadvantage that computation costs considerably increase with the number of information points. Solving the resulting equation system in the finite difference method by means of conjugate gradients is a seconds relief, as it solves only a part of the problem. No matter

which solver we would choose, unlike finite differences or finite elements, the weighted least squares approach has the advantage to be able to provide a harmonic continuation with information on only two sides of the domain instead of all. This holds at least as long as the test data comes from potential–typed functions lying outside of the cuboid where information points are available.

For each of the considered test cases, i.e., for each full grid $\Omega_{\#}$ and the appropriate subset ${P_\Gamma}^{fd}$, we found consequently that for the incomplete boundary data set ${P_\Gamma}^{1,0}$ $E_{2,\mathrm{mid}}(u_{fd}) < E_{2,\mathrm{mid}}(u_\eta)$. This holds for the best η and independent from the considered level. The finite difference provided practically slightly better results than the approximate continuation with basis level $l = 3$, even when using the rather generous boundary data set ${P_\Gamma}^{3,2}$. But for $l = 4$ the performance of the least squares approach is superior: $E_{2,\mathrm{mid}}(u_{fd}) \sim E_{2,\mathrm{mid}}(u_\eta)$ for ${P_\Gamma}^{1,1}$ which entails a fraction of the information points of ${P_\Gamma}^{fd}$.

We can state at this point, that the approximate continuation employing a sufficient basis level solves the Laplace equation for ${P_\Gamma}^{1,1} \subset {P_\Gamma}^{fd}$ at least as well as finite differences. Yet, all other approximate continuations for boundary datasets containing at least two layers of points at the boundary, the approximate continuations are more exact than u_{fd}.

6.3.4 Variation of the Weight Parameter

In order to better understand the regulatory effect of the second term in (4.8) we analyze the influence of the weight parameter over the solution. Figures 6.4– 6.7 depict the error measurements $E_{2,\mathrm{mid}}$, $E_{\infty,\mathrm{mid}}$ and spectral condition number for the continuation problem with synthetic harmonic test function $V^{3,0} - V^{8,0}$ on two full grids, ${\Omega_\#}^{32\times32\times16}$ and ${\Omega_\#}^{64\times64\times32}$, with levels 3 and 4 of the (tensor product) B-Spline basis. First, the boundary data set P_Γ is fixed to ${P_\Gamma}^{1,1}$ and ${P_\Gamma}^{2,0}$ and then the level of the B-Spline basis is varied, see Figures 6.4 and 6.5. We find that the continuation quality increases indeed with the basis level on both middle of the domain and boundary data. Notice secondly that the continuation using ${P_\Gamma}^{2,0}$ is almost as good as the one using ${P_\Gamma}^{1,1}$ for each considered level and weight parameters $\eta \in [10^{-10}, 10^{-4}]$. We still see that ${P_\Gamma}^{1,1}$ leads to better results than ${P_\Gamma}^{2,0}$, as the solution is more sensitive with respect to the value of η. For $\eta \in [10^{-4}, 10^{-1}]$, the continuation results for ${P_\Gamma}^{1,1}$ are good, but with ${P_\Gamma}^{2,0}$ they get constantly worse with increasing η. This can be expected considering that we continue a harmonic function within a cuboid with input information on just one of the six sides.

Next, we fix the B-Splines basis level to $l = 3$ or to $l = 4$. We vary the structure of the boundary set P_Γ by considering sets with data at one or two sides of the cuboid and increase the number of layers:

$$ {P_\Gamma}^{2,0},\ {P_\Gamma}^{1,1},\ {P_\Gamma}^{2,1},\ {P_\Gamma}^{2,2},\ {P_\Gamma}^{3,2}, \tag{6.27} $$

thus increasing the available boundary information. Figure 6.6 shows the behavior of the solution of each stated continuation problem using the level 3 basis for an interval of weight parameters η. The continuation for ${P_\Gamma}^{2,0}$ is the poorest, the others are similar in quality. Hence, increasing the boundary information does not lead necessarily to a better solution, as the system seems to get saturated under the the influence of the term

enforcing the harmonicity. Still, the additional information is mirrored by the condition number, which gets lower with every supplementary layer. We presume, that a similar effect should be noticed when using a finer B-Spline basis with the saturation occurring at a larger information content, as more information can be represented by the basis. This is true indeed, as one can see in Figure 6.7, which depicts the behavior of the solution of each stated continuation problem using a level 4 basis and a finer full grid ${\Omega_\#}^{64\times64\times32}$ for an interval of weight parameters η. Here, we find that ${P_\Gamma}^{2,1}$, ${P_\Gamma}^{2,2}$ and ${P_\Gamma}^{3,2}$ provide about the same saturated error in the maximum norm over the middle of the domain $E_{\infty,\text{mid}}$. This error is considerably smaller than the saturated error resulting in the level 3 basis case. However, the respective spectral condition number for each considered boundary points set is larger when using the finer basis.

It is interesting to notice that, to a certain extent, a similar saturation effect also occurs in the evolution of the spectral condition number. Just as the continuation error for varying η is similar for ${P_\Gamma}^{2,2}$, ${P_\Gamma}^{3,2}$, so is the condition number of the resulting equation system $\text{cond}(\mathbf{M}+\eta\mathbf{G})$. This fact support our theory, that in spite of missing boundary data on the other sides of the cuboid, the system becomes sufficiently well posed under the influence of the additional regularization term enforcing the harmonicity in (4.8).

Figure 6.4. *Error $E_{2,mid}$ (left), $E_{\infty,mid}$ (middle) and spectral condition number (right) for the continuation problem with synthetic harmonic test function $V^{3,0}-V^{8,0}$ on ${\Omega_\#}^{32\times32\times16}$, boundary data ${P_\Gamma}^{1,1}$ and varying basis level.*

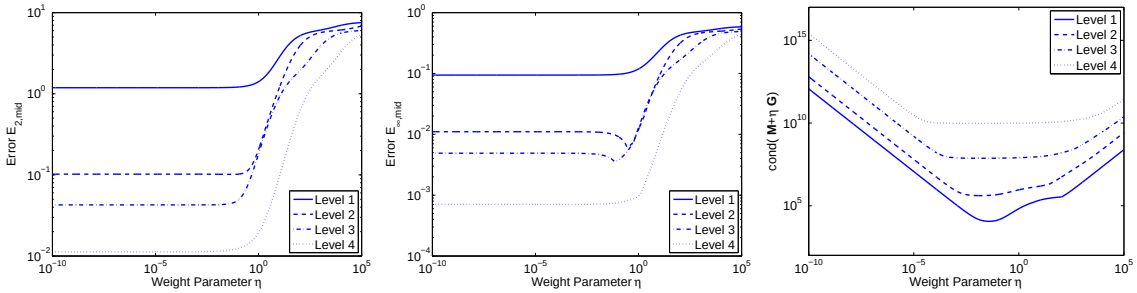

Figure 6.5. *Error $E_{2,mid}$ (left), $E_{\infty,mid}$ (middle) and spectral condition number (right) for the continuation problem with synthetic harmonic test function $V^{3,0}-V^{8,0}$ on ${\Omega_\#}^{32\times32\times16}$, boundary data ${P_\Gamma}^{2,0}$ and varying basis level.*

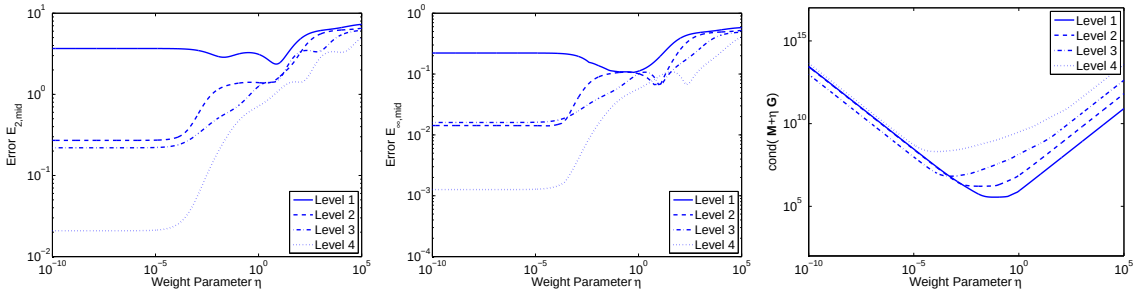

Figure 6.6. *Error $E_{2,mid}$ (left), $E_{\infty,mid}$ (middle) and spectral condition number (right) for the continuation problem with synthetic harmonic test function $V^{3,0} - V^{8,0}$ on ${\Omega_\#}^{32\times32\times16}$, level 3 (tensor product) B-Spline basis and varying boundary data P_Γ.*

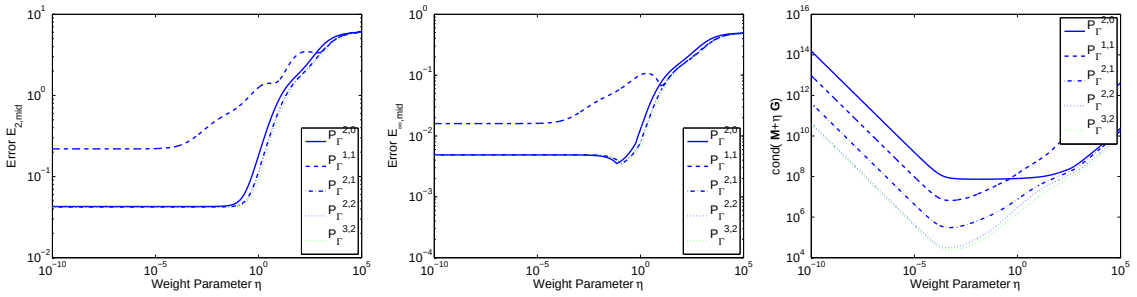

Figure 6.7. *Error $E_{2,mid}$ (left), $E_{\infty,mid}$ (middle) and spectral condition number (right) for the continuation problem with synthetic harmonic test function $V^{3,0} - V^{8,0}$ on ${\Omega_\#}^{64\times64\times32}$, level 4 (tensor product) B-Spline basis and varying boundary data P_Γ.*

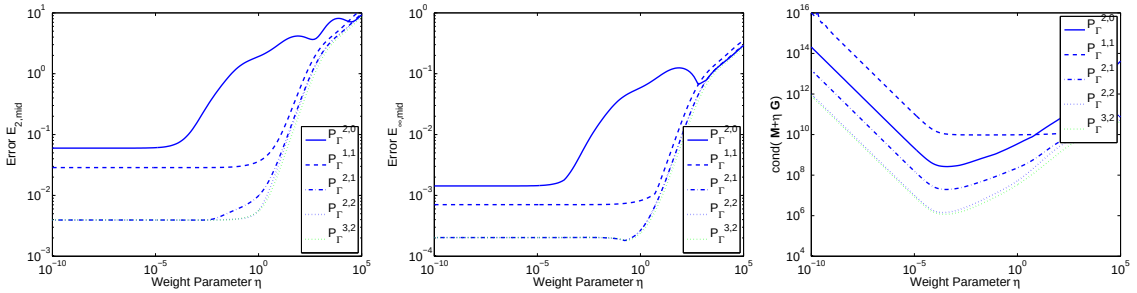

6.4 Experiments with Earth's Potential Field Data

Test Data Sets

Our second row of computations refers to several potential field datasets generated using the Geopotential Model EGM96, The NASA GSFC and NIMA Joint Geopotential Model [92]. Recall from Section 3.4 that the earth's gravitational potential and thus the undulation of the geoid can be expressed as infinite series of spherical harmonics outside the topographic surface of the earth. In order to compute the gravitational potential outside the topographic mass, one evaluates the series of spherical harmonics as follows. For $x = (r, \theta, \lambda)$ the spherical coordinates of a computation point x with the geocentric radius r, the spherical co-latitude θ and the longitude λ of x, we have

$$V^\infty(r,\theta,\lambda) = \frac{GM_1}{r} \sum_{n=0}^{\infty} \sum_{m=0}^{n} \left(\frac{a_1}{r}\right)^n \left(C_{n,m}\cos(m\lambda) + S_{n,m}\sin(m\lambda)\right) P^{n,m}(\cos\theta) \qquad (6.28)$$

with the gravity-mass constant GM_1, the equatorial scale factor a_1, that is the best fitting earth ellipsoid, and the (fully normalized) Legendre functions $P^{n,m}$. But as the geodetic information is limited, the geopotential models embody a truncated set of harmonic coefficients and are available with four components: the set of (fully normalized) coefficients

$C_{n,m}$ and $S_{n,m}$ for degrees $n = 0, \ldots, N$ and order $m = 0, \ldots, n$, the gravity-mass constant GM_1, the equatorial scale factor a_1 and the permanent tide system.

Remember at this point the degree variance of a spherical harmonics geoid model. The smaller the degree $n = 1, \ldots$, the greater the influence of the terms with spherical harmonics of degree n in the summation (3.30). The exponential drop of the model coefficients with the degree and the factor $\left(\frac{a_1}{r}\right)^n$ underline the fact that the smaller degree terms strongly dominate when computing the undulation values. Considering that the long-waved components of the geoid, that are the low-degree terms of the decomposition, are already known, numerical experiments will then work on blocks or truncated summation of spherical harmonics at the bottom. That is, we omit the evaluation of the low-degreed terms up to a point.

The potential field data sets [128–130] employed in this section have been provided by Prof. Dr. Schuh. Undulation values are obtained from the Geopotential Model EGM96. We are going to investigate the behavior of our weighted least squares approach, depending on the range of potential field frequencies. For this we consider three frequencies groups, i.e. datasets computed using spherical harmonics of degrees on three different intervals. For the first data set we employ spherical harmonics of degree 51 until 180 [128] (see Figure 6.8). The second one captures a large part of the lower frequencies and is computed with spherical harmonics of degree 20 until 180 [129] (see Figure 6.9). The third set considers the higher frequencies, going up to the highest available degree of EGM96: spherical harmonics of degree 51 until 360 [130] (see Figure 6.10). They use a grid $\widetilde{\Omega_\#}$ of $41 \times 41 \times 26$ observation points located between

$$\widetilde{\Omega_\#} \;=\; (6380, 10, 6630)[\text{km}] \times (-2000, 100, 2000)[\text{km}] \times (-2000, 100, 2000)[\text{km}] \qquad (6.29)$$

for the first two considered datasets [128, 129] and between

$$\widetilde{\Omega_\#} \;=\; (6380, 10, 6630)[\text{km}] \times (-1000, 50, 1000)[\text{km}] \times (-1000, 50, 1000)[\text{km}] \qquad (6.30)$$

for the third one [130]. Notice that the data is very low sampled, considering the high degree of the spherical harmonics used in the expansion. Fine oscillations will then not be sufficiently captured by the discretization grid, which leads to an aggravation in the ill-posedness of our continuation problem. For the computations this grid $\widetilde{\Omega_\#}$ has been scaled to $\Omega_\# \subset [0, 1]^3$.

6.4.1 Some Approximate Continuations

We begin with the tests for the first data set [128]. The continuation results are presented in Tables 6.16 and 6.19. For an intuitive evaluation of the performance of the proposed approximate continuations, we look at a vertical section of the original data field in Figure 6.8. One can notice the propagation of the gravity anomalies with the height as this vertical section depicts their interaction. This is one of the cases where we have observed that field continuation seems to be problematic.

Further, we test the weighted least squares approach for three reasonable information point sets P_Γ. Again, ${P_\Gamma}^{b,t}$ denotes an information point set with b layers of information points at the bottom side and t layers of information points at the top side of our cuboid

Table 6.16. *Continuation results for original dataset 1 [128] using a level 3 (tensor product) B-Spline basis, varying boundary dataset P_Γ and best η. Results for continuation using finite differences, finite elements and ${P_\Gamma}^{fd}$.*

P_Γ	best η	$E_{2,\text{mid}}$	$E_{\infty,\text{mid}}$	$E_{2,\text{bnd}}$	$E_{\infty,\text{bnd}}$	$\int_\Omega \lvert\Delta u_\eta\rvert^2 dx$	$\text{cond}(\mathbf{M}+\eta\mathbf{G})$
${P_\Gamma}^{1,0}$	1.0471e+09	1.8571e+00	9.4369e-02	7.9319e-01	9.4369e-02	6.7780e-10	1.9620e+18
${P_\Gamma}^{1,1}$	2.1380e+09	1.2734e+00	1.1067e-01	9.6229e-01	1.1067e-01	9.4594e-10	2.3270e+17
${P_\Gamma}^{2,0}$	3.1623e+09	2.1862e+00	1.0611e-01	1.1160e+00	1.0611e-01	7.1361e-10	3.9371e+18
${P_\Gamma}^{2,1}$	8.9125e-06	8.1697e-01	2.8704e-02	1.1232e-01	1.1457e-02	8.9457e+02	4.4502e+05
${P_\Gamma}^{2,2}$	5.7544e-06	6.0892e-01	2.1748e-02	9.9773e-02	1.0123e-02	1.3890e+03	2.8075e+05
${P_\Gamma}^{3,2}$	1.0000e-10	6.1546e-01	2.2861e-02	2.6344e-02	2.5688e-03	1.0780e+04	1.9321e+09
FD	–	4.6931e+00	8.3883e-02	–	–	–	–
FE	–	2.2099e+00	8.0870e-02	–	–	–	–

Table 6.17. *Continuation results for original dataset 2 [129] using a level 3 (tensor product) B-Spline basis, varying boundary dataset P_Γ and best η. Results for continuation using finite differences, finite elements and ${P_\Gamma}^{fd}$.*

P_Γ	best η	$E_{2,\text{mid}}$	$E_{\infty,\text{mid}}$	$E_{2,\text{bnd}}$	$E_{\infty,\text{bnd}}$	$\int_\Omega \lvert\Delta u_\eta\rvert^2 dx$	$\text{cond}(\mathbf{M}+\eta\mathbf{G})$
${P_\Gamma}^{1,0}$	2.3988e+00	2.8486e+00	1.0897e-01	1.2096e-01	1.6180e-02	1.3632e-02	1.4631e+18
${P_\Gamma}^{1,1}$	9.3325e+08	1.3034e+00	9.7179e-02	1.2153e+00	1.4585e-01	5.7968e-09	2.4356e+16
${P_\Gamma}^{2,0}$	1.4791e+09	4.1551e+00	1.2887e-01	1.3123e+00	1.4970e-01	4.3388e-09	2.9818e+18
${P_\Gamma}^{2,1}$	1.0000e-05	8.9758e-01	2.9314e-02	1.1338e-01	1.1489e-02	7.2683e+02	4.5078e+05
${P_\Gamma}^{2,2}$	6.0256e-06	6.5014e-01	2.1432e-02	9.9444e-02	9.9911e-03	1.2836e+03	2.8312e+05
${P_\Gamma}^{3,2}$	1.0000e-10	6.0514e-01	2.2618e-02	2.6010e-02	2.5350e-03	1.0333e+04	1.9321e+09
FD	–	7.8203e+00	1.6516e-01	–	–	–	–
FE	–	2.0328e+00	7.6449e-02	–	–	–	–

Table 6.18. *Continuation results for original dataset 3 [130] using a level 3 (tensor product) B-Spline basis, varying boundary dataset P_Γ and best η. Results for continuation using finite differences, finite elements and ${P_\Gamma}^{fd}$.*

P_Γ	best η	$E_{2,\text{mid}}$	$E_{\infty,\text{mid}}$	$E_{2,\text{bnd}}$	$E_{\infty,\text{bnd}}$	$\int_\Omega \lvert\Delta u_\eta\rvert^2 dx$	$\text{cond}(\mathbf{M}+\eta\mathbf{G})$
${P_\Gamma}^{1,0}$	5.1286e-05	1.5092e+00	7.1752e-02	1.0963e-03	1.3359e-04	2.1878e-04	3.5469e+19
${P_\Gamma}^{1,1}$	8.1283e+09	7.6162e-01	1.9761e-02	2.8611e-01	3.3538e-02	-5.5828e-11	1.8615e+16
${P_\Gamma}^{2,0}$	2.0893e+09	2.1682e+00	9.7629e-02	4.5806e-01	4.8319e-02	-1.2448e-10	3.1418e+18
${P_\Gamma}^{2,1}$	1.1749e-04	4.8295e-01	1.0936e-02	6.1922e-02	2.9010e-03	2.5761e+01	1.4076e+05
${P_\Gamma}^{2,2}$	5.4954e-05	3.5570e-01	8.4474e-03	5.0667e-02	2.1342e-03	5.6104e+01	8.8466e+04
${P_\Gamma}^{3,2}$	1.0000e-10	3.4408e-01	8.2143e-03	1.3713e-03	1.3358e-04	2.8112e+02	1.3522e+10
FD	–	2.1611e+00	3.4364e-02	–	–	–	–
FE	–	1.1462e+00	2.9015e-02	–	–	–	–

domain. If more than one layer is included at one side, then the layers are successive horizontal parallel layers from $\Omega_\#$. In this case we have 26 layers spanning a total of 250 km, thus a distance of 10 km between them.

The continuation tests for this datasets underline the fact, that information points on both the upper and lower side of the cuboid are needed in order to obtain reasonable results. Let us take a more detailed look for example at the approximate continuations for the first test data set [128]. For ${P_\Gamma}^{2,0}$, the most accurate continuation in view of the error E_{mid} is obtained for weight parameter $\eta = 8.9125e+09$. In fact, ${P_\Gamma}^{1,1}$, though slightly better, has also proved to be quite insufficient. The best continuation for ${P_\Gamma}^{1,1}$ is obtained for weight parameter $\eta = 1.0232e+09$. As one can see in Figure 6.8, the results are not satisfactory since the continuations do not reproduce the interaction between the

Table 6.19. *Continuation results for original dataset 1 [128] using a level 4 (tensor product) B-Spline basis, varying boundary dataset P_Γ and best η. Results for continuation using finite differences, finite elements and ${P_\Gamma}^{fd}$.*

P_Γ	best η	$E_{2,\text{mid}}$	$E_{\infty,\text{mid}}$	$E_{2,\text{bnd}}$	$E_{\infty,\text{bnd}}$	$\int_\Omega \lvert\Delta u_\eta\rvert^2 dx$	$\text{cond}(\mathbf{M}+\eta\mathbf{G})$
${P_\Gamma}^{1,0}$	6.7608e+08	1.2402e+00	9.9720e-02	1.3998e+00	9.9720e-02	9.9678e-09	4.9060e+18
${P_\Gamma}^{1,1}$	2.5119e+08	1.2484e+00	1.0645e-01	9.2144e-01	1.0645e-01	7.6451e-09	9.1057e+17
${P_\Gamma}^{2,0}$	3.8019e+08	1.3464e+00	1.0719e-01	1.0770e+00	1.0719e-01	7.1527e-09	5.6409e+17
${P_\Gamma}^{2,1}$	8.7096e-06	8.1477e-01	2.7432e-02	1.0815e-01	9.2825e-03	9.2080e+02	2.1434e+06
${P_\Gamma}^{2,2}$	5.6234e-06	6.0712e-01	2.0669e-02	9.5166e-02	7.9579e-03	1.4228e+03	1.2566e+06
${P_\Gamma}^{3,2}$	1.0000e-10	6.0730e-01	2.2416e-02	8.0448e-04	1.2049e-04	1.0065e+04	1.3547e+09
FD	–	4.6931e+00	8.3883e-02	–	–	–	–
FE	–	2.2099e+00	8.0870e-02	–	–	–	–

Table 6.20. *Continuation results for original dataset 2 [129] using a level 4 (tensor product) B-Spline basis, varying boundary dataset P_Γ and best η. Results for continuation using finite differences, finite elements and ${P_\Gamma}^{fd}$.*

P_Γ	best η	$E_{2,\text{mid}}$	$E_{\infty,\text{mid}}$	$E_{2,\text{bnd}}$	$E_{\infty,\text{bnd}}$	$\int_\Omega \lvert\Delta u_\eta\rvert^2 dx$	$\text{cond}(\mathbf{M}+\eta\mathbf{G})$
${P_\Gamma}^{1,0}$	5.2481e+04	1.6080e+00	7.5072e-02	6.2901e-01	7.5072e-02	1.1308e-06	5.2318e+17
${P_\Gamma}^{1,1}$	7.4131e+07	1.2838e+00	9.6289e-02	9.2168e-01	9.6289e-02	-4.5912e-08	1.7465e+16
${P_\Gamma}^{2,0}$	6.7608e+07	3.3156e+00	1.0004e-01	9.7792e-01	9.2972e-02	-3.8383e-08	1.6064e+18
${P_\Gamma}^{2,1}$	9.7724e-06	8.9226e-01	2.7949e-02	1.0923e-01	9.3548e-03	7.4628e+02	2.1826e+06
${P_\Gamma}^{2,2}$	6.0256e-06	6.4571e-01	2.0719e-02	9.5818e-02	7.9453e-03	1.2793e+03	1.2743e+06
${P_\Gamma}^{3,2}$	1.0000e-10	5.9783e-01	2.2172e-02	7.9981e-04	1.2462e-04	9.6449e+03	1.3547e+09
FD	–	7.8203e+00	1.6516e-01	–	–	–	–
FE	–	2.0328e+00	7.6449e-02	–	–	–	–

Table 6.21. *Continuation results for original dataset 3 [130] using a level 4 (tensor product) B-Spline basis, varying boundary dataset P_Γ and best η. Results for continuation using finite differences, finite elements and ${P_\Gamma}^{fd}$.*

P_Γ	best η	$E_{2,\text{mid}}$	$E_{\infty,\text{mid}}$	$E_{2,\text{bnd}}$	$E_{\infty,\text{bnd}}$	$\int_\Omega \lvert\Delta u_\eta\rvert^2 dx$	$\text{cond}(\mathbf{M}+\eta\mathbf{G})$
${P_\Gamma}^{1,0}$	1.8197e-03	4.4669e+00	1.1665e-01	1.0741e-04	8.2618e-06	1.1950e-05	9.1869e+18
${P_\Gamma}^{1,1}$	7.9433e+08	7.6200e-01	1.9033e-02	2.8949e-01	2.5714e-02	-1.2117e-09	1.0293e+16
${P_\Gamma}^{2,0}$	3.8019e+05	7.5540e+00	2.0886e-01	1.7783e-01	1.0995e-02	5.2190e-09	3.0510e+15
${P_\Gamma}^{2,1}$	1.1749e-04	4.8120e-01	1.0538e-02	6.0966e-02	2.9211e-03	2.5157e+01	6.8346e+06
${P_\Gamma}^{2,2}$	5.3703e-05	3.5339e-01	8.3935e-03	4.9139e-02	2.1100e-03	5.6062e+01	6.0711e+05
${P_\Gamma}^{3,2}$	1.0000e-10	3.4471e-01	8.2665e-03	2.3547e-04	8.2463e-06	2.6297e+02	8.2545e+09
FD	–	2.1611e+00	3.4364e-02	–	–	–	–
FE	–	1.1462e+00	2.9015e-02	–	–	–	–

anomalies. But the results for ${P_\Gamma}^{2,1}$ are above expectations. With a more consistent set of information points on the lower side of the domain, where the oscillations are the strongest, we get significantly preciser results than using the finite differences and the finite elements approach.

The experiments with the second [129] and third [130] undulation data depicted in Figures 6.9, 6.10 and detailed in Tables 6.17, 6.18 show a quite similar behavior: the approximate continuation for ${P_\Gamma}^{2,0}$ is bad, the one for ${P_\Gamma}^{2,1}$ is better than the one obtained with finite differences.

Figure 6.8. *Original data set 1. Approximate continuation using weighted least squares: Level 3 cubic splines and each best η for each P_Γ. Continuation using finite elements and finite differences. Vertical section in the reconstruction at* $(6380, 6630)$ *[km]*$\times$ (0)*[km]* $\times$ $(-2000, 2000)$*[km].*

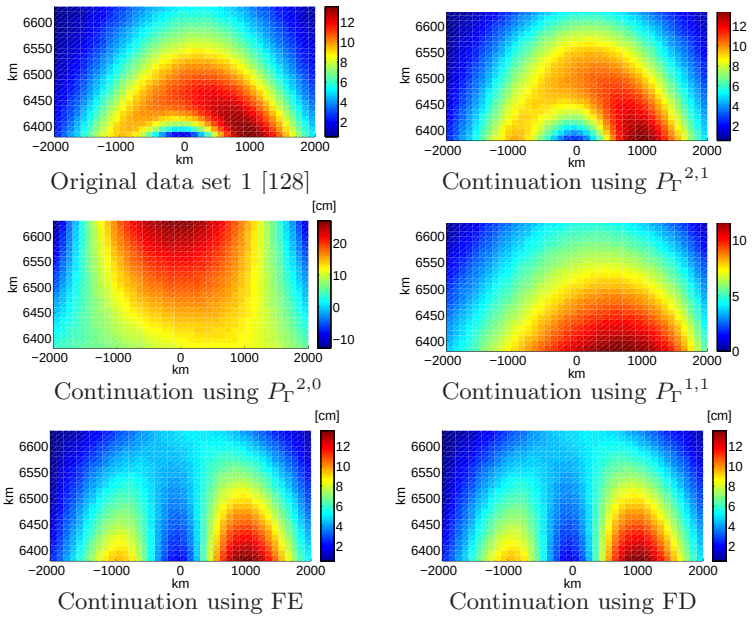

Figure 6.9. *Original dataset 2 [129]. Approximate continuation using weighted least squares: Level 3 cubic splines and best η for each P_Γ. Continuation using finite differences. Vertical section in the reconstruction at* $(6380, 6630)$ *[km]* $\times$ (0)*[km]* $\times$ $(-2000, 2000)$*[km].*

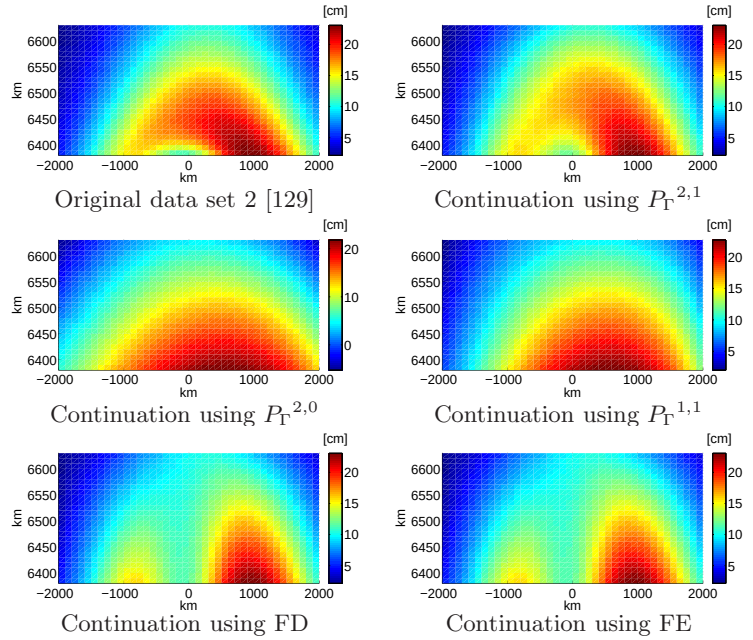

Figure 6.10. *Vertical section of third set of original data [130]. Approximate continuation using finite differences. Approximate continuation using weighted least squares: Level 3 cubic splines and best η for each P_Γ. Vertical section in the reconstruction at* $(6380, 6630)$ *[km]*$\times(0)$ *[km]*$\times(-1000, 1000)$*[km].*

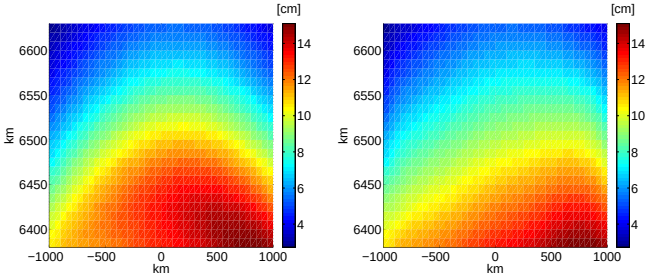

Original data set 3 [130] Continuation using FD

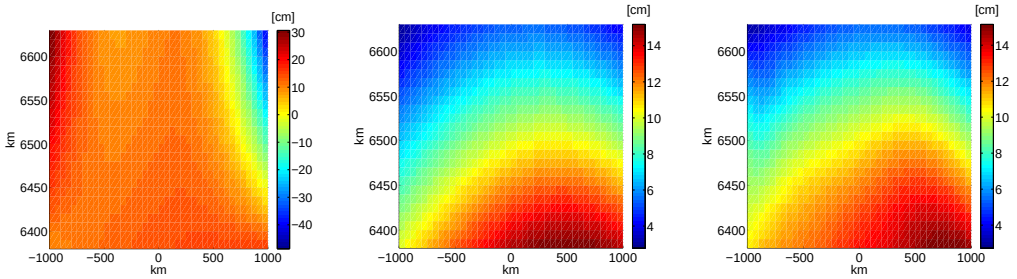

Continuation using ${P_\Gamma}^{2,0}$ Continuation using ${P_\Gamma}^{1,1}$ Continuation using ${P_\Gamma}^{2,1}$

6.4.2 Comparison to Finite Differences and Finite Elements

We find that the finite element method and the finite differences are not able to properly reconstruct the test fields in the middle of the domain, where the anomalies interact, see Figure 6.8. It is interesting to see how both finite elements and finite differences fail to reconstruct the data set, despite the fact that both methods have been proven to solve the Laplace equation.

See Figure 6.11 to find a comparison of the discrete Laplacian of the data set, the solution using ${P_\Gamma}^{2,1}$ and the solution obtained using finite differences. We have chosen the discrete Laplacian as the data is only discrete available. The discrete Laplacian of the data set [128] shows deviations from zero in the immediate neighborhood of the anomaly. This is where the high degree components are incompletely resolved and hence lead to a considerably non harmonic part to the test function. We suspect that the poor resolution, i.e., the bad sampling of the data, corroborated with the high degree of the spherical harmonic components that have been evaluated, lead to these difficulties. This behavior resides mostly in the fact, that the dataset at this mesh size is not consistent with the harmonicity constraint.

Of course, one cannot try to reconstruct a non–harmonic function by enforcing that the Laplacian is 0. The strict approach of solving the Laplace equation by the finite elements and finite differences, though successful in the case of the synthetic dataset, fails here. As it can be expected, the solution obtained by finite differences has a discrete Lapla-

cian of practically 0. Yet, the better result is obtained by the approximate continuation using ${P_\Gamma}^{2,1}$. Here, the harmonicity constraint is only fulfilled to a certain extent. This motivates us more to investigate the weighted least-squares approach, which targets on an arbitrary, deliberate approximate fulfillment of Laplace's equation with respect to the given boundary condition.

Figure 6.11. *Discrete Laplacian for the original data set 1 (top), best continuation using weighted least squares and* ${P_\Gamma}^{2,1}$ *(middle) and continuation using finite differences (bottom). Vertical section at* $(6380, 6630)$ *[km]*$\times(0)$*[km]* $\times(-2000, 2000)$ *[km].*

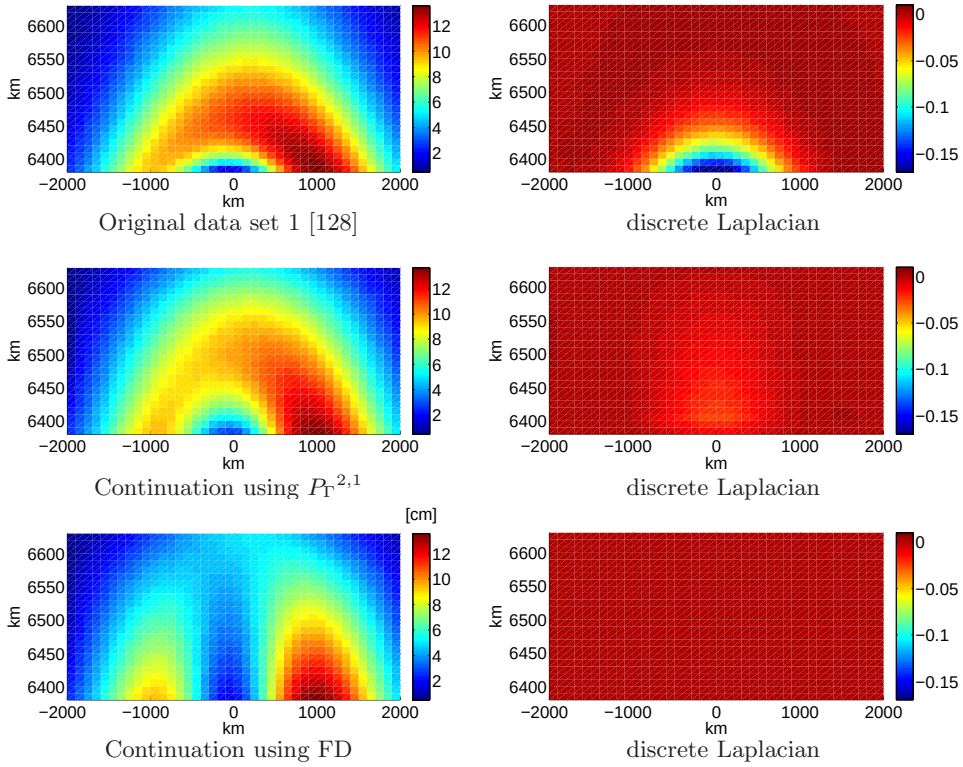

6.5 Constraints of the Least-Squares-Approach for Potential Field Datasets

As we have already seen, the gravity potential of the earth is classically represented by a spherical harmonics decomposition as

$$V(r,\theta,\lambda) = \frac{GM_1}{r}\sum_{n=0}^{N}\sum_{m=0}^{n}\left(\frac{a_1}{r}\right)^n \left(C_{n,m}\cos(m\lambda) + S_{n,m}\sin(m\lambda)\right) P^{n,m}(\cos\theta) \qquad (6.31)$$

for some point in spherical coordinates $x = (r, \theta, \lambda)$, the (fully normalized) Legendre functions $P^{n,m}$, the gravity-mass constant GM_1 and the equatorial scale factor a_1. The fundamental gravity field unknowns $C_{n,m}$ and $S_{n,m}$, the set of (fully normalized) coefficients,

have been determined up to a resolvable degree. For the Geopotential Model EGM96 the coefficients are available up to the maximal degree $N = 360$, which corresponds to a minimal wavelength for $a_1 = 6378.135$ km of

$$w = \frac{2\pi a_1}{2N+1} \;=\; 55.5825 \text{ km}. \tag{6.32}$$

See Figure 3.7 to find the wavelength per degree of the spherical harmonic decomposition. The factor

$$F_h^n = \left(\frac{a_1}{a_1+h}\right)^n = \left(\frac{a_1}{r}\right)^n \tag{6.33}$$

for a point with radius

$$r = a_1 + h \tag{6.34}$$

describes the field attenuation with the altitude, which is dependent on the degree n, which further correlates to the wavelength $w = 2\pi a_1/(2n+1)$.

This means, that the attenuation of the potential field and its anomalies, that is the decay with the distance to the earth, is dependent on the wavelength, such that short wavelength anomalies decay faster than the long-waved ones. At an altitude h above the topographic surface of the earth, the potential is affected by the (spherical harmonic) component of degree n reduced by the factor $\left(\frac{a_1}{a_1+h}\right)^n$ compared to directly at the surface.

In conclusion, the attenuation is a function of both the distance from the source and the wavelength. This is why satellite data alone cannot deliver a fine geoid model, as fine oscillations of the geoid have attenuated at satellite height. The critical wavelength, that is the minimal wavelength that can be resolved by a satellite flying at height h is approximately equal to h. For example, a satellite flying at $h = 250$km height will resolve the spherical harmonic coefficients up to a maximal degree $n_h = 80$. The determination of components with higher spherical harmonic degree from satellite data needs otherwise to be amplified by the reciprocals of the attenuation factors to produce a gravity field on the surface – which means to construct a downward continuation – and thus magnifying measurements errors (see [109]). Only components of spherical degree not larger than $n_h = 80$ do not attenuate up to satellite height. Components of higher degrees have been smoothed and practically do not contribute to the geoid height at that point.

Another question to be considered is, how good does the data to be upward continued resolve the undulation of the geoid at the given height? The dimension of the space spanned by spherical harmonics of degree n is $2n+1$. Further, since the minimal wavelength is related to the maximal degree as $w = 2\pi a_1/(2N+1) \;=\; 55.5825$ km, we can compute up to which degree a certain dataset resolves the geoid undulation or potential values. We compute the highest degree

$$n_{\max}^{P_\Gamma} = \left\lfloor \frac{1}{2}\left(\frac{2\pi a_1}{\Delta x} - 1\right)\right\rfloor \tag{6.35}$$

where we consider the mesh size Δx of the available data points grid. When constructing the upward continuation, the missing points in the middle of our cuboid domain can be counter valued by the existence of the term in the functional (4.8) forcing the harmonicity.

However, the continuation cannot be more accurate than the given data at the boundaries. This means, the frequencies lost by the data resolution at the surface will also miss in the upward continuation. This is not dramatic, because high frequencies attenuate very fast. The missing higher frequencies will cause a continuation error, which attenuates itself as the higher frequencies would have attenuated. Practically, the continuation error caused by the finer frequencies than the data points grid can resolve will remain a constitute of the continuation solution but only within the lower section of the domain, where the height is approximately as large as the wavelength of the missed frequencies.

Further, the incomplete sampled short waved component leads to a non-harmonic constituent in the data, as we have noticed in Section 6.4.2. This constituent will also attenuate with the altitude. In conclusion, the further we are from the source, the more correct should the continuation be.

Lastly, we discuss to which extent the chosen (tensor product of) B-Spline basis Ψ is relevant for the quality of the upward continuation. To this end, we bring the support of the B-Spline basis functions in relation to the wavelength of a spherical harmonic. The one dimensional B-Spline basis has been defined on the interval $[0, 1]$ and the cuboid domain $\Omega_\#$ has been scaled, so that

$$\Omega_\# \subset [0, 1]^3. \tag{6.36}$$

Let L be the original length of the cuboid, then the support of a B-Spline basis of level l with respect to length L of the grid is

$$H_L^l = L\frac{4}{2^l}. \tag{6.37}$$

Now take a look at Figure 3.30. A set of points with mesh size

$$\Delta x = 2\pi a/(2n + 1) \tag{6.38}$$

over the entire surface of the sphere will uniquely determine a spherical harmonic component of degree n. However, in order to fit such a curve with B-splines, which are locally supported and not intrinsically harmonic, one needs at least twice as many points. By further setting the distance between points Δx to the half of the wavelength

$$\Delta x = w/2 = H_L^l/4 \tag{6.39}$$

we have $\frac{w}{2} = \frac{L}{2^l}$ and

$$w = H_L^l/2. \tag{6.40}$$

This is because a cubic spline needs four control points. We see that, without further regarding the curvature of the earth, the finest spherical harmonic component that can be approximated by the B-Spline basis of level l living on an interval of size L is approximately

$$n_{\max}^{\Psi} \approx \frac{1}{2}\left(\frac{2\pi a_1}{\frac{H_L^l}{2}} - 1\right) = \frac{1}{2}\left(2\pi a_1 \frac{2^l}{2L} - 1\right) = \frac{1}{2}\left(\frac{\pi a_1 2^l}{L} - 1\right). \tag{6.41}$$

Figure 6.12. *B-Spline basis function with support $H_L = 4L/s^l$ and spherical harmonic component of wavelength $w = 2L/2^l$ living on an uniform set of 2^l data points of length L and mesh size $\Delta x = L/2^l$.*

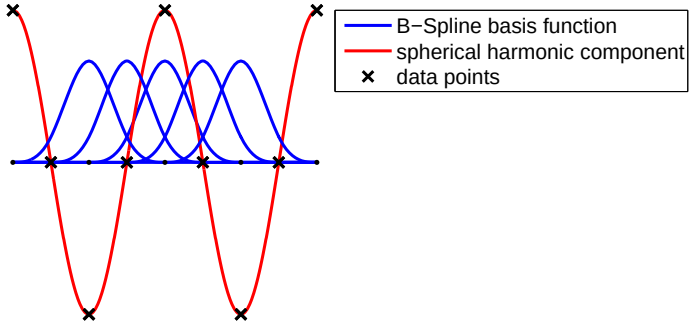

The finest frequency that can be resolved in a given upward continuation setup is bounded by the maximum degree dictated by the information available in the boundary data and the chosen B-Spline basis. In conclusion, the maximal spherical harmonic degree that can be resolved by a given boundary dataset P_Γ with width L, grid mesh w and a B-Spline basis of level l is

$$n_{\max} = \min\left\{n_{\max}^{P_\Gamma}, n_{\max}^{\Psi}\right\}. \tag{6.42}$$

We can then a priori choose a sufficient B-Spline Basis of level l living on an interval of length L and support $H_L^l = 4L/2^l$ that resolves the data by looking at the highest frequency component of the data. From equation (6.41) this is

$$n_{\max}^{P_\Gamma} = n_{\max}^{\Psi} \approx \frac{1}{2}\left(\frac{\pi a_1 2^l}{L} - 1\right) = \frac{\pi a_1 2^l}{2L} - \frac{1}{2} = \frac{2\pi a_1}{H_L^l} - \frac{1}{2}. \tag{6.43}$$

This translates to a support of

$$H_L^l \approx \frac{2\pi a_1}{n_{\max}^{P_\Gamma} + \frac{1}{2}} \tag{6.44}$$

and yields the level l from $H_L^l = 4L/2^l$ as

$$l = \log_2 \frac{4L}{H_L^l} \approx \log_2 4L \frac{n_{\max}^{P_\Gamma} + \frac{1}{2}}{2\pi a_1}. \tag{6.45}$$

The minimal mesh size Δx with $H_L^l = 4\Delta x$ is

$$\Delta x = \frac{H_L^l}{4} = \frac{\pi a_1}{2\, n_{\max}^{P_\Gamma} + 1}. \tag{6.46}$$

Remember that spherical harmonics are globally supported. In order to resolve the field up to a fixed maximal degree n of the spherical harmonics, one needs a grid of mesh width w necessarily distributed over the entire surface of the sphere. Yet, when using the least-squares approach and cubic B-Splines one needs a finer mesh with $\Delta x = w/2$ covering only the given cubical domain.

We go back to the original dataset 1 considered for the upward continuation experiments: we employ a grid $\widetilde{\Omega_{\#}}$ of $41 \times 41 \times 26$ observation points located between

$$(6380, 10, 6630)[\text{km}] \times (-2000, 100, 2000)[\text{km}] \times (-2000, 100, 2000)[\text{km}]$$

and spherical harmonics of degrees 20 – 180 [128] (see Figure 6.8). We have then a grid of the boundary dataset with $\Delta x = 100km$. The highest frequented component for degree $n_{\max} = 180$ corresponds to the wavelength

$$w = \frac{2\pi a_1}{2n_{\max} + 1} = 111.01km. \tag{6.47}$$

Then, the highest degree $n^{\Psi}_{\max}$ that can be resolved using the least squares approach and the B-Spline basis by fitting a grid with $\Delta x = 100km$ results from $\Delta x = \pi a_1/(2\, n^{\Psi}_{\max} + 1)$ as

$$n^{\Psi}_{\max} \approx \frac{\pi a_1}{2\Delta x} - \frac{1}{2} \approx 100. \tag{6.48}$$

The highest degree $n^{P_\Gamma}_{\max}$ that could be computed by the spherical harmonics approach can be derived from $\Delta x = w = 2\pi a_1/(2n^{P_\Gamma}_{\max} + 1)$ as

$$n^{P_\Gamma}_{\max} \approx \frac{\pi a_1}{\Delta x} - \frac{1}{2} \approx 200. \tag{6.49}$$

However, the spherical harmonics approach requires the data given over the entire surface of the earth with given Δx. Yet as long as the data is only locally given, the spherical harmonic approach is impracticable.

This comparison shows the price of locality of the available data when resolving a sampled spherical harmonic component of a certain degree. Within the data fitting step for the approximate continuation, the low frequencies will be resolved. The highest ones are only captured as noise. When constructing the upward continuation of this local data, we have to keep in mind some other important aspects. First, we have the presence of the weighted factor forcing the harmonicity in our functional to be minimized (4.8). This term significantly determines the equation system and compensates for data missing over the middle of the domain. Second, we point to the the higher frequented constituents. Some of them might cause harmonicity violations due to poor sampling. Yet, they carry less information as they are much less weighted, as we have seen in the Figure 3.8 describing the amplitude per degree of the spherical harmonic coefficients. Further, these higher frequented constituents are stronger attenuated with the height.

By variation of the weight parameter η controlling the harmonicity and the approximate fulfillment of the Laplace equation, we are able to produce a good upward continuation of the boundary data. This in contrast to the finite differences and finite elements approach, which fail as a cause of absolute harmonicity constraints.

6.6 Estimating the Weight Parameter

The functional to be minimized (4.8) is of the generic type

$$J_\eta(u) = \sum_{i=1}^{N} (u(x_i) - z_i)^2 + \eta \|u\|_X^2 \tag{6.50}$$

with X some Sobolev norm, e.g. H^1 or H^2, and weight parameter $\eta > 0$ controlling the regularization term. This is the classical way to make sure that the data fitting results with the least squares method are also smooth. The literature on regularization in terms of splines includes [37,53,55,65,133]. The results of formulations using weighted least squares depend essentially on the choice of the weight parameter η. As we have already seen in Chapter 5, the choice strongly influences the results of the approximate continuation.

6.6.1 Classical Regularization Strategies

Ordinary and Generalized Cross Validation

One of the most established and verified methods are the *Ordinary Cross Validation* method and the less computationally expensive *Generalized Cross Validation method* , both to be found e.g. in [144]. These methods require no a priori knowledge of the data. The general idea of the cross validation method is to divide the data into an estimation subset, which is used to obtain a parameter estimate, and a validation subset on which the performance is checked under the estimate. In fact, the best solution is the one that best predicts each measurement as a function of the others. The Ordinary Cross Validation is based on the so called *leave one out* principle. That is, we search for the weight parameter leading to the reconstruction that is least affected by any single data point. Let for $\ell = 1, \ldots, N$ be u_η^ℓ the approximation of the whole set of data without the point x_ℓ, with respect to a weight parameter η, i.e.:

$$u_\eta^\ell \text{ minimizes } \sum_{i=1,\, i\neq\ell}^{N} \left(u_\eta^\ell(x_i) - z_i \right)^2 + \eta \|u_\eta^\ell\|_X^p. \tag{6.51}$$

The Ordinary Cross-Validation Estimate of η is the one which minimizes the *Ordinary Cross Validation* function for η defined as

$$OCV(\eta) := \sum_{\ell=1}^{N} \left(z_\ell - u_\eta^\ell(x_\ell) \right)^2. \tag{6.52}$$

Since one system of equation has to be solved for each ℓ and the cardinality of our data sets is high, the formulation in equation (6.52) is not practicable. The computational cost can be reduced to some extent by employing the *leave-one-out Lemma* stated by Craven and Wahba ([26]). However, the method remains very expensive.

The Ordinary Cross–Validation technique has been further modified to the Generalized Cross Validation in order to fulfill additional invariance properties. In [17], the method is adapted to a formulation in terms of splines where $u_\eta = \sum_{\lambda\in\Lambda} d_\lambda \psi_\lambda$ with $\{d_\lambda\}_{\lambda\in\Lambda}$ is the

solution of the system (4.27). The weight parameter η then minimizes the Generalized Cross–Validation functional

$$GCV(\eta) = \frac{1}{N} \frac{\sum_{i=1}^{N} (u_\eta^\ell(x_i) - z_i)^2}{\sum_{i=1}^{N} (1 - h_{i,i})^2} = \frac{\|(I - \mathbf{H}(\eta))z\|^2}{(\mathrm{tr}(I - \mathbf{H}(\eta)))^2} \tag{6.53}$$

where $H \in I\!R^{N \times N}$ with entries $h_{i,j}$ is the *influence matrix* of the problem, defined as

$$\mathbf{H} := \mathbf{A} \left(\mathbf{A}^T \mathbf{A} + \eta \mathbf{G} \right)^{-1} \mathbf{A}^T. \tag{6.54}$$

This again involves the solution of a linear system for each η. The trace can be further stochastically estimated as

$$\mathrm{tr}(\mathbf{H}(\eta)) = \mathbf{x}^T \mathbf{H}(\eta) \mathbf{x}, \tag{6.55}$$

with a random vector $\mathbf{x}$ with entries 1 and -1, see [76]. In [17], a multilevel version of the generalized cross validation method is also provided.

We have decided not to use the Ordinary or the Generalized Cross-Validation because of two reasons. First, the methods are computationally intensive and dependent on the choice of the tested weight parameters. The second and more important argument considers the availability of the data. In our context, the data points are available mainly at the boundaries, in particular at the bottom and eventually at the top side of the domain. In such a setting, the data is too scattered for the weight parameter to be computed by the minimization of the functional (6.53).

Figure 6.13. *Generalized Cross-Validation function for continuation using* ${P_\Gamma}^{2,1}$ *and test function* $f_1 = V^{3,0} - V^{8,0}$ *on* ${\Omega_\#}^{32\times32\times16}$.

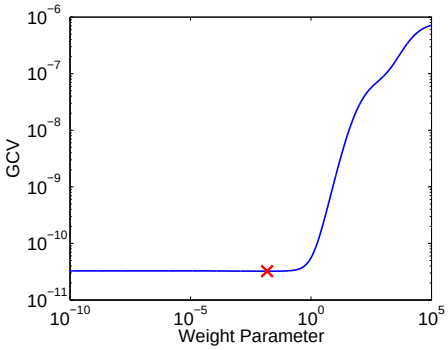

Figure 6.14. *Generalized Cross-Validation function for continuation using* ${P_\Gamma}^{2,1}$ *and geopotential original data set 1 [128].*

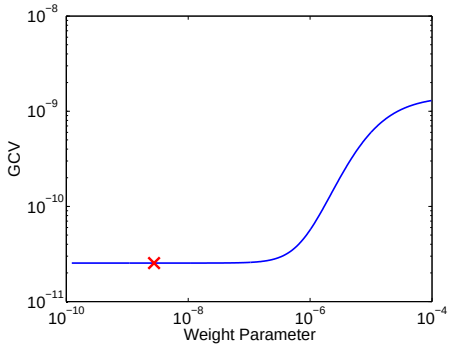

We present in Figures 6.13 and 6.14 the Generalized Cross-Validation functional for the approximate continuation of the test function $f_1 = V^{3,0} - V^{8,0}$ and the original dataset 1 [128]. The red marker points to the minimum of the respective function. To this end we have considered the partial data set ${P_\Gamma}^{2,1}$. In the case of f_1, we have a wide range of

weight parameter for which similar good results have been obtained, see Table 6.6. The weight parameter determined by the Generalized Cross-Validation does indeed belong to that range. In case of the results obtained for the original dataset 1, the minimization Generalized Cross-Validation functional did not point to a reasonable weight parameter. Further, both functionals are smooth and the determined minimum depends strongly on the sampling of the interval of weight parameter candidates.

L-Curve Method

Another common tool for balancing the regularization term and the quality of the datafit is the L-Curve method. It provides an intuitive tool for displaying the trade-off between the norm of a solution and the approximation over the available data for varying weight parameter η.

For a set of weight parameters η, one successively computes the corresponding approximations $\{d_\eta\}_{\eta\in\mathcal{N}}$. There are various choices of the involved norms depending on the approach, but all formulation regard at the end the curvature of the L-curve. We stay with the adapted formulation as in [17]. One plots the norm of the approximations, here chosen as $\|d^\eta\|_{\ell_2}$, versus the norm of the data fitting residuals $\|z - f_\eta\|_{\ell_2}$. The L-Curve criterion is to select the weight parameter value lying at the corner of this curve. This is usually the value of η that maximizes the curvature defined as

$$\kappa(\eta) = \frac{\xi''(\eta)\zeta'(\eta) - \xi'(\eta)\zeta''(\eta)}{(\xi'(\eta)^2 + \zeta'(\eta)^2)^{\frac{3}{2}}} \tag{6.56}$$

with $\xi(\eta) = \|z - f^\eta\|_{\ell_2}, \quad \zeta(\eta) = \|d^\eta\|_{\ell_2}$.

Figure 6.15. *L-Curve for continuation using* ${P_\Gamma}^{2,1}$ *and test function* f_1 *on* ${\Omega_\#}^{32\times32\times16}$.

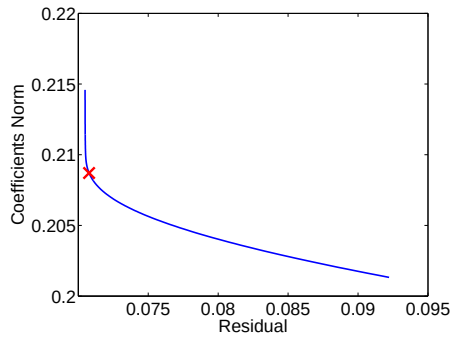

Figure 6.16. *L-Curve for continuation using* ${P_\Gamma}^{2,1}$ *and geopotential original data set 1 [128].*

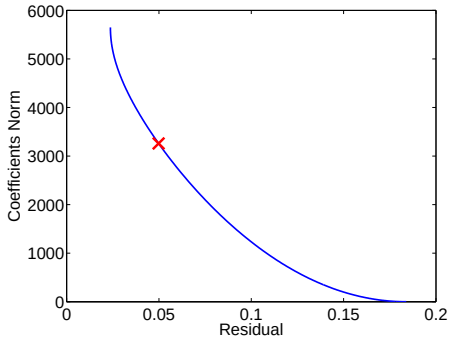

We have still decided against the L-curve method. Figures 6.15 and 6.16 show the L-Curves for the approximate continuation with the partial data set ${P_\Gamma}^{2,1}$ for the test function $f_1 = V^{3,0} - V^{8,0}$ and for the original dataset 1 [128]. The red marker shows the corner determined by equation (6.56). The corner of the curve for the test function $f_1 = V^{3,0} - V^{8,0}$ points again to one of the many good weight parameters. The value

determined for the geopotential data set is wrong. Both determined corners are highly sensitive to the choice of weight parameter candidates.

In fact, it has been shown in [64], that the L-curve criterion will fail for smooth solutions. It is explained, that the smoother the solution u, the worse the results with the weight parameter η computed by the L-curve criterion. In comparison to the data fitting ansatz of [17], we deal in the geodetic setup indeed with relatively smooth functions. Recall, the solution u_η is supposed to be harmonic.

6.6.2 Estimators Based on the System Matrices

Our experiments inspired two rules of thumb that may help us to find an adequate weight parameter more easily. First, for a given configuration, the best continuation obtained with information points at both the upper and lower side of the cuboid required a smaller η than the best continuation obtained with information points only at the bottom facet. Secondly, a higher number of basis functions whose support contains available information points is associated with a lower value of the appropriate weight parameter.

The initial consideration was that the value of the weight parameter η should have little or no influence on the solution of the equation system derived for the minimization of the functional (4.8). Any value should lead to the same solution, because the second term, namely $\eta \int_\Omega |\Delta u(x)|^2 \, dx$, would be evaluated to 0 for any harmonic function u. But the solution is written as a sum of (tensor product of) B-splines and is not implicitly harmonic. The harmonicity is then constrained directly by the second term, that is, by η, which should be greater than 0. We will later see, that in general the system cannot be solved for $\eta = 0$, as the matrix $\mathbf{M}$ is not invertible. This is to expect, as $\mathbf{M}$ accumulates information from data situated on some boundary alone instead from scattered information points over the entire domain. Thereby, the support of several basis functions does not contain any data points. The coefficients for those basis functions cannot be determined by data fitting alone.

Because the boundary data is available only on parts of the boundary of the domain, the solution of our problem is not unique. Through the second term in (4.8), there is an unique solution of the equation system for each given weight parameter η. This solution may or may not be equal to the solution of the system for another value of η. So the issue remains, how should the weight parameter be chosen, for the solution to be a reasonable continuation of the given boundary data. To this extent, we will see, how a too large weight parameter becomes an impairment, as boundary conditions get disregarded. Heuristically, the weight parameter η should be chosen to balance between matrices in the resulting equation system $(\mathbf{M} + \eta\mathbf{G})\mathbf{d} = \mathbf{b}$.

We begin with the argumentation, why the lower Laplacian of a solution does not correlate with a lower reconstruction error. That is, a more harmonic solution does not necessarily point at a better one. When the harmonicity constrained is too large, the solution tends to become very smooth and the boundary conditions are ignored. The result is a quasi plain continuation averaging the available data. Further, when the data itself is noised or very sparsely sampled, some harmonicity gets lost. It does not make sense to force a condition, which the solution does not properly fulfill.

First Indicator: Minimizing the Condition Number

For a better understanding of the influence of the weight parameter η in the minimization of the functional (4.8), we present series of results for the first original data set 1 [128], boundary information points ${P_\Gamma}^{2,1}$ and different values of η. Take a look at Figure 6.17. Recall that this dataset has proven problematic: both finite elements and finite differences failed to reconstruct it due to the intrinsic inflexible approach of the harmonicity constraint. We see that for some large values of the weight parameter η, e.g. $\eta = 10^{-2}$, the reconstruction strongly resembles the poor reconstructions that we obtain with the other two considered methods, the finite elements and the finite differences approach. The harmonicity constraint is here basically too strong, considering also the discrete Laplacian over the domain is only approximately null. Also supporting this presumption is the continuation for $\eta = 10^4$, which is characteristic for a wide interval of higher values of the weight parameter. This continuation reminds us of the continuation obtained for ${P_\Gamma}^{1,1}$, which suggests that the additional information in ${P_\Gamma}^{2,1} \setminus {P_\Gamma}^{1,1}$ has been lost in favor of a much to smooth yet more harmonic solution.

Another important aspect is, that we witness a gradual transit from this solution to the best one for this information points set. In general, a small variation of η leads to a small change in the approximate continuation u_η.

Figure 6.17. *3-dimensional approximate continuation of the reference data set 1 using weighted least squares, boundary data* ${P_\Gamma}^{2,1}$ *and varying weight parameter* η*. Vertical section of the reconstruction at* $(6380, 10, 6630)$ *[km]*$\times(0)$ *[km]*$\times(-2000, 100, 2000)$*[km].*

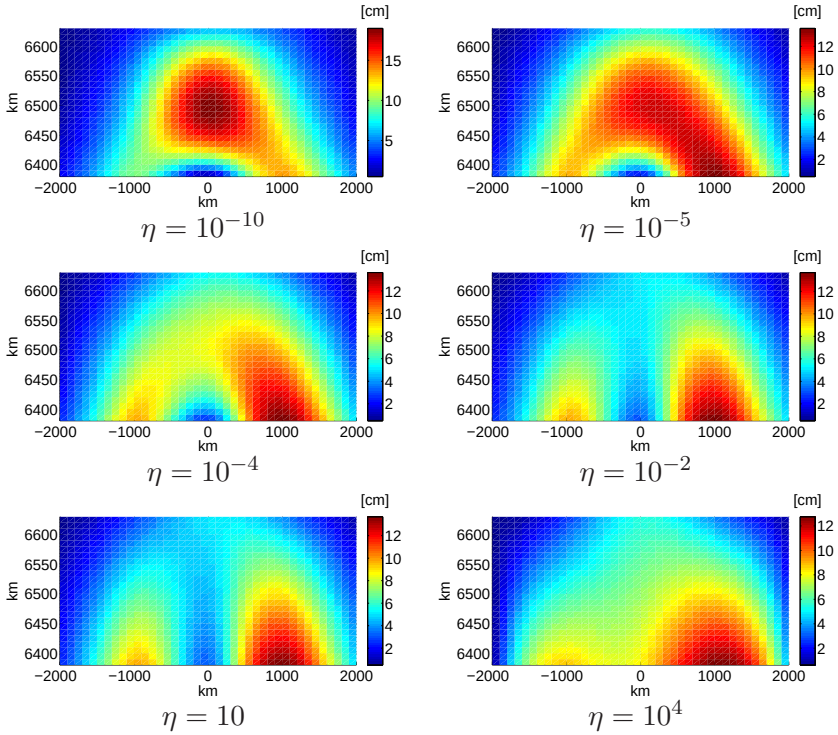

Further, we suggest the reader to take a look at Figures 6.18 and 6.19 to find experiments with synthetic harmonic functions. For each pair of plots, the first one depicts for each continuation case the error in the middle of the domain $E_{2,\mathrm{mid}}$ and the second plot depicts the spectral condition number of the matrix $\mathbf{M}+\eta\mathbf{G}$ for varying weight parameter η. We see some correlation between the error in the middle of the domain that we wish to minimize and the spectral condition number of the equation system on the variation of η. Namely, for the value of the weight parameter η, for which the smallest spectral condition number of the system matrix has been attained, the error over the middle of the domain is practically at its lowest level or near to it.

Also notice that the evolution of $\mathrm{cond}(\mathbf{M}+\eta\mathbf{G})$ with η is not very spectacular; in spite of the presence of some different local minima, a strong saddle-typed trend can be detected. Once the spectral condition number has attained its minimum and starts to get greater, so will the error over the middle of the domain increase, not just the error over the boundary of the domain. This error over the boundaries increases with the value of η over the entire considered interval anyway, as boundary conditions get more and more disregarded.

Figure 6.18. *Error $E_{2,mid}$, $E_{\infty,mid}$ and spectral condition number for the continuation problem with synthetic harmonic test function $V^{3,0}-V^{8,0}$ on ${\Omega_{\#}}^{32\times32\times16}$, levels 1, 2, 3 and 4 (tensor product) B-Spline basis, boundary data ${P_\Gamma}^{1,1}$.*

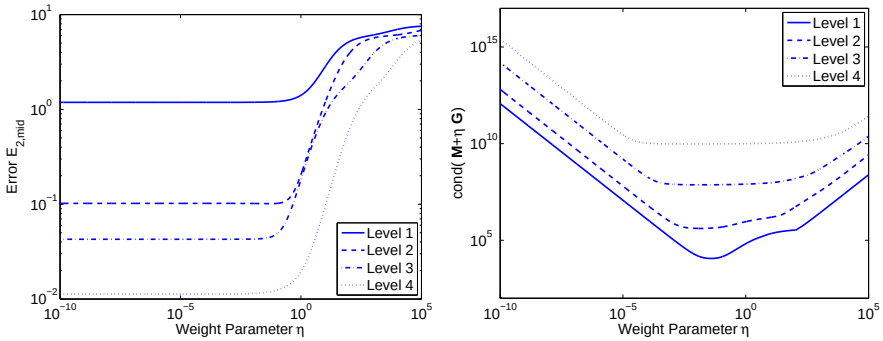

Figure 6.19. *Error $E_{2,mid}$, $E_{\infty,mid}$ and spectral condition number for the continuation problem with synthetic harmonic test function $V^{3,0}-V^{8,0}$ on ${\Omega_{\#}}^{64\times64\times32}$, level 4 (tensor product) B-Spline basis and varying boundary data P_Γ.*

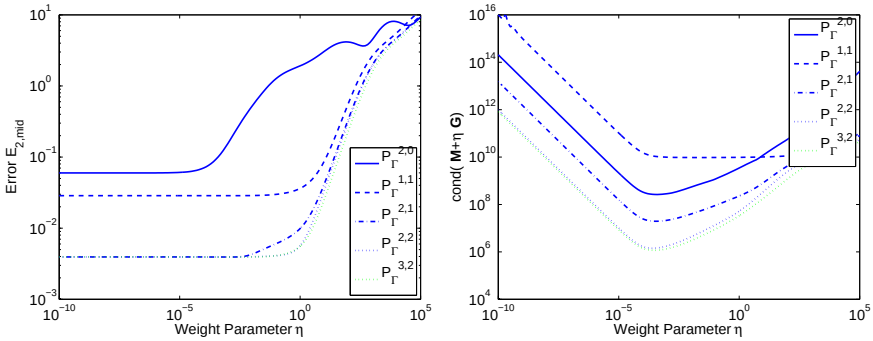

We can then suggest as development of Algorithm 6.1.1 an additional step in constructing the approximate continuation. That is, we should chose the weight parameter η such that the condition number of the system matrix is minimized. Not only that this value is expected to belong to the interval of good weight parameter values. Choosing the weight parameter that minimizes the spectral condition number is also very convenient, especially when working with iterative system solvers. A lower condition number is also associated in fact with a faster convergence of iterative system solvers.

Algorithm 6.6.1.

1. *Preprocessing: scale the given domain and the information points set* $P_\Gamma = \{(x_i, z_i), i = 1, \ldots, M\}$ *to* $\Omega = [0,1]^3$.

2. *Choose resolution* $2^{-\ell}$ *for the cubic splines* $\Psi = \{\psi_\lambda : \lambda \in \Lambda\}$ *defined on* Ω *and build the matrices* $\mathbf{A}$, $\mathbf{M}$, $\mathbf{G}$ *and the vector* $\mathbf{b}$ *as*

$$\mathbf{A} = (\mathbf{A}_{i\ell})_{\substack{i=1,\ldots,M \\ \ell=1,\ldots,L}},\ \mathbf{A}_{i\ell} = \psi_\ell(x_i), \quad \mathbf{M} = \mathbf{A}^{\mathbf{T}}\mathbf{A}, \quad \mathbf{b} = \mathbf{A}^T\mathbf{z},$$

$$\mathbf{G} = (\mathbf{G}_{\ell\ell'})_{\ell,\ell'=1,\ldots,L},\ \mathbf{G}_{\ell\ell'} = \int \Delta\psi_\ell(x)\Delta\psi_{\ell'}(x)dx.$$

3. *Choose* Υ *a set of candidate values for the weight parameter; select* $\eta = \eta_{cond}$ *computed as*

$$\eta_{cond} = \{\eta, cond(\mathbf{M} + \eta\mathbf{G}) = \min\}.$$

4. *Solve* $(\mathbf{M} + \eta\mathbf{G})\,\mathbf{d} = \mathbf{b}$ *to determine the spline coefficients* $\mathbf{d} = (d_\lambda)_{\lambda\in\Lambda}$ *of the approximate continuation*

$$u_\eta(x) = \sum_{\lambda\in\Lambda} d_\lambda\psi_\lambda(x),\ x \in \Omega.$$

Let η_{cond} be the weight parameter η for which the minimal condition number of the system matrix for a given continuation problem has been attained, that is,

$$\eta_{\text{cond}} = \{\eta, \text{cond}(\mathbf{M} + \eta\mathbf{G}) = \min\}. \tag{6.57}$$

This indicator appears in Figures 6.20-6.23 depicted by a blue line.

One could choose a wide yet sparse set of values Υ for the weight parameter η. Further, the spectral condition number of $\mathbf{M} + \eta\mathbf{G}$ is calculated for each of the values $\eta \in \Upsilon$. Considering the saddle-typed behavior of the condition number observed in Figures 6.18 and 6.4, one can choose the sub-interval where the minimum of $\text{cond}(\mathbf{M}+\eta\mathbf{G})$ would most probably be attained and refine the search. This iterative search can be repeated until η is determined with some fixed accuracy.

Approximative Minimization of the Condition Number

Inspired by the computationally expensive indicator η_{cond}, we will consider minimizing an estimator of the spectral condition number, namely CONDEST. This is a MATLAB function that computes a lower bound for the 1-norm condition number of a square matrix. CONDEST is based on the 1-norm condition estimator of Hager [62] and a block oriented generalization of Hager's estimator given by Higham and Tisseur [70]. The algorithm involves an iterative search to estimate 1-norm of the inverse matrix without computing the inverse explicitly and calls the random function. Let η_{condest} be the weight parameter η belonging to some candidate set Υ for which the lowest estimated 1-norm condition number of the system matrix for a given continuation problem has been attained, that is

$$\eta_{\text{condest}} = \{\eta, \text{condest}(\mathbf{M} + \eta\mathbf{G}) = \min\}. \tag{6.58}$$

This indicator appears in Figures 6.20-6.23 depicted by a red line.

In order to compute η_{cond} and η_{condest} it is necessary to compute the spectral condition number or the 1-norm condition estimator respectively for each η belonging to the considered interval. This fact raises some concerns regarding their effectiveness. Another idea would be to estimate the weight parameter η without the burden of too many repetitive computations of the spectral condition number of the system matrix $\mathbf{M} + \eta\mathbf{G}$ for a sequence of values for η. We proceed our search for another indicator.

To recapitulate: we have a set of boundary information points whose values are known, we choose a level for the (tensor product of) B-splines basis and we build the two system matrices $\mathbf{M}$ and $\mathbf{G}$. These steps are mandatory. Our intuition says: heuristically η should be chosen in such a way, that it determines some kind of compensation. Instead of computing or estimating the condition number of $\mathbf{M} + \eta\mathbf{G}$ for varying η, we look only at the spectral condition number of the two system matrices and at their largest eigen values. These values for the matrix $\mathbf{M}$ (see Table (6.22)) depend only on the structure of the boundary data set P_Γ and on the chosen B-splines basis level, but not on the right side of the normal equation system, namely, the values that the function to be continued takes on the boundaries. Also, the condition number and the greatest eigen value of $\mathbf{G}$ in Table (6.23) change only with the chosen basis. Table (6.22) also shows the importance of the matrix $\mathbf{G}$ for even obtaining some solution to the problem. One can see how the cross product matrix $\mathbf{M}$ is most of the times not invertible. This is to expect as the continuation problem, especially in this incomplete, local field continuation setting, is ill-posed.

We are now ready to discuss the last alternative indicator. Because η should lead to some balance within $(\mathbf{M} + \eta\mathbf{G})$, we chose another indicator η_{eigs} computed as the ratio between the highest eigenvalue of $\mathbf{M}$ and the highest eigenvalue of $\mathbf{G}$

$$\eta_{\text{eig}} = \frac{\max(\text{eig}(\mathbf{M}))}{\max(\text{eig}(\mathbf{G}))}. \tag{6.59}$$

This indicator does not depend on the considered interval for η, as in the case of the two other considered indicators, and is computed only once; it appears in Figures 6.20-6.23 depicted by a green line.

Table 6.22. *Condition number and the greatest eigenvalue of* $\mathbf{M}$ *for differently designed* P_Γ *and levels* $l = 3, 4$.

$\Omega_\#$	P_Γ	level $l=3$		
		cond($\mathbf{M}$)	max(eig($\mathbf{M}$))	$\frac{\max(\text{eig}(\mathbf{M}))}{\max(\text{eig}(\mathbf{G}))}$
$\Omega_\#^{16\times16\times8}$	$P_\Gamma^{1,0}$	Inf	6.9567e-03	5.2307e-05
$\Omega_\#^{16\times16\times8}$	$P_\Gamma^{1,1}$	Inf	6.9567e-03	5.2307e-05
$\Omega_\#^{16\times16\times8}$	$P_\Gamma^{2,0}$	Inf	6.9567e-03	5.2307e-05
$\Omega_\#^{16\times16\times8}$	$P_\Gamma^{2,1}$	Inf	6.9567e-03	5.2307e-05
$\Omega_\#^{16\times16\times8}$	$P_\Gamma^{2,2}$	1.9447e+85	6.9567e-03	5.2307e-05
$\Omega_\#^{16\times16\times8}$	$P_\Gamma^{3,2}$	5.7618e+81	6.9567e-03	5.2307e-05
$\Omega_\#^{32\times32\times16}$	$P_\Gamma^{1,0}$	Inf	2.7829e-02	2.0924e-04
$\Omega_\#^{32\times32\times16}$	$P_\Gamma^{1,1}$	Inf	2.7829e-02	2.0924e-04
$\Omega_\#^{32\times32\times16}$	$P_\Gamma^{2,0}$	Inf	2.8566e-02	2.1478e-04
$\Omega_\#^{32\times32\times16}$	$P_\Gamma^{2,1}$	Inf	2.8566e-02	2.1478e-04
$\Omega_\#^{32\times32\times16}$	$P_\Gamma^{2,2}$	3.2745e+87	2.8566e-02	2.1478e-04
$\Omega_\#^{32\times32\times16}$	$P_\Gamma^{3,2}$	6.4363e+84	2.8804e-02	2.1657e-04
$\Omega_\#^{64\times64\times32}$	$P_\Gamma^{1,0}$	Inf	1.1132e-01	8.3698e-04
$\Omega_\#^{64\times64\times32}$	$P_\Gamma^{1,1}$	Inf	1.1132e-01	8.3698e-04
$\Omega_\#^{64\times64\times32}$	$P_\Gamma^{2,0}$	Inf	1.3627e-01	1.0246e-03
$\Omega_\#^{64\times64\times32}$	$P_\Gamma^{2,1}$	Inf	1.3627e-01	1.0246e-03
$\Omega_\#^{64\times64\times32}$	$P_\Gamma^{2,2}$	3.6986e+87	1.3627e-01	1.0246e-03
$\Omega_\#^{64\times64\times32}$	$P_\Gamma^{3,2}$	7.7638e+87	1.4713e-01	1.1063e-03
$\Omega_\#$	P_Γ	level $l=4$		
		cond($\mathbf{M}$)	max(eig($\mathbf{M}$))	$\frac{\max(\text{eig}(\mathbf{M}))}{\max(\text{eig}(\mathbf{G}))}$
$\Omega_\#^{16\times16\times8}$	$P_\Gamma^{1,0}$	Inf	2.4414e-04	6.7215e-06
$\Omega_\#^{16\times16\times8}$	$P_\Gamma^{1,1}$	Inf	2.4414e-04	6.7215e-06
$\Omega_\#^{16\times16\times8}$	$P_\Gamma^{2,0}$	Inf	2.4414e-04	6.7215e-06
$\Omega_\#^{16\times16\times8}$	$P_\Gamma^{2,1}$	Inf	2.4414e-04	6.7215e-06
$\Omega_\#^{16\times16\times8}$	$P_\Gamma^{2,2}$	Inf	2.4414e-04	6.7215e-06
$\Omega_\#^{16\times16\times8}$	$P_\Gamma^{3,2}$	Inf	2.4414e-04	6.7215e-06
$\Omega_\#^{32\times32\times16}$	$P_\Gamma^{1,0}$	Inf	9.5025e-04	2.6161e-05
$\Omega_\#^{32\times32\times16}$	$P_\Gamma^{1,1}$	Inf	9.5025e-04	2.6161e-05
$\Omega_\#^{32\times32\times16}$	$P_\Gamma^{2,0}$	Inf	9.5025e-04	2.6161e-05
$\Omega_\#^{32\times32\times16}$	$P_\Gamma^{2,1}$	Inf	9.5025e-04	2.6161e-05
$\Omega_\#^{32\times32\times16}$	$P_\Gamma^{2,2}$	6.0900e+239	9.5025e-04	2.6161e-05
$\Omega_\#^{32\times32\times16}$	$P_\Gamma^{3,2}$	3.6287e+207	9.5025e-04	2.6161e-05
$\Omega_\#^{64\times64\times32}$	$P_\Gamma^{1,0}$	Inf	3.8010e-03	1.0465e-04
$\Omega_\#^{64\times64\times32}$	$P_\Gamma^{1,1}$	Inf	3.8010e-03	1.0465e-04
$\Omega_\#^{64\times64\times32}$	$P_\Gamma^{2,0}$	Inf	3.9017e-03	1.0742e-04
$\Omega_\#^{64\times64\times32}$	$P_\Gamma^{2,1}$	Inf	3.9017e-03	1.0742e-04
$\Omega_\#^{64\times64\times32}$	$P_\Gamma^{2,2}$	3.9498e+239	3.9017e-03	1.0742e-04
$\Omega_\#^{64\times64\times32}$	$P_\Gamma^{3,2}$	8.9007e+238	3.9342e-03	1.0831e-04

Table 6.23. *Condition number and the greatest eigen value of* $\mathbf{G}$ *for levels* $l = 3, 4$.

level $l=3$		level $l=4$	
cond($\mathbf{G}$)	max(eig($\mathbf{G}$)	cond($\mathbf{G}$)	max(eig($\mathbf{G}$)
1.7334e+18	1.3300e+02	1.6435e+18	3.6323e+01

We find in Figures 6.20-6.23 for each single continuation problem the weight parameters determined by our three indicators. We see that when handling synthetic data, that is

Figures 6.20-6.23, the η_{condest} and η_{eig} indicators are sufficient. For the case of the real data [128], η_{condest} is more exact.

Remember from the two previous sections, in case of the synthetic data we had a large interval of good values for η for each continuation problem. For the test functions f_1 and f_2, the considered grids were fine enough. Here the boundary points subset was consistent with the harmonicity constraint. This is reflected by the fact that we obtain a correct continuation for a very wide range of values of the weight parameter η. This did not happened for the experiments with earths potential field data. There, we had much less flexibility in choosing an appropriate parameter. But this fact strongly correlates with another recurrent issue when solving a given continuation problem, namely, the harmonicity of the boundary data. We have observed in the previous section, that the EGM96 data, at the given discretization, is not harmonic anymore. The $26 \times 41 \times 41$ grid can not properly discretize, for e.g., the reference data set [128] computed with spherical harmonics of degree 51 until 180 using the Geopotential Model EGM96 over

$$(0, 250)\ [\text{km}]\ \times (-2000, 2000)\ [\text{km}]\ \times (-2000, 2000)\ [\text{km}]\ .$$

The fine oscillations near to the earth are lost and the harmonicity of the data set at this discretization is broken. Trying to reconstruct a harmonic function using this boundary data and the harmonicity constraint is a difficult task.

Figure 6.20. *Error $E_{2,mid}$ and condition numbers for the continuation problem with level 3 B-Spline basis, $P_\Gamma^{2,1}$ and reference data set 1.*

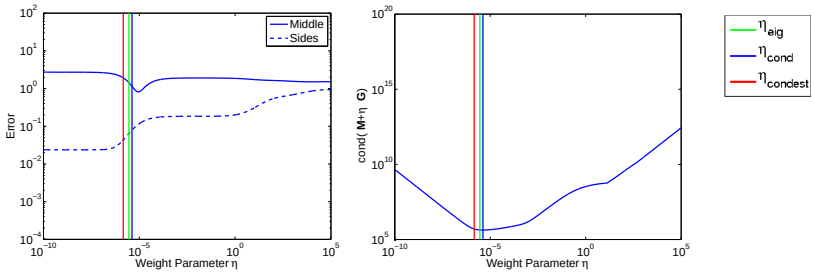

Figure 6.21. *Error $E_{2,mid}$ and condition numbers for the continuation problem with level 4 B-Spline basis, $P_\Gamma^{2,1}$ and reference data set 1.*

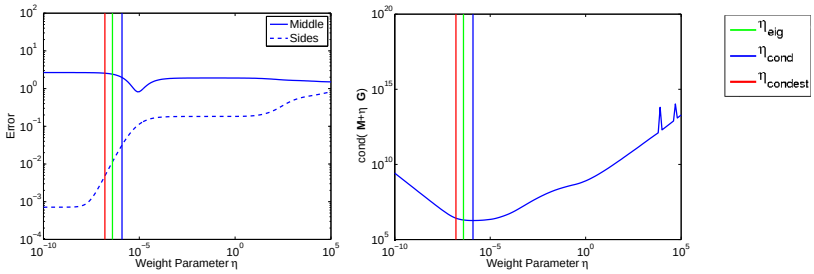

Figure 6.22. *Error $E_{2,mid}$ and condition numbers for the continuation problem with a level 3 B-Spline basis, ${P_\Gamma}^{2,0}$ and test function $V^{3,0} - V^{8,0}$ on ${\Omega_\#}^{32\times32\times16}$.*

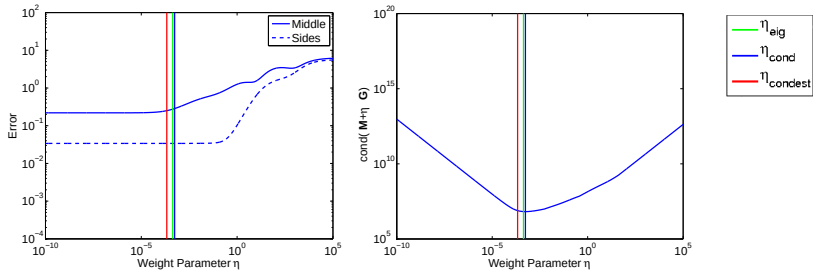

Figure 6.23. *Error $E_{2,mid}$ and condition numbers for the continuation problem with a level 3 B-Spline basis, ${P_\Gamma}^{1,1}$ and test function $V^{3,0} - V^{8,0}$ on ${\Omega_\#}^{32\times32\times16}$.*

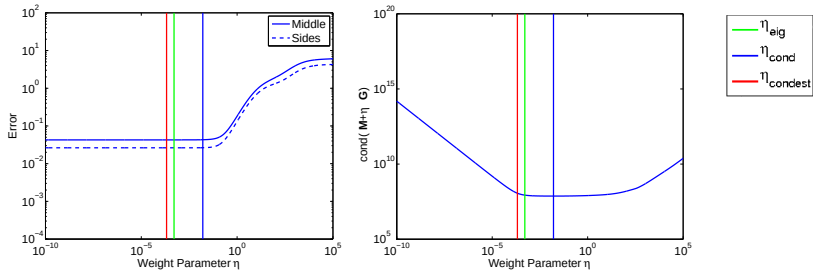

Figure 6.24. *Error $E_{2,mid}$ and condition numbers for the continuation problem with level 3 B-Spline basis, ${P_\Gamma}^{2,1}$ and test function $V^{3,0} - V^{8,0}$ on ${\Omega_\#}^{32\times32\times16}$.*

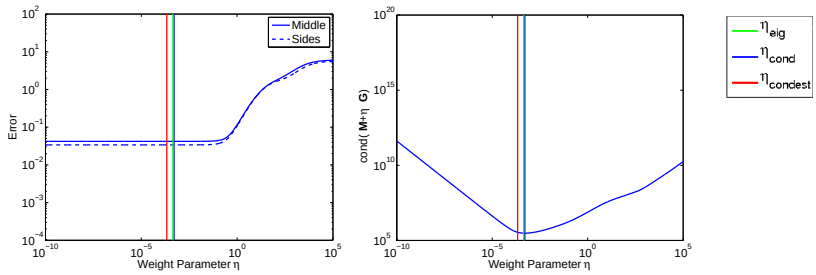

Figure 6.25. *Error $E_{2,mid}$ and condition numbers for the continuation problem with a level 3 B-Spline basis, ${P_\Gamma}^{2,1}$ and test function $V^{3,0} - V^{8,0}$ on ${\Omega_\#}^{64\times64\times32}$.*

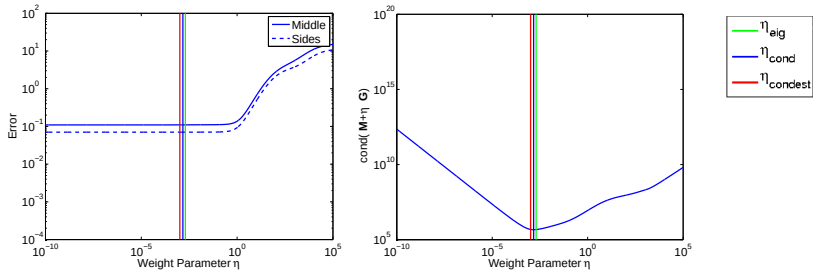

Figure 6.26. *Error $E_{2,mid}$ and condition numbers for the continuation problem with level 3 B-Spline basis, ${P_\Gamma}^{2,0}$ and test function $V^{3,0} - V^{8,0}$ on ${\Omega_\#}^{64\times64\times32}$.*

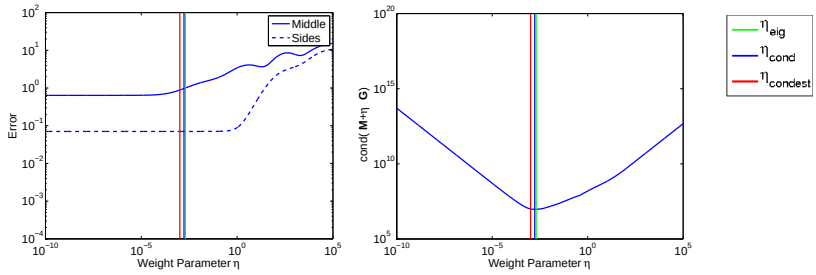

Figure 6.27. *Error $E_{2,mid}$ and condition numbers for the continuation problem with level 4 B-Spline basis, ${P_\Gamma}^{2,0}$ and test function $V^{3,0} - V^{8,0}$ on ${\Omega_\#}^{64\times64\times32}$.*

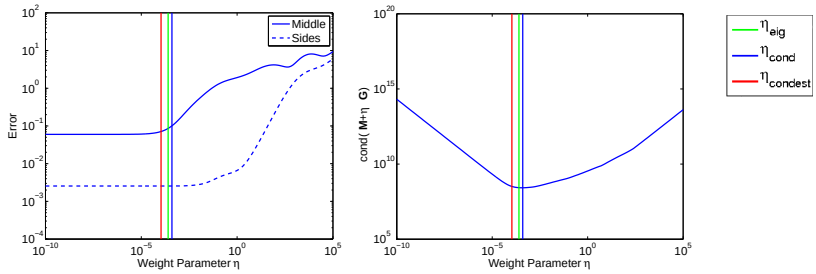

Figure 6.28. *Error $E_{2,mid}$ and condition numbers for the continuation problem with level 3 B-Spline basis, ${P_\Gamma}^{1,1}$ and test function $V^{3,0} - V^{8,0}$ on ${\Omega_\#}^{64\times64\times32}$.*

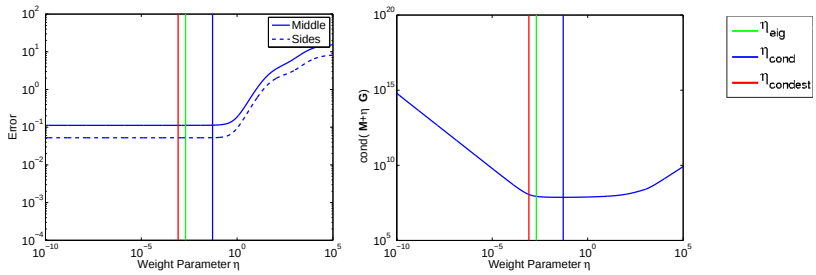

Figure 6.29. *Error $E_{2,mid}$ and condition numbers for the continuation problem with level 4 B-Spline basis, ${P_\Gamma}^{1,1}$ and test function $V^{3,0} - V^{8,0}$ on ${\Omega_\#}^{64\times64\times32}$.*

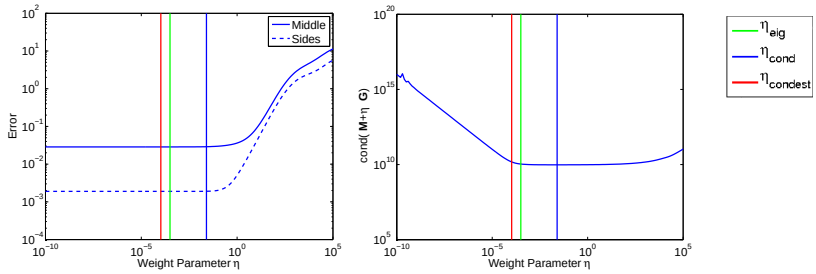

Height of the continuations

We also investigate how the three estimators of the weight parameter for the approximate continuation of harmonic function with our least squares approach variate with the structure of the full grids and of the boundary points set. In general, the domain is broader than high, which is to expect, as the continuation is a badly posed problem and also dictated by the geodetic set up. This experiment is inspired by the intuition that a higher upward continuation is associated with a worse posed problem. Otherwise, the more narrow the domain, the stronger the influences of the field and of the oscillation sources outside of the domain over the field inside of it. Conversely, the spherical harmonics approach, that was implicitly harmonic, required input data sampled over the entire surface of the sphere.

Let Ω be a cuboid of breadth and length 1 and varying height H, that is

$$\Omega = [0,1]^2 \times [0,H] \subset [0,1]^3. \tag{6.60}$$

Over Ω lie the full grids ${\Omega_\#}^{64\times64\times32}$ or ${\Omega_\#}^{32\times32\times16}$ and the partial grids ${P_\Gamma}^{1,1}$, ${P_\Gamma}^{2,0}$ or ${P_\Gamma}^{2,1}$. We choose the B-Spline basis level 3. For each of this general formulated continuation problems we will variate the height of the domain and compute the three indicators η_{cond}, η_{condest} by testing weight parameter candidates $\eta \in \{10^{-10}, 10^{-9.95}, 10^{-9.90} \dots 10^{9.90}, 10^{9.95}, 10^{10}\}$ as defined in equations (6.57,6.58) and η_{eig} as in equation (6.59).

Figure 6.30. *Variation of the indicators η_{cond}, $\eta_{condest}$ and η_{eigs} with the scaling of the height of a domain $\Omega \in [0,1]^3$ for fixed grid $\Omega_\#$ and boundary data P_Γ.*

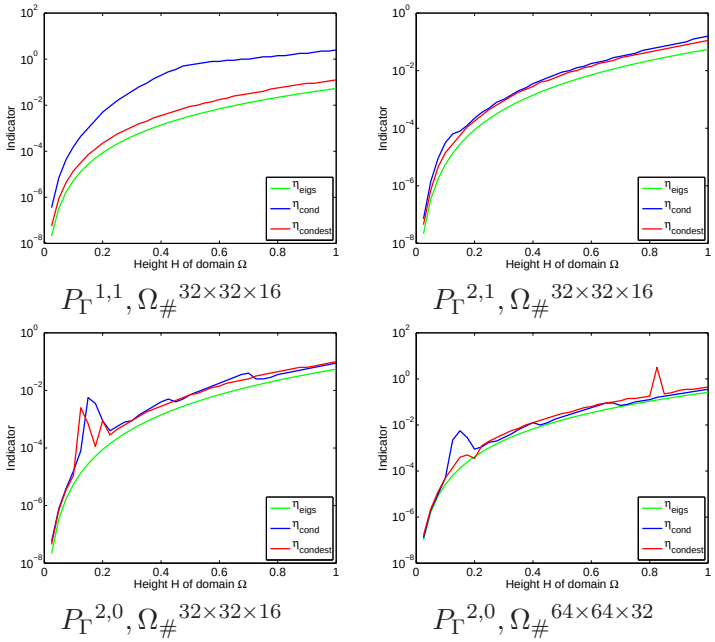

${P_\Gamma}^{1,1}, {\Omega_\#}^{32\times32\times16}$ ${P_\Gamma}^{2,1}, {\Omega_\#}^{32\times32\times16}$

${P_\Gamma}^{2,0}, {\Omega_\#}^{32\times32\times16}$ ${P_\Gamma}^{2,0}, {\Omega_\#}^{64\times64\times32}$

We were content to see in Figure 6.30 that the variation of the three indicators is in some degree synchronous and stays within limits. For each continuation problem setup, the indicators point to compensatory weight parameters which lead to an equitable stabilization of the solution. Most notably is the steady evolution of the computationally

less expensive indicator η_{eig} with the height of the domain. This makes it more reliable than the other two ones, whose calculation depends on a discrete set of weight parameter candidates. The indicator η_{eig} can also be regarded as a starting point within an iterative search for the weight parameter that minimizes the condition number of the system.

We still do not assume, that any of the three indicators would point to the best possible weight parameter. Their computation did not regard the available data, i.e., the right hand side of the equation system. Especially in the case of badly sampled harmonic functions, where the harmonicity in the available discretization is lost, the interval of best weight parameters is narrow. This interval could eventually strongly variate with the values that the function takes. The three indicators presented here may not pinpoint it exactly, but only to a neighborhood of it.

6.6.3 Final Strategy

In view of the considered three indicators, our expectancy remains, that the better formulated the given continuation problem, that is, the better the boundary data and the better the selected basis discretize the function to be continued, the greater the interval of good weight parameters. We found the employment of the η_{eig} indicator of the weight parameter and the following version of Algorithm 6.1.1 as the most promising for the construction of the approximate continuation.

Algorithm 6.6.2.

1. *Preprocessing: scale the given domain and the information points set* $P_\Gamma = \{(x_i, z_i), i = 1, \ldots, M\}$ *to* $\Omega = [0,1]^3$.

2. *Choose resolution* $2^{-\ell}$ *for the cubic splines* $\Psi = \{\psi_\lambda : \lambda \in \Lambda\}$ *defined on* Ω *and build the matrices* $\mathbf{A}$, $\mathbf{M}$, $\mathbf{G}$ *and the vector* $\mathbf{b}$ *as*

$$\mathbf{A} = (\mathbf{A}_{i\ell})_{\substack{i=1,\ldots,M \\ \ell=1,\ldots,L}},\ \mathbf{A}_{i\ell} = \psi_\ell(x_i), \quad \mathbf{M} = \mathbf{A}^{\mathbf{T}}\mathbf{A}, \quad \mathbf{b} = \mathbf{A}^T\mathbf{z},$$

$$\mathbf{G} = (\mathbf{G}_{\ell\ell'})_{\ell,\ell'=1,\ldots,L},\ \mathbf{G}_{\ell\ell'} = \int \Delta\psi_\ell(x)\Delta\psi_{\ell'}(x)dx.$$

3. *Set* $\eta = \eta_{eig}$ *computed as*

$$\eta_{eig} = \frac{\max(eig(\mathbf{M}))}{\max(eig(\mathbf{G}))}.$$

4. *Solve* $(\mathbf{M} + \eta\mathbf{G})\,\mathbf{d} = \mathbf{b}$ *to determine the spline coefficients* $\mathbf{d} = (d_\lambda)_{\lambda\in\Lambda}$ *of the approximate continuation* $u_\eta(x) = \sum_{\lambda\in\Lambda} d_\lambda\psi_\lambda(x),\ x \in \Omega$.

6.7 Working with Iterative Solvers

We have mentioned in Section 4.4 that we may turn to iterative system solvers. We investigate their influence over the results of our least squares approach for the approximate continuation of harmonic functions and justify their employment. In Table 6.3 we have presented results obtained via preconditioned conjugate gradients method. There, the iterative solver has been allowed the necessary number of iterations in order to achieve a low residual of 10^{-10}. We want to see how the results change when the solver stops earlier. The regularization effect of cutting off the iterative process has already been studied for data fitting with splines in [145] or for more generalized ill–posed problems in [63]. Considering that our target functions are harmonic and smooth, choosing a reasonable iteration abort criteria should not lead to an essential loss in accuracy. It is also interesting, whether cutting of the iterative procedure interferes with the harmonicity constraint.

To test the effects of the interruption of the solver, we consider the test function $V^{3,0} - V^{8,0}$ on ${\Omega_{\#}}^{32\times32\times16}$. We set the weight parameter to some arbitrary value $\eta = 10^{-5}$ and consider the boundary datasets ${P_\Gamma}^{1,1}$, ${P_\Gamma}^{2,0}$ and ${P_\Gamma}^{2,1}$. We solve the resulting equation system using one of the following iterative system solvers for large and sparse matrices: the conjugate gradients method [7,135], the minimum residual method [7,113], the biconjugate gradients method [7] and the stabilized biconjugate gradients [7, 142] as implemented in MATLAB. The conjugate gradient method, one of the most used iterative system solvers, is an algorithm for the numerical solution of systems of linear equations whose matrix is symmetric and positive-definite. For the minimum residual method, the coefficient matrix must be symmetric but does not need be positive definite. The biconjugate gradient method provides a generalization to non-symmetric matrices and involves replacing the orthogonal sequence of residuals in the conjugate gradient method by two mutually orthogonal sequences. Since the biconjugate gradient method is numerically unstable, we consider also the stabilized biconjugate gradient method.

See the results in Figures 6.31 – 6.34. Sometimes the methods converge even before the half of necessary iterations, but not always. For this continuation case, the minimum residual and the stabilized biconjugate method were the fastest to reach the lowest error over the middle of the domain for the friendliest boundary data points set ${P_\Gamma}^{2,1}$. The results for the other two configurations are not very concluding. In some of these cases, $E_{2,\mathrm{mid}}$ reached the proper values only within the last iterations of the system solver. We cannot say, which method generally is less sensitive to cutting off the iterative procedure. Since the approximate continuation problem is generally ill–omened with respect the conditioning due to the incorporated ill–posedness, we cannot depend on fast convergence.

The rational conclusion in corroboration with the high accuracy demands of the method is that one should prudently cut off the iterative procedure. Experiments show that the defects caused by the interruption do not deposit on the harmonic part of the minimization problem. The main thing to be regarded is the ill–posedness of the problem. The more ill–posed the problem, the worse the equation system matrix is conditioned and the iterative solver converges more slowly. In our case, with less or poorly distributed available information points, the iterative solver converges later. This behavior is reflected here in spite of the intrinsic regulatory aspect of the approximate continuation method.

Figure 6.31. *Results obtained with the conjugate gradients method. Error* $E_{2,\mathrm{mid}}$ *and relative residual for boundary data configurations* ${P_\Gamma}^{1,1}$, ${P_\Gamma}^{20}$, ${P_\Gamma}^{2,1}$.

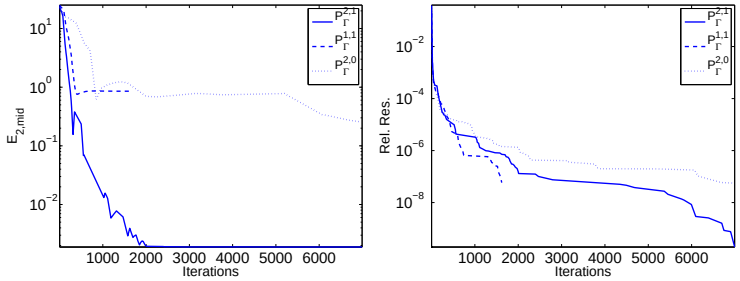

Figure 6.32. *Results obtained with the minimum residuals method. Error* $E_{2,\mathrm{mid}}$ *and relative residual for boundary data configurations* ${P_\Gamma}^{1,1}$, ${P_\Gamma}^{20}$, ${P_\Gamma}^{2,1}$.

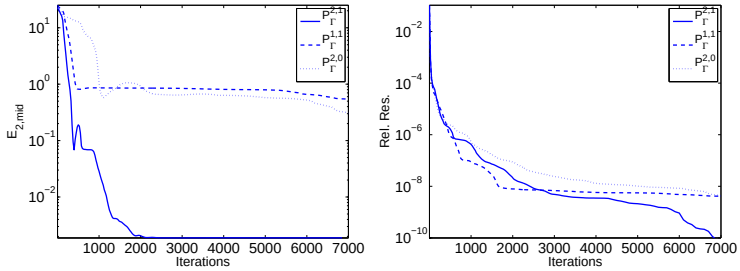

Figure 6.33. *Results obtained with the biconjugate gradients method. Error* $E_{2,\mathrm{mid}}$ *and relative residual for boundary data configurations* ${P_\Gamma}^{1,1}$, ${P_\Gamma}^{20}$, ${P_\Gamma}^{2,1}$.

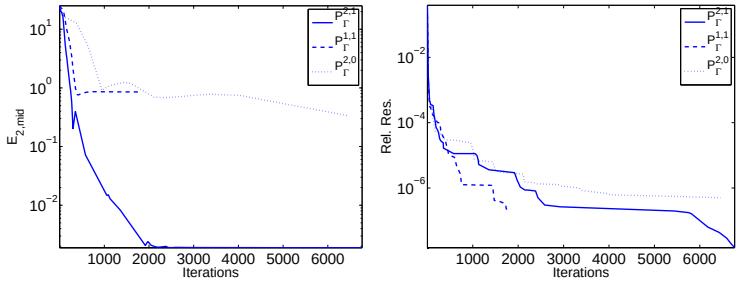

Figure 6.34. *Results obtained with the stabilized biconjugate gradients method. Error* $E_{2,\mathrm{mid}}$ *and relative residual for boundary data configurations* ${P_\Gamma}^{1,1}$, ${P_\Gamma}^{20}$, ${P_\Gamma}^{2,1}$.

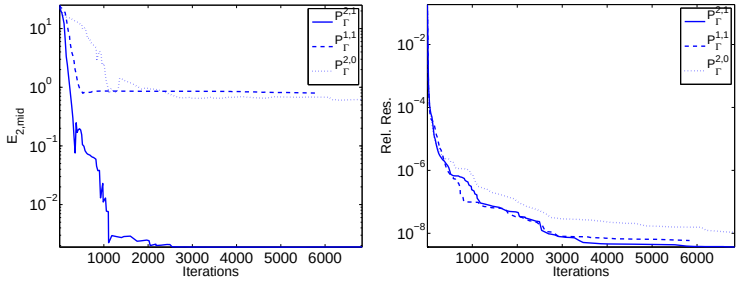

Chapter 7

Adaptivity: Experiments with the Hierarchical Cubic B-spline Basis

Le mieux est l'ennemi du bien.

La Bégueule, Voltaire

As a substantial enhancement of our least squares with regularization approach for the approximate continuation of harmonic functions, we attempt to construct an adaptive development. We seek to determine a representation of the continuation in terms of some basis functions, yet with a minimal number of degrees of freedom. This means that we should not loose essential accuracy in comparison e.g. to the uniform, full tensor product basis considered in the previous chapters. Yet the representation should not contain redundant information, i.e., it should not contain degrees of freedom that are neglectable. So, starting from this full grid setup, the most direct approach would be to ignore all basis functions of a sufficient accurate representation for which the coefficients have a value smaller than a threshold. But solving such large systems for full grid approximations, where all basis functions up to some high, necessary level are included, is not always practicable, as in the case of badly distributed data.

Moreover, we want degrees of freedom to accumulate where necessary, i.e., basis functions of higher level should be considered where they resolve detail informations of the approximate continuation. This is where the hierarchical or wavelet decompositions of finite element spaces comes into play. Inspired by [22] and by [17], we suggest therefore an iterative, coarse–to–fine strategy.

In this chapter, we will first need to present some functional analysis prerequisites in order to explain the concept of nested spaces and multiscales. We further present some literature on (multivariate) hierarchical constructions in terms of splines. In order to construct the multi-frequency basis functions for our adaptive approach to the approximate continuation of harmonic functions, we discuss our hierarchical decomposition in terms of tensor product cubic B-splines; we also explain our choice over established (multi–dimensional) wavelet constructions, like cubic B-spline wavelets, or linear hierarchic finite elements.

7.1 Prerequisites

The fundamental theoretical set up of functional analysis presented here is based on [3] and [60]. Let X, Y be normed linear spaces over the field $\mathbb{R}$.

Definition 7.1.1 (Linear Operators and Operator Norms). *The space of linear operators from X to Y is denoted by*

$$L(X;Y) := \{T : X \to Y;\ T \text{ is continuous and linear}\}. \tag{7.1}$$

For any $T \in L(X;Y)$, the associated operator norm is defined by

$$\|T\|_{L(X;Y)} := \sup_{x\in X,\ \|x\|_X=1} \|Tx\|_Y. \tag{7.2}$$

Definition 7.1.2. *A* Banach space *is a complete vector space B with a norm $\|\cdot\|_B$.*

The norms $\|\cdot\|_{B_1}$ and $\|\cdot\|_{B_2}$ associated with a Banach space are called *equivalent* if they induce the same topology. This is equivalent to the existence of positive finite constants c and C such that for all $v \in B$

$$\|v\|_{B_1} \le c\|v\|_{B_2} \text{ and } \|v\|_{B_2} \le C\|v\|_{B_1}. \tag{7.3}$$

This is commonly written as

$$\|v\|_{B_1} \lesssim \|v\|_{B_2} \text{ and } \|v\|_{B_2} \gtrsim \|v\|_{B_1} \quad \text{or} \quad \|v\|_{B_1} \sim \|v\|_{B_2}. \tag{7.4}$$

Definition 7.1.3. *A* Hilbert space $\mathcal{H}$ *is a complete vector space with an inner product $(\cdot,\cdot)_{\mathcal{H}}$ such that the norm is induced by the inner product as $\|\cdot\|_{\mathcal{H}} := \sqrt{(\cdot,\cdot)_{\mathcal{H}}}$.*

A Hilbert space is always a Banach space. By definition, a Hilbert space is complete with respect to the norm associated with its inner product. But the converse does not need to hold and not every Banach space is a Hilbert space. Further, a Hilbert space is called *separable* if it contains a countable dense subset, this means

$$V = \{v_i : i = 1, 2, \ldots\} \subset \mathcal{H}, \quad \operatorname*{clos}_{\mathcal{H}} V = \mathcal{H}. \tag{7.5}$$

Separability is essential for numerical analysis and for the study of partial differential equations as equation (7.5) is equivalent to

$$\operatorname{dist}(f;V) = 0, \quad \text{for all } f \in \mathcal{H}. \tag{7.6}$$

In other words, every element of $\mathcal{H}$ can be approximated using the subspace V with arbitrary precision.

Definition 7.1.4. *The dual space X^* of a Banach space X is the space of all linear continuous functions from X onto the underlying field $\mathbb{R}$:*

$$X^* := L(X;\mathbb{R}). \tag{7.7}$$

The elements $v' \in X^*$ are called *linear functionals* and the dual form is defined as

$$\langle x, x' \rangle_{X \times X^*} := x'(x). \tag{7.8}$$

The theory on Sobolev spaces presented here has been borrowed from the books of [2], [60] and [94]. We consider again $\Omega \subset \mathbb{R}^n$ to be a bounded domain with piecewise smooth boundary $\partial\Omega$ and Ω being locally on one side of $\partial\Omega$. The space $L_2(\Omega)$ is the space of all real-valued square Lebesgue integrable functions on Ω. It is associated with the inner product

$$(u, v)_{L_2(\Omega)} := \int_\Omega u(x)v(x)\, d\mu, \tag{7.9}$$

where $\mu = \mu(x)$ is the Lebesgue measure. Generally, the spaces $L_p(\Omega)$, $1 \leq p < \infty$, and the subspaces $H^s(\Omega)$ of $L_2(\Omega)$ defined in equation (7.1.6) are typical (separable) Hilbert spaces in functional analysis. Conversely, $L_\infty(\Omega)$ is not separable.

Definition 7.1.5. *A function $u \in L_2(\Omega)$ has the weak derivative $v := \partial^\alpha u$, if $v \in L_2(\Omega)$ and*

$$(\phi, v)_{L_2} = (-1)^{|\alpha|}(\partial^\alpha \phi, u)_{L_2}, \quad \text{for all } \phi \in C_0^\infty(\Omega) \tag{7.10}$$

with $\alpha := (\alpha_1, \ldots, \alpha_n) \in \mathbb{N}_0^n$ a multi-index.

If such a partial derivate v exists, it is unique (in the L_2-sense). We recall that two functions $u, v \in L_2(\Omega)$ are considered *equal* if $u(x) = v(x)$ holds almost everywhere, i.e., for all $x \in \Omega \setminus A$ and $\mu(A) = 0$. When $u \in C^m(\Omega)$, the weak derivative is in fact the classical strong derivative.

Definition 7.1.6. *For $m \in \mathbb{N}$ we denote by $H^m(\Omega)$ the Hilbert space of all functions $u \in L_2(\Omega)$ for which the weak derivatives $\partial^\alpha u$ for all $|\alpha| \leq m$ exist.*

The inner product is formulated as

$$(u, w)_{H^m} := \sum_{|\alpha| \leq m} (\partial^\alpha u, \partial^\alpha w)_{L_2}. \tag{7.11}$$

The associated norm and seminorm are defined as

$$\|u\|_{H^m} := \sqrt{(u, u)_{H^m}} = \sqrt{\sum_{|\alpha| \leq m} \|\partial^\alpha u\|_{L_2}^2}, \tag{7.12}$$

$$|u|_{H^m} := \sqrt{\sum_{|\alpha| = m} \|\partial^\alpha u\|_{L_2}^2}. \tag{7.13}$$

Sobolev spaces are important since solutions of partial differential equations can be constructed in Sobolev spaces, profiting from the formulation in terms of the weak derivatives. Also, the Sobolev spaces are nested, i.e., $H^{m+1} \subset H^m$. It has been commonly written

$$H^0 := L_2. \tag{7.14}$$

Further, the series of spaces $H^m, m \in \mathbb{N}_0$, can be extended to a scale of spaces with continuous smoothness indices. These spaces of non-integral order build subspaces of spaces with integral order H^m. First,

Definition 7.1.7. *For $s = m + \sigma, m \in \mathbb{N}_0, 0 < \sigma < 1$, we define the inner product*

$$(u,v)_{H^s} := (u,v)_{H^m} + \sum_{|\alpha|\leq m} \left(\int_\Omega \int_\Omega \frac{|\partial^\alpha u(x) - \partial^\alpha u(y)||\partial^\alpha v(x) - \partial^\alpha v(y)|}{|x-y|^{n+2\sigma}} \, d\mu(x) \, d\mu(y) \right). \tag{7.15}$$

Then the space $H^s(\Omega)$ is the closure of all functions in $H^m(\Omega)$ for which the norm

$$\|u\|_{H^s} := \sqrt{(u,u)_{H^s}} \tag{7.16}$$

is finite. This is also a Hilbert space.

For $\Omega \subseteq \mathbb{R}^n$ and any two constants s_1 and s_2 not necessarily integers the nesting yields

$$H^{s_1} \subset H^{s_2} \subset L_2, \quad s_1 > s_2 > 0. \tag{7.17}$$

Subspaces in Sobolev Spaces

Considering a domain $\Omega \subseteq \mathbb{R}^n$, $H^s(\Omega)$ coincides with the space of restrictions to Ω of the elements of $H^s(\mathbb{R}^n)$. Further, the spaces $H_0^s(\Omega)$ entail the elements of the spaces $H^s(\Omega)$ with compact support in Ω. In general, the spaces $H_0^s(\Omega)$ are closed subspaces of $H^s(\Omega)$. Considering that $C^\infty(\Omega) \cap H^m(\Omega)$ is dense in $H^m(\Omega)$ for $m \in \mathbb{N}_0$, we have:

Definition 7.1.8. *$H_0^s(\Omega)$ is defined as the closure of $\mathcal{D}(\Omega) := C_0^\infty(\Omega)$ with respect to the norm of $H^s(\Omega)$, i.e.,*

$$H_0^s(\Omega) := \{\phi \,|\, \exists \{\phi_n\} \in \mathcal{D}(\Omega) \text{ and } \phi_n \to \phi \text{ is a Cauchy sequence in } \|\cdot\|_{H^s(\Omega)}\}. \tag{7.18}$$

The equivalent characterization of equation (7.18) holds [59, 60]

$$H_0^s(\Omega) = \{u \,|\, u \in H^s(\Omega), \partial^\alpha u = 0 \text{ on } \partial\Omega, |\alpha| \leq s - \frac{1}{2}\}. \tag{7.19}$$

For the Sobolev spaces of integral orders the following inclusions are dense and the embeddings continuous:

$$\begin{array}{ccccccccc} L_2(\Omega) & = & H^0(\Omega) & \supset & H^1(\Omega) & \supset & H^2(\Omega) & \supset \ldots \\ & & \shortparallel & & \cup & & \cup & \\ & & H_0^0(\Omega) & \supset & H_0^1(\Omega) & \supset & H_0^2(\Omega) & \supset \ldots \end{array} \tag{7.20}$$

Dual of Sobolev Spaces

The dual space of $H^s(\Omega)$ is generally denoted by $(H^s(\Omega))^*$. We know from the *Riesz Representation Theorem* [122] that $(L_2)^* = L_2$. The dual form is given as

$$\langle u, v \rangle_{L_2 \times (L_2)^*} := \int u(x)\, v(x)\, d\mu, \quad u, v \in L_2. \tag{7.21}$$

In case $\Omega = I\!R^n$ we have the following result from [94]. It employs an alternative definition of fractional Sobolev spaces by means of Fourier Analysis.

Theorem 7.1.9. *For all $s > 0$ one has*

$$(H^s(I\!R^n))^* = H^{-s}(I\!R^n). \tag{7.22}$$

The following definition is to be employed when the domain Ω is bounded.

Definition 7.1.10. *For $\Omega \subset I\!R^n$ and $s \in I\!R_+$ we define a norm for $u \in L_2(\Omega)$ by*

$$\|u\|_{H^{-s}(\Omega)} := \sup_{v \in H_0^s(\Omega)} \frac{\langle u, v \rangle_{(L_2)^* \times L_2}}{\|v\|_{H_0^s(\Omega)}}, \quad s > 0. \tag{7.23}$$

The closure of $L_2(\Omega)$ with respect to this norm is $H^{-s}(\Omega) = (H_0^s(\Omega))^*$. Further, the following nesting holds:

$$\ldots \supset H^{-2}(\Omega) \supset H^{-1}(\Omega) \supset L_2(\Omega) \supset H_0^1(\Omega) \supset H_0^2(\Omega) \supset \ldots\ . \tag{7.24}$$

Multiresolution

The basic multiscale decompositions of function spaces discussed here is based on [27, 88, 124]. For Λ be a (possibly infinite) index set defined over a basis functions set Φ with $\#\Lambda$ elements, $\ell_2(\Lambda)$ is the Banach space of elements $\mathbf{v} \in \ell_2(\Lambda)$ for which the norm

$$\|\mathbf{v}\|_{\ell_2(\Lambda)} := \left(\sum_{\lambda \in \Lambda} |v_\lambda|^2 \right)^{1/2} \tag{7.25}$$

is finite. We introduce the following shorthand notation for an expansion of Φ with a coefficient vector $\mathbf{c} = \{c_\lambda\}_{\lambda \in \Lambda}$,

$$\mathbf{c}^T \Phi := \sum_{\lambda \in \Lambda} c_\lambda \phi_\lambda. \tag{7.26}$$

Consider a Hilbert space H embedded in L_2. Let $\{V_j\}_{j \geq 0}$ be a sequence of nested spaces approximating H, that is

$$V_0 \subset V_1 \subset \ldots \subset V_j \subset \ldots \subset H, \tag{7.27}$$

where their union is dense in H

$$\overline{\bigcup_{j\geq 0} V_j} = H. \tag{7.28}$$

Each of these so called multiresolution spaces V_j is spanned by a finite dimensional set of level dependent basis functions, also called single scale basis,

$$\Phi_j := \{\phi_\lambda\}_{\lambda\in\Lambda_j}, \quad V_j := \operatorname{span}(\Phi_j). \tag{7.29}$$

The basis functions $\{\phi_\lambda\}_{\lambda\in\Lambda_j}$ are chosen such that they are compactly supported on intervals depending on the scale j and

$$\operatorname{diam}(\operatorname{supp}\phi_\lambda) \sim 2^{-j}, \quad \lambda \in \Lambda_j. \tag{7.30}$$

Often, these basis functions can be written as translation and dilation of a single function known as *generator*. Since the support of the basis functions decreases with the level j they can represent more local information.

Another approach is to consider the complements of two successive spaces V_j, V_{j+1} and their decomposition in terms of orthogonal complements, here W_j:

$$V_j \oplus W_j = V_{j+1}. \tag{7.31}$$

We then consider a basis Ψ_j of the complement space:

$$W_j = \operatorname{span}(\Psi_j). \tag{7.32}$$

We fix a basis Φ_0 for the lowest nested space V_0 and construct a multi–scale basis Ψ_j^{MS} of V_j for each $j \geq 1$ by

$$\Psi_j^{MS} = \Phi_0 \cup \bigcup_{j'\geq 0}^{j-1} \Psi_{j'}. \tag{7.33}$$

In order to be able to work with this construction, the expansion coefficients in a basis Φ of any function $v \in \mathcal{H}$ should be *unique* and *stable*. For that we are interested in the following definitions.

Definition 7.1.11. *A multiresolution basis $\Psi_j^{MS} = \Phi_0 \cup \bigcup_{j'\geq 0}^{j-1} \Psi_{j'}$ of a separable Hilbert space $\mathcal{H}$ is called to be uniformly stable, if and only if the functions in $\Psi_j = \{\psi_{j,k}\}_k$ are linearly independent and*

$$\|\mathbf{v}_j\|_{\ell_2(\Lambda_j)} \sim \|\mathbf{v}_j^T \Psi_j\|_{\mathcal{H}}, \tag{7.34}$$

holds for every $\mathbf{v}_j \in \ell_2(\Lambda_j)$ and for every $j \geq 0$.

This means, there exist positive finite constants c_1, c_2 independent of j such that

$$c_1\|\mathbf{v}_j\|_{\ell_2(\Lambda_j)} \leq \|\mathbf{v}_j^T \Psi_j\|_H \leq c_2\|\mathbf{v}_j\|_{\ell_2(\Lambda_j)}. \tag{7.35}$$

7.2 Background on Multivariate and Multiscale Constructions

Univariate and Multivariate Uniform Splines

We have presented in Section 4.3.1 the construction of univariate B-splines for arbitrary degree and presented their properties. For a knot sequence $\Delta = \{\tau_i\}_{i=0,\dots,l+1}$ with $a = \tau_0 < \tau_1 < \ldots < \tau_{l+1} = b$ we defined the B-splines $N_{i,k}(x)$ of order k with respect to $\tau_i, \dots, \tau_{i+k}$ for $k = 1, \dots, l$ and $i = 0, \dots, l-k+1$ recursively. Recall at this point the following properties as in (4.3.6): local support, non-negativity, piecewise polynomial, partition of unity. We have later discussed the B-spline dual basis and in Proposition 4.3.13 the stability of B-spline series $\sum_{i=1}^{n} c_i N_{i,k}$ in the L_∞ norm.

At this point we present a more general result from [132]. We define for the knot sequence Δ and B-splines of order k the constants

$$d_i := \frac{\tau_{i+k} - \tau_i}{k},\ i = 0, \dots, l-k+1. \tag{7.36}$$

We deal in our work with uniform knot sequences, up to the multiple knots at the boundary. However, for the spline space we define its L_p-normalized basis in terms of the d_i coefficients and obtain:

Theorem 7.2.1. *There exists a constant $0 < D_k < \infty$ such that for each spline $S = \sum_{i=1}^{n} c_i N_{i,k}$ of order k and for each $0 < p \leq \infty$*

$$D_k \|\mathbf{c}'\|_p \leq \|S\|_p \leq \|\mathbf{c}'\|_p, \quad 1 \leq p \leq \infty, \tag{7.37}$$

$$D_k \|\mathbf{c}'\|_p \leq \|S\|_p \leq k^{1/p} \|\mathbf{c}'\|_p, \quad 0 < p < 1. \tag{7.38}$$

with $\mathbf{c}' := \{c_i'\},\ c_i' = c_i d_i^{1/p},\ i = 0, \dots, l-k+1$.

Corollary 7.2.2. *For $p = 2$, the B-spline basis is stable.*

The literature entails several types of multivariate spline spaces. Their definitions differ at least in the structure of the underlying partition for the polynomial segments, e.g. rectangular or triangular ones. We cite just some works e.g., [20, 28, 72]. The most direct construction is in term of tensor products of uniform B-splines. We have seen in Section 4.3 some theory on tensor products and their construction in terms of B-splines. In [107], the authors argue that the uniform stability of tensor product B-spline bases in $\mathbb{R}^d$ is known, citing further [34]. The standard result on the uniform stability of B-splines for $\mathbb{R}^d$ states that the condition number, for a suitably normalized B-spline basis, is bounded by a constant. This constant depends only on the degree and the dimension, but not on the choice of knots. Still, when approximating functions on a domain $\Omega \subset \mathbb{R}^d$, the stability of the basis is lost because the support of some basis functions intersects the boundary and has only small parts lying inside the domain, see e.g. [28]. There are different strategies in the literature to construct a uniformly stable family of bases for tensor product spline approximations on bounded domains in $\mathbb{R}^d$. The most direct strategy is to chose only the tensor product B-splines whose support intersects the domain. In [107], the authors start from the standard B-spline basis by normalization with respect to the L_p-norm.

Further, they employ a selection process in terms of Boor-Fix functionals [35]. Other alternatives are based on the concept of extension as in [72–74]. The outer, boundary B-splines causing instability are attached to inner ones. The result is a uniformly stable basis with full approximation power.

Hierarchical Multivariate B-Splines

Hierarchical constructions have also been widely present in literature for different problems statements. Just as an example, in [6], the author discusses the use of different hierarchically constructed bases on triangulations for the finite element method and positive definite elliptic operator equations. The author solves a problem for a finite element space V then adds certain hierarchical basis functions to the initial basis function set. The resulting space $\bar{V}$ has the hierarchical decomposition as a direct sum

$$\bar{V} = V \oplus W, \tag{7.39}$$

where W is the space spanned by the additional basis functions. It is expected that the component of the solution using $\bar{V}$ and restricted to V has not changed significantly to the solution obtained using V alone. For the two dimensional case, hierarchical basis methods are expected to have a growth of the condition number of order j^2 with j the number of levels and exponential in j for the three dimensional set up. The author still argues for the use for multigrid method mainly due to mesh handling, see [6] for the detailed discussion on error estimates and the associated inequalities.

Further, the authors of [44–46] employ the local refinement of a representation in terms of the hierarchical B-splines for object modeling. In this set up, the refinement is a local process and additional degrees of freedom accumulate where necessary. The authors present a method of localizing the effect of refinement through the use of overlays, which are hierarchically controlled subdivisions. As long as data points have not been fitted up to the required tolerance, one solves the least squares problem on the overlay for each separate out–of–tolerance region at a given level. After computing the resulting residuals, one can determine any remaining out–of–tolerance regions. The method recursively fits a hierarchical surface to a set of data by first fitting a coarse approximation. The approximation at a coarse level is successively improved with a correction term from the next finer level. Although their construction is adaptive, this method is not appropriate for scattered data. Still, working with gridded data allows for particularly efficient computations, since the surface fitting problem decomposes into a sequence of curve fitting processes. Also interestingly, the authors advocate in [46] the use of hierarchical splines for such data fitting problems instead of wavelet-based multiresolution analysis. It is explained that wavelet techniques are of advantage only in a setting in which refinements are known and fixed in advance. Further, wavelets have been developed for continuous inner products and in a functional setting. On the other side, the data fitting ansatz requires a discrete inner product and is designed for a parametric setting. In [52], the authors use an explicit spline representation of smooth free-form surfaces combined with a hierarchy of meshes. Here, finer-level patches replace coarse-level patches. Localized-hierarchy Surface Splines (LeSS) are based on surface splines and extend the modeling paradigm from [46]. Further, [58]

aim at conforming, hierarchical, adaptive refinement methods by refining basis functions, not elements. The approach is versatile as it is independent of domain dimension, element type, and basis function order.

Hierarchical B-splines were also treated in [72, 86]. The authors consider a multilevel linear spline in terms of tensor product B-splines on different, hierarchically ordered grid levels. A selection mechanism for B-splines is provided such that linear independence to form a basis is guaranteed. The proceedings are appropriate for intricated domains and singularities. A subset of the relevant B-splines for a grid with grid width h, e.g., those basis functions whose support intersects the boundary of the domain, are replaced by B-splines of grid width $h/2$ via subdivision. From these additional basis functions, a further subset is selected and refined. A B-spline either belongs to the hierarchical basis or is represented as a linear combination of B-splines with smaller grid width via subdivision. According to the authors, the local approximation power of the resulting basis corresponds to the level of refinement. Stability with respect to the number of grid levels is not achieved. However, the basis is proven to be weakly stable, i.e., stability constants grow like $\mathcal{O}(j)$ with j the number of grid levels.

A generalization of the traditional tensor-product construction of bivariate spline spaces is provided in [148]. The authors studied so-called semi-regular bases which lead to spaces of piecewise polynomials with an irregular, locally refinable knot structure. They considered the domain partition with knot segments and knot rays with endpoints in the interior of the domain. The dimension of these generalized tensor-product spline spaces is also investigated.

Another approach on multilevel B-splines but not in the strict hierarchical sense can be found in [91]. The authors describe an algorithm for scattered data interpolation and approximation. Multilevel B-splines are introduced to compute a $\mathcal{C}^2$–continuous surface through a set of irregularly spaced points. They employ a coarse-to-fine hierarchy of control lattices to generate a sequence of bicubic B-spline functions whose sum approaches the desired interpolation function. Later, the representation is reduced to one equivalent B-spline function using B-spline refinement. The results remain experimental.

These approaches are still adapted for data fitting, be it uniform or scattered. We deal in our approximate continuation problem with an ill posed problem. The data fitting ansatz is corroborated with the harmonicity constraint. It is only the boundary data that must be fitted, and preferably adaptive. The constructed approximation over the domain entails practically no data points and the continuation is controlled only by the weighted term minimizing the Laplacian of the continuation. This is why we decided to adapt the initial tensor product splines to a method whose construction is less dependent on the available control points.

At this point we wish to shortly point out the distinction between hierarchical and wavelet decompositions, the main approach to multiresolution analysis or to tensor product spline functions. In the case of wavelets, the orthogonal complement of two successive spaces is constructed. Spline wavelets for tensor-products and decompositions were investigated e.g. in [8, 79, 117]. These citations do not include the vast literature on spline wavelets alone. We will later explain in this work why we chose the hierarchical construction over the wavelet method.

Adaptive Methods for PDEs and Scattered Data Problems

We have mentioned at the beginning of this chapter the main influential works for these thesis. To these we count [22] which discussed the construction and analysis of wavelet-based adaptive algorithms for the numerical solution of elliptic PDEs, and [16, 17], which studied the use of (tensor products of) linear spline wavelets for adaptive data-fitting. Later, we have considered alternative bases and employed sparse grids as e.g. in [14].

Modern approaches to partial differential equations do not rely anymore on the refinement of a mesh, as in the case of adaptive Finite Element Methods, but on the refinement of the considered locally supported basis. Within some iterative process, suitably selected further basis functions are added to those that are already used to approximate the current solution. The assumption is that representation coefficients locally describe the function and that large coefficients indicate that some information still has to be represented. As in the case of Finite Elements, in-depth studies were undertaken in order to understand the theoretical aspects for the optimality of the solution and error reduction rate.

In [22], the authors search algorithms to approximate the solution u of an elliptic operator equation by a linear combination of N wavelets. The considered benchmark is given by the rate of the best N-term approximation where only the N largest wavelet coefficients of the real solution are retained. This selection process is known as *thresholding*. Determining the best N-term coefficients requires the thresholding of the exact, but not known solution discretized in wavelet coordinates. The authors look therefore for an optimal adaptive wavelet algorithm including a thresholding of the coefficients, which performs like thresholding the exact one. They also approach the computational optimality of the method investigating the number of necessary arithmetic operations. In addition to the fact that an optimal algorithm is presented and its convergence is proved, another relevant issue regards the Riesz property of the basis. E.g., a linear boundary value problem is equivalent to its representation in a basis, if the Riesz property for the chosen basis holds. In this case, the thresholding procedure with respect to the coefficient values makes sense. Further literature includes [29, 30].

For data fitting, [16] and the dissertation [17] presents an algorithm that constructs a least squares approximation to a given set of unorganized points in terms of particular B-spline based wavelets. A hierarchy of approximations to the data with increasing level of detail is constructed within a multiresolution setting. The author designed this coarse–to–fine algorithm in such a way that overfitting effects should be avoided. For that, the authors consider within the iterative procedure two types of thresholding. First, the horizontal thresholding requires that only basis functions, in whose support lie a prescribed number q of data points, are admitted to the basis Ψ_j. Secondly, for the selected basis, the magnitude of the coefficients can be interpreted as a local smoothness estimator. The vertical thresholding procedure then eliminates degrees of freedom that are detected not to make a significant contribution. Since the ansatz deals with scattered data, the author presents conditions to allow for a stable growth of the basis and invertibility of the resulting system matrices. Further, the equivalence relation between wavelets and Besov spaces is employed to formulate the problem of data fitting with regularization. In [38], this least squares data fitting method is used for the evaluation of the non-linear term in the wavelet-Galerkin formulation of nonlinear PDE problems.

Sparse Grids

Another modern development which contributed to the results of this thesis are sparse grids. We refer at this point without assuming completeness to [14], citing further the precursor and initiator [152]. They present a survey of the fundamentals and the applications of sparse grids and discuss their use to the solution of partial differential equations. The motivation of sparse grid in general resides in the dreaded curse of dimensionality. When working with uniform grids and with piecewise polynomial functions as in our set up, the computational cost and storage requirements with respect to the order of accuracy grow exponentially with the number of dimensions of the problem. The additional argument is that stronger assumption on the smoothness of the solution alone will not help to compensate for the exponential growing complexity.

The sparse grid method [14, 50, 51] assumes that the functions belong to spaces of functions with bounded mixed derivatives. Consider w.r.o.g. for the d-dimensional unit interval $\bar{\Omega} := [0,1]^d$ the multivariate functions u

$$u(x) \in I\!R, x := (x_1, \ldots, x_d) \in \bar{\Omega}, \tag{7.40}$$

with (in some sense) bounded weak mixed derivatives

$$D^{\alpha}(u) := \frac{\partial^{|\alpha|_1} u}{\partial x_1^{\alpha_1} \cdots \partial x_d^{\alpha_d}}, \quad \alpha = (\alpha_1, \ldots, \alpha_d) \in I\!N_0^d, \ |\alpha|_1 := \sum_{i=1}^{d} \alpha_i. \tag{7.41}$$

For example for

$$|\alpha| \leq 2 \tag{7.42}$$

these functions belong to the Sobolev space H^2_{mix} defined as

$$H^2_{\text{mix}} := \left\{ u : \bar{\Omega} \to I\!R : D^{\alpha}(u) \in L_2(\Omega), |\alpha| \leq 2, u|_{\partial\Omega} = 0 \right\}. \tag{7.43}$$

Sparse grids further require a one dimensional multilevel basis, which is preferably also L_2 stable. One works, for example, with the piecewise linear hierarchical basis. This basis is extended into higher space dimensions by a plain tensor product construction to obtain a multilevel basis. In contrast to the hierarchical multivariate approaches from computer graphics, e.g. of [44,46,72,86], the sparse grid method allows for anisotropic support bases, i.e. entailing functions tensoring one dimensional basis functions living on different levels. It can be proven, that for a function belonging e.g. to H_2^{mix} and by employing tensors of the one dimensional piecewise linear basis holding

$$\mathcal{O}(2^{2|l|_1}) \tag{7.44}$$

degrees of freedom, the resulting coefficients of u in this basis decrease as

$$\mathcal{O}(2^{-2|l|_1}) \tag{7.45}$$

where $l = (l_1, \ldots, l_d)$ is the level in the d–variate set up. This is followed by a thresholding procedure. An optimization with respect to the number of degrees of freedom and the

resulting approximation accuracy is at this point provided, leading directly to sparse grid spaces. Instead of working the full grid space

$$V_n := \oplus_{|l|_\infty \leq n} W_l \tag{7.46}$$

yielding a computational and storage requirement order

$$\mathcal{O}(2^{nd}), \tag{7.47}$$

one considers only the so called *sparse grid* spaces containing only basis functions such that

$$V_n^{sparse} := \oplus_{|l|_1 \leq n+d-1} W_l. \tag{7.48}$$

Here, one has a reduced complexity of order

$$\mathcal{O}(2^n n^{d-1}). \tag{7.49}$$

Further, within the sparse grid construction, the number of degrees of freedom is significantly reduced, whereas the accuracy is only slightly deteriorated [51]. This sparse grid method has been applied to partial differential equations or numerical integration.

We are still mostly interested in the extension of sparse grids employing higher-order basis functions. Some proven alternatives to the piecewise linear hierarchical basis are one dimensional polynomial bases of arbitrary degree or prewavelets. The authors of [13] introduced the so-called hierarchical Lagrangian interpolation which uses a hierarchical basis of piecewise polynomials of arbitrary degree p. $\mathcal{C}_0$–elements are considered with just one degree of freedom per node or per grid point for a higher grade. An alternative hierarchical multiscale basis with higher-order functions are the interpolets from [36] which can be used in simple multilevel algorithms for the evaluation of nonlinear terms. Although interpolets are defined on the whole of $\mathbb{R}$, their construction can easily be adapted to a bounded interval, see [85]. These approaches take advantage of higher regularity assumptions and provide better approximation rates. It has been explained in [111] that these hierarchical multiscale bases are not stable in the multidimensional case and do not provide a stable multiscale splitting.

In [56, 84], the authors provide a technique to take one dimensional, two-sided error norm estimates to the higher-dimensional case based on the representation of Sobolev spaces $H^s([0,1]^d), s \geq 0$, as

$$H^s([0,1]^d) = \bigcap_{i=1}^{d} \underbrace{L_2([0,1]) \otimes \cdots \otimes L_2([0,1])}_{(i-1) \text{ times}} \otimes H^s([0,1]) \otimes \underbrace{L_2([0,1]) \otimes \cdots \otimes L_2([0,1])}_{(d-i) \text{ times}}. \tag{7.50}$$

The Sobolev space $H^s_{\text{mix}}([0,1]^d), s \geq 0$ is further defined as the simple tensor product

$$H^s_{\text{mix}}([0,1]^d) = \underbrace{H^s([0,1]) \otimes \cdots \otimes H^s([0,1])}_{d \text{ times}}. \tag{7.51}$$

For the different components of the tensor product, two-sided norm estimates are obtained if the univariate multiscale functions ϕ_{l_j,k_j} on level l_j allow two-sided norm estimates for both H^s and L_2. We present this result from [14].

Theorem 7.2.3. *Let the univariate multiscale basis $\Phi = \{\phi_{l_j,k_j}\}$ satisfy the norm equivalence*

$$\|u\|_{H^s}^2 \sim \sum_{l_j} 2^{-l_j} \sum_{k_j} 2^{2l_j s} |d_{l_j,k_j}|^2, \tag{7.52}$$

with

$$u(x_j) = \sum_{l_j,k_j} d_{l_j,k_j} \phi_{l_j,k_j}(x_j), \tag{7.53}$$

$$-\gamma_1 < s < \gamma_2, \gamma_1, \gamma_2 > 0. \tag{7.54}$$

Then, the multivariate basis functions $\{\phi_{l,k}\}$ with levels $l = (l_1, \ldots, l_d)$ and indices $k = (k_1, \ldots, k_d)$ for the d–variate set up fulfill the norm equivalences

$$\|u\|_{H^s}^2 = \left\| \sum_{l,k} d_{l,k} \phi_{l,k} \right\|_{H^s}^2 \sim \sum_{l,k} 2^{2s|l|_\infty} |d_{l,k}|^2 2^{-|l|_1}, \tag{7.55}$$

$$\|u\|_{H^s_{mix}}^2 = \left\| \sum_{l,k} d_{l,k} \phi_{l,k} \right\|_{H^s_{mix}}^2 \sim \sum_{l,k} 2^{2s|l|_1} |d_{l,k}|^2 2^{-|l|_1} \tag{7.56}$$

where $u(\mathbf{x}) = \sum_{l,k} d_{l,k}(x) \phi_{l,k}(x)$.

The authors of [14] point for proof and further details to [56,84,85]. The bounds γ_1, γ_2 for the range of the regularity parameter s depend on the specific choice of the mother function ϕ. In fact, the L_2-stability of the 1D hierarchical basis $\{\phi_{l_j,k_j}\}$, is a prerequisite in Theorem 7.2.3. Most linear hierarchical bases like the construction in [13, 36] are also not L_2-stable. In this case, only the upper estimates can be verified. It has further been explained in [14] that the hierarchical coefficients $d_{l,k}$ in the multivariate setup can still be employed after suitable weighting as error indicators in a refinement procedure, but not as a true error estimator. The resulting solution is within the prescribed global error tolerance but eventually by employing more than the optimal number of degrees of freedom. Further, the condition number of the resulting linear system still depends of the finest considered refinement level. One could otherwise consider established wavelet constructions known to fulfill the stability condition, see again [14] for further insight and citations.

7.3 Multiscale Constructions

Hierarchical methods are based upon hierarchically defined bases Ψ_j with locally supported functions to discretize the subspaces

$$V_0 \subset V_1 \subset \ldots \subset V_j,\ j > 0, \tag{7.57}$$

on uniformly and dyadically refined partitions over the given domain Ω. An initial analysis of hierarchical basis functions for finite element approaches for the elliptic partial differential equation setting can be found in [153] and an overview in [151]. Other literature on hierarchical constructions includes [149, 150].

7.3.1 Monovariate Hierarchical and Wavelet Basis

Linear hierarchical (B-spline) basis

In view of the splittings of function spaces presented here, let us take a look at one of the most commonly used approaches, namely the linear hierarchical basis. There are various definitions, via nodal bases on iteratively divided partitions as e.g. in [15, 151] or via translation and constructions of an initial hat function, as e.g. in [17]. Remember the construction we had for the B-splines in Section 4.3.1, applied to the first degree case. Consider the j-th level uniform knot sequence

$$\Delta_j = \{\tau_i\}_{i=0,\ldots,2^j} \tag{7.58}$$

defined without loss of generality over $[0, 1]$ with

$$0 = \tau_0 < \tau_1 = \tau_0 + 2^{-j} < \ldots < \tau_{2^j} = 1. \tag{7.59}$$

The nodal basis functions are defined by ϕ_i, $i = 0, \ldots, 2^j$, the piecewise linear function over the intervals determined by the knots of Δ_j, such that

$$\phi_i(\tau_k) = \delta_{ik}, \quad \tau_k \in \Delta_j. \tag{7.60}$$

Obviously, all the elements have the same frequency and a maximal support of 2^{j-1}. Based on this construction, we can define further the functions $\psi_{j,i}$ of the hierarchical basis such that

$$\psi_{j,i}(\tau_k) = 0, \quad \tau_k \in \Delta_{j-1}. \tag{7.61}$$

We hereby obtain a set with the same dimension as in the case of the nodal basis. But this time, the frequency of the basis function varies with the level of the knot sequence refinement: the higher the level j, the higher the frequency of the basis function.

Otherwise, one can construct the same basis function up to scaling by considering the hat function $\psi(x)$ centered around $1/2$

$$\phi(x) := \begin{cases} x & : \quad 0 \leq x \leq \frac{1}{2}, \\ 1 - x & : \quad \frac{1}{2} \leq x \leq 1, \end{cases} \tag{7.62}$$

and defining the translations and contractions $\psi_{j,k}(x)$ on level j as

$$\psi_{j,k}(x) := \phi(2^j x - k). \tag{7.63}$$

Accordingly, we obtain a hierarchical decomposition of the piecewise linear function space on the uniform knot sequence Δ_j for $\psi_{j,k}$ defined either as in equation (7.61) or in equation (7.62)

$$\Psi_N^{HB} := \left\{\psi_{j,k} : j \leq N;\ k = 0, \ldots, 2^{j-1}\right\}. \tag{7.64}$$

The reader can compare the nodal basis functions in Figure 7.4 and the hierarchical decomposition of the same piecewise linear space in Figure 7.1.

The desirable property of stability should not be taken for granted, not even in this elementary set up. It is known that the standard hierarchical basis is uniformly stable after

appropriate rescaling in one dimension; it is still unstable in two dimensions [150, 153]. It has been proven in [95] that the rescaled, i.e. normalized, linear hierarchical basis is a Riesz basis in $H^s(\Omega)$ if and only if

$$d/2 < s < 3/2,\ d \leq 2. \tag{7.65}$$

Considering the uniform stability in L_2, look at [17] to see with the help of an insightful example how the mechanism of instability works, i.e. the norm of the resulted coefficient vector and of the function do not meet the conditions anymore.

Figure 7.1. *The standard linear hierarchic basis as in e.g. [17, 149].*

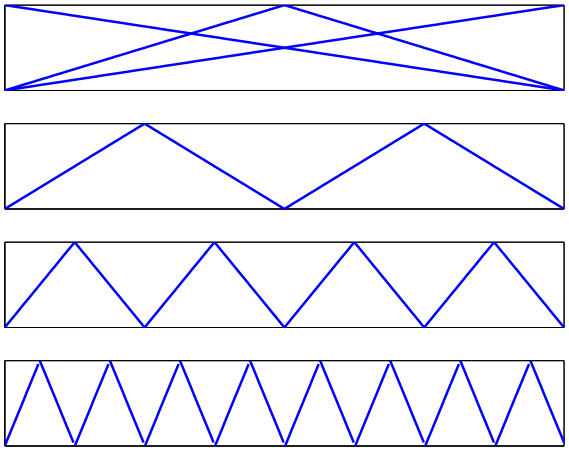

The Wavelet Linear B-Spline Basis

We have discussed at the beginning of this section the possibility of constructing nested spaces and multiresolution decompositions in terms of orthogonal complements: consider two successive spaces V_{j-1}, V_j and construct an orthogonal complement W_j such that

$$V_j \oplus W_j = V_{j+1}. \tag{7.66}$$

This idea resides at the core of wavelet constructions.

For Ψ_0 a basis for an initial space V_0, we construct a basis Ψ_j^{WB} of subsequent nested spaces V_j of the form

$$\Psi_j^{WB} = \Psi_0 \bigcup_{j'\geq 0}^{j} S_{j'}, \quad S_j = \operatorname{span}(W_j) \tag{7.67}$$

for each $j \geq 1$. We will not discuss here the actual construction of these basis functions. There are various wavelet families and intricated constructions of them having different properties. We just mention the wavelet linear B-spline basis Ψ^{WB} associated to the same function space as the linear hierarchic (B-spline) basis Ψ^{HB} discussed here. Their construction can be found e.g. in [140]. The reader can find Figure 7.2 for the first basis functions of the decomposition.

Figure 7.2. *Linear wavelets on the interval as e.g. in [17, 140].*

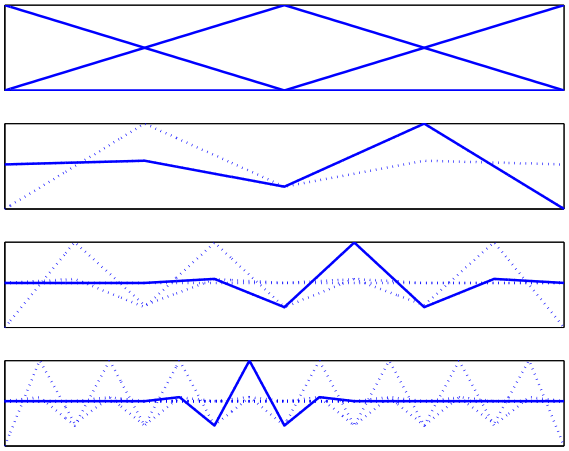

Quadratic hierarchical basis

As a distinctive example in exercising hierarchical decompositions, we show the polynomial quadratic hierarchical basis functions as constructed in [15]. They start with nodal bases on iteratively divided partitions as the j-th level uniform knot sequence Δ^j as in equation (7.58) and define the polynomial quadratic basis functions over two neighboring intervals of Δ_j as the functions $\psi_{j,l}$

$$\psi_{j,l}(\tau_l) = 0, \quad \tau_l \in \Delta_{j-1}. \tag{7.68}$$

Figure 7.3, left shows the first basis functions set of this decomposition. The authors suggest a further development. They explain that by replacing some selected quadratic basis functions with linear ones, the spanned space should not change. Figure 7.3 provides a comparative illustration.

Figure 7.3. *Alternative hierarchic developments as in [15]. Left: Quadratic hierarchical basis functions spanning a 17-dimensional, quadratic finite element space. Right: An alternate set of quadratic hierarchical basis functions spanning the same 17-dimensional, quadratic finite element space.*

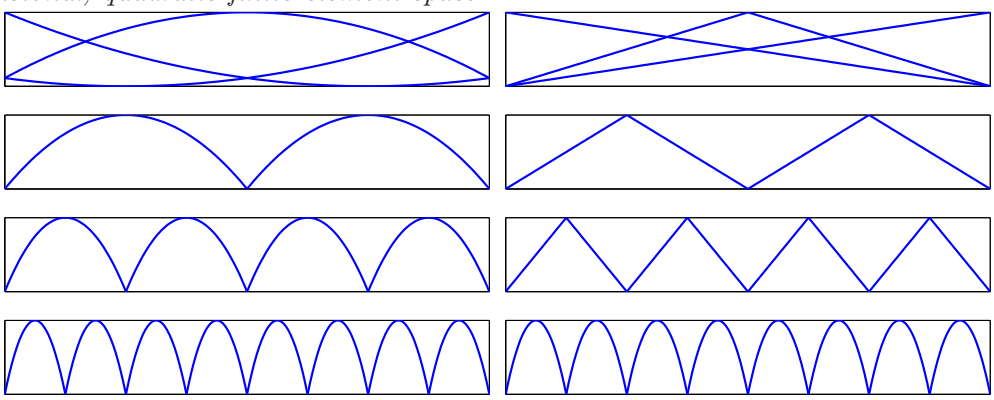

The Hierarchical and Wavelet Cubic B-Spline Basis

When dealing with multiscale decompositions of piecewise cubic function spaces, the common approach considers the wavelet cubic B-spline basis [19, 21, 140]. Wavelet functions can be expressed as a linear combination of the scaling functions, which are in this case the cubic B-splines. In view of our application, we are interested in the endpoint interpolating B-splines on the unit interval. Later, we also describe the hierarchical (end-point interpolating) cubic B-spline setup and argue as our multiscale approach choice.

In the multiresolution analysis set up, the basis functions for Ψ_j for level j can be given by translation and dilation of a single function. The resulted spaces are nested and we have the refinement or subdivision coefficients

$$\{m_k\}_{k\in\mathbb{Z}} \in \ell_2(\mathbb{Z}) \tag{7.69}$$

such that for every $x \in \Omega$

$$\phi(x) = \sum_{k\in\mathbb{Z}^m} m_k \phi(2x-k). \tag{7.70}$$

This relation has been formulated in the literature in matrix form. For any of the functions $\phi_{j,k},\ j \geq j_0$, the matrices

$$\mathbf{M}_{j,0} = (m^{j,0}_{r,k})_{r\in\Delta_{j+1},k\in\Delta_j} \tag{7.71}$$

have been defined such that the two-scale relation

$$\phi_{j,k} = \sum_{r\in\Delta_{j+1}} m^{j,0}_{r,k}\phi_{j+1,r}, \quad k \in \Delta_j \tag{7.72}$$

holds. The sequence

$$\mathbf{m}^j_k := (m^{j,0}_{r,k})_{r\in\Delta_{j+1}} \in \ell_2(\Delta_{j+1}) \tag{7.73}$$

is called mask and each element a mask coefficient. Recall that we are considering only locally supported basis functions. Only the refinement coefficients of the function on level $j+1$ whose support intersects the support of a function on the previous level j can carry non-zero mask coefficients. Furthermore, we have the matrix-vector formulation

$$\Phi_j = \mathbf{M}^T_{j,0}\Phi_{j+1}. \tag{7.74}$$

with $\mathbf{M}^T_{j,0}$ uniformly sparse.

We proceed with the construction in terms of B-splines. For that, we first define the scaling functions for a nested set of function spaces. Remember the recursive definition 4.3.5 of generalized B-splines $N_{i,k}$ of order k for a given knot sequence Δ. As in the previously presented approaches, we consider iteratively divided uniform knot sequences Δ_j on the unit interval $[0,1]$. For the construction of the end-point interpolating version, a certain padding of Δ_j is required, such that the first and last $k+1$ knots are set to 0 and 1 respectively. We hereby obtain the basis function set

$$\Phi = \{\phi_{i,k}\},\ \phi_{i,k} := \{N_{i,k}\}_{i=0,\ldots,2^n+k-1} \tag{7.75}$$

for the space of piecewise-polynomials of degree k. These are in fact known also as the level n end-point interpolating B-spline scaling functions. We denote them for our cubic case as N_i^n.

We take a look at the nested spaces property. Let V_n be the space spanned by the cubic B-spline scaling functions on knot sequence of level j on the interval

$$V_j := \text{span}\{N_i^j : i = 1, \ldots, 2^j + 3\}. \tag{7.76}$$

We have to make sure that the spaces $\{V_j\}_{j=1,2,\ldots}$ are nested as required by multiresolution analysis. It is often met in literature to write scaling functions $N_{i,3}^j$ a given level j as a combination of scaling functions $N_{i,3}^{j+1}$ on the next finer level $j+1$. This is done in view of the fact, that the condition stating, that the subspaces V_j are nested, is equivalent to requiring refinable scaling functions. Formulated in matrix form, there must exist a matrix of constants $\mathbf{M}_{j,0}^T, j \geq j_0$, such that

$$\Phi_j = \mathbf{M}_{j,0}^T \Phi_{j+1}, \quad \Phi_j := \left[N_0^j \ldots N_{2^j+3}^n \right], \quad \mathbf{M}_{j,0} \in I\!R^{(\#\Phi_{j+1})\times(\#\Phi_j)}. \tag{7.77}$$

How to determine the appropriate matrices $\mathbf{M}_{j,0}^T$ can be found in [19, 140].

We consider again the example of the hierarchical linear basis. The functions $\psi_{j,i}$ of the hierarchical basis were defined in equation (7.61). Here, only every other second basis function in the level $j+1$ nodal basis belongs to the hierarchical complement on level j. We translate this alternation principle to the endpoint interpolating cubic splines to obtain our hierarchical cubic B-spline construction.

We have

$$\#\Lambda_j = 2^j + 3, \quad \#\Lambda_{j+1} = 2^{j+1} + 3 \tag{7.78}$$

so a number of

$$\#W_j = \#V_{j+1} - \#V_j = 2^j \tag{7.79}$$

basis functions are missing up to the nodal basis on level $j+1$. We take the additional 2^j degrees of freedom as functions of the nodal level j and distributed over the 2^j intervals of size 2^{-j} such that each one is centered at each of the additional nodes

$$\Delta_{j+1} \backslash \Delta_j. \tag{7.80}$$

We hereby have that W_j is a subset of the nodal basis on level $j+1$. Considering the subdivision formula for B-splines, each function contained in the nodal B-spline basis on level $j+1$ but not in W_j can be written as a linear combination of the basis functions in V_j and W_j. The functions in the hierarchically decomposed $V_j \oplus W_j$ are linearly independent and span the same space as the nodal basis of level $j+1$. See Figure 7.5 for a hierarchical cubic B-spline decomposition.

Figure 7.4. *Comparison of a level 3 cubic (top) and linear (bottom) B-spline complete set of scaling basis functions. Every other second basis function, here continuously lined, belongs to the hierarchical complement on the previous level.*

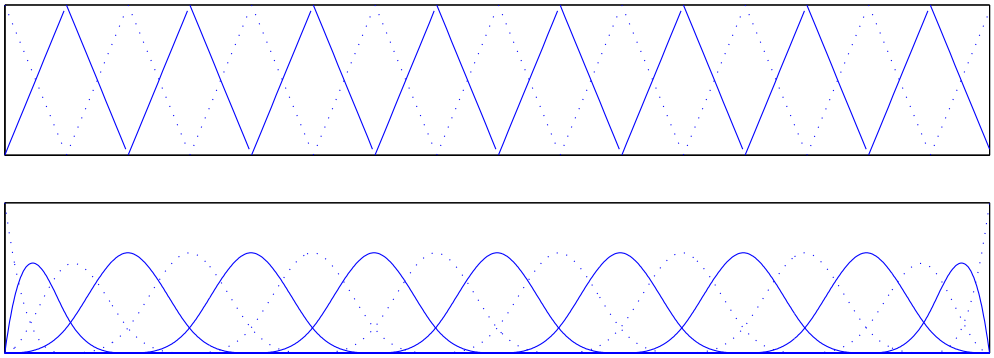

The matrix formulation technique is applied in case of the wavelets, where we need to find basis functions for the orthogonal complements for two sequent nested spaces. Since by definition

$$W_j \subset V_{j+1}, \tag{7.81}$$

we can write the wavelet basis functions

$$\Psi_j = \{\psi_{j,k}\}_{i=0,\ldots,2^n} \tag{7.82}$$

as linear combinations of the scaling functions. This formulation can be further used to express the orthogonality or biorthogonality conditions. But since the possible constructions are unlimited, wavelets must fulfill additional conditions, like minimal support. The B-spline wavelets constructed as in [43] or [19] are biorthogonal, and share other good properties with the B-splines scaling functions e.g. compact support, smoothness, symmetry and can be efficiently implemented.

Still, in spite of the very clean image of the cubic B-spline wavelets which includes stability, we had problems considering them for our adaptive approximate continuations of harmonic functions. As mentioned earlier in our work, encouraged also by the experience gained in our inspirational reference [99], we had decided to work with cubic polynomial spaces. Notice by comparison in Figures 7.5 and 7.7, how a wavelet on level n has a support of

$$7 \cdot 2^{-n}, \tag{7.83}$$

almost twice as large as the support of a scaling B-spline function on the same level, namely

$$4 \cdot 2^{-n}. \tag{7.84}$$

This can be also argued by analyzing the columns in the matrices $\mathbf{M}_{j,0}$ and $\mathbf{M}_{j,1}$ for end-point interpolating cubic B-spline scaling functions wavelets as presented in [140]. The columns of $\mathbf{M}_{j,0}$ for $j \geq 3$ for the scaling functions $\phi_{j,i}$ not containing the ending points of the interval have the entries:

$$\mathbf{M}^i_{j,0} = \frac{1}{16}[\ldots 0\ 2\ 8\ 12\ 8\ 2\ 0 \ldots]. \tag{7.85}$$

Figure 7.5. *First basis functions in a hierarchical cubic B-spline decomposition.*

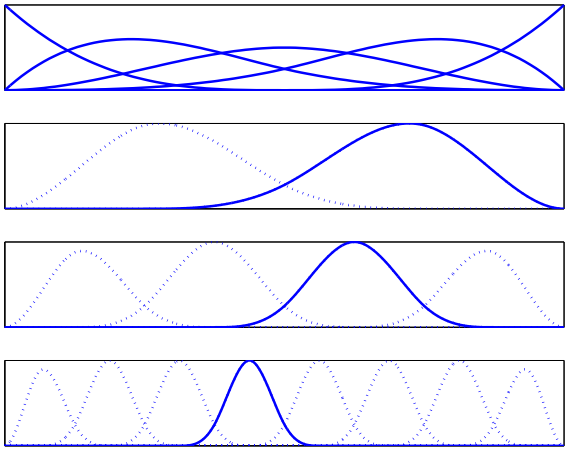

Figure 7.6. *First basis functions in a cubic B-spline wavelet decomposition.*

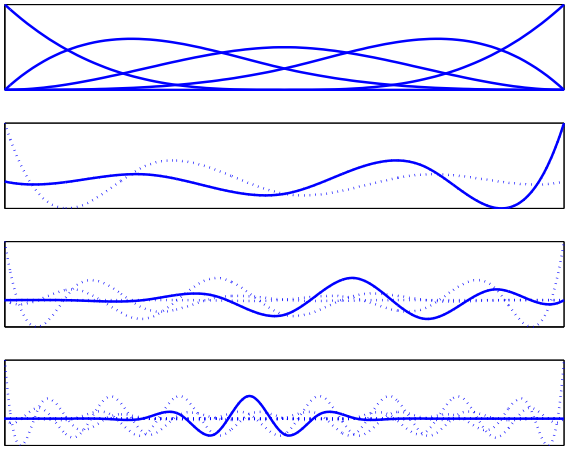

The columns of $\mathbf{M}_{j,1}$ for $j \geq 4$ for the basis functions $\psi_{j,i}$ not containing the ending points of the interval have the entries:

$$\mathbf{M}^i_{j,1} = \sqrt{\frac{5 \cdot 2^j}{675221664}}[\ldots 0,\ -1,\ 124,\ -1677,\ 7904,\ -18482,\ 24264,\\ -18482,\ 7904,\ -1677,\ 124,\ -1,\ 0,\ldots].$$

So, a scaling function on level j is the weighted sum of five successive scaling functions on level $j-1$ covering a support of eight 2^{j-1} segments as opposed to eleven successive scaling functions and a support of fourteen 2^{j-1} segments in the case of wavelets. This means, a wavelet has an almost twice as large support than a scaling function on the same level. Recall, approximate harmonic function continuation method targets in fact three dimensional domains. The data fitting ansatz requires the evaluation of all basis functions over all available data points. But a larger support means that a bigger number of data points might be included by the support and this for each dimension. It translates to

Figure 7.7. *Left: Comparison of a level 3 cubic B-spline scaling (dotted line) and wavelet (continuous line) functions, together with a delimiting of their supports. Right: Detail, wavelet only apparently zero at the outer support segments.*

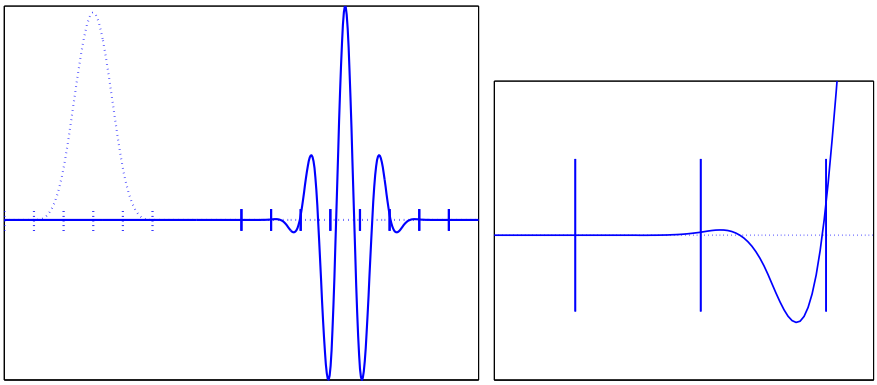

eventually up to

$$\left(\frac{14}{8}\right)^3 \sim 5.36 \tag{7.86}$$

times more non-zero entries to be considered, which significantly affects the sparse nature of the resulting system matrices and is associated with memory requirements. The factor $\left(\frac{14}{8}\right)^3$ is orientational, since variations determined by data point distribution, e.g. them being given only at the boundaries, may occur. This convinced us to consider working with a hierarchic construction in terms of cubic B-splines scaling functions over the classical cubic B-spline wavelet approach.

For a better insight we present a comparison of the matrices cross product matrices $\mathbf{M}$ resulting within the first successive iterative steps of an adaptive approximate harmonic continuation procedure containing functions up to level 3, 4 and 5 respectively. When using the hierarchical cubic B-spline basis, we obtained the matrices denoted here by

$$M^3_{\mathrm{HB}},\ M^4_{\mathrm{HB}} \text{ and } M^5_{\mathrm{HB}}, \tag{7.87}$$

using the wavelet cubic B-spline basis the matrices denoted here by

$$M^3_{\mathrm{WB}},\ M^4_{\mathrm{WB}} \text{ and } M^5_{\mathrm{WB}}. \tag{7.88}$$

In view of the adaptive setting, one needs to set up these matrices explicitly and we deal with problems regarding memory requirements. Matrix structures do variate greatly with the considered indexing of the basis functions and of the data points. Anyway, it turns out that the sparsity patterns of the matrices resulting with the hierarchical basis is thinner due to the smaller support of the basis functions. Notice in Figure 7.3.1 the number of non zero entries of each considered matrix. Although wavelets, unlike hierarchical constructions, profit from the numerical and computational advantage of low coupling between levels due to orthogonality conditions, we found memory issues more stringent.

Figure 7.8. *Comparison of the cross product matrices resulted within the iterative steps of an adaptive procedure involving basis functions up to levels 3, 4 5 respectively. The matrices M^3_{HB}, M^4_{HB} and M^5_{HB} have been obtained using the tensor product hierarchical cubic B-spline basis and the matrices M^3_{WB}, M^4_{WB} and M^5_{WB} using the tensor product cubic B-spline wavelets basis. nz denotes the number of non zero entries of the matrix.*

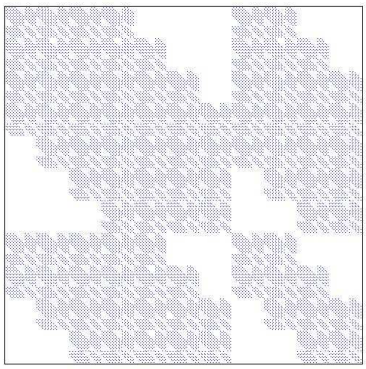

$M^3_{\mathrm{HB}},\ nz = 26562$

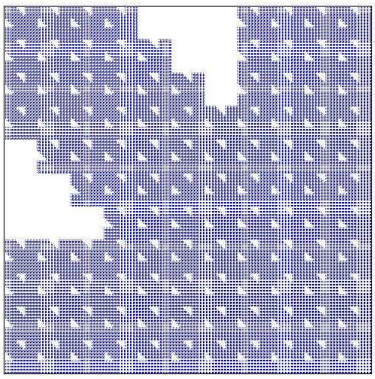

$M^3_{\mathrm{WB}},\ nz = 95048$

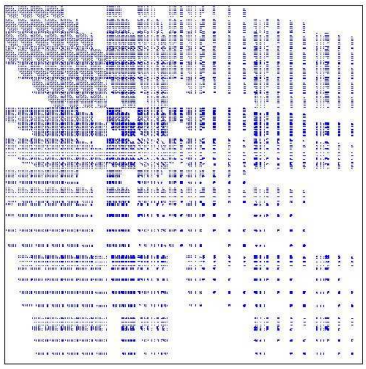

$M^4_{\mathrm{HB}},\ nz = 40344$

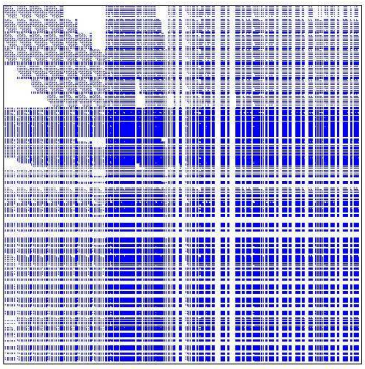

$M^4_{\mathrm{WB}},\ nz = 286636$

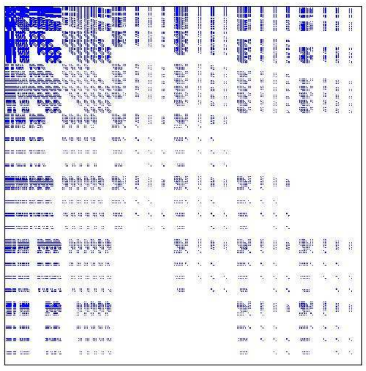

$M^5_{\mathrm{HB}},\ nz = 652082$

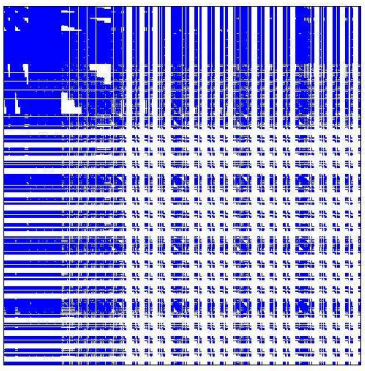

$M^5_{\mathrm{WB}},\ nz = 32578592$

7.3.2 Tensored Nested Spaces

We have seen in the previous section how to construct a multiresolution basis, e.g. in terms of one dimensional B-splines, by considering the nested sequence (7.27). We are now ready to regard the construction in terms of tensor product considering the nested spaces property. For clarity yet without restriction of generality, we consider the two dimensional tensoring $V_J \otimes V_J$ of the one–dimensional space V_J decomposed as:

$$V_J = V_{j_0} \oplus W_{j_0} \oplus W_{j_0+1} \oplus \ldots \oplus W_{J-1}. \tag{7.89}$$

We write the tensor product space $V_J \otimes V_J$ as

$$V_J \otimes V_J = (V_{j_0} \oplus W_{j_0} \oplus W_{j_0+1} \oplus \ldots \oplus W_{J-1}) \otimes (V_{j_0} \oplus W_{j_0} \oplus W_{j_0+1} \oplus \ldots \oplus W_{J-1}) \,. \tag{7.90}$$

At this point we can differentiate between three main approaches in constructing a tensor product basis. For that we consider three different refinement strategies: anisotropic, isotropic and sparse. For each of the refinement strategies, different set of refined basis functions are admitted to the (tensor-product) basis on the next level. We can describe the decompositions in terms of the basis on the initial level j_0, $\Phi_j := \{\phi_{j_0,k}\}_{k=0,\ldots,2^{j_0}+3}$, spanning the space V_{j_0}, and the sets $\Psi_j := \{\psi_{j,k}\}_{k=0,\ldots,2^j-1}$, basis for each succeeding complement W_j as follows.

The (full) anisotropic basis

Practically, the full tensor-product space $V_J \otimes V_J$ up to the maximal level J allows all possible basis elements, including those tensoring basis functions on different scales. For j_x and j_y scales on the two dimensions x and y we have for tensoring of the form $V_{j_0} \otimes V_{j_0}$, $V_{j_0} \otimes W_j$ and $W_{j_x} \otimes V_{j_y}$ with $j_0 \le j, j_x, j_y \le J-1$ respectively:

$$\Phi_{j_0} \otimes \Phi_{j_0} := \left\{\phi_{j_0,k_x}(x) \cdot \phi_{j_0,k_y}(y)\right\}_{k_x=0,\ldots,2^{j_0}-1+m;\; k_y=0,\ldots,2^{j_0}-1+m}, \tag{7.91}$$

$$\Phi_{j_0} \otimes \Psi_{j_y} := \left\{\phi_{j_0,k_x}(x) \cdot \psi_{j_y,k_y}(y)\right\}_{k_x=0,\ldots,2^{j_0}-1+m;\; k_y=0,\ldots,2^{j_0}-1}, \tag{7.92}$$

$$\Psi_{j_x} \otimes \Psi_{j_y} := \left\{\psi_{j_x,k_x}(x) \cdot \psi_{j_y,k_y}(y)\right\}_{k_x=0,\ldots,2^{j_x}-1;\; k_y=0,\ldots,2^{j_y}-1}, \tag{7.93}$$

yielding the representation of full tensor-product space $V_J \otimes V_J$ as span of $\mathbf{\Phi}^{\text{aniso}}$ with

$$\mathbf{\Phi}^{\text{aniso}} = \Phi_{j_0} \otimes \Phi_{j_0} \bigcup_{\substack{j_x=j_0 \\ j_0 \le j_y \le J-1}} \Phi_{j_x} \otimes \Psi_{j_y} \bigcup_{\substack{j_0 \le j_x \le J-1 \\ j_y=j_0}} \Psi_{j_x} \otimes \Phi_{j_y} \bigcup_{\substack{j_0 \le j_x \le J-1 \\ j_0 \le j_y \le J-1}} \Psi_{j_x} \otimes \Psi_{j_y}. \tag{7.94}$$

Considering anisotropic candidates for the tensor product basis is a challenging issue. (Bi/tri)-variate basis functions, having elongated supports in one direction, may or may not be desirable when making refinements. This depends on the structure of the data to be reconstructed. If the data is rather scattered, with strong local variation and less global connected topology, plate- or stick-formed basis function may not be viable. However, the data could indeed present anisotropic structures, e.g a mountain within a landscape.

The isotropic basis

In this case, the tensoring considers only one-dimensional basis functions situated on the same level $V_j, j = j_0, \ldots, J$ for each dimension, or equivalently on the previous dyadic level and its complement to the next level $V_j = V_{j-1} \oplus W_{j-1}, j = j_0, \ldots, J$. This means we decompose for the finest space V_J:

$$\begin{aligned} V_J \otimes V_J &= (V_{J-1} \oplus W_{J-1}) \otimes (V_{J-1} \oplus W_{J-1}) && (7.95) \\ &= (V_{J-1} \otimes V_{J-1}) \oplus (V_{J-1} \otimes W_{J-1}) \oplus \\ &\quad \oplus (W_{J-1} \otimes V_{J-1}) \oplus (W_{J-1} \otimes W_{J-1}) \,. && (7.96) \end{aligned}$$

Now we can iterate using the reduced approximation of $V_{J-1} \otimes V_{J-1}$ further up to the smallest, initial level j_0. We obtain the isotropic decomposition of $V_J \otimes V_J$ by retaining only tensor product of basis functions on the same level. For example, tensor products like $(W_{J-1} \otimes W_J)$ are left out. At the end, only tensor-products of basis functions with the same support will be accepted as candidates in the isotropic basis. Notice, we do not use the equality sign in the following equation, since the isotropic decomposition includes only some terms of the complete, anisotropic decomposition of $V_J \otimes V_J$:

$$\begin{aligned} V_J \otimes V_J \sim\ & (V_{j_0} \otimes V_{j_0}) \oplus \\ & (V_{j_0} \otimes W_{j_0}) \oplus (W_{j_0} \otimes V_{j_0}) \oplus (W_{j_0} \otimes W_{j_0}) \\ & \oplus \ldots \oplus \\ & (V_{J-1} \otimes W_{J-1}) \oplus (W_{J-1} \otimes V_{J-1}) \oplus (W_{J-1} \otimes W_{J-1}) \,. \end{aligned} \tag{7.97}$$

We write the representation of the isotropic tensor-product space $V_J \otimes V_J$ as span of $\mathbf{\Phi}^{\text{iso}}$ with

$$\mathbf{\Phi}^{\text{iso}} = \Phi_{j_0} \otimes \Phi_{j_0} \bigcup_{j_0 \le j \le J-1} \Phi_j \otimes \Psi_j \bigcup_{j_0 \le j \le J-1} \Psi_j \otimes \Phi_j \bigcup_{j_0 \le j \le J-1} \Psi_j \otimes \Psi_j. \tag{7.98}$$

The sparse basis

In contrast to the isotropic decomposition, the sparse decomposition, also a subset of the full decomposition, includes preferentially anisotropic basis functions. In fact, tensor product basis functions will tensor one dimensional basis functions such that the sum of their levels $j_x,\ j_y$ for each direction z, y of the tensor does not exceed a certain given value

$$j_x + j_y \le J_{\max}. \tag{7.99}$$

This type of refinement avoids that finer refinements occur in several directions simultaneously. The maximal sum the levels $J_{\max}$ is chosen as:

$$dj_0 \ \le J_{\max} \ \le dJ \tag{7.100}$$

for d the number of dimensions, j_0 the coarsest level and J the finest level. If $J_{\max}$ is exactly the number of dimensions times the maximal available level, we obtain the

full (anisotropic) decomposition. The main literature [14] on sparse grids considers for $j = (j_1, j_2, \ldots, j_d)$ the level vector for a d–dimensional tensoring

$$J_{\max} = J + d - 1. \tag{7.101}$$

For the two dimensional case with j_x and j_y scales on direction x and y we have for tensor product of the form $V_{j_0} \otimes V_{j_0}$, $V_{j_0} \otimes W_j$ and $W_{j_x} \otimes V_{j_y}$ with $j_0 \leq j, j_x, j_y \leq J-1$ respectively:

$$\Phi_{j_0} \otimes \Phi_{j_0} := \left\{\phi_{j_0,k_x}(x) \cdot \phi_{j_0,k_y}(y)\right\}_{\substack{k_x=0,\ldots,2^{j_0}-1+m;\\ k_y=0,\ldots,2^{j_0}-1+m}}, \; j_0 + j_0 \leq J_{\max}, \tag{7.102}$$

$$\Phi_{j_0} \otimes \Psi_{j_y} := \left\{\phi_{j_0,k_x}(x) \cdot \psi_{j_y,k_y}(y)\right\}_{\substack{k_x=0,\ldots,2^{j_0}-1+m;\\ k_y=0,\ldots,2^{j_0}-1}}, \; j_x + j_0 \leq J_{\max}, \tag{7.103}$$

$$\Psi_{j_x} \otimes \Psi_{j_y} := \left\{\psi_{j_x,k_x}(x) \cdot \psi_{j_y,k_y}(y)\right\}_{\substack{k_x=0,\ldots,2^{j_x}-1;\\ k_y=0,\ldots,2^{j_y}-1}}, \quad j_x + j_y \leq J_{\max}, \tag{7.104}$$

yielding the representation of the sparse tensor-product space $V_J \otimes V_J$ as span of $\mathbf{\Phi}^{\text{sparse}}$ with

$$\mathbf{\Phi}^{\text{sparse}} = \Phi_{j_0} \otimes \Phi_{j_0} \bigcup_{\substack{j_x=j_0\\ j_0 \leq j_y \leq J-1\\ j_0+j_0 \leq J_{\max}}} \Phi_{j_x} \otimes \Psi_{j_y} \bigcup_{\substack{j_0 \leq j_x \leq J-1\\ j_y=j_0\\ j_x+j_y \leq J_{\max}}} \Psi_{j_x} \otimes \Phi_{j_y} \bigcup_{\substack{j_0 \leq j_x \leq J-1\\ j_0 \leq j_y \leq J-1\\ j_x+j_y \leq J_{\max}}} \Psi_{j_x} \otimes \Psi_{j_y}. \tag{7.105}$$

7.3.3 Stability Issues

Considering the adaptive nature of our set up, we should consider at this point the L_2–stability of our hierarchical basis in terms of tensor products of B-splines.

For Δ_j a d–dimensional knot sequence of level j, let

$$V_j = S_k^r(\Delta_j) \cap L_2(I\!R^d) \tag{7.106}$$

be the L_2 subspaces of tensor product splines of degree k and global smoothness r, $0 \leq r \leq k$ as defined in Definition 4.3.5 with respect to the uniform knot sequence Δ_j. Then, the sets V_j for each level j form an increasing sequence of subspaces of the Sobolev spaces $H^s(I\!R^d)$, $0 \leq s < r + 3/2$ and locally contain all algebraic polynomials of degree less equal k [112]. We know from [107, 132] that, for each level, the tensor product B-splines are L_2-stable.

We can assume that $\phi_\lambda \in \Psi$ are in

$$H^s([0,1]^d), \; 0 \leq s < r + 3/2 \tag{7.107}$$

since the (tensor products of) cubic B-splines are of smoothness $r = 2$. Each $u \in H^s([0,1]^d)$ has the expansion $u = \mathbf{u}^T \Psi := \sum_{\lambda \in \Lambda} u_\lambda \phi_\lambda$ with $\mathbf{u}$ the set of coefficients for the basis functions in Ψ. We are looking at estimates of the type

$$\|u\|_{H^s([0,1]^d)} \sim \|\mathbf{u}\|_{\ell_2(\Lambda)}. \tag{7.108}$$

Figure 7.9. *Full (anisotropic) refinement of tensor product spaces*

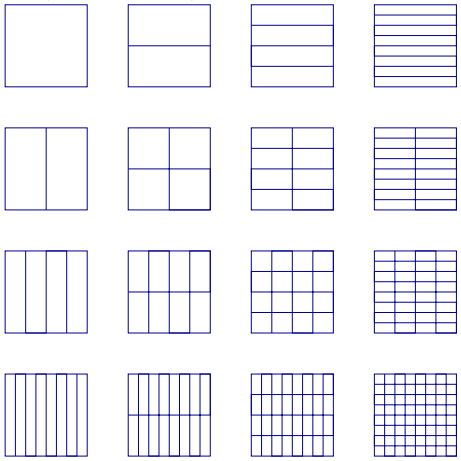

Figure 7.10. *Isotropic refinement of tensor product spaces*

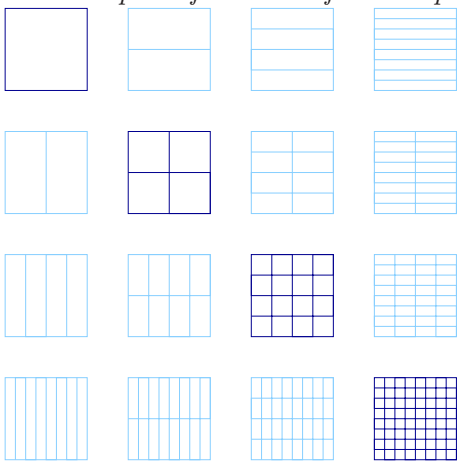

Figure 7.11. *Sparse refinement of tensor product spaces*

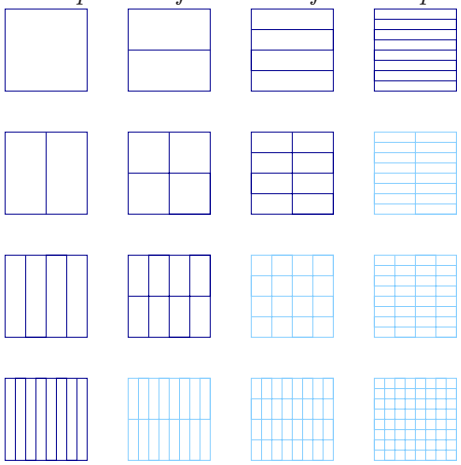

For $s = 0$ we have

$$H^s([0,1]^d) = H^0([0,1]^d) = L_2([0,1]^d), \tag{7.109}$$

corresponding to the L_2-stability. In general, the verification mechanism of the Riesz basis property of a hierarchical system in Sobolev spaces is based on tools like Jackson and Bernstein inequalities for scales of approximating spaces and with the study of associated biorthogonal systems [27, 95, 96, 111]. We have also learned from [14] how to carry this stability to the tensor product case, see Theorem 7.2.3.

In the one dimensional case, we know that equation (7.108) holds for $s = 0$ in the case of the B-spline wavelets. For the standard linear hierarchical basis, we know from [95] that equation (7.108) holds in $d \leq 2$ dimensions for

$$d/2 < s < 3/2. \tag{7.110}$$

Considering at last the hierarchical construction of B-splines, as in the case of other hierarchical bases investigated in [95], we do not expect the estimate to hold for $s = 0$. It is still not so far away from it. In fact, under proper scaling, the constants in (7.108) are expected to depend mildly on the highest level J.

The author of [112] explains that hierarchical constructions which do not lead to stable splittings setting may well be successful in some other applications. The author further points for example to the linear hierarchical basis method of [151] designed for H^1 elliptic problems on two–dimensional domains. The practical performance depends on a non–asymptotical range of small to moderate finest level J. Still, the stability of the multiscale splitting becomes crucial in an adaptive refinement where larger levels are expected. Further, as explained in [14], we can still use the coefficients for adaptive refinement, but loose eventually the optimality of the representation with respect to the number of employed degrees of freedom.

In view of the ill-posed nature of the problem, this is not considered dramatic. Discussing the stability of a hierarchical tensor product B-spline basis in our context is still idealistic. Recall that we deal with incomplete boundary conditions. The data is insufficient for both the data fitting ansatz, since data is missing over the domain, and for the partial differential equation solution, since the boundary data is not available over the complete boundary. Considering the data fitting term, [17] explained that in order for the matrix $\mathbf{M}_{\mathbf{\Lambda_j}}$ to be if at all invertible, the support of each basis function of the (adaptively) constructed basis must contain a sufficient number of properly distributed data points. For a good choice of η, the system matrix

$$\mathbf{M}_{\Lambda_j} + \eta \mathbf{G}_{\Lambda_j} \tag{7.111}$$

is invertible. Recall, the matrices $\mathbf{M}_{\Lambda_j} = \mathbf{A}^T\mathbf{A}$ should also have uniformly bounded condition numbers if the considered basis is uniformly stable [17]. But our method considers basis functions whose support does not contain data points at all. Consequently, common stability considerations fail and we are bound to deal with ill conditioning issues, regardless of the selected basis.

7.4 General Adaptive Set-up

7.4.1 Coarse–to–Fine Strategy

We construct recursively for each level j starting from some level j_0 a series of basis function sets Λ_j such that each one of them contains the adequate basis functions up to the level j that represent the data without overfitting effects. We understand by overfitting effects the consideration of basis functions that do not contribute to the representation or of basis functions that may generate unrelated information like oscillations in poorly resolved areas of the continuation. Once we have Λ_{j-1}, we have to construct the next basis function set Λ_j by means of the determined coefficient set $\mathbf{d}_{\Lambda_{j-1}}$ and some selection strategy and stopping criteria. We determine a set of refinement candidates $\delta(\Lambda_j)$ from Λ_j as

$$\tilde{\Lambda}_j = \Lambda_{j-1} \cup \delta(\Lambda_{j-1}) \tag{7.112}$$

and minimize the functional (4.8) by solving the normal equations for level–dependent weight parameter η_j

$$J_\eta(u_{\eta_j}) = \sum_{i=1}^{M} \left(u_{\eta_j}(x_i) - z_i\right)^2 + \eta_j \int_\Omega \left|\Delta u_{\eta_j}(x)\right|^2 \, dx \to \min \tag{7.113}$$

with

$$u_{\eta_j}(x) := \sum_{\lambda \in \tilde{\Lambda}_j} d_\lambda \psi_\lambda(x), \quad x \in \Omega. \tag{7.114}$$

Later we sort out less informative basis functions and thus obtain Λ_j.

Our general setup for the coarse–to–fine adaptive approximate continuation of harmonic functions rely on two main ingredients. First, we have a coefficients thresholding procedure, where in each iteration we select only the basis functions whose coefficients are larger than a threshold parameter ε_j eventually dependent on the level j. Secondly, as stopping criterion we choose the most natural extinction criterion, i.e., when in one iteration no more basis functions have been added to the representation in comparison to the previous step, then the algorithm terminates.

Remember, the higher the frequency of a basis function, the smaller its support. A smaller support means less data points intersect the support of each basis function and less non–zero entries in the matrix $\mathbf{M}$. Considering this correlation between the size of the basis functions support and the resulting matrix pattern and its sparsity, we could take the strategy indicated in [15]. This means to work initially with the finest nodal basis as much as possible and than undertake further hierarchical refinements. Still, we deal with baldy scattered datasets. We assume the results of the continuation would profit from some kind of level–to–level coupling via larger basis function supports. We make a compromise and choose the starting level empirically. Motivated by the ill–posed nature of the problem and little available information, our strategy is to start the adaptive procedure at a lower level, so that useless basis functions get lost earlier and less basis function coefficients must be determined in that subsequent iterations.

Algorithm 7.4.1 (General Set-up)**.**

1. *Given: boundary data points* P_Γ.
   Set: start level j_0*, highest available level* J*, weight parameter* η_j *and thresholding value* $\epsilon_j > 0$ *for each level* j.

2. *Create (tensor product) basis functions set* $\tilde{\Lambda}_{j_0}$.
   Compute $\{d_\lambda^{j_0}\}_{\lambda\in\Lambda_{j_0}}$ *that solves*

$$(\mathbf{M}_{\tilde{\Lambda}_{j_0}} + \eta_{j_0}\mathbf{G}_{\tilde{\Lambda}_{j_0}})\mathbf{d} = \mathbf{b}.$$

   Select $\Lambda_{j_0}^{\varepsilon_{j_0}} = \{\lambda \in \tilde{\Lambda}_{j_0} : |d_\lambda^{j_0}| \geq \varepsilon_{j_0}\}$.

3. *For each level* $j = j_0 + 1, \ldots, J$

   (a) *Create children set* $\delta(\Lambda_{j-1})$.

   (b) *Set preliminary basis* $\tilde{\Lambda}_j = \Lambda_{j-1} \cup \delta(\Lambda_{j-1})$.

   (c) *Compute* $\{d_\lambda^j\}_{\lambda\in\Lambda_j}$ *that solves*

$$(\mathbf{M}_{\tilde{\Lambda}_j} + \eta_j\mathbf{G}_{\tilde{\Lambda}_j})\mathbf{d} = \mathbf{b}.$$

   (d) *Select* $\Lambda_j^{\epsilon_j} = \{\lambda \in \delta(\Lambda_j) : |d_\lambda^{j+1}| \geq \epsilon_j\}$.

   (e) *If* $\Lambda_j^{\epsilon_j} = \emptyset$ *stop, else set basis* $\Lambda_{j+1} = \Lambda_j \cup \Lambda_j^{\epsilon_j}$.

Algorithm 7.4.2 (Create full children set $\delta(\Lambda_{j-1})$)**.**
For all $\psi_\lambda = \psi_{j_x,k_x} \cdot \psi_{j_y,k_y} \cdot \psi_{j_z,k_z}$*, the following children of* ψ_λ *are uniquely added to* $\delta(\Lambda_{j-1})$

$\psi_{j_x,k_x} \cdot \psi_{j_y,k_y} \cdot \psi_{j_z+1,2k_z}$
$\psi_{j_x,k_x} \cdot \psi_{j_y,k_y} \cdot \psi_{j_z+1,2k_z+1}$
$\psi_{j_x,k_x} \cdot \psi_{j_y+1,2k_y} \cdot \psi_{j_z,k_z}$
$\psi_{j_x,k_x} \cdot \psi_{j_y,2k_y+1} \cdot \psi_{j_z,k_z}$
$\psi_{j_x,k_x} \cdot \psi_{j_y+1,2k_y} \cdot \psi_{j_z+1,2k_z}$
$\psi_{j_x,k_x} \cdot \psi_{j_y+1,2k_y+1} \cdot \psi_{j_z+1,2k_z}$
$\psi_{j_x,k_x} \cdot \psi_{j_y+1,2k_y} \cdot \psi_{j_z+1,2k_z+1}$
$\psi_{j_x,k_x} \cdot \psi_{j_y+1,2k_y+1} \cdot \psi_{j_z+1,k_z+1}$
$\psi_{j_x+1,2k_x} \cdot \psi_{j_y,k_y}\psi_{j_z+1,2k_z}$
$\psi_{j_x+1,2k_x+1} \cdot \psi_{j_y,k_y} \cdot \psi_{j_z+1,2k_z}$
$\psi_{j_x+1,2k_x} \cdot \psi_{j_y,k_y} \cdot \psi_{j_z+1,2k_z+1}$
$\psi_{j_x+1,2k_x+1} \cdot \psi_{j_y,k_y} \cdot \psi_{j_z+1,2k_z+1}$
$\psi_{j_x+1,2k_x} \cdot \psi_{j_y+1,2k_y} \cdot \psi_{j_z,k_z}$
$\psi_{j_x+1,2k_x+1} \cdot \psi_{j_y+1,2k_y} \cdot \psi_{j_z,k_z}$
$\psi_{j_x+1,2k_x} \cdot \psi_{j_y+1,2k_y+1} \cdot \psi_{j_z,k_z}$
$\psi_{j_x+1,2k_x+1} \cdot \psi_{j_y+1,2k_y+1} \cdot \psi_{j_z,k_z}$
$\psi_{j_x+1,2k_x} \cdot \psi_{j_y+1,2k_y} \cdot \psi_{j_z+1,2k_z}$
$\psi_{j_x+1,2k_x+1} \cdot \psi_{j_y+1,2k_y} \cdot \psi_{j_z+1,2k_z}$
$\psi_{j_x+1,2k_x} \cdot \psi_{j_y+1,2k_y+1} \cdot \psi_{j_z+1,2k_z}$
$\psi_{j_x+1,2k_x+1} \cdot \psi_{j_y+1,2k_y+1} \cdot \psi_{j_z+1,2k_z}$
$\psi_{j_x+1,2k_x} \cdot \psi_{j_y+1,2k_y} \cdot \psi_{j_z+1,2k_z+1}$
$\psi_{j_x+1,2k_x+1} \cdot \psi_{j_y+1,2k_y} \cdot \psi_{j_z+1,2k_z+1}$
$\psi_{j_x+1,2k_x} \cdot \psi_{j_y+1,2k_y+1} \cdot \psi_{j_z+1,k_z+1}$
$\psi_{j_x+1,2k_x+1} \cdot \psi_{j_y+1,2k_y+1} \cdot \psi_{j_z+1,k_z+1}$.

We comment on our decision how to sort out useless basis functions without knowledge of the final solution. Inspired by [16, 17] and works on adaptive methods for partial differential equations, e.g. [22,30], we have chosen the coefficient thresholding. This means, basis functions with large coefficients alone are retained for further refinement within the next iteration. We have explained in Section 7.3.3 the main arguments. Although the employed hierarchical basis is not expected to be L_2–stable, thresholding with respect to coefficient values can still be used under correct scaling as an error indicator. This is the only thresholding we employ. The algorithm finishes when at some level j, none of coefficients of the additional, children basis functions indexed by $\delta(\Lambda_{j-1})$ are larger than the thresholding parameter ϵ_j. We interpret $\Lambda_j^{\epsilon_j} = \emptyset$ as that no information is left to be represented and no further refinement is necessary.

Other strategies in literature dealing with data-fitting issues, e.g. [17], suggest the *horizontal thresholding*, that is, keeping basis functions containing at least a given number of information data points. This approach is not adequate for our method, as given data points are available only at the boundaries. We can still adapt this idea to our setup to help us estimate the finest acceptable level by taking a look at the boundary conditions: levels should not get finer than the boundary data can resolve. The argumentation relies on the fact that in geodetic problems the information has the strongest oscillations at the boundaries. This is why the adaptive strategy should concentrate the degrees of freedom there. But remember that we are not dealing with a pure data fitting problem, since the harmonicity constraint adds a significant amount information. Therefore, we allow the method to refine to higher levels than the boundary data indicates.

Another classic idea is the *error thresholding*, that is refine, where the reconstruction error is large. This is also not adequate for our purposes, since the information data points are only at the boundaries anyway and the target function is not a priori known. Also, the boundary data itself might be noisy and would profit from some harmonic regularization. In this case, the boundary error is not associated with the continuation error. We could conversely check to which extent the Laplacian condition has been fulfilled. Yet, we have already discussed in previous sections that the Laplacian does not directly correlate with the reconstruction error. A high value of the Laplacian can point not only to the correct solution, but often erroneously to some smooth or planed function that averages the boundary data.

In addition to the choice of the thresholding value ϵ_j, there is another parameter influencing the outcome of the algorithm. This is the weight parameter η_j controlling the harmonicity of the continuation. The legitimate question is, whether the weight parameter η_j should indeed variate with the level j? The first solution would be to choose at each iteration some estimator, e.g. the

$$\eta_{\text{eig}} = \frac{\max(\text{eig}(\mathbf{M}_{\Lambda_j}))}{\max(\text{eig}(\mathbf{G}_{\Lambda_j}))} \tag{7.115}$$

estimator for the weight parameter (see Section 6.6 for details). Yet, considering that in each level we only add some more basis functions, the system matrices should not be completely different from level to level. Our hope is that the weight parameter does not variate that much; but when too many degrees of freedom are added, a new estimation

of the parameter might be required. For the experimental results presented here we have decided to reestimate the value of the weight parameter using the η_{eig} estimator within each iteration. In conclusion, we still have some parameters of the algorithm to control: the start level j_0, the finest available level J of the basis functions and the threshold value for sorting coefficients ε_η.

7.4.2 Test Data

For the experiments using the adaptive development of our least squares approach to the continuation of harmonic functions we have constructed a challenging data set. Recall Section 3.5.2 where we considered Example 3.2 showing the gravity anomaly generated by one sphere and Example 3.3 showing the gravity anomaly generated by a series of buried spheres. We construct here a test case similar to these examples. This time we assume again a series of seven buried spheres with radius r_i and deviating densities $\rho_i, i = 1, \ldots, 7$. The anomalous gravity as a function of the position of the observation point (x, y, z) translates then to

$$\delta g = \sum_{i=1}^{7} \frac{4\pi G z \rho_i r_i^3}{((x - x_i)^2 + (y - y_i)^2 + (z - z_i)^2)^{3/2}}. \tag{7.116}$$

See Figure 7.12 for a view of the constructed dataset which we denote by $u := \delta g$. It is on purpose constructed such that the reconstruction is difficult. Notice the dissipation of the anomalies with the height. Notice also the sharp anomaly near the middle of the lower boundary of the domain. It is created by the presence of a small sphere with negative density deviation, e.g, a hole, near to the surface. The difficulties for the continuation problem set ups to come reside within the fact that the anomaly is not completely resolved by the $65 \times 65 \times 33$ points data set. Therefore, all considered methods will have some difficulties to properly handle the anomalies generated in this test case. We hereby simulate the behavior of real data where measurements cannot always resolve sharp changes of the field and high–degree spherical harmonic constituents. See Table 7.1 for a comparison of the available number of information points carried by the most used partial grids for the here constructed data set and corresponding full grid.

Figure 7.12. *3D surface view of the test function u(left), section through the middle of the domain (middle) and close up of the sharp anomaly (right).*

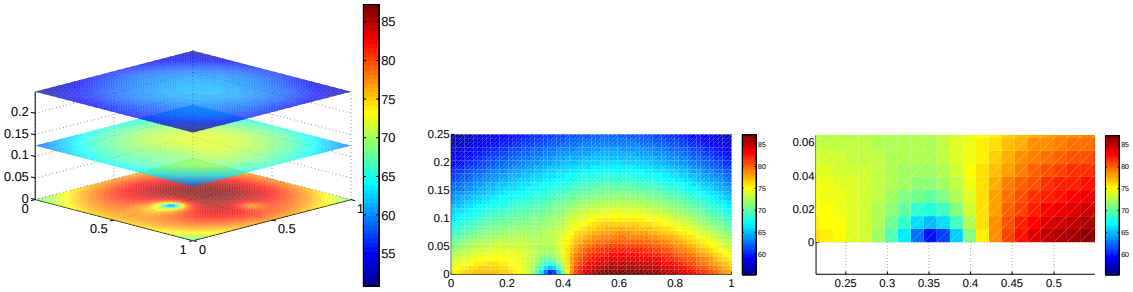

Table 7.1. *Number of information points for common partial grids P_Γ and for the full grid $\Omega_\#$.*

Data configuration	data points
${P_\Gamma}^{1,1}$	$65 \times 65 \times (1+1) = 8540$
${P_\Gamma}^{2,1}$	$65 \times 65 \times (2+1) = 12675$
${P_\Gamma}^{fd}$	16386
$\Omega_\#$	$65 \times 65 \times 33 = 139426$

In addition to the error measures $E_{2,\text{bnd}}$, $E_{2,\text{mid}}$, $E_{\infty,\text{bnd}}$ and $E_{\infty,\text{mid}}$ defined in Section 6.2.3, equations 6.10, we will depict later the pointwise error of the continuation computed as

$$E_{\Omega_\#} := |u_\eta(x_i) - u(x_i)|,\ x_i \in \Omega_\#. \tag{7.117}$$

Non–adaptive approximate continuations

For comparison purposes we present in Table 7.2 the continuation results obtained using the full, non adaptive grid presented in the previous chapters. We consider as in our original, fully gridded approach for the approximate continuation of harmonic functions the boundary data geometries ${P_\Gamma}^{1,1}$ and ${P_\Gamma}^{2,1}$.

We chose the full basis functions set of B-splines level three, four and five. The levels have been chosen to give a hint about what to expect when using all basis functions of a certain level. The weight parameter has been computed using the n_{eig} indicator. The systems of equations resulting for levels three and four have been solved directly. The results obtained using finite differences are also included. Error measurements are again computed over the boundaries or over the middle of the domain, as defined in 6.10. We mention that the problematic points, where the maximal $E_{\infty,\text{mid}}$ and maximal $E_{\infty,\text{bnd}}$ are attained, are situated in the immediate neighborhood of the sharp anomaly.

Table 7.2. *Continuation results obtained using the full grid approach for boundary data sets ${P_\Gamma}^{1,1}$, ${P_\Gamma}^{2,1}$ and tensor product B-splines basis of levels 3, 4 and 5. Results obtained using finite differences.*

P_Γ	level	d.o.f.	η_{eig}	$E_{\infty,\text{mid}}$	$E_{2,\text{mid}}$
${P_\Gamma}^{1,1}$	3	1331	8.3697e-04	8.9987e+00	7.4106e+01
${P_\Gamma}^{1,1}$	4	6859	1.0464e-04	3.3483e+00	6.1918e+01
${P_\Gamma}^{1,1}$	5	42875	3.9921e-10	1.9853e+00	6.0257e+01
${P_\Gamma}^{2,1}$	3	1331	1.0246e-03	9.1895e+00	5.8906e+01
${P_\Gamma}^{2,1}$	4	6859	1.0741e-04	3.4178e+00	6.0024e+01
${P_\Gamma}^{2,1}$	5	42875	3.9921e-10	1.2773e+00	6.2941e+01
${P_\Gamma}^{fd}$	–	–	–	2.0683e+00	6.0084e+01

The worse results are for level 3, see Table 7.2. This basis cannot resolve the boundary data. It is still interesting how in both cases, ${P_\Gamma}^{1,1}$ and ${P_\Gamma}^{2,1}$, the smoothed boundary data allowed for the continuation to be still more correct on the upper side of the cuboid domain. In view of the error $E_{\infty,\text{mid}}$, i.e., in the maximum sense, the best approximate

Figure 7.13. *Error of the continuation $E_{\Omega_\#}$ obtained using the full grid approach for boundary data sets ${P_\Gamma}^{1,1}$, ${P_\Gamma}^{2,1}$ and tensor product B-splines basis of level 3, 4 and 5. Error of the continuation $E_{\Omega_\#}$ obtained using the classical finite differences approach.*

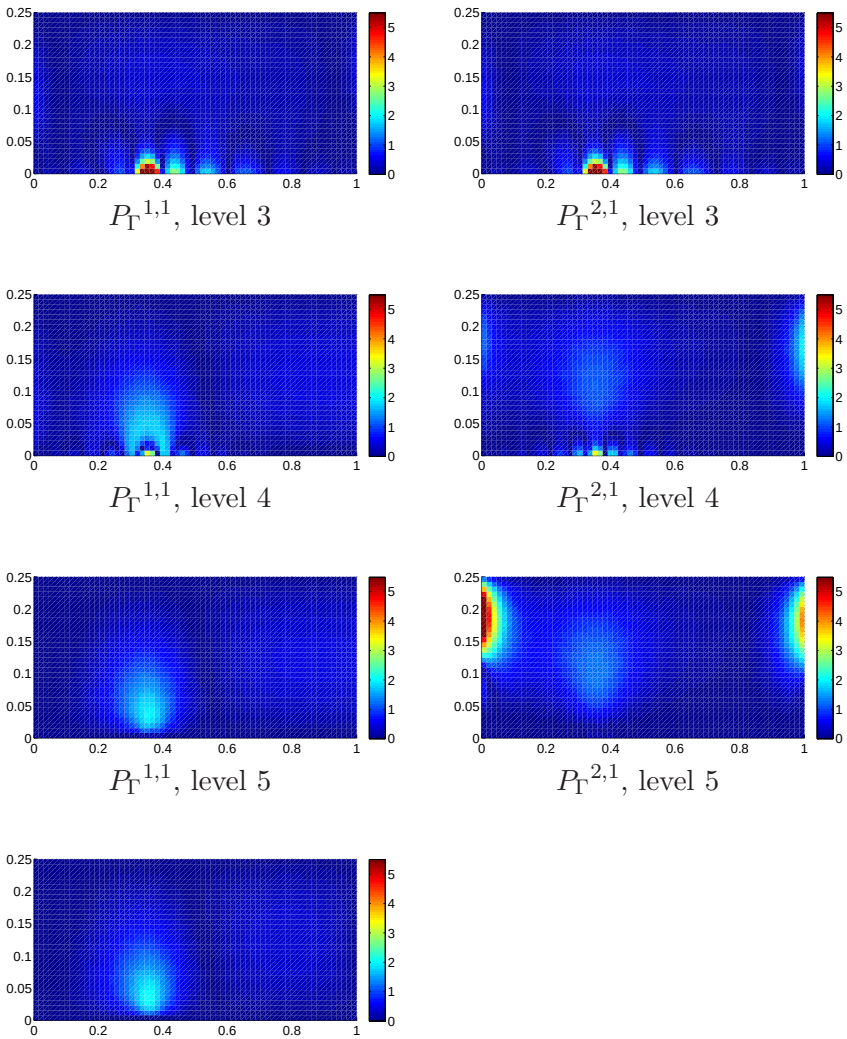

continuation in the full grid setup has been obtained for ${P_\Gamma}^{2,1}$ and basis level 5. For the weighted L_2 norm $E_{\infty,\mathrm{mid}}$ the best continuation has been obtained for ${P_\Gamma}^{2,1}$ and basis level 4, followed by ${P_\Gamma}^{1,1}$ and basis level 5 and the finite differences approach. Recall, the finite difference approach requires complete boundary conditions, i.e., uniform grid on all sides of the cuboid domain. Notice also how a level 5 basis is required in order to properly resolve the available boundary data and the sharp anomaly.

By comparison with the finite difference results, we can at this point acknowledge the good performance of the n_{eig} indicator for the weight term controlling the harmonicity.

We did not assume that n_{eig} points to the best possible weight parameter, such that the continuation error is minimized. But we find the estimated value dependable since it provides better results than finite differences for a basis of sufficient level.

7.4.3 3D Grid Visualization

We also give an intuitive view over the refinement process by showing the resulting refinement grid. Recall, each one of the three one–dimensional tensor basis functions is compactly supported. In fact, the support of a basis function for some level l per dimension will cover four segments constructed on the knot succession Δ_l. So for all three dimensional basis functions $\psi_\lambda = \psi_{j_x,k_x} \cdot \psi_{j_y,k_y} \cdot \psi_{j_z,k_z} \in \Lambda_l$ of levels j_x, j_y and j_z respectively we print a point in the middle of the cuboid support. This representation is insightful but not complete. One cannot say if an isolated point on a grid is associated with a basis function of level l or $l+1$ in some direction since no information about the size of the support is available. But the points seen as grid nodes are still intuitive enough, since an agglomeration of points indicates agglomeration of degrees of freedom and higher–leveled basis functions. Recall also that we deal with end–point interpolating basis functions. This means, the support of the basis function near the boundary of the domain does not cover four but one, two or three segments of size 2^l. So the middle of the support, i.e., the associated grid points, for the external basis function of an uniform basis are not uniformly distributed. This concentration of points does not indicate a change of level. One could alternatively plot each of the four segments of the support as lines, per direction separately, but this would significantly overload the picture. Further, since visualizing such a three–dimensional grid on a two dimensional media is still confusing, we suggest a horizontal, lateral view of the grid. We project the resulting grid in horizontal direction. We refer later to this representation as *lateral view of the grid nodes.*

For better insight, we construct the refinement grid for a one–dimensional case. We consider the decomposition of an arbitrary one dimensional function in B-spline bases of levels two, three, four and six. Figure 7.14 shows the grid nodes representation associated with the multiscale resulting basis. On the right side of the plot, the refinement is uniform. The grid point agglomeration occurs here due to the end-point interpolating basis functions. Conversely, notice on the left side of the interval the superposition of basis functions with different levels. We can see here the high density of grid points showing to the accumulation of degrees of freedom.

Also, we found it interesting to see the refinement of the bottom boundary of the domain. Remember, in our approximate continuation approach, the most relevant available information is situated there and is associated with the source of the field. Due to the maximum property of harmonic functions, the maximal and minimal values of the function to be continued are attained at the boundary. This is where we expect for the refinement grid to be most dense. Further, a good resolving of the boundary information is essential for the quality of the resulting continuation. For this representation we print a point in the middle of the cuboid support for each basis function of the the final Λ_l living on the bottom boundary. Subsequently, we plot the vertical projection of the resulting grid. We refer later to this representation as *final refinement of the bottom boundary.*

Figure 7.14. *Grid nodes representation for an arbitrary one–dimensional function and its decomposition in B-spline basis functions of levels 2, 3, 4 and 6.*

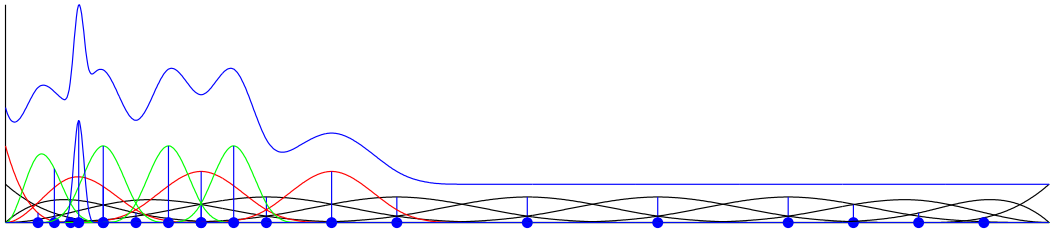

7.4.4 Refinement Process

Tables for the experiments with the adaptive approximate continuation show the results as follows: for each described iteration, we show the maximum available level. Further, $\#\tilde{\Lambda}_l = \#\Lambda_{l-1} + \#\delta\Lambda_{l-1}$ is the number of basis functions considered at the beginning of a new iteration and $\#\Lambda_l$ is the number of basis functions remaining after the thresholding procedure. For better insight the effects of basis function dumping, error measurements over the middle of the domain will be shown for the approximate continuation obtained for each of the basis function sets $\tilde{\Lambda}_l$ and Λ_l respectively. For the last iteration, $\#\Lambda_l$ is the final number of degrees of freedom of the adaptively determined basis function set.

We continue in Tables 7.3–7.6 with some results obtained using the adaptive strategy in Algorithm 7.4.1 and the boundary data geometries ${P_\Gamma}^{1,1}$ and ${P_\Gamma}^{2,1}$. We chose as start point the full basis functions set of B-splines level three. In each successive iteration, viable basis functions will eventually be refined. The resulting basis function attain thereby a maximum level consisting of the sum between the initial level and the allowed number of iterations for each direction, respectively. We also choose between two thresholding parameters, $\varepsilon = 0.1$ and $\varepsilon = 1$. The weight parameter η_l has been computed using the n_{eig} indicator.

The effectiveness of the adaptive procedure in view of the thresholding can be seen by comparing the refinement grids in the pair Figures 7.15–7.16 and 7.17–7.18. The grids obtained within the iterative adaptive procedure for $\varepsilon = 0.1$ are significantly more dense as for $\varepsilon = 1$ since more basis function are retained to Λ_l and more children basis functions have been added to $\tilde{\Lambda}_l$ within each iterative step. The quality of the representation is reflected by the error measurements in Tables 7.3–7.6. It remains more or less constant for both values of the thresholding parameter ε although the final set contains less than half of the number of degrees of freedom.

A slight improvement of the continuation has been achieved, as expected, by considering two instead of one layers of information points on the lower boundary of the domain. This additional information helps the adaptive procedure to better distribute the degrees of freedom. The lowest point wise maximum measured error $E_{\infty,\text{mid}}$ of the approximate continuation has been obtained for ${P_\Gamma}^{2,1}$, basis level 5 and threshold parameter $\varepsilon = 1$. The representation involved 8915 basis functions, less than a quarter of the level 5 full grid basis. The lowest $E_{\infty,\text{mid}}$ has been obtained for ${P_\Gamma}^{2,1}$, basis level 5 and threshold parameter $\varepsilon = 0.1$. Here, almost 30.000 degrees of freedom have been employed.

Table 7.3. *Results per iteration for* ${P_\Gamma}^{1,1}$, $l_{\min} = 3$, $\varepsilon = 0.1$; *final solution and* $E_{\Omega_\#}$.

level l	$\#\tilde{\Lambda}_l$	$E_{\infty,\mathrm{mid}}$	$E_{2,\mathrm{mid}}$	$\#\Lambda_l$	$E_{\infty,\mathrm{mid}}$	$E_{2,\mathrm{mid}}$	η_l
3	1331	9.0042e+00	7.4094e+01	901	9.0042e+00	7.4084e+01	6.6345e-03
4	4021	3.3937e+00	6.1950e+01	3667	3.3937e+00	6.1950e+01	6.6548e-03
5	23277	1.9745e+00	6.0225e+01	20812	1.9744e+00	6.0224e+01	6.6548e-03

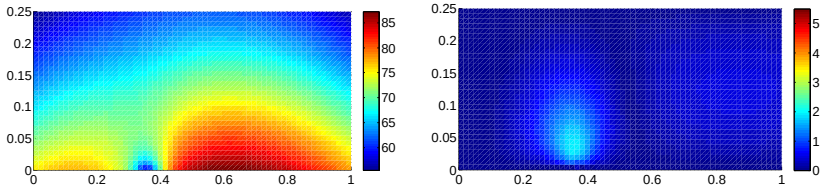

Table 7.4. *Results per iteration for* ${P_\Gamma}^{1,1}$, $l_{\min} = 3$, $\varepsilon = 1$; *final solution and* $E_{\Omega_\#}$.

level l	$\#\tilde{\Lambda}_l$	$E_{\infty,\mathrm{mid}}$	$E_{2,\mathrm{mid}}$	$\#\Lambda_l$	$E_{\infty,\mathrm{mid}}$	$E_{2,\mathrm{mid}}$	η_l
3	1331	9.0042e+00	7.4094e+01	635	9.0042e+00	7.4194e+01	6.6345e-03
4	2167	3.4010e+00	6.1910e+01	1863	3.4010e+00	6.1909e+01	6.6805e-03
5	10178	1.9742e+00	6.0324e+01	6953	1.9746e+00	6.0328e+01	6.6804e-03

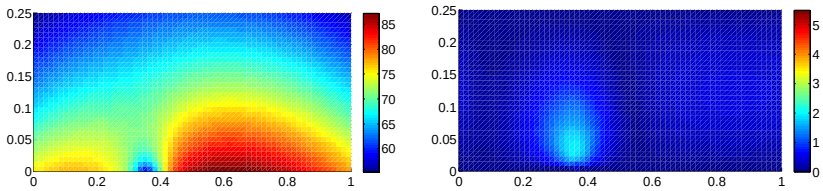

Table 7.5. *Results per iteration for* ${P_\Gamma}^{2,1}$, $l_{\min} = 3$, $\varepsilon = 0.1$; *final solution and* $E_{\Omega_\#}$.

level l	$\#\tilde{\Lambda}_l$	$E_{\infty,\mathrm{mid}}$	$E_{2,\mathrm{mid}}$	$\#\Lambda_l$	$E_{\infty,\mathrm{mid}}$	$E_{2,\mathrm{mid}}$	η_l
3	1331	9.3335e+00	6.3150e+01	1084	9.3335e+00	6.3118e+01	9.8243e-03
4	5128	3.8328e+00	4.5547e+01	4816	3.8328e+00	4.5547e+01	9.8618e-03
5	29932	1.8025e+00	1.0062e+01	28143	1.8025e+00	1.0061e+01	4.4760e-02

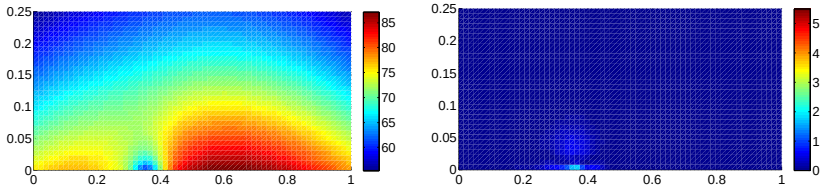

Table 7.6. *Results per iteration for* ${P_\Gamma}^{2,1}$, $l_{\min} = 3$, $\varepsilon = 1$; *final solution and* $E_{\Omega_\#}$.

level l	$\#\tilde{\Lambda}_l$	$E_{\infty,\mathrm{mid}}$	$E_{2,\mathrm{mid}}$	$\#\Lambda_l$	$E_{\infty,\mathrm{mid}}$	$E_{2,\mathrm{mid}}$	η_l
3	1331	9.3335e+00	6.3150e+01	698	9.3335e+00	6.2839e+01	9.8243e-03
4	2434	3.8414e+00	4.5869e+01	2164	3.8414e+00	4.5870e+01	9.8915e-03
5	11518	1.5087e+00	4.3545e+01	8915	1.5092e+00	4.3552e+01	9.8921e-03

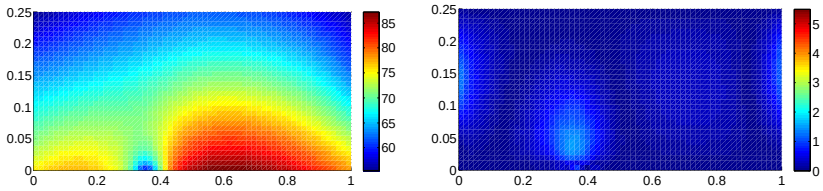

Figure 7.15. *Lateral view of the grid nodes computed within each iteration of the adaptive method and final refinement of the bottom boundary for partial grid* ${P_\Gamma}^{1,1}$, $l_{\min} = 3$, $\varepsilon = 0.1$.

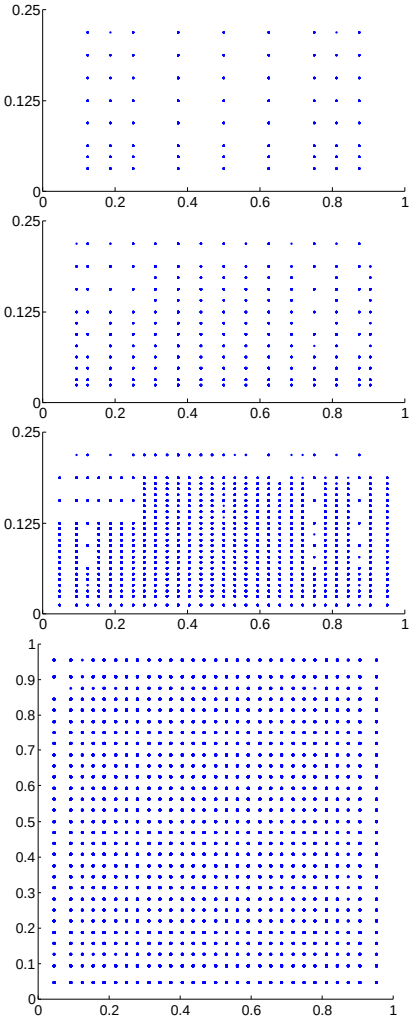

Figure 7.16. *Lateral view of the grid nodes computed within each iteration of the adaptive method and final refinement of the bottom boundary for partial grid* ${P_\Gamma}^{1,1}$, $l_{\min} = 3$, $\varepsilon = 1$.

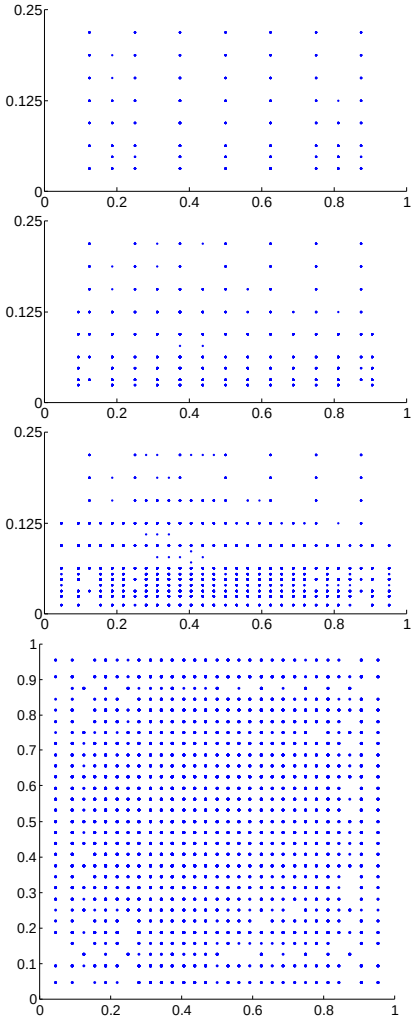

Figure 7.17. *Lateral view of the grid nodes computed within each iteration of the adaptive method and final refinement of the bottom boundary for partial grid* ${P_\Gamma}^{2,1}$, $l_{\min} = 3$, $\varepsilon = 0.1$

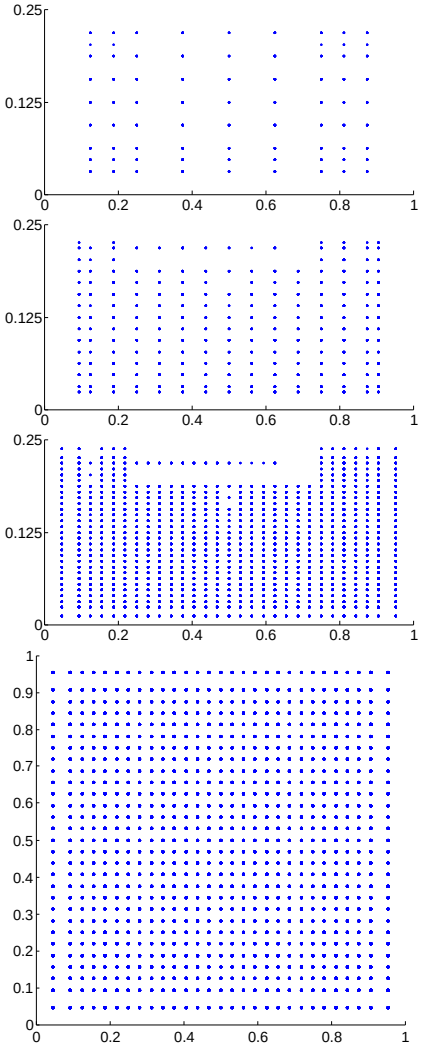

Figure 7.18. *Lateral view of the grid nodes computed within each iteration of the adaptive method and final refinement of the bottom boundary for partial grid* ${P_\Gamma}^{2,1}$, $l_{\min} = 3$, $\varepsilon = 1$.

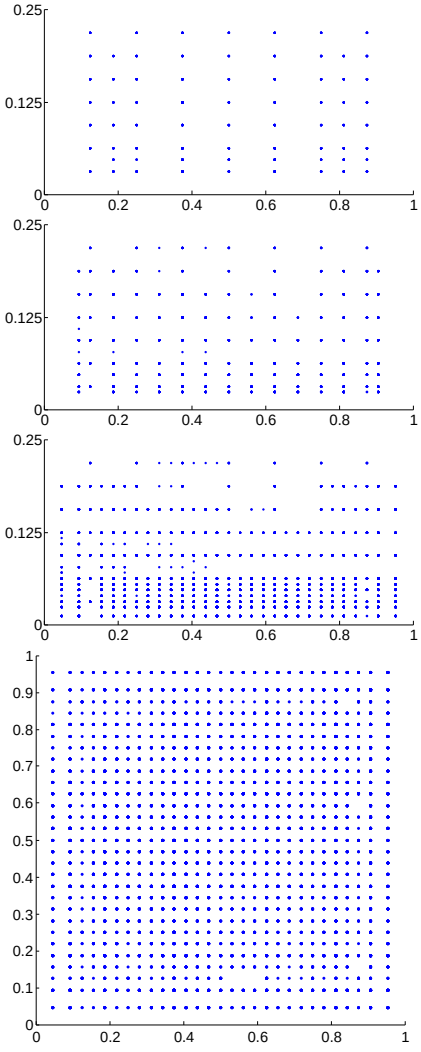

7.5 Alternative Refinement Strategies

The starting point for an alternative approach is Algorithm 7.4.1 which considers a (full) anisotropic basis. An obvious idea would be to restrain the candidate set by performing one of the two alternative refinements: the isotropic and the sparse refinement.

7.5.1 The Isotropic Refinement

Recall that the isotropic refinement considers only basis functions tensoring one-dimensional basis functions situated on the same level V_j, $j = j_0, \ldots, J$ for all directions.

Algorithm 7.5.1 (Create isotropic children set $\delta^{\text{iso}}(\Lambda_{j-1})$)**.**

1. *Create children set* $\delta(\Lambda_{j-1})$
2. *For all* $\psi_{j_x,k_x} \cdot \psi_{j_y,k_y} \cdot \psi_{j_z,k_z} \in \delta(\Lambda_{j-1})$, *add* $\psi_{j_x,k_x} \cdot \psi_{j_y,k_y} \cdot \psi_{j_z,k_z}$ *to* $\delta^{\text{iso}}(\Lambda_{j-1})$ *only if* $j_x = j_y = j_z$

As an example, a function of type $\psi_{3,k_x} \cdot \psi_{3,k_y} \cdot \psi_{3,k_z}$ would be added to the children set, but $\psi_{3,k_x} \cdot \psi_{3,k_y} \cdot \psi_{4,k_z}$ would have been rejected.

The results in Tables 7.7-7.10 show the bad behavior of this strategy. For both considered boundary data geometries and threshold parameters no proper continuation could be successfully constructed. Constricting the course–to–fine procedure to only isotropic basis functions has deep drawbacks. Not only is the final result poor, but the quality of the constructed approximation remains constant from iteration to iteration. The additional children have no significant contribution to the representation. The rather large number of degrees of freedom have not been sufficient. It could indeed be, had the method been allowed to proceed for longer, the results might have been better. Another iteration was not possible due to the strongly increasing number of basis functions and due to memory requirements. Further, since the number of information points remains constant, we cannot expect to determine an even further increasing number of basis function coefficients. The motivation for this behavior lies most probably within the asymmetric structure of the domain and of the test function.

Considering the error pattern of the continuation, we notice a strong resemblance with the results obtained using the full grid set-up for level 3, see Figure 7.13. The most direct conclusion we can make is that the isotropic setup cannot resolve the boundary data properly. Hereby, some of the information given by the available data points gets lost and the results are affected.

It is also irritating to see how the degrees of freedom within the representation do indeed seem to concentrate correctly around the anomaly, but still without improving the representation itself. This is in fact a strong alarm signal. It does not only state that the isotropic refinement fails. It is a warning, that an apparently nicely refined grid still is no guarantee for properly resolved boundary data and even less for a good continuation.

Table 7.7. *Results for* $\delta^{\mathrm{iso}}(\Lambda_{j-1})$, ${P_\Gamma}^{1,1}$, $l_{\min}=3$, $\varepsilon=0.1$*; final solution and* $E_{\Omega_\#}$.

level l	$\#\tilde{\Lambda}_l$	$E_{\infty,\mathrm{mid}}$	$E_{2,\mathrm{mid}}$	$\#\Lambda_l$	$E_{\infty,\mathrm{mid}}$	$E_{2,\mathrm{mid}}$	η_l
3	1331	9.0042e+00	7.4094e+01	901	9.0042e+00	7.4084e+01	6.6345e-03
4	1221	9.0042e+00	7.4107e+01	1157	9.0042e+00	7.4107e+01	6.6550e-03
5	3205	9.0042e+00	7.4108e+01	2915	9.0042e+00	7.4108e+01	6.6550e-03
6	16979	9.0042e+00	7.4108e+01	15114	9.0042e+00	7.4108e+01	6.6550e-03

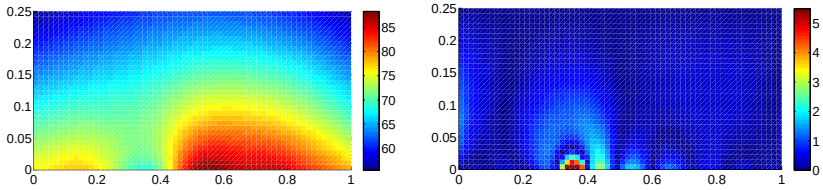

Table 7.8. *Results for* $\delta^{\mathrm{iso}}(\Lambda_{j-1})$, ${P_\Gamma}^{1,1}$, $l_{\min}=3$, $\varepsilon=1$*; final solution and* $E_{\Omega_\#}$.

level l	$\#\tilde{\Lambda}_l$	$E_{\infty,\mathrm{mid}}$	$E_{2,\mathrm{mid}}$	$\#\Lambda_l$	$E_{\infty,\mathrm{mid}}$	$E_{2,\mathrm{mid}}$	η_l
3	1331	9.0042e+00	7.4094e+01	635	9.0042e+00	7.4194e+01	6.6345e-03
4	763	9.0044e+00	7.4029e+01	704	9.0044e+00	7.4029e+01	6.6805e-03
5	1256	9.0044e+00	7.4029e+01	1156	9.0044e+00	7.4029e+01	6.6805e-03
6	4772	9.0043e+00	7.4029e+01	4028	9.0043e+00	7.4029e+01	6.6805e-03
7	27004	9.0043e+00	7.4029e+01	21788	9.0043e+00	7.4029e+01	6.6805e-03

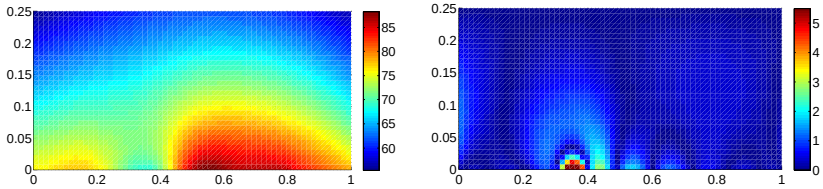

Table 7.9. *Results for* $\delta^{\mathrm{iso}}(\Lambda_{j-1})$, ${P_\Gamma}^{2,1}$, $l_{\min}=3$, $\varepsilon=0.1$*; final solution and* $E_{\Omega_\#}$.

level l	$\#\tilde{\Lambda}_l$	$E_{\infty,\mathrm{mid}}$	$E_{2,\mathrm{mid}}$	$\#\Lambda_l$	$E_{\infty,\mathrm{mid}}$	$E_{2,\mathrm{mid}}$	η_l
3	1331	9.3335e+00	6.3150e+01	1084	9.3335e+00	6.3118e+01	9.8243e-03
4	1460	9.3327e+00	6.3153e+01	1433	9.3327e+00	6.3153e+01	9.8615e-03
5	4225	9.3326e+00	6.3143e+01	3958	9.3326e+00	6.3143e+01	9.8615e-03
6	24158	9.3326e+00	6.3143e+01	22061	9.3326e+00	6.3143e+01	9.8615e-03

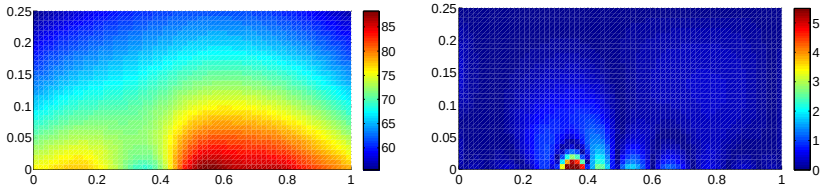

Table 7.10. *Results for* $\delta^{\mathrm{iso}}(\Lambda_{j-1})$, ${P_\Gamma}^{2,1}$, $l_{\min}=3$, $\varepsilon=1$*; final solution and* $E_{\Omega_\#}$.

level l	$\#\tilde{\Lambda}_l$	$E_{\infty,\mathrm{mid}}$	$E_{2,\mathrm{mid}}$	$\#\Lambda_l$	$E_{\infty,\mathrm{mid}}$	$E_{2,\mathrm{mid}}$	η_l
3	1331	9.3335e+00	6.3150e+01	698	9.3335e+00	6.2839e+01	9.8243e-03
4	834	9.3329e+00	6.3137e+01	787	9.3329e+00	6.3137e+01	9.8912e-03
5	1499	9.3328e+00	6.3127e+01	1360	9.3328e+00	6.3127e+01	9.8912e-03
6	5944	9.3328e+00	6.3126e+01	4855	9.3328e+00	6.3126e+01	9.8912e-03
7	32815	9.3328e+00	6.3126e+01	27457	9.3328e+00	6.3126e+01	9.8912e-03

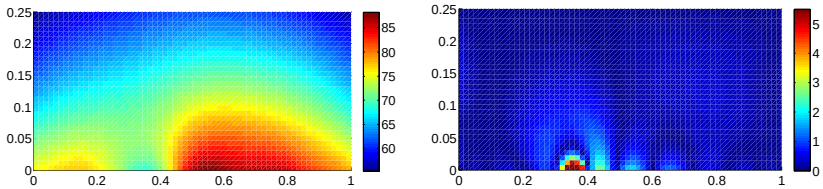

Figure 7.19. *Lateral view of the grid nodes computed within each iteration of the isotropic adaptive method and final refinement of the bottom boundary for* $P_\Gamma{}^{1,1}$, $l_{\min} = 3$, $\varepsilon = 0.1$.

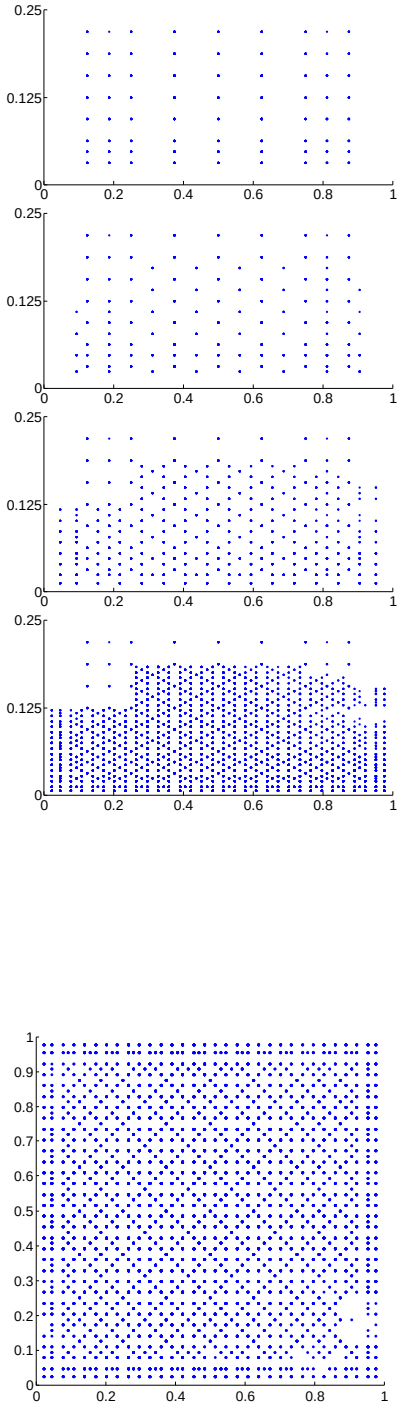

Figure 7.20. *Lateral view of the grid nodes computed within each iteration of the isotropic adaptive method and final refinement of the bottom boundary for* $P_\Gamma{}^{1,1}$, $l_{\min} = 3$, $\varepsilon = 1$.

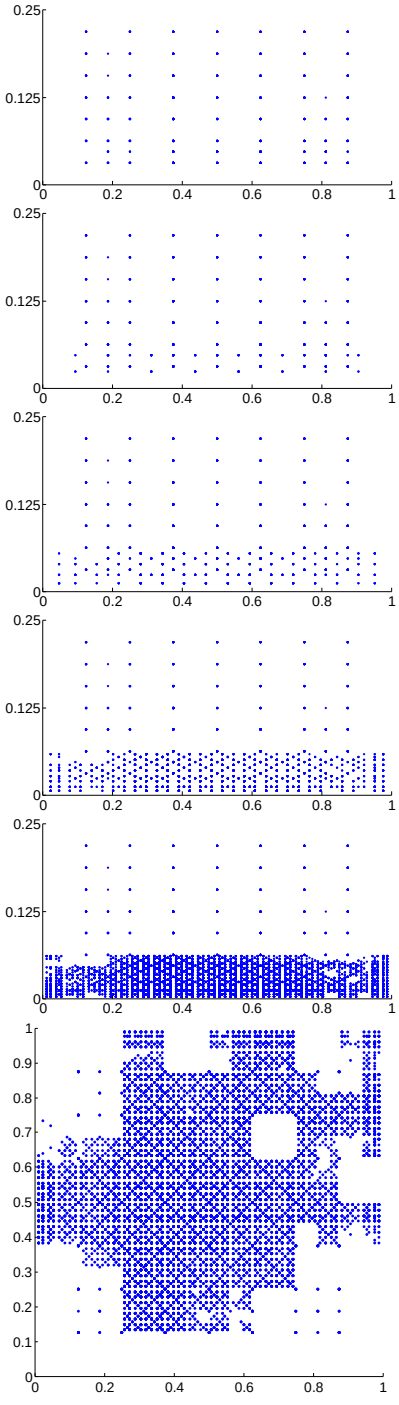

Figure 7.21. *Lateral view of the grid nodes computed within each iteration of the isotropic adaptive method and final refinement of the bottom boundary for* $P_\Gamma{}^{2,1}$, $l_{\min} = 3$, $\varepsilon = 0.1$.

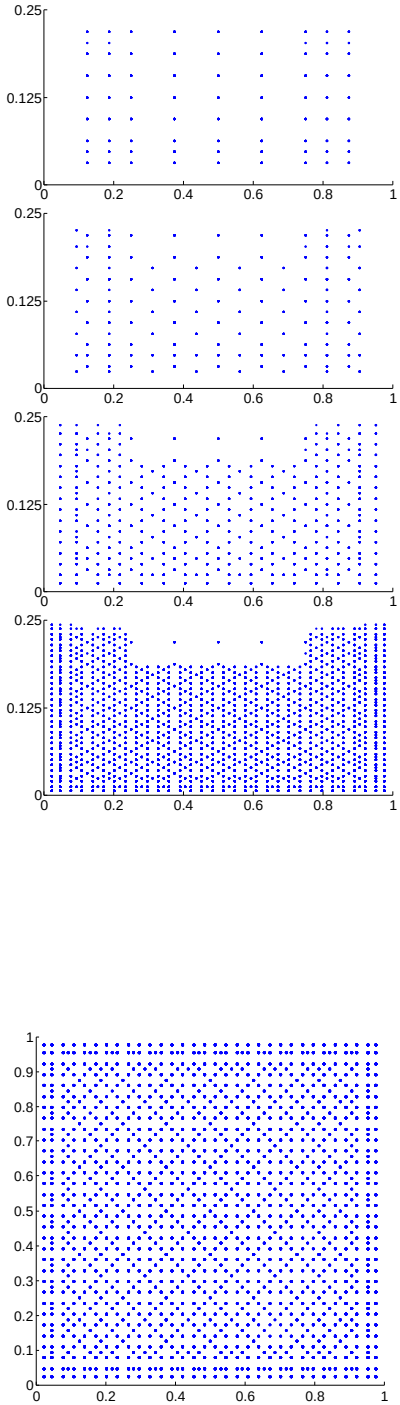

Figure 7.22. *Lateral view of the grid nodes computed within each iteration of the isotropic adaptive method and final refinement of the bottom boundary for* $P_\Gamma{}^{2,1}$, $l_{\min} = 3$, $\varepsilon = 1$.

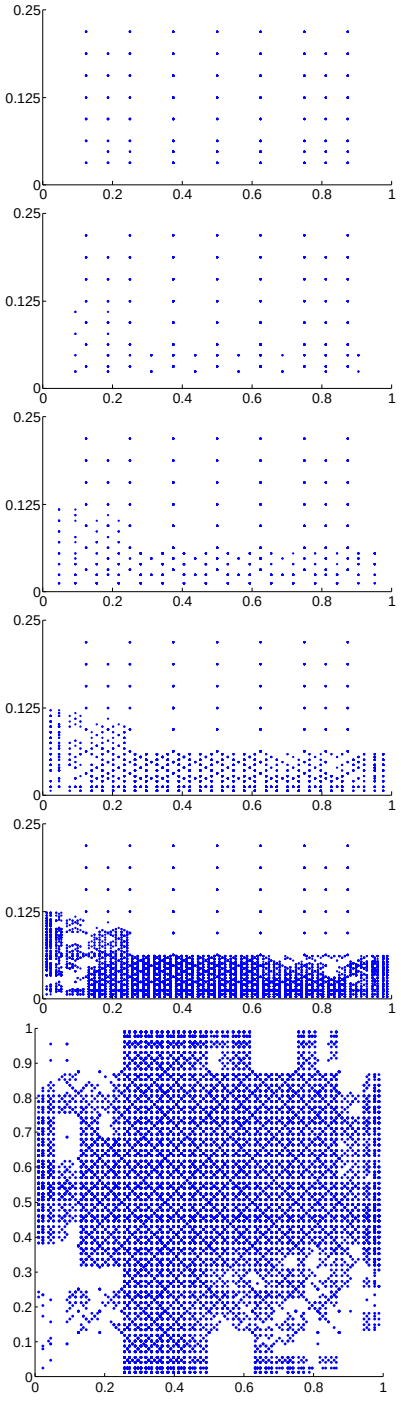

7.5.2 The Sparse Refinement

Within our second alternative refinement, namely the sparse adaptive refinement, candidate basis functions will tensor one dimensional basis functions such that the sum of their levels does not exceed a certain given value $J_{\max}$, thus avoiding finer refinements in more directions simultaneously.

Algorithm 7.5.2 (Create sparse children set $\delta^{\text{sparse}}(\Lambda_{j-1})$)**.**

1. *Create children set* $\delta(\Lambda_{j-1})$
2. *For all* $\psi_{j_x,k_x}\cdot\psi_{j_y,k_y}\cdot\psi_{j_z,k_z} \in \delta(\Lambda_{j-1})$*, add* $\psi_{j_x,k_x}\cdot\psi_{j_y,k_y}\cdot\psi_{j_z,k_z}$ *to* $\delta^{\text{sparse}}(\Lambda_{j-1})$ *only if* $j_x + j_y + j_z \leq J_{\max}$

We have set in our experiments $J_{\max} = 11$. This means, a basis function of type $\psi_{3,k_x} \cdot \psi_{3,k_y} \cdot \psi_{5,k_z}$ would be added to the children set, but a basis function of type $\psi_{5,k_x} \cdot \psi_{5,k_y} \cdot \psi_{5,k_z}$ would have been rejected.

Notice that the value of the weight parameter does again not change significantly for subsequent iterations despite the great variation in considered degrees of freedom. Empirically, one may choose to skip evaluating it within each iteration of the coarse-to-fine process.

Also, two layers on the bottom side are necessary to obtain better results as with the continuation obtained via finite differences. A lower threshold, i.e., more retained degrees of freedom, does not compensate for the missing information within the boundary data. Using just one layer on each of the top and bottom side provides still results similar to finite differences.

Both the lowest point wise maximum measured error $E_{\infty,\text{mid}}$ and the weighted error $E_{2,\text{mid}}$ for the sparse adaptive continuation have been obtained for ${P_\Gamma}^{2,1}$, basis level 5 and threshold parameter $\varepsilon = 1$, see Table 7.12. The representation involved 3361 basis functions, less than a tenth of the level 5 full grid basis. The last iteration, allowing basis functions up to level 6, did not positively contribute to the continuation. The error is, compared to the previous iteration, slightly larger. The additional basis function coefficients could not have been correctly determined. A considerable number of additional degrees of freedom remaining after the thresholding but are still redundant for the representation.

The additional layer of points in the data set ${P_\Gamma}^{2,1}$ brought a lower continuation error when measured with $E_{2,\text{mid}}$, but not when measured with $E_{\infty,\text{mid}}$. The highest value of $E_{\infty,\text{mid}}$ for ${P_\Gamma}^{2,1}$ has been attained anyway at the boundary, in the middle of the sharp anomaly.

The reader may notice in Figures 7.23-7.26 how the representation of the degrees of freedom shows the typical sparse grid structure. This adaptive and direction–wise accumulation of the grid nodes is consistent with the data set, since degrees of freedom still concentrate over the high-oscillating parts of the test function, i.e. vertically centered and near the bottom boundary of the domain.

Table 7.11. *Results for* $\delta^{\text{sparse}}(\Lambda_{j-1})$, ${P_\Gamma}^{1,1}$, $l_{\min} = 3$, $\varepsilon = 0.1$; *final solution and* $E_{\Omega_\#}$.

level l	$\#\tilde{\Lambda}_l$	$E_{\infty,\text{mid}}$	$E_{2,\text{mid}}$	$\#\Lambda_l$	$E_{\infty,\text{mid}}$	$E_{2,\text{mid}}$	η_l
3	1331	9.0042e+00	7.4094e+01	901	9.0042e+00	7.4084e+01	6.6345e-03
4	3221	3.4552e+00	6.1952e+01	2996	3.4552e+00	6.1952e+01	6.6548e-03
5	5659	1.8242e+00	6.0574e+01	5051	1.8242e+00	6.0574e+01	6.6548e-03
6	6975	1.8263e+00	6.0815e+01	5969	1.8263e+00	6.0815e+01	6.6548e-03

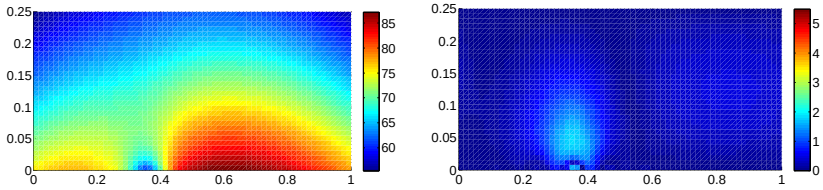

Table 7.12. *Results for* $\delta^{\text{sparse}}(\Lambda_{j-1})$, ${P_\Gamma}^{1,1}$, $l_{\min} = 3$, $\varepsilon = 1$; *final solution and* $E_{\Omega_\#}$.

level l	$\#\tilde{\Lambda}_l$	$E_{\infty,\text{mid}}$	$E_{2,\text{mid}}$	$\#\Lambda_l$	$E_{\infty,\text{mid}}$	$E_{2,\text{mid}}$	η_l
3	1331	9.0042e+00	7.4094e+01	635	9.0042e+00	7.4194e+01	6.6345e-03
4	1847	3.4575e+00	6.1915e+01	1652	3.4575e+00	6.1917e+01	6.6805e-03
5	2969	1.8174e+00	6.0510e+01	2561	1.8173e+00	6.0508e+01	6.6803e-03
6	3361	1.8188e+00	6.0509e+01	2806	1.8187e+00	6.0512e+01	6.6803e-03

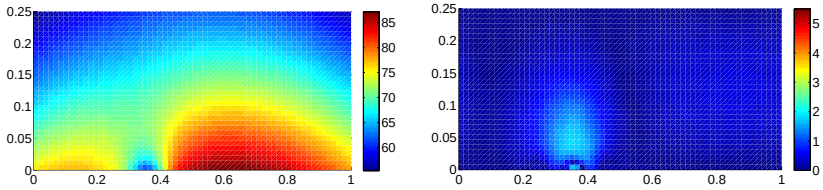

Table 7.13. *Results for* $\delta^{\text{sparse}}(\Lambda_{j-1})$, ${P_\Gamma}^{2,1}$, $l_{\min} = 3$, $\varepsilon = 0.1$; *final solution and* $E_{\Omega_\#}$.

level l	$\#\tilde{\Lambda}_l$	$E_{\infty,\text{mid}}$	$E_{2,\text{mid}}$	$\#\Lambda_l$	$E_{\infty,\text{mid}}$	$E_{2,\text{mid}}$	η_l
3	1331	9.3335e+00	6.3150e+01	1084	9.3335e+00	6.3118e+01	9.8243e-03
4	4188	3.8983e+00	4.5562e+01	3922	3.8983e+00	4.5562e+01	9.8618e-03
5	7603	2.1186e+00	4.2785e+01	6910	2.1186e+00	4.2785e+01	9.8624e-03
6	9660	2.1338e+00	4.2073e+01	8332	2.1338e+00	4.2073e+01	9.8624e-03

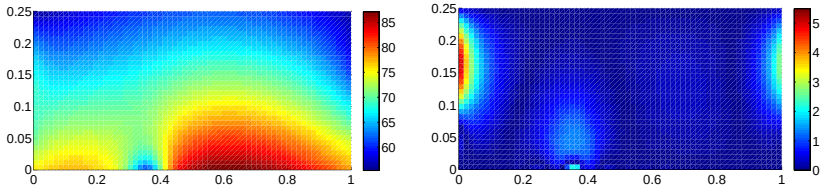

Table 7.14. *Results for* $\delta^{\text{sparse}}(\Lambda_{j-1})$, ${P_\Gamma}^{2,1}$, $l_{\min} = 3$, $\varepsilon = 1$; *final solution and* $E_{\Omega_\#}$.

level l	$\#\tilde{\Lambda}_l$	$E_{\infty,\text{mid}}$	$E_{2,\text{mid}}$	$\#\Lambda_l$	$E_{\infty,\text{mid}}$	$E_{2,\text{mid}}$	η_l
3	1331	9.3335e+00	6.3150e+01	698	9.3335e+00	6.2839e+01	9.8243e-03
4	2094	3.9012e+00	4.5884e+01	1915	3.9012e+00	4.5873e+01	9.8915e-03
5	3542	2.1409e+00	4.3969e+01	3016	2.1409e+00	4.3965e+01	9.8920e-03
6	4030	2.1565e+00	4.3903e+01	3267	2.1565e+00	4.3905e+01	9.8915e-03

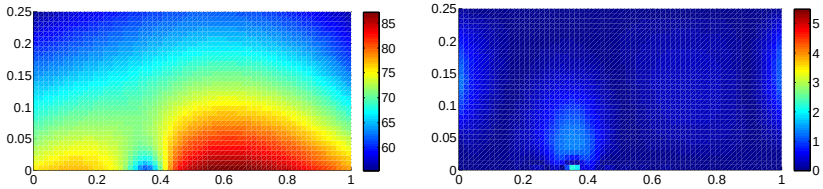

Figure 7.23. *Lateral view of the grid nodes computed within each iteration of the anisotropic adaptive method and final refinement of the bottom boundary for* $P_\Gamma{}^{1,1}$, $l_{\min} = 3$, $\varepsilon = 0.1$.

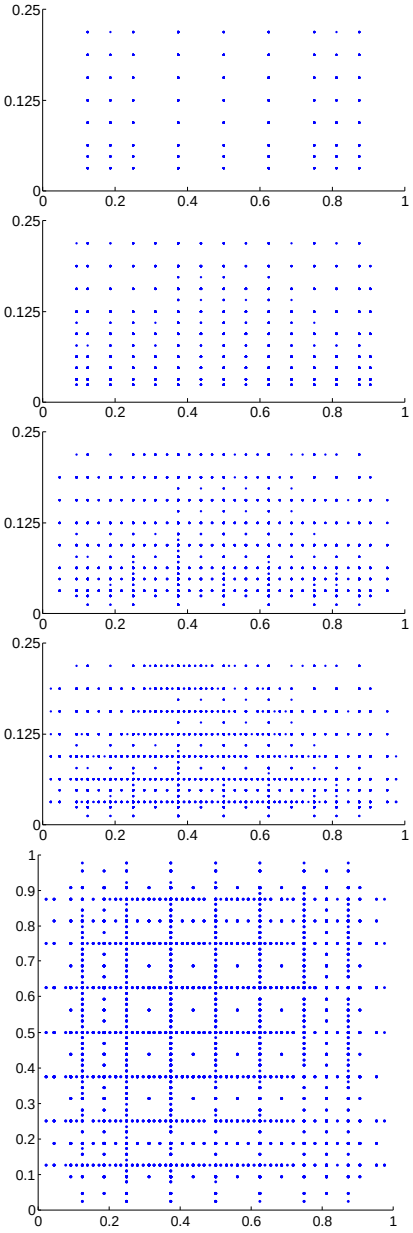

Figure 7.24. *Lateral view of the grid nodes computed within each iteration of the anisotropic adaptive method and final refinement of the bottom boundary for* $P_\Gamma{}^{1,1}$, $l_{\min} = 3$, $\varepsilon = 1$.

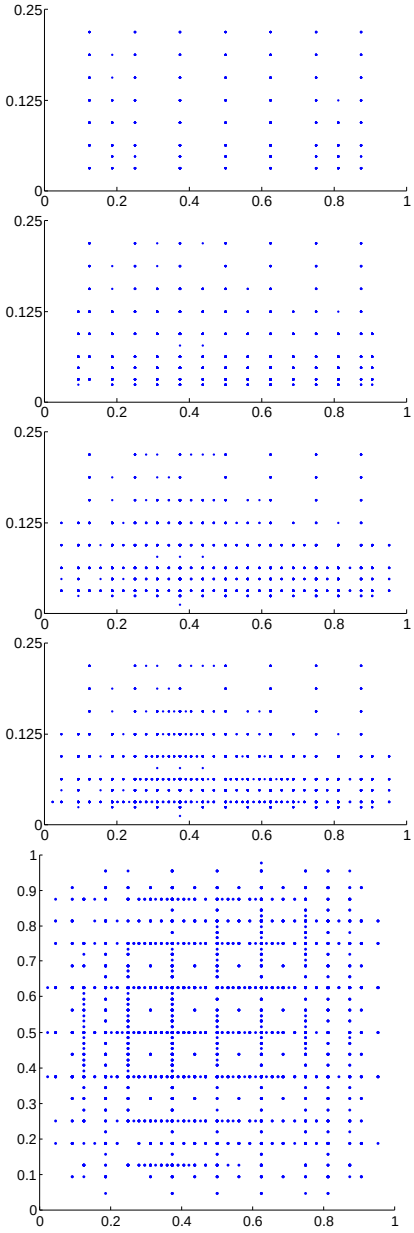

Figure 7.25. *Lateral view of the grid nodes computed within each iteration of the anisotropic adaptive method and final refinement of the bottom boundary for* $P_\Gamma{}^{2,1}$, $l_{\min} = 3$, $\varepsilon = 0.1$.

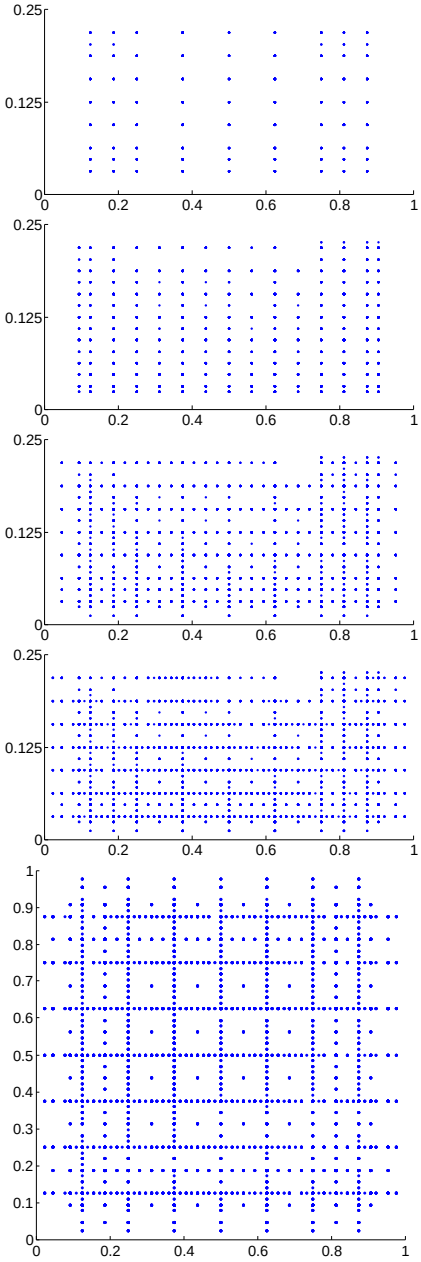

Figure 7.26. *Lateral view of the grid nodes computed within each iteration of the anisotropic adaptive method and final refinement of the bottom boundary for* $P_\Gamma{}^{2,1}$, $l_{\min} = 3$, $\varepsilon = 1$.

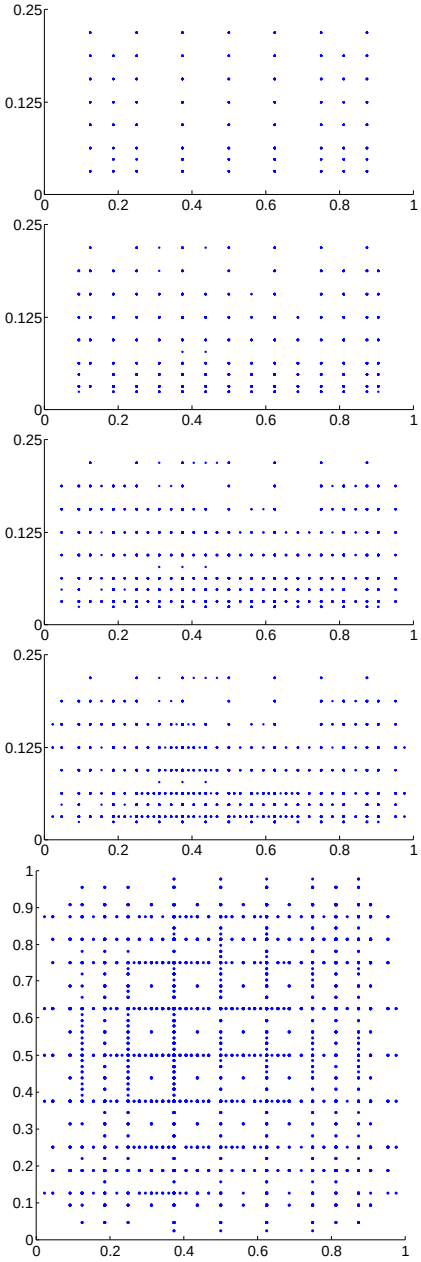

7.5.3 Comparative Draw

In retrospect, the most promising adaptive approaches for the salt lake data set have been the complete, anisotropic adaptive refinement from Section 7.4.1 and the sparse adaptive refinement from Section 7.4.1.

The most direct comparison between the full and adaptive construction of an approximate continuation for the salt lake data resides however in the error pattern. We are interested for the continuation to be as exact as possible in the middle of the domain. In view of the point wise maximum measured error $E_{\infty,\mathrm{mid}}$ the best approximate continuation has been obtained using complete, that is, anisotropic adaptive set up for ${P_\Gamma}^{2,1}$, basis level 5 and threshold parameter $\varepsilon = 1$, see Table 7.6. For the weighted L_2 norm $E_{2,\mathrm{mid}}$ the best continuation has been obtained for again using the complete adaptive set–up for ${P_\Gamma}^{2,1}$, basis level 5 but for threshold parameter $\varepsilon = 0.1$, see Table 7.5. Both the full adaptive and the sparse setup top without doubt the finite difference approach and provide similar results. Yet, with the sparse refinement, less than the half of degrees of freedom as in the complete adaptive set up for each choice of the threshold parameter ε respectively have been employed. Further, the sparse approach requires an average of about one tenth of the degrees of freedom needed and the full gridded approach by practically the same performance.

We find the estimated value for the adaptive construction again η_{eig} reliable, i.e., the quality of the thereby resulting continuation is as good as working with finite differences. It is interesting to see that η does not variate directly dependent from the number of unknowns. In the full grid approach, the estimated value changes radically from level 3 holding 1331 degrees of freedom and $\eta_3 = 8.3697e-4$ to $\eta_5 = 3.9921e-10$ by level 5 holding 42875 degrees of freedom. But the estimated weight parameter stays practically constant from iteration to iteration within all adaptive strategies. The greatest change occurred within the adaptive refinements for ${P_\Gamma}^{2,1}$, $\varepsilon = 0.1$ from $\eta_3 = 9.8243e-03$ to $\eta_5 = 4.4760e-02$ by a change in the number unknowns from 1331 to 29332.

It is too early to decide which strategy is the most successful one. The sparse setup provides results comparable with the full adaptive one when the isotropic refinement failed. Yet, we do not praise either one as the categorical best choice. We would rather point two main, distinctive ingredients of our problem statement relevant for the behavior of the adaptive techniques. They are in our opinion: first, the regulatory term counteracting by its nature adaptivity, and second, the structure of the domain and its normalization to unity. In geodetical statements, domains are rather flat. This calls for anisotropic representations but does not discriminate the isotropic approach for other domains or domain normalizations. The essential point is that the adaptive approach helps to save a considerable number of degrees of freedom compared to the full grid set-up. However, we do not expect to reach the accuracy of the costly full grid approach due to the intrinsic regulatory nature of the method. Further research and understanding of the involved parameters is seen as future work.

Last but not least, recall the sharp but poorly resolved anomaly within the boundary data. Notice also the defects of the continuation generated. They are similar to those seen in the experiments with real potential data sets. We assume therefore at this point that the rather weak performance of our method for the real dataset is indeed associated

with insufficiently well discretized boundary conditions. Recall also the good results obtained with well resolved boundary data, as in the case of the experiments with synthetic test functions based on summation of low spherical harmonics. Also, the continuation constructed by either of the full gridded or the full adaptive and sparse refinement are confirmed by the classical finite difference approach. We can conclude that our method based on weighted least squares does indeed solve the Dirichlet's problem for the Laplace equation with incomplete boundary conditions.

Chapter 8

Conclusions

A conclusion is the place where you got tired of thinking.

Harold Fricklestein

The task of this thesis is the approximate continuation of real valued potential functions on bounded domains with incomplete boundary conditions. We looked for an alternative to the classical continuation method in terms of spherical harmonics, which is computationally very expensive and confined to spherical domains. We reconstruct a harmonic function u on a cuboid domain $\Omega \subset \mathbb{R}^3$ from given information on a sub-domain $\Gamma \subset \Omega$ under the requirement that u should be approximately harmonic in Ω and that u approximates the given values over Γ. For that, we presented a weighted least squares approach and a formulation of the solution in terms of (tensor product of) B-spline. One has to include all given data in the information point set Γ. The minimization of the functional (4.8) for a (tensor product of) B-spline basis and for an adequate weight parameter $\eta \geq 0$ leads to the system of equations (4.27), which can be solved directly or iteratively. We thereby obtain the representation coefficients and we can evaluate the resulting reconstruction over the entire domain Ω. We have learned how to choose a good weight parameter depending on information points and on the available basis function set by the employment, e.g., of the indicator n_{eigs} (6.59).

We compare the results obtained by the weighted least-squares approach with a finite element and finite differences simulation on a cuboid for both synthetic and original undulation data, particularly with regard to quality. We thereby also verified that our weighted least squares approach does indeed solve Dirichlet's problem for the Laplace equation.

We recall some of the main advantages of the weighted least-squares approach over the classical continuation methods that rely on spherical harmonics. The power of the weighted least-squares method lies in the fact that it facilitates the computation of a representation on bounded domains and in terms of locally supported basis functions. Our approach can handle irregularly distributed data. The representation in terms of locally supported basis functions leads to sparse instead of full system matrices. We thus have the advantage of much lower memory requirements. Further, vis-á-vis to the finite differences and finite elements approach, recall that these methods require that data is

available over the entire boundary of the domain. Since this restriction does not hold for our approximate continuation approach based on weighted least squares, we investigated the effects of the missing boundary conditions over the reconstructed solution. Incomplete boundary conditions are acceptable for potential–typed functions when boundary data is available at the boundary near the source of the potential. Further, the variation of the weight parameter controlling the regularization term allows for an approximate fulfillment of the harmonicity constraint. This helps us to better continue insufficiently resolved or noised boundary data.

As a substantial further advancement of the proposed method, we have also provided an adaptive coarse–to–fine strategy which returns the solution of the continuation with efficient representation. The formulation in terms of hierarchical (tensor product of) B-splines basis allows for adaptive representations of the potential field and thereby an additional substantially reduced complexity. The adaptive refinement iteratively concentrates the degrees of freedom where needed. Without the necessity of an uniform grid, well surveyed areas can be so properly represented. We argued the use of the hierarchical decomposition over wavelet approaches and further compared several alternative refinement strategies, namely the isotropic and the sparse one.

As the experiments have shown, the main compromise of the weighted-least squares approach is that the continuation of real undulation data can only take place, when information points are available on both the upper and the lower side of the continuation domain. This is obligatory in order to compensate for missing boundary data on the vertical sides of the cuboid and for the poor fulfillment of the harmonicity due to low data sampling. We therefore cannot strictly characterize the method as an upward continuation problem. However, this is not a substantial drawback. In real applications, data is not available only at the surface of the earth, but is the result of additional various airborne measurements. Also, only low–frequency, already known or predictable components of the field reach satellite height. This means, boundary data on the upper side of the cuboid can be regarded as available. Alternatively, one may compute the upward continuation to greater distances where the field has practically attenuated. The boundary data at the side of the domain remote from the source can be set to 0.

Outlook

This (adaptive) weighted least-squares method for the approximate continuation of harmonic functions can be directly successfully employed for several other tasks in geodesy. Designed for the reconstruction of the earth's potential field, the method can be used, for example, for gridding and denoising of potential field measurements, with the advantage of the locality of the representation.

The employment of our method is not restricted to geodetic applications. It can handle other not necessarily two– or three dimensional, potential field typed setups. Since we numerically solve the Laplace equation in case of deficitary boundary conditions, we can handle similar difficulties in problems in electromagnetism, astronomy, and fluid dynamics.

Our approach can in fact find use in any kind of applications involving harmonic function over intricated domains. We have seen in Section 2.3 some applications of harmonic

function in the natural sciences. They require that some harmonic function is constructed depending on some boundary restrictions. The simple formulation in terms of tensor, locally supported basis functions could replace the analytic formulation or the one in terms of spherical harmonics, which were anyway more suitable for spherical domains. We have discussed only the direct application dealing with the classical geodetical problems. However, several applications from computer graphics and motion planning can profit from this construction of harmonic functions and the resulting sparse, adaptive and easy–to–evaluate representation.

Appendix A

Separable Solution of the Laplace Equation

The derivation of the separable solution of the Laplace equation coincides explicit derivation and construction of spherical harmonics. We have written the Laplace operator in spherical coordinates:

$$\Delta = \frac{1}{r^2}\frac{\partial}{\partial r}\left(r^2\frac{\partial\varphi}{\partial r}\right) + \frac{1}{r^2\sin(\theta)}\frac{\partial}{\partial\theta}\left(\sin(\theta)\frac{\partial}{\partial\theta}\right) + \frac{1}{r^2\sin^2(\theta)}\frac{\partial^2}{\partial\phi^2}. \tag{A.1}$$

Now we assume that $\varphi(r,\theta,\phi) = R(r)\Gamma(\theta,\phi)$, and separate the radial and angular variables: when the solution of the Laplace equation φ can be indeed written as the product of a function of r, $R(r)$, and a function of the angles θ and ϕ, namely $\Gamma(\theta,\phi)$, the function Γ is called a spherical harmonic. Let us further assume the existence of a variable separable solution of the form $\varphi(r,\theta,\phi) = R(r)\Theta(\theta)\Phi(\phi)$. We insert $\varphi(r,\theta,\phi)$ in the Laplace equation based upon the spherical coordinates version of the operator (2.11) to obtain

$$\Delta R(r)\Theta(\theta)\Phi(\phi) = \frac{\Theta\Phi}{r^2}\frac{d}{dr}\left(r^2\frac{dR}{dr}\right) + \frac{R\Phi}{r^2\sin(\theta)}\frac{d}{d\theta}\left(\sin(\theta)\frac{d\Theta}{d\theta}\right) + \frac{R\Theta}{r^2\sin^2(\theta)}\frac{d^2\Phi}{d\phi^2} \;=\; 0. \tag{A.2}$$

and proceed with the separation of variables as follows.

Step 1: Azimuthal Separation

We divide further both hand sides of equation (A.2) by the solution $\varphi(r,\theta,\phi) = R(r)\Theta(\theta)\Phi(\phi)$ and move the ϕ–dependence completely to the right hand side of the equation; to isolate it, multiply through by $r^2\sin^2(\theta)$. The last equation then becomes

$$\frac{1}{R}\sin^2(\theta)\frac{d}{dr}\left(r^2\frac{dR}{dr}\right) + \frac{1}{\Theta}\sin(\theta)\frac{d}{d\theta}\left(\sin(\theta)\frac{d\Theta}{d\theta}\right) \;=\; -\frac{1}{\Phi}\frac{d^2\Phi}{d\phi^2} \;=\; m^2. \tag{A.3}$$

The radial, azimuthal and the polar angle separation can now indeed follow. We proceed with the azimuthal part, i.e. the one regarding ϕ, and deal with the ordinary differential, Sturm-Liouville equation

$$\frac{d^2\Phi}{d\phi^2} = -m^2\Phi, \tag{A.4}$$

whose solutions are $\sin(m\phi)$ and $\cos(m\phi)$. These can also be formulated in terms of the complex exponential function $\exp(\pm im\phi)$. But we must obey the so called Single-valuedness Principle. This enforces that, in order to guarantee a physically correct result, we must have the same solution at ϕ and at $\phi + 2\pi n$. We hereby restrict m on the right side of equation (A.4) to an integer value, positive or negative.

$$\Theta_m(\theta) = e^{im\theta}, \quad m = \ldots, -3, -2, -1, 0, 1, 2, 3, \ldots. \tag{A.5}$$

Step 2: Polar Angle Separation

In order to carry out the polar angle separation, i.e. of θ, we must first isolate θ from r in equation (A.3) of the previous step; division through $\sin^2\theta$, grouping the θ terms on the right hand side yields the separation of the dependence with a separation constant $\ell(\ell+1)$,

$$\frac{1}{R}\frac{d}{dr}\left(r^2\frac{dR}{dr}\right) \;=\; -\frac{1}{\Theta\sin(\theta)}\frac{d}{d\theta}\left(\sin(\theta)\frac{d\Theta}{d\theta}\right) + \frac{m^2}{\sin^2(\theta)} \;=\; l(l+1). \tag{A.6}$$

We refine the last equality in (A.6) in terms of θ by multiplying with Θ and bringing all terms on the left hand side

$$\frac{1}{\sin(\theta)}\frac{d}{d\theta}\left(\sin(\theta)\frac{d\Theta}{d\theta}\right) + \Theta\left(\ell(\ell+1) - \frac{m^2}{\sin^2(\theta)}\right) \;=\; 0. \tag{A.7}$$

The following step is the change of variable $x = \cos(\theta)$: than $dx = -\sin(\theta)d\theta$, $d/dx = 1/\sin(\theta)d/d\theta$ and with the help of basis trigonometric identities we come to

$$(1-x^2)\frac{d^2\Theta}{dx^2} - 2x\frac{d\Theta}{dx} + \Theta\left(\ell(\ell+1) - \frac{m^2}{1-x^2}\right) \;=\; 0, \tag{A.8}$$

which is in fact an ordinary differential equation known as the associated Legendre differential equation

$$(1-x^2)\,y'' - 2xy' + \left(\ell[\ell+1] - \frac{m^2}{1-x^2}\right)y = 0, \tag{A.9}$$

where the indices ℓ and m are referred to as the degree and order of the associated Legendre function respectively. Please notice for clarity, the meaning of degree ℓ and order m for an associated Legendre function P_ℓ^m or for a spherical harmonic differs the common meaning of degree and order as in the case of classic polynomials; there we say, a polynomial of degree n has order $k = n + 1$. The associated Legendre functions $P_\ell^m(x)$ are then the canonical solutions of the general Legendre equation and they are defined in terms of the derivatives of the ordinary Legendre polynomials. These derivatives of the ordinary Legendre polynomials, sometimes called Legendre functions of the first kind, are the solution of the associated Legendre equation for $m = 0$, also known as the general Legendre equation:

$$(1-x^2)\frac{d^2y}{dx^2} - 2x\frac{dy}{dx} + \ell(\ell+1)y \;=\; 0. \tag{A.10}$$

Figure A.1. *The P_1, P_2, P_3, P_4 and P_5 Legendre polynomials.*

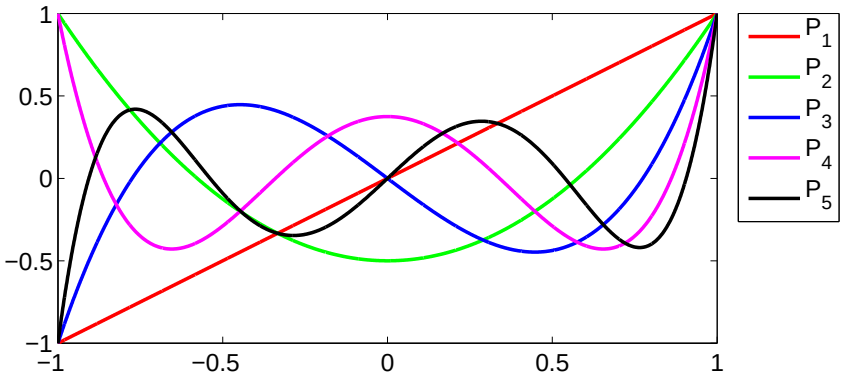

The Legendre differential equation can be solved using the standard power series method, see [1]. These solutions for $\ell = 0, 1, 2, \ldots$ are normalized such that $P_\ell(1) = 1$ form a polynomial sequence of orthogonal polynomials.

Definition A.0.3. *Each Legendre polynomial $P_\ell(x)$, $x \in [-1, 1]$ is a polynomial of degree ℓ and can be expressed using Rodrigues' formula:*

$$P_\ell(x) := \frac{1}{2^\ell \ell!} \frac{d^\ell}{dx^\ell} \left[(x^2 - 1)^\ell \right]. \tag{A.11}$$

The Legendre polynomials $P_\ell(x)$ are defined on the interval $[-1, 1]$ since x has been obtained through the variable transformation $x = \cos(\theta)$ with θ e.g. from equation (A.7).

Proposition A.0.4. *Their essential property is their orthogonality with respect to the L_2 inner product on the interval $-1 \leq x \leq 1$:*

$$\int_{-1}^{1} P_k(x) P_\ell(x)\, dx = \frac{2}{2\ell + 1} \delta_{k,\ell}. \tag{A.12}$$

Proposition A.0.5. *Essential for computational purposes, the Legendre polynomials can be constructed using the recurrence relation*

$$(n + 1)P_{n+1} = (2n + 1)xP_n - nP_{n-1}, \quad n \geq 1. \tag{A.13}$$

Now that we characterized the Legendre polynomials, we return to the associated Legendre functions.

Definition A.0.6. *The associated Legendre functions of degree ℓ and order m are defined as*

$$P_\ell^m(x) := (-1)^m \, (1 - x^2)^{\frac{m}{2}} \, \frac{d^m}{dx^m} \left(P_\ell(x) \right). \tag{A.14}$$

The factor $(-1)^m$ in formula (A.14)is known as the Condon-Shortley phase, see [23]. We obtain as a consequence of Rodriguez formula the identity

$$P_\ell^m(x) = \frac{(-1)^m}{2^\ell \ell!}(1-x^2)^{m/2}\ \frac{d^{\ell+m}}{dx^{\ell+m}}(x^2-1)^\ell. \tag{A.15}$$

Proposition A.0.7. *The associated Legendre functions are also orthogonal over* $[-1,1]$*: for* $0 \le m \le \ell$ *and fixed* m*, one has*

$$\int_{-1}^{1} P_k^m P_\ell^m dx = \frac{2(\ell+m)!}{(2\ell+1)(\ell-m)!}\ \delta_{k,\ell}. \tag{A.16}$$

Further, for fixed ℓ

$$\int_{-1}^{1} \frac{P_\ell^m P_\ell^n}{1-x^2}dx = \begin{cases} 0 & \text{if } m \neq n, \\ \frac{(\ell+m)!}{m(\ell-m)!} & \text{if } m = n \neq 0, \\ \infty & \text{if } m = n = 0. \end{cases} \tag{A.17}$$

The associated Legendre functions for negative m are proportional to those of positive m:

$$P_\ell^{-m} = (-1)^m \frac{(\ell-m)!}{(\ell+m)!} P_\ell^m. \tag{A.18}$$

Essential is that for $|m| > \ell$ one has $P_\ell^m = 0$. For implementation purposes, the following recurrence relations for the associated Legendre polynomials can also be considered:

Proposition A.0.8. *Other recurrence identities of the associated Legendre polynomials :*

$$P_{\ell+1}^m(x) = \frac{(2\ell+1)xP_\ell^m(x) - (\ell+m+1)P_{l-1}^m(x)}{l-m+1} \tag{A.19}$$

$$P_{\ell+1}^m(x) = P_{\ell-1}^m(x) - (2\ell+1)\sqrt{1-x^2}P_\ell^{m-1}(x) \tag{A.20}$$

$$\sqrt{1-x^2}P_\ell^{(m+1)}(x) = (\ell-m)xP_\ell^m(x) - (\ell+m)P_{ell-1}^m(x) \tag{A.21}$$

$$(x^2-1)P_\ell^{m\prime}(x) = \ell x P_\ell^m(x) - (\ell+m)P_{\ell-1}^m(x) \tag{A.22}$$

$$(x^2-1)P_\ell^{m\prime}(x) = -(\ell+m)(\ell-m+1)\sqrt{1-x^2}P_\ell^{m-1}(x) - mxP_\ell^m(x) \tag{A.23}$$

Recall now that we have made in equation (A.7) the change of variable $x = \cos(\theta)$. This is why x belongs to the interval $[-1,1]$. We can write then the associated Legendre functions in terms of θ as

$$P_\ell^{(m)}(\cos\theta) = (-1)^m(\sin\theta)^m\ \frac{d^m}{d(\cos\theta)^m}\left(P_\ell(\cos\theta)\right). \tag{A.24}$$

Step 3: Radial Separation

In order to carry out the last separation in the solution of the Laplace equation by means of separation of the variables, we deal with the following equation derived from (A.6)

$$\frac{1}{R}\frac{d}{dr}\left(r^2\frac{dR}{dr}\right) \;=\; l(l+1). \tag{A.25}$$

Once we multiply by $R(r)$ and express the derivative accordingly, we obtain

$$r^2\frac{d^2R}{dr^2} + 2r\frac{dR}{dr} \;=\; \ell(\ell+1)R. \tag{A.26}$$

Inspired by the attenuation of the potential field to be modeled by means of spherical harmonics, it is near to try to write $R(r)$ as a power of the radius, i.e.

$$R(r) = r^n. \tag{A.27}$$

By inserting this form in (A.26) we conclude that n can only be $n = \ell$ or $n = -(\ell+1)$, providing the general formulation for the radial factor as a sum of the two possible powers

$$R(r) \;=\; ar^{\ell} + br^{-(\ell+1)}. \tag{A.28}$$

We assemble the separable solution of the form $\varphi(r,\theta,\phi) = R(r)\Theta(\theta)\Phi(\phi)$ of the Laplace equation in spherical coordinates as product of the azimuthal, polar and radial terms described in (A.5,A.14, A.28):

$$\varphi(r,\theta,\phi) \;=\; \sum_{l=0}^{\infty}\sum_{m=-\ell}^{\ell}\left(a_{\ell m}r^{\ell} + b_{\ell m}r^{\ell+1}\right)P_{\ell}^{m}(\cos\theta)e^{im\phi}. \tag{A.29}$$

Appendix B

Notation

Chapter 2. Harmonic Functions

$\mathbb{N}$, $\mathbb{N}_0$	the natural numbers (including zero)
$\mathbb{Z}$	integers
$\mathbb{Q}$	the rational numbers
$\mathbb{R}$, $\mathbb{R}^n$	the real numbers, the n-dimensional Euclidean vector space
$\mathbb{R}_+$, $\mathbb{R}^n_+$	the positive real numbers, $\{(x_1, \ldots, x_n) \,\vert\, x_i > 0 \text{ for } 1 \leq i \leq n\}$
$\Omega \in \mathbb{R}^n$, $\partial\Omega$, $\bar{\Omega}$	domain, boundary of Ω, $\Omega \cup \partial\Omega$
$x = (x_1, \ldots, x_n)$	point in $\mathbb{R}^n$
(x, y, z)	Cartesian coordinates of a point in $\mathbb{R}^3$
(r, θ, ϕ)	spherical coordinates of a point in $\mathbb{R}^3$, r radius, θ co-latitude or polar angle $0 \leq \theta \leq \pi$, φ the azimuth or longitude, $0 \leq \varphi < 2\pi$
∇, Δ	differential and Laplace operator
$C^k(\Omega)$	all $\phi : \Omega \to \mathbb{R}$ such that all derivatives $\partial^\alpha \phi$ of order $\vert\alpha\vert \leq k$ are continuous in Ω (and such that $\operatorname{supp}\phi \subset\subset \Omega$)
$C^k(\bar{\Omega})$	all $\phi \in C^k(\Omega)$ such that all derivatives $\partial^\alpha \phi$ of order $\vert\alpha\vert \leq k$ have continuous extensions to $\bar{\Omega}$
$C^{k,1}(\Omega)$	Lipschitz continuous functions
$C^\infty(\Omega)$	space of infinitely differentiable functions on Ω with values in $\mathbb{R} = \bigcap_{k\in\mathbb{N}} \{C^k(\Omega)\}$
$\mathcal{D}(\Omega)$, $C_0^\infty(\Omega)$	space of infinitely differentiable functions with values in $\mathbb{R}$ and with compact support fully contained in Ω
$L_2(\Omega)$	space of real valued square Lebesque-integrable functions on Ω
$f, g, u, F : \Omega \to \mathbb{R}$	real valued function defined on Ω
φ	generic solution of the Laplace equation
$B(x, r)$	a ball with center x and radius r
$\mathcal{S}^{d-1}$	the sphere in d dimensions
$\varphi(r, \theta, \phi) = R(r)\Theta(\theta)\Phi(\phi)$	separable solution of the Laplace equation

$P_\ell^m(x)$	associated Legendre function of degree m and order ℓ
$P_\ell(x)$	associated Legendre polynomial of and order ℓ
$Y_\ell^m(\theta,\phi)$	spherical harmonic of degree m and order ℓ
$Y_\ell^{mc}(\theta,\phi), Y_\ell^{ms}(\theta,\phi)$	real part of spherical harmonics
A_ℓ^m	expansion coefficients in terms of Y_ℓ^m
S_ℓ^m, C_ℓ^m	expansion coefficients in terms of Y_ℓ^{mc}, Y_ℓ^{ms}

Chapter 3. The Earth's Gravitational Field

$\mathbf{r}$	radius vector
$\mathbf{a}_r$	dimensionless unit vector for direction
M, m, M_s	points of mass
g $\mathbf{g}$	gravitational attraction per unit mass, gravity vector
δg	anomalous gravity
F, $\mathbf{F}$	gravitational (vector) force
$Gal,\ mGal$	unit, force per mass
G	universal gravitational constant
GM	gravity–mass constant
a_1	equatorial scale factor
Vol, V_{Earth}	volume, earth's volume
$S = \partial V$	volume surface
ρ	volume density
$\delta\rho$	deviating volume density
$\mathbf{n}$	the outward pointing unit normal
H	orthometric height, surface's elevation above the geoid
h	ellipsoid height to the surface
n	spherical harmonic degree (of geoid model)
γ	normal gravity on the surface
U	undulation (geoid height) above the ellipsoid
U^n	approximation of the undulation in terms of spherical harmonics up to degree and order n
V	gravitational potential
V^n	approximation of the gravitational potential in terms of spherical harmonics up to degree and order n
N	the normal potential
T	disturbing potential
w	wavelength
C_n^m, S_n^m	geopotential model coefficients for (fully normalized) spherical harmonics of degree n and order m
δC_n^m	undulation model coefficients for (fully normalized) spherical harmonics of degree n and order m
σ_n^2	signal amplitude per degree n of the spherical harmonic coefficients, degree variance
F_h^n	attenuation factor per spherical degree n and height h

Chapter 4. New Approach: Least Squares with Regularization

f, g, u	real valued functions
$\Omega \subset I\!R^3$	domain
$\partial\Omega$	boundary of Ω
$\Gamma \subset \Omega$	sub-domain
$\Omega_\#$	uniformly gridded observation points on Ω
$\Gamma_\# \subset \Omega_\#$	boundary grid points on $\Gamma \subset \Omega$.
P_Γ	set of input observation points
$\Psi = \{\psi_\lambda : \lambda \in \Lambda\}$	basis defined on Ω, Λ index set
$L = \#\Lambda$	number of elements in Λ
$\lambda, \lambda' \in \Lambda$	basis function indices
η	weight parameter
$J(u)$	functional of u with data fitting term
$J_\eta(u)$	functional of u, dependent on η with both data fitting term and harmonicity constraint
$u_\eta = \sum_{\lambda\in\Lambda} d_\lambda \psi_\lambda(x_i)$	solution, approximate continuation
$\mathbf{d} = (d_\lambda)_{\lambda\in\Lambda}$	expansion coefficients
$\mathbf{z} = (z_i)_{(x_i,z_i)\in P_\Gamma}$	vector of boundary values
$\mathbf{b} = \mathbf{A}^T\mathbf{z}$	right hand side of equation system (4.27)
$\mathbf{A}$	observation matrix
$\mathbf{M}$	crossed-product matrix
$\mathbf{G}$	harmonicity constraint matrix
$\mathbf{M} + \eta\mathbf{G}$	system matrix of equation system (4.27)
Π_{n-1}	space of all polynomials in one variable of order at most n
b^n	uniform B-spline of degree n on the uniform mesh
Δ, Δ^d	(d–dimensional) knot sequence
T, T^h	knot sequence of length n and meshsize h extended by means of knot multiplicity k at the boundaries
s	spline series
$S_{k,\Delta}$	spline space of order k and knot sequence Δ
$\mathcal{S} = \otimes_{j=1}^d S_{k^j,\Delta^j}$	space of tensor-product polynomial splines
f_+^n	truncated power function
$N_{i,k}(x)$	B-splines of order k with respect to points $\tau_i, \ldots, \tau_{i+k}$
$T = \{\theta_i\}_{i=1,\ldots,n+k}$	knot sequence with multiplicity at the boundaries
$\mathcal{N}_k(T)$	the set of linear combinations of the B-splines over T
$N_{i,k}^h(x)$	refinable B-Splines for knot sequence with mesh h
V, W	vector space
V^*	dual vector space
$\otimes$	tensor product operator
$N_{\mathbf{i},\mathbf{k}} = \prod_{j=1}^d N_{i^j,k^j}$	d-variate tensor product spline

Chapter 6. Two Dimensional Illustration of the Method

$\Omega \subset I\!R^2$	domain
$f_1, f_2 : \mathbb{R}^2 \to \mathbb{R}$,	test functions: $f_1(x_1, x_2) = \exp^{-10x_1} \cdot \sin(10x_2) + \exp^{-10+10x_1} \cdot \sin(10 - 10x_2)$, $f_2(x_1, x_2) = \exp^{-10+10x_1} \cdot \sin(10 - 10x_2)$
$E_{bnd,\infty}$, $E_{\Omega,\infty}$, $E_{\Omega,\Delta}$	error measurements
l	basis level

Chapter 6. Numerical Results

$\Omega \subset I\!R^3$	domain
u_η	approximate continuation for weight parameter η
u_{fd}	approximate continuation using finite differences
Υ	set with weight parameter candidates
$E_{2,\text{bnd}}$, $E_{2,\text{mid}}$, $E_{\infty,\text{bnd}}$, $E_{\infty,\text{mid}}$, $E_{\Delta,\Omega}$	error measurements defined in equations (6.10) and (6.14)
cond	spectral condition number
${\Omega_\#}^{n\times e\times h}$	full grid consisting of $n \cdot e \cdot h$ uniformly gridded observation points
${P_\Omega}^{n\times e\times h}$	data on full grid $\Omega_\#$
d_n, d_e, d_h	mesh size per axis
${P_\Omega}^{mid} \subset P_\Omega$	middle of the domain
${P_\Gamma}^{b,t}$	set of input information points with b layers of data points at the bottom and t layers of data points at the top side of a cuboid domain
${P_\Gamma}^{fd}$	partial grid for finite differences and finite elements setup
$V^{n,m}$	component of the spherical harmonic representation of potential V of degree n and order m
$f_1, f_2 : \mathbb{R}^3 \to \mathbb{R}$,	test functions, $f_1 = V^{3,0} - V^{8,0}$, $f_2 = V^{3,1} - V^{6,1}$
Δx	mesh size
w	wavelength
L	the original length of the cuboid
l	basis function level with resolution 2^{-l}
H_L^l	support of a B-Spline basis of level l with respect L
$n_{\max}$, $n_{\max}^{P_\Gamma}$, $n_{\max}^{\Psi}$	spherical harmonic degrees
$OCV(\eta)$, $GCV(\eta)$	ordinary and generalized cross validation functionals
η_{cond}, η_{condest}, η_{eigs}	weight parameter indicators

Chapter 7. Adaptivity: Experiments with the Hierarchical Cubic B-spline Basis

$H^m(\Omega)$	Sobolev space of order $m \in \mathbb{N}$, all $\phi \in L_2(\Omega)$, $\frac{\partial \phi}{\partial x_i} \in L_2(\Omega), \ldots, D^\alpha \phi \in L_2(\Omega)$ for all α multi-index with $\lvert\alpha\rvert \leq m$
$H_0^m(\Omega)$	all $\phi \in H^m(\Omega), D^\alpha \phi = 0$ on $\partial\Omega, \lvert\alpha\rvert \leq m-1$
$H^s(\Omega)$	Sobolev space of fractional order s on Ω
$H^{-s}(\Omega)$	dual space of $H_0^s(\Omega)$
H	Hilbert space
$\{V_j\}_{j\geq 0}$	sequence of nested spaces approximating H
$\ell_2(\Lambda)$	the Banach space of elements $\mathbf{v} \in \ell_2(\Lambda)$ for which the norm $\lVert\mathbf{v}\rVert_{\ell_2(\Lambda)} := \left(\sum_{\lambda\in\Lambda} \lvert v_\lambda\rvert^2\right)^{1/2}$ is finite
$\operatorname{span}(\Phi)$	space spanned by Φ
$\oplus$	set plus
$\otimes$	tensor product
j, l	basis function levels
J	finest level
$J_{\max}$	maximal sum the levels for the sparse refinement
Λ	index of basis function set
$\#\Lambda$	number of elements in Λ
$\lambda \in \Lambda$	basis function index
u, u_η	solution
$\mathbf{c}, \mathbf{u}$	coefficient vector
$\mathbf{d}_{\Lambda_{j-1}}$, $\mathbf{d}_{\Lambda_j}$	determined coefficient set for levels $j-1$,j
Φ_j	single scale basis on level j
$\phi_\lambda \in \Phi_j$	basis function of Φ_j
$W_j = \operatorname{span}(\Psi_j)$	complement of two successive spaces V_j, V_{j+1}
Ψ_j^{MS}	the multi-scale basis on level j
Ψ_j^{WB}	wavelet linear B-spline basis
Ψ^{HB}	linear hierarchic (B-spline) basis
$\mathbf{M}_{j,0}^T$, $\mathbf{M}_{j,1}$	matrices for the two–scale relation
$\Delta_j = \{\tau_i\}_{i=0,\ldots,2^j}$	j-th level uniform knot sequence
η_j	weight parameter on level j
j_0, $l_{\min}$	start level
$\psi_{j_x,k_x} \cdot \psi_{j_y,k_y} \cdot \psi_{j_z,k_z}$	three dimensional tensor product basis function of levels j_x, j_y and j_z
ϵ	thresholding value
$\delta(\Lambda_{j-1})$	complete children basis functions set of Λ_{j-1}
$\delta^{\text{iso}}(\Lambda_{j-1})$	isotropic children basis functions set of Λ_{j-1}
$\delta^{\text{sparse}}(\Lambda_{j-1})$	sparse children basis functions set of Λ_{j-1}
$\tilde{\Lambda}_j = \Lambda_{j-1} \cup \delta(\Lambda_{j-1})$	preliminary basis function set
$E_{\infty,\text{mid}}$, $E_{2,\text{mid}}$, $E_{\infty,\text{bnd}}$, $E_{2,\text{bnd}}$	error measurement over the boundaries or over the middle of the domain, as defined in (6.10)
$E_{\Omega_\#}$	pointwise error of the continuation, as defined in (7.117)

Bibliography

[1] M. Abramowitz and I. A. Stegun, *Handbook of Mathematical Functions with Formulas, Graphs, and Mathematical Tables*, Dover, New York, ninth dover printing, tenth gpo printing ed., 1964.

[2] R. Adams, *Sobolev Spaces*, vol. 65 of Pure and applied mathematics, New York: Academic Press, 1978.

[3] H. Alt, *Lineare Funktionalanalysis: eine anwendungsorientierte Einführung*, Springer, 2002. (In German).

[4] D. A. Armitage and S. J. Gardiner, *Classical Potential Theory*, Springer Monographs in Mathematics, Springer; 1 edition, 2000.

[5] S. Axler, P. Bourdon, and W. Ramey, *Harmonic Function Theory*, Graduate Texts in Mathematics, Springer; 2nd ed. edition, 2001.
`http://www.axler.net/HFT.pdf`.

[6] R. E. Bank, *Hierarchical bases and the finite element method*, in Acta numerica, vol. 5, Univ. Press, 1996, pp. 1–43.

[7] R. Barrett, M. Berry, T. F. Chan, J. Demmel, J. Donato, J. Dongarra, V. Eijkhout, R. Pozo, C. Romine, and H. V. der Vorst, *Templates for the Solution of Linear Systems: Building Blocks for Iterative Methods, 2nd Edition*, SIAM, Philadelphia, PA, 1994.

[8] G. Beylkin, R. Coifman, and V. Rokhlin, *Fast wavelet transforms and numerical algorithms I*, Communications on Pure and Applied Mathematics, 44 (1991), pp. 141–183.

[9] A. Bierce, *The devil's dictionary*, Doubleday, 1911.
`http://ebooks.ub.uni-muenchen.de/12166/`.

[10] C. Boxhammer and W.-D. Schuh, *GOCE gravity field modeling: computational aspects - free kite numbering scheme*, Observation of the Earth System from Space, (2006), pp. 209–224.

[11] D. Braess, *Finite Elemente, Theorie, schnelle Löser und Anwendungen in der Elastizitätstheorie*, Springer, Berlin, Heidelberg, New York, 2nd ed., 1997.

[12] J. M. Brockmann, B. Kargoll, I. Krasbutter, W.-D. Schuh, and M. Wermuth, *GOCE data analysis - from calibrated measurements to the global earth gravity field*, System Earth via Geodetic-Geophysical Space Techniques, (2010).

[13] H.-J. Bungartz, *Finite Elements of Higher Order on Sparse Grids*, Berichte aus der Informatik, Shaker Verlag, Aachen, November 1998.

[14] H.-J. Bungartz and M. Griebel, *Sparse grids*, Acta Numerica, 13 (2004), pp. 147–269.

[15] M. Calhoun-Lopez and M. D. Gunzburger, *The efficient implementation of a finite element, multi-resolution viscosity method for hyperbolic conservation laws*, J. Comput. Phys., 225 (2007), pp. 1288–1313.

[16] D. Castano and A. Kunoth, *Adaptive fitting of scattered data by spline–wavelets*, Curves and Surfaces, (2003), pp. 65–78.

[17] D. Castano Diez, *Adaptive Scattered Data Fitting with Tensor Product Spline-Wavelets*, PhD thesis, Mathematisch-Naturwissenschaftliche Fakultät, Rheinische Friedrich-Wilhelms-Universität Bonn, 2005.

[18] D. Castano Diez, G. Jager, and A. Kunoth, *Multiscale analysis of multivariate data*, 18th International Conference on the Application of Computer Science and Mathematics in Architecture and Civil Engineering (Electronic Proceedings), K. Gürlebeck and C. Könke (eds.), Weimar, Germany, (July 2009).

[19] C. Chui and E. Quak, *Wavelets on a bounded interval*, in Numerical Methods of Approximation Theory, D. Braess and L. L. Schumaker, eds., vol. 9, Birkhauser-Verlag, Basel, Switzerland, 1992, pp. 1–24.

[20] C. K. Chui, *Multivariate Splines*, vol. 54 of CBMS-NSF Series in Applied Mathematics, SIAM, Philadelphia, 1988.

[21] C. K. Chui, *An introduction to wavelets*, Academic Press Professional, Inc., San Diego, CA, USA, 1992.

[22] A. Cohen, W. Dahmen, and R. Devore, *Adaptive wavelet methods for elliptic operator equations - convergence rates*, Math. Comp., 70 (1999), pp. 27–75.

[23] E. U. Condon and G. H. Shortley, *The theory of atomic spectra*, Cambridge University Press, 1970.

[24] C. I. Connolly, J. B. Burns, and R. Weiss, *Path planning using Laplace's equation*, Proceedings IEEE International Conference on Robotics & Automation, (1990), pp. 2102–2106.

[25] C. I. Connolly and R. A. Grupen, *Applications of harmonic functions to robotics*, tech. rep., University of Massachusetts, Amherst, MA, USA, 1992.

[26] P. Craven and G. Wahba, *Smoothing noisy data with spline functions: estimating the correct degree of smoothing by the method of generalized cross-validation*, Numer. Math., 31 (1979), pp. 377–403.

[27] W. Dahmen, *Wavelet and multiscale methods for operator equations*, Acta Numerica, 6 (1997), pp. 55–228.

[28] W. Dahmen, R. De Vore, and K. Scherer, *Multi-dimensional spline approximation*, SIAM Journal on Numerical Analysis, 17 (1980), pp. 380–402.

[29] W. Dahmen and A. Kunoth, *Multilevel preconditioning*, Numer. Math., 63 (1992), pp. 315–344.

[30] W. Dahmen, A. Kunoth, and K. Urban, *Biorthogonal spline-wavelets on the interval – stability and moment conditions*, Appl. Comp. Harm. Anal., 6 (1999), pp. 132–196.

[31] W. Dahmen, S. Müller, and T. Schlinkmann, *Multigrid and multiscale decompositions*, Large-Scale Scientific Computations of Engineering and Environmental Problems, Notes on Numerical Fluid Mechanics, 62 (1998), pp. 18–41.

[32] J. d'Alembert, *Opuscules mathmatiques*, 1761. Some bands digitized by Google from the library of the University of Michigan.

[33] I. Daubechies, *Ten Lectures on Wavelets*, Society for Industrial and Applied Mathematics, Philadelphia, 1992.

[34] C. de Boor, *On local linear functionals which vanish at all B-splines but one*, in Theory of Approximation with Applications, A. G. Law and B. N. Sahney, eds., New York, 1976, Academic Press, pp. 120–145.

[35] C. de Boor, *A practical guide to splines*, no. 27 in Applied Mathematical Sciences, Springer-Verlag, New York-Berlin, 1978.

[36] G. Deslauriers and S. Dubuc, *Symmetric iterative interpolation processes*, Constructive Approximation, 5 (1989), pp. 49–68.

[37] P. Dierckx, *Curve and Surface Fitting with Splines*, Clarendon Press, Oxford, 1993.

[38] D. C. Diez, M. Gunzburger, and A. Kunoth, *An adaptive wavelet viscosity method for hyperbolic conservation laws*, Numer. Meths. for PDEs 24, 6 (2008), pp. 1388–1404.

[39] A. Eicker, T. Mayer-Guerr, and K. Ilk, *Improved resolution of a GRACE gravity field model by regional refinements*, Observing our Changing Earth, (2008), pp. 99–104.

[40] ESA, *European space agency's gravity mission GOCE*, 2009. `http://www.esa.int/esaLP/ESAYEK1VMOC_LPgoce_0.html`.

[41] L. Euler, *An identity for spline functions with applications to variation-diminishing spline approximation*, Novi Commentarii Acad. Sci. Petropolitanae, (1761).

[42] L. C. Evans, *Partial Differential Equations (Graduate Studies in Mathematics, V. 19) GSM/19*, American Mathematical Society, June 1998.

[43] A. Finkelstein and D. H. Salesin, *Multiresolution curves*, in SIGGRAPH '94: Proceedings of the 21st annual conference on Computer graphics and interactive techniques, New York, NY, USA, 1994, ACM, pp. 261–268.

[44] D. R. Forsey and R. H. Bartels, *Hierarchical B-spline refinement*, in SIGGRAPH '88: Proceedings of the 15th annual conference on Computer graphics and interactive techniques, New York, NY, USA, 1988, ACM, pp. 205–212.

[45] D. R. Forsey and R. H. Bartels, *Tensor products and hierarchical fitting*, in In Volume 1610 Curves and Surfaces in Computer Vision and Graphics II, 1991, pp. 88–96.

[46] D. R. Forsey and R. H. Bartels, *Surface fitting with hierarchical splines*, ACM Trans. Graph., 14 (1995), pp. 134–161.

[47] W. Freeden, T. Gervens, and M. Schreiner, *Constructive Approximations on the Sphere (With Applications to Geomatics)*, Oxford Science Publications, Clarendon Press, 1998.

[48] W. Freeden and V. Michels, *Multiscale Potential Theory: With Applications to Geoscience (Applied and Numerical Harmonic Analysis)*, Birkhäuser; Auflage: 1, 2004.

[49] W. Freeden and M. Schreiner, *Spherical Functions of Mathematical Geosciences (A Scalar, Vectorial, and Tensorial Setup)*, Advances in Geophysical and Environmental Mechanics and Mathematics, Springer Verlag, 2008.

[50] J. Garcke, M. Griebel, and M. Thess, *Data mining with sparse grids*, Computing, 67 (2001), pp. 225–253.

[51] T. Gerstner and M. Griebel, *Sparse grids*, in Encyclopedia of Quantitative Finance, R. Cont, ed., John Wiley and Sons, Feb. 2010.

[52] C. Gonzalez-Ochoa and J. Peters, *Localized-hierarchy surface splines (less)*, in I3D '99: Proceedings of the 1999 symposium on Interactive 3D graphics, New York, NY, USA, 1999, ACM, pp. 7–15.

[53] S. J. Gortler and M. Cohen, *Hierarchical and variational geometric modeling with wavelets*, Proc. Symposium on Interactive 3D Graphics, (1995).

[54] R. D. Gregory, *Uniform bounds for $P_n^m(\cos\theta)$ and the absolute convergence of series expansions in spherical surface harmonics*, Quarterly Journal of Mechanics and Applied Mathematics, 50 (1997), pp. 467–479.

[55] G. Greiner and K. Hormann, *Interpolating and approximating scattered 3d-data with hierarchical tensor product splines*, Surface Fitting and Multiresolution Methods, (1996), pp. 163–172.

[56] M. Griebel and P. Oswald, *Tensor product type subspace splittings and multilevel iterative methods for anisotropic problems*, Adv. Comput. Math, (1995), pp. 171–206.

[57] D. J. Griffiths, *Introduction to quantum mechanics*, Prentice Hall,Upper Saddle River, NJ, 1995.

[58] E. Grinspun, P. Krysl, and P. Schröder, *CHARMS: a simple framework for adaptive simulation*, in SIGGRAPH '02: Proceedings of the 29th annual conference on Computer graphics and interactive techniques, New York, NY, USA, 2002, ACM, pp. 281–290.

[59] P. Grisvard, *Elliptic Problems in Nonsmooth Domains*, vol. 24 of Monographs and studies in mathematics, Boston : Pitman Advanced Pub. Program, 1985.

[60] W. Hackbusch, *Elliptic Differential Equations. Theory and Numerical Treatment*, Springer, 2003.

[61] J. Hadamard, *Lectures on Cauchy's problem in linear partial differential equations*, Dover Phoenix Editions, 1923.

[62] W. W. Hager, *Condition estimates*, SIAM Journal on Scientific and Statistical Computing, 5 (1984), pp. 311–316.

[63] M. Hanke, *Conjugate Gradient type methods for ill-posed Problems*, vol. 327 of Pitman Research Notes in Mathematics, Longman Scientific $ Tenchical, New York, 1995.

[64] M. Hanke, *Limitations of the L-curve method in ill-posed problems*, BIT, (1996), pp. 287–301.

[65] M. Hegland, S. Roberts, and I. Altas, *Finite element thin plate splines for surface fitting*, Computational Techniques and Applications: CTAC97, (1997), pp. 289–296.

[66] E. Heine, *Handbuch der Kugelfunctionen*, G. Reimer, 1861.

[67] W. A. Heiskanen and H. Moritz, *Physical Geodesy*, Freeman, San Francisco, California, 1967.

[68] T. Helmholtz Centre Potsdam GFZ, German Research Centre for Geosciences, *The CHAMP mission*, 2009.
`http://www-app2.gfz-potsdam.de/pb1/op/champ/index_CHAMP.html`.

[69] R. Hersh and R. Griego, *Brownian motion and potential theory*, Scientific American, (1969), p. 6674.

[70] N. J. Higham and F. Tisseur, *A block algorithm for matrix 1-norm estimation, with an application to 1-norm pseudospectra*, SIAM J. Matrix Anal. Appl., 21 (2000), pp. 1185–1201.

[71] E. Hobson, *The Theory of Spherical and Ellipsoidal Harmonics*, New York: Chelsea, 1955.

[72] K. Höllig, *Finite Element Methods with B-splines*, SIAM, 2003.

[73] K. Höllig and U. Reif, *Nonuniform web-splines*, Comput. Aided Geom. Des., 20 (2003), pp. 277–294.

[74] K. Höllig, U. Reif, and J. Wipper, *Weighted extended B-spline approximation of dirichlet problems*, SIAM J. Numer. Anal., 39 (2001), pp. 442–462.

[75] R. House, *Dictionary.com unabridged (v 1.1).* Based on the Random House Unabridged Dictionary, Random House, Inc., Feb 2009. `http://dictionary.reference.com/browse/harmonic`.

[76] M. F. Hutchinson and F. R. de Hoog, *Smoothing noisy data with spline functions*, Numer. Math., 47 (1985), pp. 99–106.

[77] J. T. Kajiya, *The rendering equation*, SIGGRAPH Comput. Graph., 20 (1986), pp. 143–150.

[78] H. Kalf, *On the expansion of a function in terms of spherical harmonics in arbitrary dimensions*, Bulletin of the Belgian Mathematical Society, 4 (1995), pp. 361–380.

[79] M. Kapl and B. Jüttler, *A multiresolution analysis for tensor-product splines using weighted spline wavelets*, J. Comput. Appl. Math., 231 (2009), pp. 828–839.

[80] W. M. Kaula, *Theory of Satellite Geodesy*, Blaisdell Publishing Co, Waltham, Massachusetts, 1966.

[81] W. Keller, *Wavelets in Geodesy and Geodynamics*, Walter de Gruyter, New York, 2004.

[82] O. D. Kellogg, *Foundations of potential theory*, originally published by Verlag von Julius Springer, 1929.

[83] O. Khatib, *Real-time obstacle avoidance for manipulators and mobile robots*, International Journal of Robotic Research, 5 (1986), pp. 90–98.

[84] S. Knapek, *Approximation und Kompression mit Tensorprodukt-Multiskalenräumen*, Phd Thesis, Universität Bonn, April 2000.

[85] F. Koster, *Multiskalen-basierte Finite Differenzen Verfahren auf adaptiven dünnen Gittern*, Phd Thesis, Universität Bonn, January 2002.

[86] R. KRAFT, *Adaptive and linearly independent multilevel B-splines*, in Surface Fitting and Multiresolution, Vanderbilt University Press, 1997, pp. 209–218.

[87] A. Kunoth, *Mathematische Methoden in der Geometrischen Datenverarbeitung (CAGD).* Lecture notes, FU Berlin, 1990.

[88] A. Kunoth, *Wavelet Methods Elliptic Boundary Value Problems and Control Problems. Advances*, Teubner Verlag, 2001.

[89] P. Laplace, *An identity for spline functions with applications to variation-diminishing spline approximation*, Hist. Acad. Sci. Paris, (1782, published 1785).

[90] ——, *Celestial mechanics*, reprinted by Chelsea, New York, Paris, 1829-1839.

[91] S. Lee, G. Wolberg, and S. Y. Shin, *Scattered data interpolation with multilevel B-splines*, IEEE Transactions on Visualization and Computer Graphics, 3 (1997), pp. 228–244.

[92] F. G. Lemoine, D. E. Smith, R. Smith, L. Kunz, N. K. Pavlis, S. M. Klosko, D. S. Chinn, M. H. Torrence, R. G. Williamson, C. M. Cox, K. E. Rachlin, Y. M. Wang, E. C. Pavlis, S. C. Kenyon, R. Salman, and R. Trimmer, *EGM96, the NASA GSFC and NIMA joint geopotential model*, 1998. `http://earth-info.nga.mil/GandG/wgsegm/egm96.html`.

[93] W. A. Light and E. W. Cheney, *Approximation theory in tensor product spaces*, in Lecture Notes in Mathematics 1169, Springer, 1985.

[94] J. Lions and E. Magenes, *Non-Homogeneous Boundary Value Problems and Applications*, vol. I,II and III, Springer, 1972.

[95] R. Lorentz and P. Oswald, *Multilevel finite element Riesz bases in Sobolev spaces*, in Proc. 9th Intern. Conf. on Domain Decomposition Methods, Bergen 1996, P. Bjorstad, ed., 1998.

[96] R. Lorentz and P. Oswald, *Criteria for hierarchical bases in Sobolev spaces*, Applied and Computational Harmonic Analysis, 8 (2000), pp. 32 – 85.

[97] M. J. Marsden, *An identity for spline functions with applications to variation-diminishing spline approximation*, Journal of Approximation Theory, (1970), pp. 7–49.

[98] T. MathWorks, 2009. `http://www.mathworks.de/`.

[99] P. Meissl, *The Use of Finite Elements in Physical Geodesy*, Reports of the Department of Geodetic Science, The Ohio State University, Ohio, 1981.

[100] V. Michel, *A multiscale method for the gravimetry problem — Theoretical and numerical aspects of harmonic and anharmonic modelling*, PhD thesis, Geomathematics Group, Department of Mathematics, University of Kaiserslautern, Shaker Verlag, Aachen, 1999.

[101] N. M. Milton and M. Lloyd-Hart, *Disk harmonic functions for adaptive optics simulations*, in Adaptive Optics: Analysis and Methods/Computational Optical Sensing and Imaging/Information Photonics/Signal Recovery and Synthesis Topical Meetings on CD-ROM, Optical Society of America, 2005.

[102] MIT, *Open courseware on earth, atmospheric, and planetary sciences, essentials of geophysics, chapter 2: The earth's gravitational field*. http://ocw.mit.edu/NR/rdonlyres/Earth--Atmospheric--and-Planetary-Sciences/12-201Fall-2004/E7A9DF78-ADC6-49A7-8812-1D8244939398/0/% ch2.pdf.

[103] H. Moritz, *Advanced Physical Geodesy*, H. Wichmann, Karlsruhe, Germany, 1980.

[104] ——, *The sand grain and the butterfly. Instability in geodesy and geophysics*, Earthprints, (1997).

[105] ——, *The strange behavior of asymptotic series in mathematics, celestial mechanics and physical geodesy*, Geod. kartogr., (2003), pp. 371–377.

[106] ——, *Working with Torben Krarup*, Presented at A Torben Krarup Workshop; Aalborg University, (2006). http://www.helmut-moritz.at/SciencePage/WorkingwithTorbenKrarup.pdf.

[107] B. Mössner and U. Reif, *Stability of tensor product B-splines on domains*, J. Approx. Theory, 154 (2008), pp. 1–19.

[108] NASA and DLR, *GRACE – gravity recovery and climate experiment*, 2009. joint partnership between the National Aeronautics and Space Administration (NASA) in the United States and Deutsche Forschungsanstalt für Luft und Raumfahrt (DLR) http://www.csr.utexas.edu/grace/.

[109] National Research Council, ed., *Satellite Gravity and the Geosphere: Contributions to the Study of the Solid Earth and Its Fluid Envelopes*, National Academy Press, England, 1997.

[110] S. Newton, Isaac, *Philosophiae naturalis principia mathematica*, Royal Society Book III, Propositions I-VII, 1686.

[111] P. Oswald, *Multilevel Finite Element Approximation*, Teubner Skripten zur Numerik, Teubner, Stuttgart, 1994.

[112] ——, *Multilevel solvers for elliptic problems on domains*, in Multiscale Wavelet Methods for Partial Differential Equations, A. J. K. Wolfgang Dahmen and P. Oswald, eds., vol. 6 of Wavelet Analysis and Its Applications, Academic Press, 1997, pp. 3 – 58.

[113] C. Paige and M. Saunders, *Solution of sparse indefinite systems of linear equations*, SIAM J. Numer. Anal., 12 (1975), pp. 617–629. http://www.stanford.edu/group/SOL/software/symmlq/PS75.pdf.

[114] R. Pail and W.-D. Schuh, *Effects of inhomogeneous data coverage on spectral analysis*, Towards an Integrated Global Geodetic Observing System (IGGOS), (2000), pp. 209–213.

[115] N. Pavlis, S. Holmes, S. Kenyon, and J. Factor, *An earth gravitational model to degree 2160: EGM2008.* presented at the 2008 General Assembly of the European Geosciences Union, Vienna, Austria, April 13-18, `http://earth-info.nga.mil/GandG/wgs84/gravitymod/egm2008/egm08_wgs84.html`.

[116] P. J. Phillips, *Potential theory, harmonic functions and volatility surfaces: An analysis of the relationship between implied volatility, strike price and expiration in equilibrium*, Social Science Research Network, University of Southern Queensland - Faculty of Business, (2007).

[117] E. Quak and N. Weyrich, *Decomposition and reconstruction algorithms for bivariate spline wavelets on the unit square*, in An international conference on curves and surfaces on Wavelets, images, and surface fitting, Fair Oaks, CA, USA, 1994, Adams-Blake Publishing, pp. 419–428.

[118] C. Reigber, P. Schwintzer, R. Stubenvoll, R. Schmidt, F. Flechtner, U. Meyer, R. König, H. Neumayer, C. Förste, F. Barthelmes, S. Y. Zhu, G. Balmino, R. Biancale, J.-M. Lemoine, H. Meixner, and J. C. Raimondo, *A high resolution global gravity field model combining CHAMP and GRACE satellite mission and surface data: EIGEN-CG01C.*, GeoForschungsZentrum-Potsdam, 2006.
urlhttp://edoc.gfz-potsdam.de/gfz/8973.

[119] F. Rellich, *Eigenwerttheorie partieller Differentialgleichungen, Teil I und Teil II, Student Lecture copy*, Gottingen Mathematisches Institut der Universität Göttingen, 1953.

[120] M. Renardy and R. C. Rogers, *An Introduction to Partial Differential Equations*, vol. 13 of Texts in Applied Mathematics, Springer, 1993.

[121] A. Renyi, *Probability Theory*, North-Holland Publishing Co., Amsterdam, 1970.

[122] F. Riesz, *Sur les operations fonctionnelles lineaires*, in Paris 149, Also appears in Oeuvres, Volume I, 1909, pp. 974–977.

[123] D. Saupe and D. V. Vranic, *3d model retrieval with spherical harmonics and moments*, in DAGM-Symposium, 2001, pp. 392–397.

[124] K. Scherer, *Approximation mit Wavelets I/II.* Lecture courses at the Universität Bonn, Summer Semester 2001 / Winter Semester 2002.

[125] A. Schmidt, K. G. Siebert, C.-J. Heine, D. Köster, and O. Kriessl, *Alberta - an adaptive hierarchical finite element toolbox.* `www.alberta-fem.de`.

[126] F. Schneider, *Inverse Problems in Satellite Geodesy and Their Approximate Solution by Splines and Wavelets*, Shaker Verlag, 1997.

[127] W.-D. Schuh, *Improved modeling of SGG-data sets by advanced filter strategies*, ESA-Project From Eötvös to mGal+, WP 2, Final-Report, (2002), pp. 113–181.

[128] W.-D. Schuh, *Reference data set 1 computed with spherical harmonics of degree 51 until 180 using the geopotential model EGM96 (the NASA GSFC and NIMA Joint Geopotential Model)*, 2006.

[129] ——, *Reference data set 2 computed with spherical harmonics of degree 20 until 180 using the geopotential model EGM96 (the NASA GSFC and NIMA Joint Geopotential Model)*, 2006.

[130] ——, *Reference data set 3 computed with spherical harmonics of degree 51 until 360 using the geopotential model EGM96 (the NASA GSFC and NIMA Joint Geopotential Model)*, 2006.

[131] W.-D. Schuh and B. Kargoll, *The numerical treatment of the downward continuation problem for the gravity potential*, V Hotine-Marussi Symposium on Mathematical Geodesy, (2004), pp. 22–31.

[132] L. L. Schumaker, *Spline Functions: Basic Theory*, Wiley & Sons, New York - London - Sydney, 1980.

[133] H. Schwetlick and T. Schütze, *Least squares approximation by splines with free knots*, BIT, 35(3) (1995), pp. 361–384.

[134] S. K. Sethi, *Cosmic microwave background radiation anisotropies and data analysis*, Pramana, 53 (1999), pp. 951–961.

[135] J. R. Shewchuk, *An introduction to the conjugate gradient method without the agonizing pain*, tech. rep., Carnegie Mellon University, Pittsburgh, PA, USA, 1994.

[136] N. H. Sleep and K. Fujita, *Principles of Geophysics*, Blackwell Science, 1997.

[137] P.-P. J. Sloan, J. Kautz, and J. Snyder, *Precomputed radiance transfer for real-time rendering in dynamic, low-frequency lighting environments*, in SIGGRAPH, 2002, pp. 527–536.

[138] G. F. Smoot, *Nobel lecture: Cosmic microwave background radiation anisotropies: Their discovery and utilization*, Rev. Mod. Phys., 79 (2007), pp. 1349–1379.

[139] W. J. Sternberg and T. L. Smith, *The theory of potential and spherical harmonics*, no. 3 in Mathematical Expositions, The University of Toronto Press, 1944.

[140] E. J. Stollnitz, T. D. DeRose, and D. H. Salesin, *Wavelets for Computer Graphics: Theory and Applications*, Morgan Kaufmann, San Francisco, 1996.

[141] W. Torge, *Gravimetry*, Walter de Gruyter, Berlin and New York, 1989.

[142] H. A. van der Vorst, *Bi-cgstab: a fast and smoothly converging variant of bi-cg for the solution of nonsymmetric linear systems*, SIAM J. Sci. Stat. Comput., 13 (1992), pp. 631–644.

[143] I. Vekua, *On metaharmonic functions (Russ., English summary)*, Trudy Tbilisskogo Mat. Inst. 12, 1943.

[144] G. Wahba, *Splines Models for Observational Data*, vol. 59 of Series in Applied Mathematics, SIAM, Philadelphia, 1990.

[145] G. Wahba, *(smoothing) splines in nonparametric regression*, El-Shaarawi, A., Piegorsch, W. (Eds.), Encyclopedia of Environmetrics, 4 (1995), pp. 2099–2112.

[146] N. Walet, *Further mathematical methods*, 2001. Lecture notes, The Theoretical Physics group at the University of Manchester
`http://walet.phy.umist.ac.uk/2C1/Notes/`.

[147] P. R. Wallace, *Mathematical analysis of physical problems*, Dover Books on Physics, Courier Dover Publications, 1984.

[148] F. Weller and H. Hagen, *Tensor-product spline spaces with knot segments*, in Mathematical Methods for Curves and Surfaces, Vanderbilt University Press, 1995, pp. 563–572.

[149] H. Yserentant, *Hierarchical bases give conjugate gradient type methods a multigrid speed of convergence*, Appl. Math. Comp., 19 (1986), pp. 347–358.

[150] ——, *On the multi-level splitting of finite element spaces*, Numer. Math., 49 (1986), pp. 379–412.

[151] ——, *Hierarchical bases*, in ICIAM 91, O'Malley and R.E., eds., Washington, DC, 1992, SIAM, Philadelphia, pp. 256–276.

[152] C. Zenger, *Sparse grids*, in Parallel Algorithms for Partial Differential Equations, volume 31 of Notes on Numerical Fluid Mechanics, 1991.

[153] O. C. Zienkiewicz, D. W. Kelly, J. Gago, and I. Babuska, *Hierarchical finite element approaches, error estimates and adaptive refinement*, in Mathematics of Finite Elements and Applications, Academic Press, 1982, pp. 313–346.